DOI: 10.14750/ME.2022.004

UNIVERSITY OF MISKOLC
FACULTY OF MATERIAL SCIENCE AND ENGINEERING

NUMERICAL SIMULATION AND EXPERIMENTAL VALIDATION OF RESIDUAL STRESSES IN A MULTI-PASS WELDED OIL AND GAS PIPE

A PhD dissertation submitted in the defence process for the degree of
Doctor of Philosophy
By

Mahmood Hasan Dakhil Alhafadhi

ANTAL KERPELY DOCTORAL SCHOOL OF MATERIALS SCIENCE & TECHNOLOGY

Head of Doctoral School
Prof. Dr Zoltán Gácsi

Scientific Supervisors:
Prof. Dr. György Krállics†
Dr. Máté Szűcs
Dr. Sándor Kovács

Institute of Metallurgy, Metal Forming and Nanotechnology

Faculty of Material Science and Engineering
University of Miskolc
Hungary, 2021

DOI: 10.14750/ME.2022.004

DOI: 10.14750/ME.2022.004

Contents

DOI: 10.14750/ME.2022.004

DOI: 10.14750/ME.2022.004

DOI: 10.14750/ME.2022.004

List of Figures

DOI: 10.14750/ME.2022.004

DOI: 10.14750/ME.2022.004

DOI: 10.14750/ME.2022.004

List of Tables

DOI: 10.14750/ME.2022.004

LIST OF SYMBOLS AND ABBREVIATIONS

Symbols Definition (Units)

p	Density
q	Heat Flux
C	Specific Heat
T	Temperature (℃ or K)
t	Time
η	Welding efficiency (%)
σ_x	Transverse residual stress, axial stress
σ_ϕ	Circumferential residual stress, hoop stress
σ_r	Radial residual stress
Q	Heat Input (joule/mm) or (joule/in)
U	Arc Voltage (volt)
I	Current (amperes)
v	Electrode Arc Speed (mm/sec)
A	Cross-Section Area (mm^2)
E	Elastic Modulus (N/m^3)
ε	Total Strain
ν	Poisson's Ratio
a	Half-length of heat source (mm)
b	Depth of heat source (mm)
c	Half-width of heat source (mm)
θ	The angle of moving the torch around the pipe
D	The outer diameter of the pipe (mm)
d	The inner diameter of the pipe (mm)
L	Length of pipe (mm)
λ	Beam wavelength or Wavelength of the X-ray
d	Inter-planar spacing (d-spacing) -the perpendicular distance between adjacent parallel crystallographic planes (Å)
d_0	Strain free inter-planar spacing (Å)
d_ψ	Inter-planar spacing of planes at an angle ψ to the surface (Å)
$\{hkl\}$	Miller indices describing a family of crystalline planes
ψ (psi)	The angle between the normal of the sample and the normal of the diffracting plane (bisecting the incident and diffracted beams)
θ	The angular position of the diffraction lines according to Bragg's Law
φ (phi)	The angle between a fixed direction in the plane of the sample and the projection in that plane of the normal of the diffracting plane
re	3-D cone radius dimension (upper part)
ri	3-D cone radius dimension (lower part)
ze	3-D cone length (upper)
zi	3-D cone length (lower)

DOI: 10.14750/ME.2022.004

Abbreviations	Definition
MMAW	Manual metal arc welding
GTAW	Gas tungsten arc welding
GMAW	Gas metal arc welding
PGTAW	Pulsed gas metal arc welding
FCAW	Flux-cored arc welding
SMAW	Shielded metal arc welding
BC	Boundary condition
FEM	Finite element method
WCL	Welding centreline
BM	Base material
HAZ	Heat affected zone
FZ	Fusion zone
WM	Weld metal
XRD	X-ray diffraction
ND	Neutron diffraction
2-D	Two-dimensional
3-D	Three-dimensional
D	X-ray detector
S	X-ray source
N	Normal to the surface
HD	Hardness test
Hv	Hardness (Vickers)
X_M	Volume fractions of martensite
X_B	Volume fractions of bainite
X_f	Volume fractions of ferrite
X_p	Volume fractions of pearlite
HV_M	Hardness of martensite
HV_B	Hardness of bainite
HV_{F+P}	Hardness of the mixture of ferrite and pearlite
CGHAZ	Coarse grained heat effect zone
FGHAZ	Fine graind heat effect zone
ICHAZ	Intrcritical heat effect zone
SCHAZ	Subcritical heat effect zone

DOI: 10.14750/ME.2022.004

DOI: 10.14750/ME.2022.004

1. INTRODUCTION AND GLOBAL AIMS

1.1 Introduction

Pipelines are the arteries of industry. These pipes are used to carry crude oil, petroleum, natural gas (pressurised into liquids known as natural gas liquids), slurries, heavy crude oil and solids flow in a multitude of the condition imposed by ongoing processes. The transportation must be continuous for a long time, which is only possible by pipeline. These pipelines may range from a few kilometres to thousand kilometres, passing through different conditions. The advantages of transporting crude oil, natural gas, and all petroleum products with pipelines as the best means of continuous and reliable operation have been well proven in the entire world. Pipelines are subject to sometimes intense stresses, temperatures, pressure and flow and combinations of these phenomena, and factors such as toxic conditions or welding residual stresses (WRS) can contribute to the hazards of corrosion, rust, erosion, fire, and explosion. For many years now, industries have increasingly shown concern about pipe safety or protection. The pipes can rust over time, or rust in the pipes can advance into the metal's internal parts, which may lead to reduce thickness and eventually pipe failure because of the crack inside or outside if left untreated. Many other factors depend significantly upon the pipe; in case of pipe failure, a section may need to be cut and joined to another metal, and the best way to join them is welding [1].

Welding is one of the most distinctive processes to join two or more pieces of material. It is a reliable and proficient metal-joining process and is broadly utilised in some industries. Commonly used types of welding include manual arc welding, shielded metal arc, submerged arc gas tungsten arc welding, etc. [2]. Among these, in the manual metal arc welding process (MMAW) an electrical arc burns between a sheathed rod electrode and the material. The basic principle of the arc welding process is illustrated in Figure 1(a). It involves joining the material pieces by liquefying the joint region, adding the filler material to form the liquid metal weld pool to make a solid weld joint. Generally, the welding consists of three distinct zones, as illustrated in Figure 1(b), divided into the following areas:

i. Weld metal (WM) or fusion zone (FZ): The metal zone is heated to a complete liquid state with a similar microstructure to casting after being solidified.
ii. Heat-affected zone (HAZ): The zone from the melting border to the base metal.
iii. Base metal (BM): The areas with temperatures less than 500 °C.

DOI: 10.14750/ME.2022.004

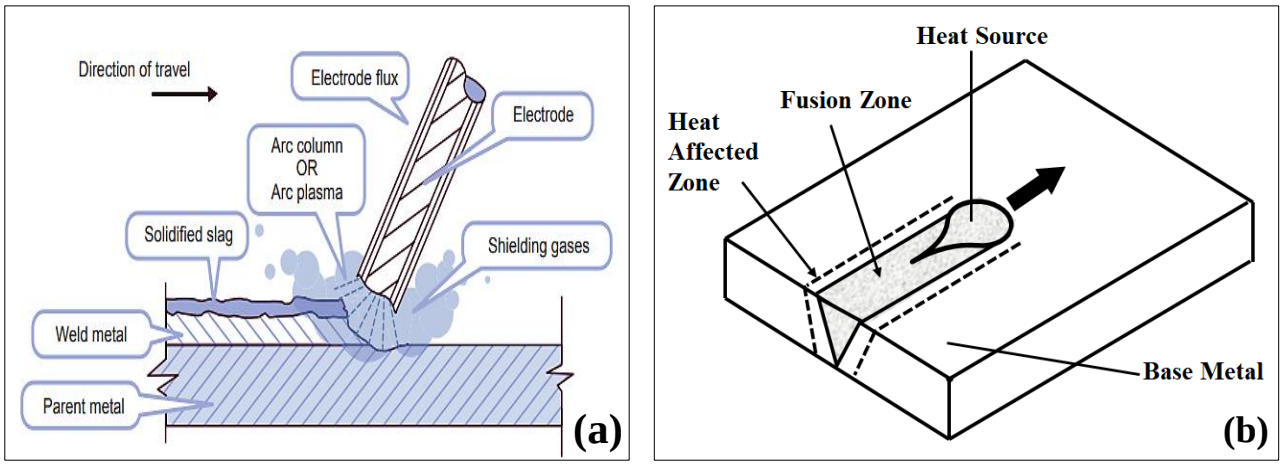

Figure 1. (a) MMAW process (b) Welded joint; BM (base material), HAZ (heat affected zone) FZ (fusion zone)

Welding similar [3] or dissimilar materials [4] usually involves heating the joint materials to fuse them together. This heat creates expansion and contraction. If heating and cooling are non-uniform, the heat from welding may cause a localised expansion in the weld zone, which is taken up during the welding by the molten area of the weld zone or another location of the part weld. After the finished weldment cools, some areas cool and contract more than others, leaving internal stresses. These internal stresses are called residual stresses [5]. Figure 2 shows the schematic diagram coupling between temperature, microstructure and stresses.

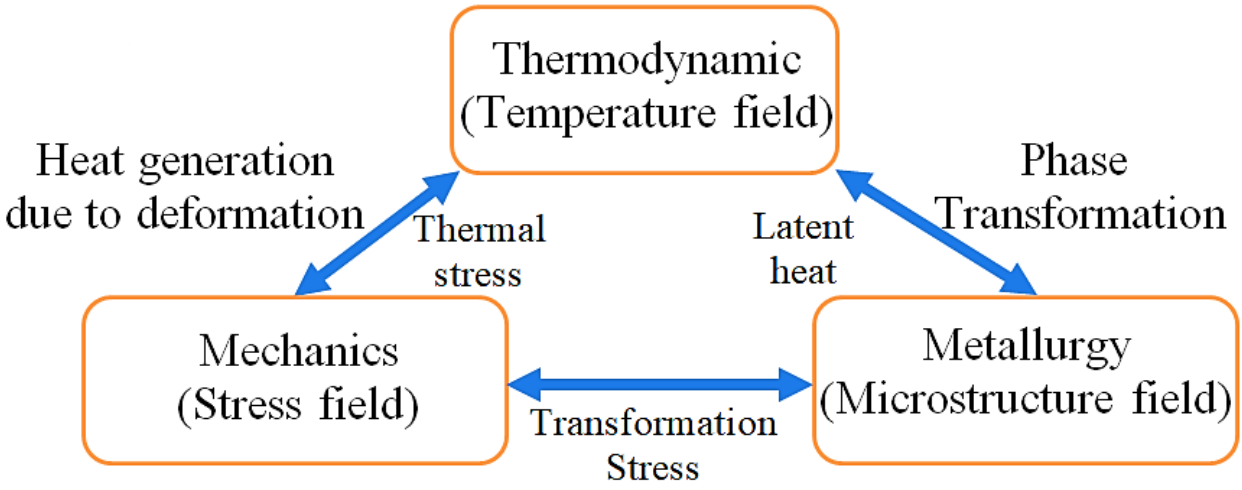

Figure 2. Schematic diagram coupling between temperature, microstructure and stresses

Residual stresses are generated in pipe welding because of non-uniform heating and cooling in the weld metal and base metal and are considered important in integrity welding assessment. Residual stresses are a crucial factor in crack formation in the pipe weld. There are two types of residual stresses, tensile or compressive, that can be found in welding. Tensile residual stresses are usually the harmful effects of welding a pipe, which causes crack growth. Residual stresses directly

affect the quality of the welding. Failures and other problems caused by residual stresses have led researchers to focus on investigation, monitoring and measuring to relieve residual stresses. Thus, residual stresses have become an important research subject of today's engineering world. So it is important to determine the welding residual stress distribution to improve the quality of welding [6]–[10].

Three groups of techniques are used to measure residual stresses, commonly known as non-destructive, semi-destructive, and destructive techniques [11]. All of the residual stress measurement methods are indirect, calculated from measured quantities, such as elastic strain or displacement. A numerical simulation using the finite element method (FEM) is a helpful tool to reduce the measurement technique for welding residual stresses [12], [13].

Many researchers have used (FEM) as a numerical tool to investigate temperature distribution and residual stresses during the fusion welding process with different materials and joints. Numerical simulation of the welding process is very complicated due to the variation in temperature, thermophysical expansion and shrinkage and variation of material properties with time and space. Software such as ANSYS, ABACUS, SYSWELD and WELDSIM are used by various researchers [14]–[23]. MSC Marc software enhanced with user subroutines is quite a familiar tool in welding process simulation and has been used with great success [24]. Numerical simulation of the welding process in finite element methods is carried out using thermo-mechanical analysis. The computational process is split into two solution steps, such as thermophysical and mechanical analyses. The sequentially coupled thermo-mechanical analysis is used to simulate the welding process. Initially, the temperature distribution and its history are computed in the welding model. Further, the thermophysical histories calculated by the model are then given as an input in the residual stress field's successive mechanical evaluation.

This research study is a significant continuation of previous research works, building upon their experience and then using our measurement results to develop the numerical simulation model using MSC Marc in order to investigate the behaviour of welding residual stresses. This dissertation is an effort to investigate residual stresses and understand the evolution of the stresses in the multi-pass welding of dissimilar pipe materials by comparing experimental measurements using X-ray diffraction technique with numerical simulation results using 2-D and 3-D models. A comprehensive list of the literature review was presented with the identification of the knowledge gap. Goals were formulated, and experiments were planned, executed, and analysed scientifically.

DOI: 10.14750/ME.2022.004

1.2 Plan of Research Work

To achieve the objectives mentioned above, it is necessary to study the essentials of finite element simulation of pipe welding reported in the literature. Hence, as a test study, it is considered essential to develop a 2-D and a 3-D finite element model of pipe welding and compare their results with experimental data for validation of the models. To validate the results of finite element predictions of residual stresses in the weld joint, residual stresses in the weld joint must be measured, which was done by two non-destructive approaches, using X-ray diffraction (XRD) and validated the model by hardness test measurements. After experimental validation of residual stresses in the weld joint, the developed finite element model will compute residual stresses in the weld zone. To achieve the simulation of MMAW process parameters such as welding current, welding speed and etc., it is necessary to construct a mathematical model in terms of the selected process parameters. Determination of residual stresses data is required for the construction of the mathematical model in the weld joint. The developed finite element model will then be run for all combinations of the parameters in the pipe weld as one step towards identifying parameters that can minimize residual stresses in the weld joint. The plan of the present research work is presented in Figure 3.

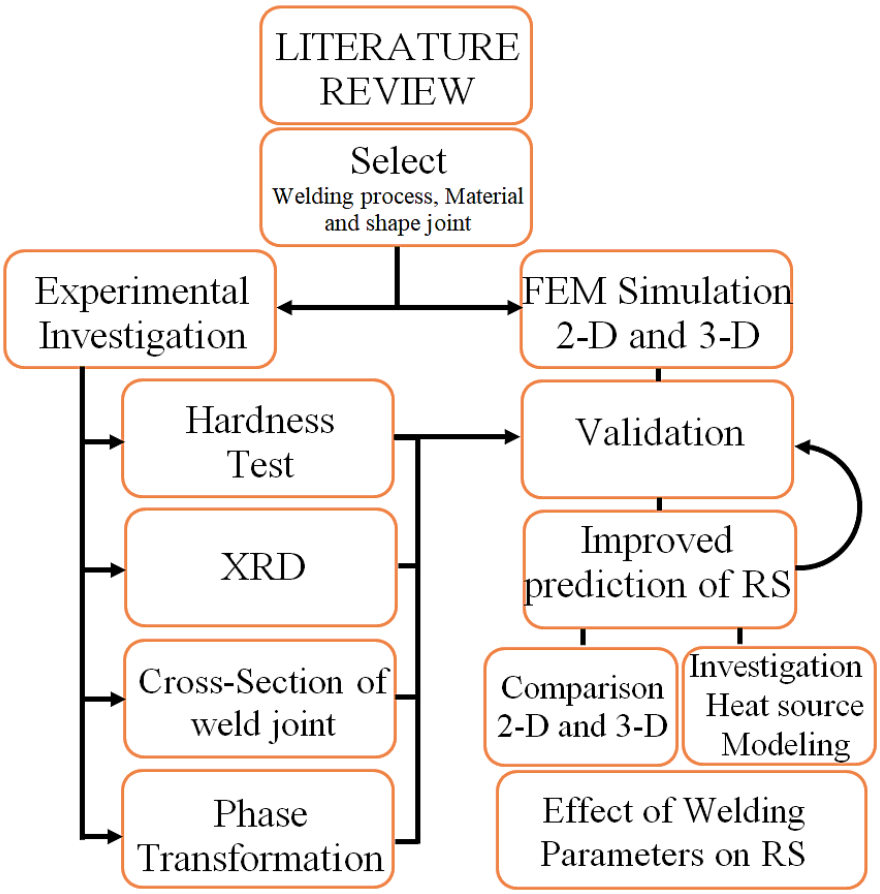

Figure 3. The plan of the present research

DOI: 10.14750/ME.2022.004

1.3 The organization of the dissertation

The research work presented in the following chapters of this dissertation was undertaken to predict temperature distribution and residual stresses in welded pipe. The effectiveness of heat source models and parameters (welding speed, thickness of the pipe, number of passes, welding current, etc.) were also investigated. Thus, the dissertation is structured accordingly as detailed below:

Chapter 2 Reviews the literature on the finite element method using 2-D and 3-D models, residual stress measurement using XRD, present the heat source models.

Chapter 3 Provides a study of the validation model using a hardness test, phase transformation, heat source model and the comparison of sectional morphology.

Chapter 4 Describes the material and method used in this work.

Chapter 5 Discusses the XRD result and finite element simulation model of the pipe welding process. The effect of temperature distribution, pipe thickness, heat source models, welding speed, and other parameters on residual stress have been studied.

Chapter 6 Compares the 3-D model with the 2-D model and investigate the accuracy of the computations.

Chapter 7 Covers the overall claims of the research work and the scope for future work.

DOI: 10.14750/ME.2022.004

2. LITERATURE REVIEW

During recent years, studies have focused on arc welding for joining oil and gas pipe, which is justified by arc welding being in common use, having relatively low cost and being suitable for out-of-position pipe welding. Most studies on welding validate numerical simulation results by comparison with welding residual stresses measurements. The experimental measurements have some uncertainties in the obtained data, making it hard to debug coding errors using the software. Some authors compare numerical simulation results with experimental data obtained from other studies.

Welding is a complex process that includes interactions among various physical and metallurgical phenomena. Several definitions are assumed when dealing with this type of problem, and not all effects are considered in a first prediction. It should be noted that several studies in the literature that presented comparisons did not model precisely the same shape of the welding part and physical phenomena or did not use the same material model of the referenced work for comparison. In addition, the lack of boundary conditions and welding parameter data makes it very hard to reproduce the measurements cases exactly.

Research on residual stresses has been a continuous interest among researchers to decrease the welding process quality's negative effect. So far, numerical and experimental investigations of residual welding stress focus on welding processes with different welding types. MMAW has several detrimental effects on the structural integrity and in-service performance of the weldments. This technique is used to join similar or dissimilar materials by the application of heat. The most important aspect is to provide high structural integrity with high joint efficiency during welding. Welding can be performed manually, semi-automatically, and fully automatically.

Sufficient literature is available on various aspects of the modelling of conventional welding processes for various situations such as plates, pressure vessels, railway rails, etc. However, only limited literature exists on modelling and simulation of residual stress in the welding of pipes. As a part of the present research, a literature review is carried out to gain an understanding of the current research status. The works of literature have been divided into different sections according to topical areas and to identify and figure out several modelling issues based on the work carried out, such as finite element method (FEM), X-ray diffraction measurement, heat source models and welding residual stress, which are presented briefly in the forthcoming subsections.

This review helped a great deal in understanding the status of residual welding stresses and gives insight into predicting and controlling residual stresses in welding, the significant contributions, and the past research limitations. The central part of this chapter focuses on identifying the various issues that can concern multiple researchers working on residual stresses in

the future. This chapter attempts to present some gaps and limitations in various research studies in the residual stresses field. The inference from the literature with the identification of the research gap is also presented at the end of this chapter.

2.1 Welding Residual Stresses (WRS)

Different processes have been developed to join the materials. Still, for simplicity, these may be classified into two groups called fusion and pressure welding, as shown in Figure 4, which lists some standard welding processes.

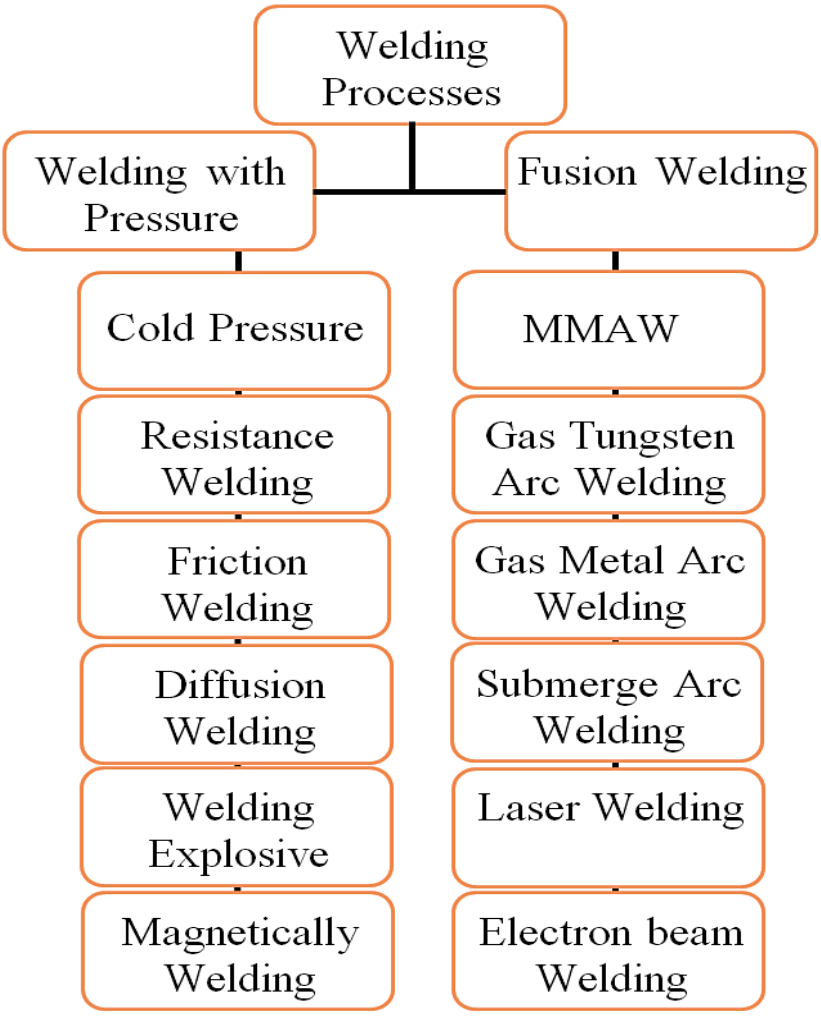

Figure 4. Some important welding processes [25]

2.2 Manual Metal Arc Welding Process (MMAW)

Different types of fusion welding techniques are used for various engineering applications. The fusion welding process includes arc welding, gas welding, electric resistance welding and thermite welding. In particular, manual metal arc welding (MMAW) is a welding process that can be used on nearly all materials suitable for welding simply, quickly and efficiently. The heat of arc

metals, the surface of the base metal and the end of the electrode is transferred through the arc metal to the sample material, where it becomes the deposited weld metal [26][27].The procedure is used, for example, when building ships, pipelines, and steel constructions and bridges outdoors. MMAW is the most widely used fusion welding process in some industries and an important component in many industrial operations. It is easily found in any industry whose products require joining pipes. It has extensive applications, particularly in oil and gas terminals. For pipeline load and suspension application, MMAW provides high joint efficiency by welding pipes of high strength steel with various thicknesses and complex shapes.

2.3 Important Issues in Manual Metal Arc Welding Process (MMAW)

Although welding is the most preferred joining technique in all manufacturing processes, it is not failure-free. Due to highly localized transient heat input, considerable residual stresses occur after welding in the weld zone [25][28]. Since the arc welding process involves highly complex thermophysical cycles, it leads to increased strains, resulting in an increase in residual stresses in a pipe weld. Residual stresses resulting from the welding represent significant problems, as reported in [29]. Residual stresses with high magnitude are problematic in fatigue or failure. Tensile residual stresses, which often exist in the weld zone, induce the farther opening of cracks.

Furthermore, residual stresses reduce fatigue strength and rust resistance [30]. Although it is impossible to eliminate residual stresses in the weld structure, it is possible to identify welding conditions that can keep the effects of residual stresses as low as possible. Hence, a need arises to develop scientific methods to determine the welding conditions that can reduce unfavourable welding effects.

- **Manufacture**

1. Either alternating (A.C.) or direct (D.C.) current is used for MMAW. When A.C. is used, the arc must re-ignite at each half-cycle, as the polarity is reversed. This causes some instability of the arc, which can be alleviated by using arc-stabilising agents in the flux coating. When D.C. is used, there is a choice of polarity – the positive pole is the hottest.
2. Arc voltages are maintained between 14 and 45 V, with open-circuit voltages of 50–150 V. Power sources range from 30 to 500 A in A.C. or D.C.
3. Coated electrodes contain slag-forming ingredients (that produce a fluid coating over the weld as it cools) and gas-forming ingredients (that generate atmospheres of CO_2, CO or H_2 around the arc). Principal materials used in electrode coatings include:

– Carbonaceous material of the cellulose type ($C_6 H_{10} O_5$) n – produces a shielding gas (CO);

DOI: 10.14750/ME.2022.004

- Silica (SiO_2) – combines with metallic oxides to form slag;
- Titanium oxide (TiO_2) – to stabilize the arc;
- Calcium carbonate ($CaCO_3$) – decomposes to form CaO, and hence a basic slag;
- Calcium fluoride (CaF_2)– increases slag fluidity;
- Sodium oxide (Na_2O) – acts as a coating binder and promotes slag fluidity;
- Ferro-silicon – acts as deoxidant;
- Iron powder – increases the rate of deposition.

4. Sizes of welding machines are designated according to their output rating, ranging from 150 to 1000 A.
5. Deposition rates are in the range of 2–5 kg h^{-1}.

• Materials

Most engineering metals and alloys can be welded by the MMAW process (a very versatile process). In welding carbon and low alloy steels, the coated electrodes are usually of low carbon steel. For alloy steels prone to hard and brittle martensite formation on cooling, low alloy steel electrodes are used. Also, these steels are prone to hydrogen embrittlement, and coatings must be free from hydrogen-forming cellulose. Instead, TiO2 and CaCO3 are added to the coating. Austenitic compositions (up to 25% chromium and 20% nickel) are also useful to prevent martensite formation.

Cast irons are welded with nickel-rich or monel electrodes (Ni - Cu). Most non-ferrous metals and alloys are welded with electrodes of a composition like the metal being welded. Aluminium alloy electrodes are coated with fluxes consisting of mixtures of fluorides and chlorides to dissolve the aluminium oxide Al_2O_3 surface layer. The precipitation hardening Al-Mg-Si alloys are welded by the TIG and MIG processes. Copper, copper-tin (bronze), and copper-zinc (brass) alloys have large coefficients of thermophysical conductivity, so they require more significant amounts of heat and need pre-heating before MMAW (up to 250–450 °C). Nickel alloys can be welded with pre-heated electrodes.

• Classification of Fluxes

In general, there are two flux types: fused flux and unfused flux (bonded flux and agglomerated flux).fluxes also can be divided into the following two categories flux classification of covered electrode and SAW flux classification.

The major components of the coating determine the four major types of covered electrodes: cellulosic, rutile, lime or lime– titania, and iron powder. Submerged arc welding fluxes (SWA)

classification by manufacturing process, based on chemical composition, based on the type of slags and based on chemical properties, as shown in Figure 5.

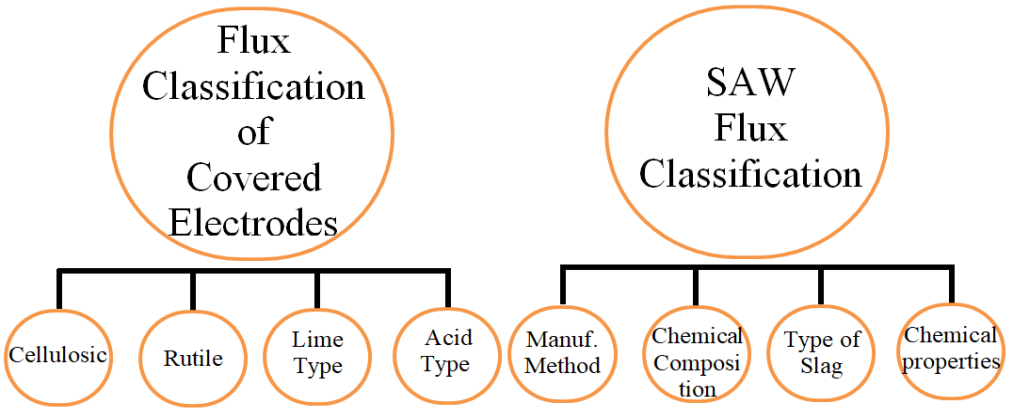

Figure 5. Classification of fluxes

- **Design**

According to the American Welding Society (AWS), American Petroleum Institute (API), and the European Union's European Committee for Standardization (CEN), manual metal arc welding (iso code 111) usually has five types of welding joints: butt, corner, lap, T-shape and edge joint. The most commonly used type of pipe joint is the butt joint, a process in which two pieces of pipes are joined in the same horizontal plane. Butt joint designs that are used with MMAW processes with similar and dissimilar material are square groove, single v-groove, and double-v-groove, as shown in Figure 6. MMAW is often the preferred method for depositing the root pass for square groove or single V-groove joints. The weld joint's remainder can then be filled using other welding processes as appropriate, with thicknesses of 5–25 mm. The minimum included angle (C) is 60° with a root opening of 0–3 mm and a root face of 0–3 mm [31].

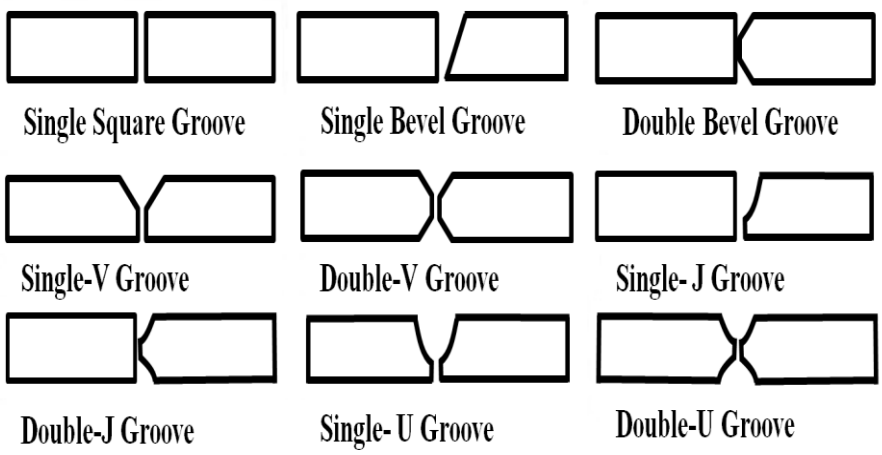

Figure 6. Typical Butt Joints for Manual Welding

DOI: 10.14750/ME.2022.004

2.4 Heat Affected Zone in welding pipe

In welding, the region next to the fusion zone (FZ) or weld pool where microstructural changes have occurred is known as the heat affect zone (HAZ); when a heat source is applied over the surface of a substrate pipe, this is the region where the microstructural and property changes occur without the melting of the substrate. The property changes in HAZ is mainly based on sensitising temperature, subsequent recooling, nature of substrate material, filler material (if used) and the quantity of heat input. The cooling rate depends on the specific heat capacity and thermal conductivity of the material, also depend on other factors unrelated to the material (e.g. intentional cooling, quenching).

With respect to heat input, higher input increases the width of HAZ. In the pass of the welding, filler material is heated and then cools as the torch moves on. The maximum temperature is reached in the weld pool. The temperature decrease away from the weld pool is inversely proportional to distance. In the pass of the welding, filler material is rapidly heated to the maximum temperature and allowed to cool more slowly by the condition of heat into the bulk of base metal (BM). Figure 7 describes the temperature-dependent phase transformations in terms of the Fe-C equilibrium phase diagram. Phase transformation changes can occur depending on the temperature reached.

Changes in the microstructure of the heat-affected zone (HAZ), including phase transformations in the solid-state, are the cause of significant changes in this area's mechanical properties compared to properties of the base material. Sufficiently far from the weld pool, the material will be unaffected. In the present work, more emphasis is devoted to the analysis in HAZ.

Microstructures in the weld zone and around, including a weld (or fusion zone) and a heat affected zone (HAZ), are different from those in a base material (BM), as shown in Figure 7.

The HAZ is divided into distinct zones based on the microstructure changes at different distances from the welding line [32] [33], known as: coarse-grained (CGHAZ), fine-grained (FGHAZ), intercortical (ICHAZ) and sub-critical (SCHAZ) heat-affected zones (a, b, c and d, respectively, in Figure 8).

New sub-zones of the HAZ are characterised by small and discontinuous features appearing. In the cooling stage, austenite transforms to different microstructures. The nature, quantity and distribution of the resulting products, are function of the chemical composition of the base metal and the thermal cycle experienced during welding. Intercritically reheated coarse grained HAZ (IC CGHAZ) is created by reheating CGHAZ to a temperature range between Ac_1 (temperature at which austenite begins to form during heating) and Ac_3 (temperature at which transformation of ferrite to austenite is completed during heating) called intercritical temperatures ($Ac_1 < T < Ac_3$).

DOI: 10.14750/ME.2022.004

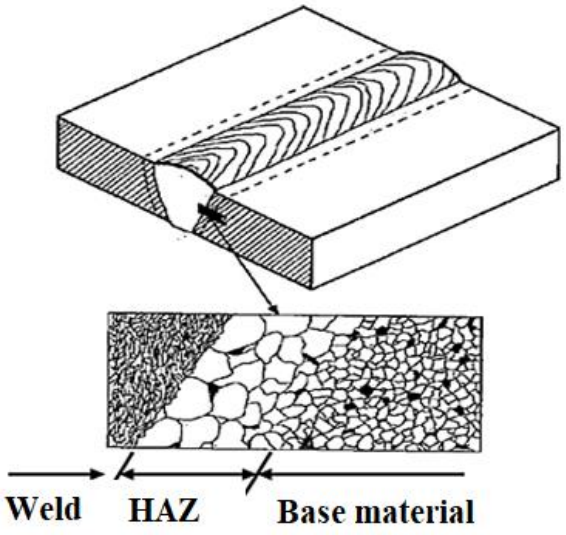

Figure 7. Microstructure near the weld

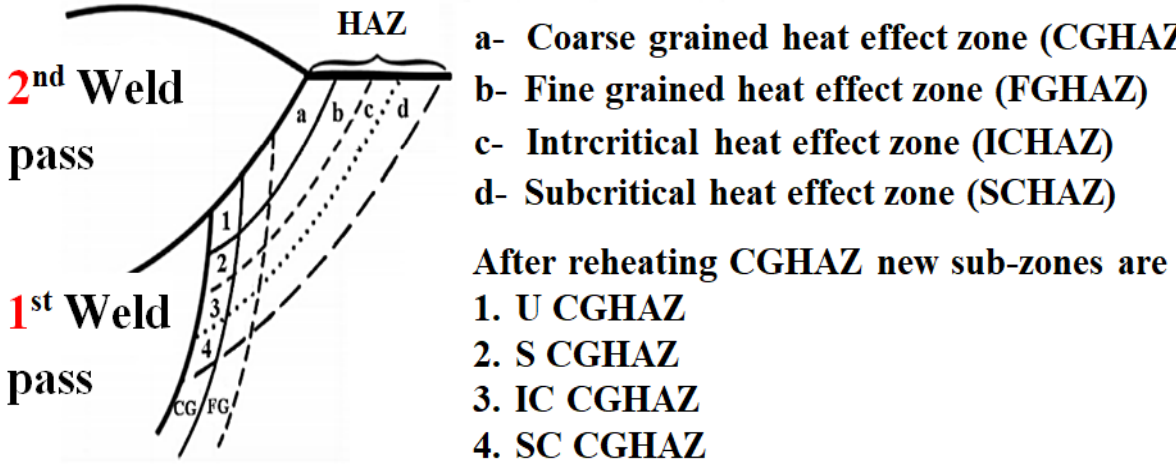

Figure 8. Sub-zones of HAZ in the welding [34]

2.5 Welding Residual Stresses (WRS)

Residual stresses (RS) are “locked-in” stresses that exist after welding, independent of the presence of any external loads. It is widely recognised that cracking associated with residual stress is classified as failure welding. The welding causes non-uniform heating and cooling in the material, thus generating inhomogeneous plastic deformation and welding residual stresses (WRS) in the weldment. Residual stress may be desirable or undesirable. Solidification and differential shrinkage of material cause large tensile and compressive residual stresses in welds. Tensile residual stresses are generally detrimental, increasing the susceptibility of a weld to fatigue damage [35], stress cracking [36], or other types of fracture [37]. Typically, residual stresses originate from:

- Differential plastic flow;
- Differential cooling rates;

- phase transformations with volume changes [38], [39].

2.6 Mechanisms for Creating Residual Stresses

Residual stresses can come from a variety of mechanisms, including:

1. Non-uniform plastic deformation, which often occurs in manufacturing processes that change the material's shape, including forging, rolling, bending, drawing and extrusion;
2. Surface modification. Examples occur in manufacturing during machining, grinding, plating, peening, carburising, and in-service by rust or oxidation;
3. Material phase, often in the presence of large thermophysical gradients. For example, this occurs in manufacture during welding, phase transformation in metals and ceramics, etc. [11].

2.7 The Length Scale Sometimes categorizes Residual Stresses

Residual stresses (RS) can be defined as either macro or micro stresses, or both may be present in a component at any one time, and hence a type of measurement technique used to study them is based on length, as shown in Figure 9 (a). They can be classified as:

Type-1 RS: macro residual stresses that extend over distances from mm upwards.

Type-2 RS: varies and self-equilibrates over the scale of several grains.

Type-3 RS: varies over less than the scale of a grain.

For pipe, three principal components coincide with the hoop or circumferential, axial and radial direction defined in Figure 9 (b).

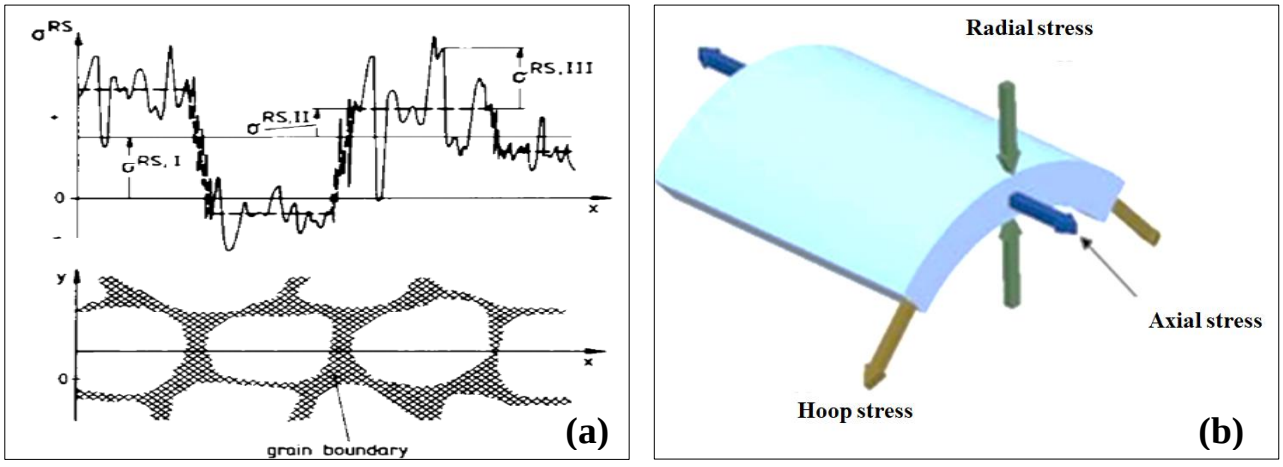

Figure 9. (a) The categorisation of residual stresses according to length scales (b) Schematic illustration of residual stress components in pipe [40]

DOI: 10.14750/ME.2022.004

2.8 Residual Stress Gradients

Figure 10 shows an example of typical stress gradients found in a pipe weld. The kind and magnitude of residual stresses change during heating and cooling. The welding residual stresses indicate a stress gradient of about 200–300 MPa adjacent and parallel to the weld. Because of concerns for welding failure through fatigue and cracking and the high-stress gradients, it is necessary to make many stress measurements on as many small sample elements as possible. In welded metal structures of pipes, a lot of attention is given to residual stresses induced by welding. Combined with other factors, the stresses can essentially affect the geometry, performance and reliability of welded structures under different conditions. Despite the fact that residual stresses are non-zero, they must be non-uniform, sometimes quite substantially do, with large stress gradients along the weld zone. Accordingly, residual stresses are not caused by forces; therefore, they must be globally balanced, i.e.:

$$\int \boldsymbol{\sigma}\, \boldsymbol{dA} = \mathbf{0} \tag{1}$$

Where σ is the residual stress, dA is an infinitesimal area in the welded part.

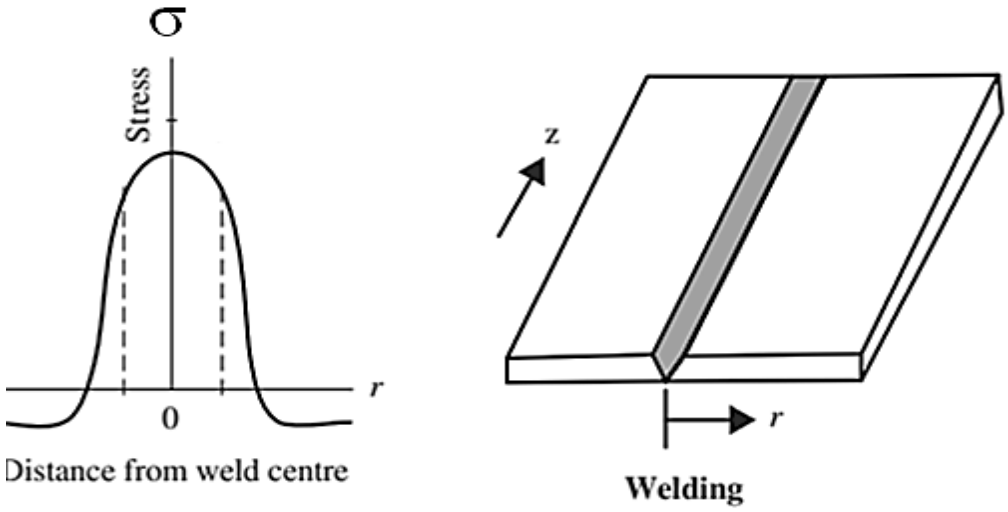

Figure 10. Illustrating typical residual stress gradients induced by various welding processes [11]

2.9 Residual Stress Profiles

Figure 11 shows the region where plastic deformation occurs during the circumferential pipe weld thermophysical cycle. During the pipe welding, the part outside the shaded area was remained elastic throughout the entire welding thermophysical cycle. The figure also shows the temperature gradients in several cross-sections through the weld zone. Section A-A crosses the base metal ahead

DOI: 10.14750/ME.2022.004

of the welding arc. The slope of the temperature gradient is zero. In section B-B, which crosses the welding arc, the slope becomes very low. The slope of the temperature gradient due to welding once again is zero along section D-D after welding. Section C-C in both of the weld metal and base metal regions has cooled and shrinking. Due to local heating during welding, complex thermophysical stresses occur; and residual stress results after welding along section D-D, where axial stresses in tensile stresses and around compressive stresses are produced farther away from the weld centerline.

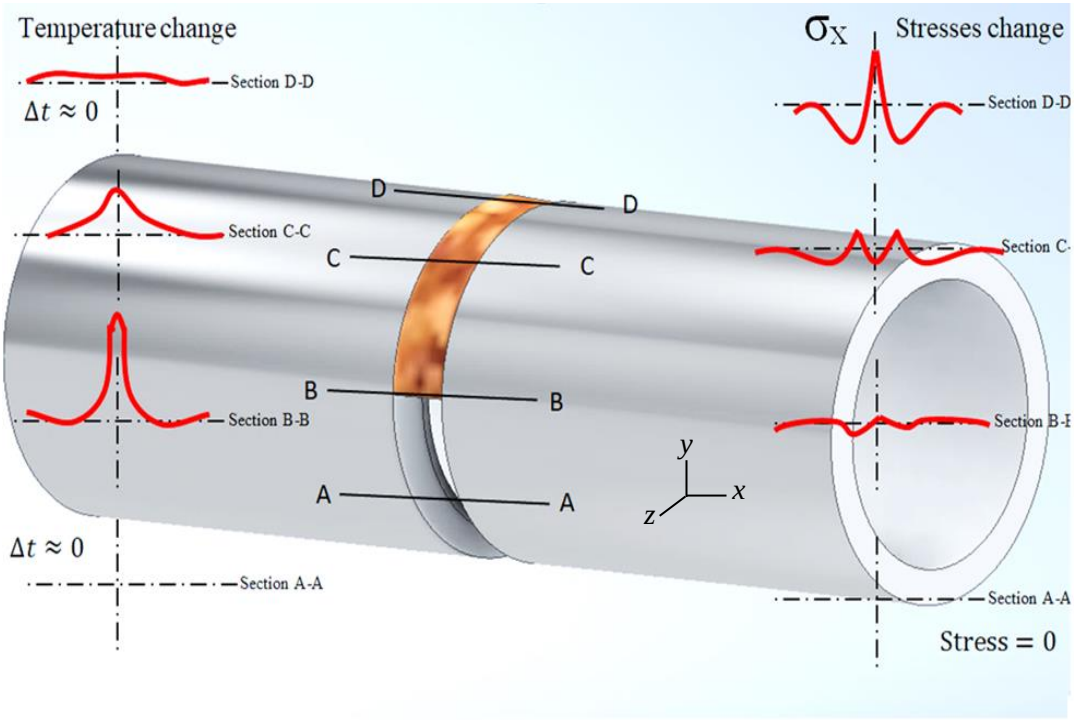

Figure 11. Schematic representations of changes in temperature and stresses during welding

2.10 Residual Stress Measurement Methods

Different methods for measuring them in various types of components have been developed. The methods are commonly categorized as non-destructive, semi destructive and destructive techniques, as shown in Figure 12. Non-destructive methods include X-ray diffraction, neutron diffraction, ultrasonic methods and magnetic methods. Semi-destructive methods are dependent on inferring the original stress from the displacement incurred by entirely or partially relieving the stress by removing material. These methods depend on the measurement of deformations due to the release of residual stresses upon the removal of material from the specimen. Contour, hole-drilling, ring-

core and deep-hole are the principal destructive and semi-destructive techniques used to measure residual stresses in structural members.

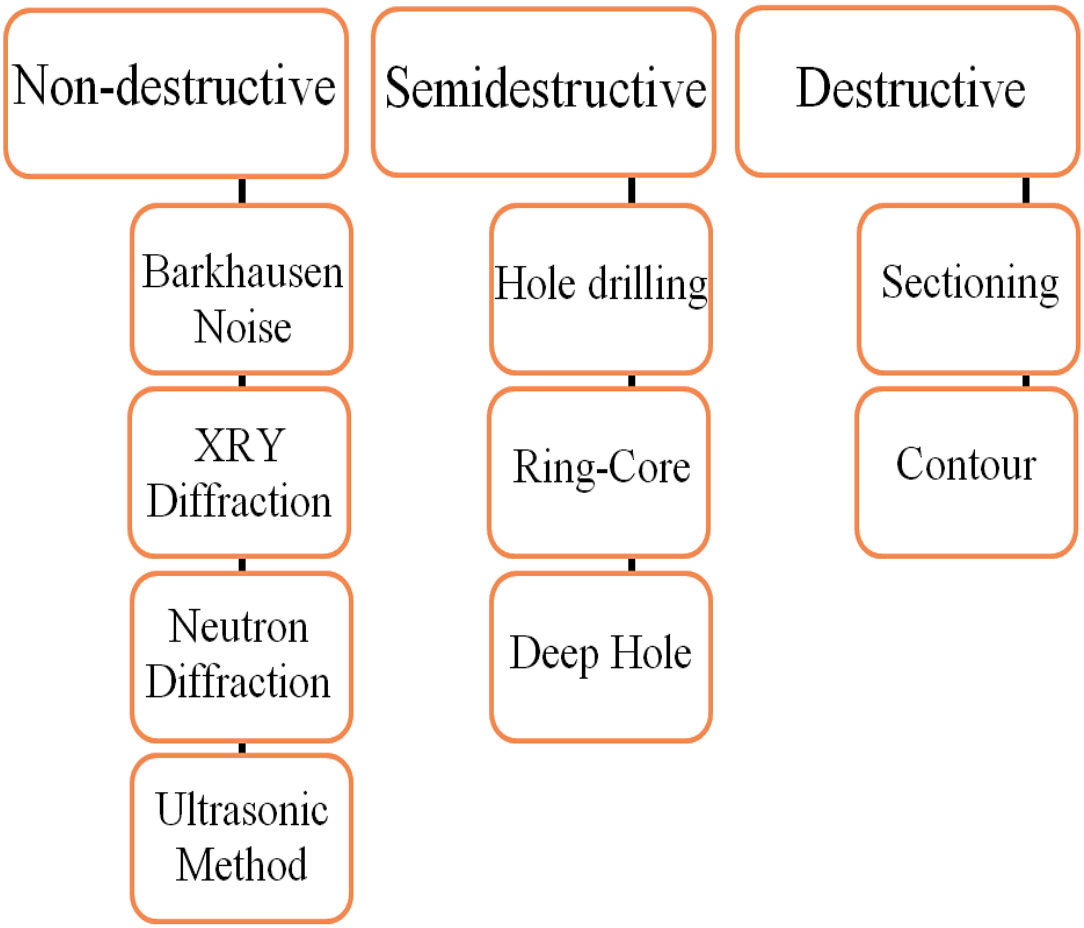

Figure 12. Residual stress measuring techniques

2.10.1 *Destructive Methods*

This method removes the sample material. The residual stress is obtained according to the displacement or strain in the weld zone. To investigate the residual stress generated during welding processing and other manufacturing processes, detection technologies that measure residual stresses at the surface have been developed. The residual stress in the surface layer cannot reflect the influence of processing on the residual stress and cannot enable a useful strength analysis. Therefore, measuring the residual stress through the thickness or more deeply came into being and gradually developed. The method proposed for measuring residual stress, the destructive process, has been studied for decades. Its high accuracy, practicability, and relatively mature theory are widely used in practical applications, as well as other less used techniques such as excision, splitting, curvature, layer removal, and slitting.

2.10.2 *Semi-Destructive Methods*

The semi destructive measurement is relatively quick and straightforward, and it is one of the most popularly used methods of residual stress evaluation, which can provide the measurement of residual stress distribution across the thickness in magnitude, direction and sense. Semi destructive techniques, called also mechanical method, are dependent on inferring the original stress from the displacement incurred by completely or partially relieving the stress by removing material. Also these methods rely on the measurement of deformations due to the release of residual stresses upon removal of material from the specimen. It has the advantages of good accuracy and reliability, standardized test procedures, and timely, practical implementation. The damage caused to the specimen is localised to a small drilled hole. Sectioning, contour, hole-drilling, ring-core and deep-hole are the principals semi destructive techniques used to measure residual stresses in structural members.

2.10.3 *Non-Destructive Methods*

Non-destructive methods or physical testing methods mainly measure residual stress based on the material's physical properties. To avoid affecting the continued use of the specimen, in some case, destructive methods are unacceptable. The non-destructive method is a reliable and effective tool and has expanded adoption and become the widely main residual stress measurement method for the future. Diffraction methods are based on determining the strain deformation, which will cause changes in the interplanar spacing, d, from their stress-free value, d_o. The strain can be calculated by using Bragg's law. It is necessary to have an accurate measure of interplanar spacing. For this, the most common diffraction methods are X-ray diffraction (XRD) and neutron diffraction. The methods are classical residual stress measurement methods, but their measurement accuracy is constantly improving.

In the last several years, the factors affecting accuracy have been investigated. The selection of the method to measure the residual stress in the welding pipe depends on the information required and the nature of the measurement sample – whether a destructive or non-destructive method is being used. Factors needed to measure residual stresses include the depth of penetration of the measurement on the surface or through-thickness of the sample's shape or geometry and location. Additionally, some of the techniques need specialized laboratory facilities [41][11][42]. For each method scope, physical limitation, accuracy, advantages and disadvantages are summarised in Table 1 and compared to the residual stresses measurement techniques.

DOI: 10.14750/ME.2022.004

Table 1. Comparison of the residual stresses measurement techniques[43].

Technique	Advantage	Disadvantage	Destructive	Accuracy
X-ray diffraction	Ductile Generally available Wide range of materials Hand-held systems Macro and Micro RS	Lab-based systems Small components Only basic measurements	non-destructive	High accuracy on the surface
Hole Drilling	Fast Easy use Generally available Hand-held Wide range of materials	Interpretation of data Limited strain sensitivity and resolution	Semi destructive	The strain gauge impacts the accuracy
Neutron Diffraction	Macro and Micro RS Optimal penetration and resolution 3-D maps	Only a specialist facility Lab-based system	non-destructive	Not on the surface
Barkhausen Noise	Very quick Sensitive to microstructure effects, especially in welds Hand-held	Only ferromagnetic materials Need to divide the microstructure signal from that due to stress	non-destructive	Accurate
Ultrasonic	Generally available Very quick Low cost Hand-held	Limited resolution Bulk measurements over the whole volume	non-destructive	The material and external factors have a great influence on the accuracy
Sectioning	Wide range of material Economy and speed Hand-held	Interpretation of data Limited strain resolution	Destructive	Accurate
Contour	High-resolution maps of the stress normal to the cut surface Hand-held Wide range of materials Larger components	held Interpretation of data Impossible to make successive slices close together	Destructive	There is a large error when obtaining results near workpiece surface
Deep hole drilling	Deep interior stresses measurement Thick section components Wide range of material	Interpretation of data Limited strain sensitivity and resolution	Semi destructive	The traditional strain gauge has a great influence

2.11 Strategies for Measurement Method Choice

An appropriate measurement technique needs to be chosen for a given measurement need. The answer is often non-unique and depends on several factors, and the essential factor to be considered when planning measurements concerns the accuracy of the measurements. A consequence of all

these challenges is that residual stresses measurements do not typically reach the accuracy or reliability that is possible when working with applied stresses. However, the various residual stress measurement methods are now quite mature, and the accuracy gap is often considerable. The X-ray diffraction (XRD) method is the most widely used general-purpose technique for measuring residual stresses in materials. It is convenient to use, has standardized procedures, and has good accuracy and reliability. The test procedure involves no damage to the specimen because of its non-destructive method. A further consideration is a balance between measurement accuracy and spatial resolution.

Figure 13 summarises several of the methods in terms of their spatial resolution and the penetration with their ability to make residual stress measurements deep within a specimen. Several factors need to be carefully considered and balanced to choose a residual stress measurement method for a given application. Appendix A shows more details about the non-destructive technique. Table 2 shows the summary of investigation residual stresses with different welding processes and different measurements technique.

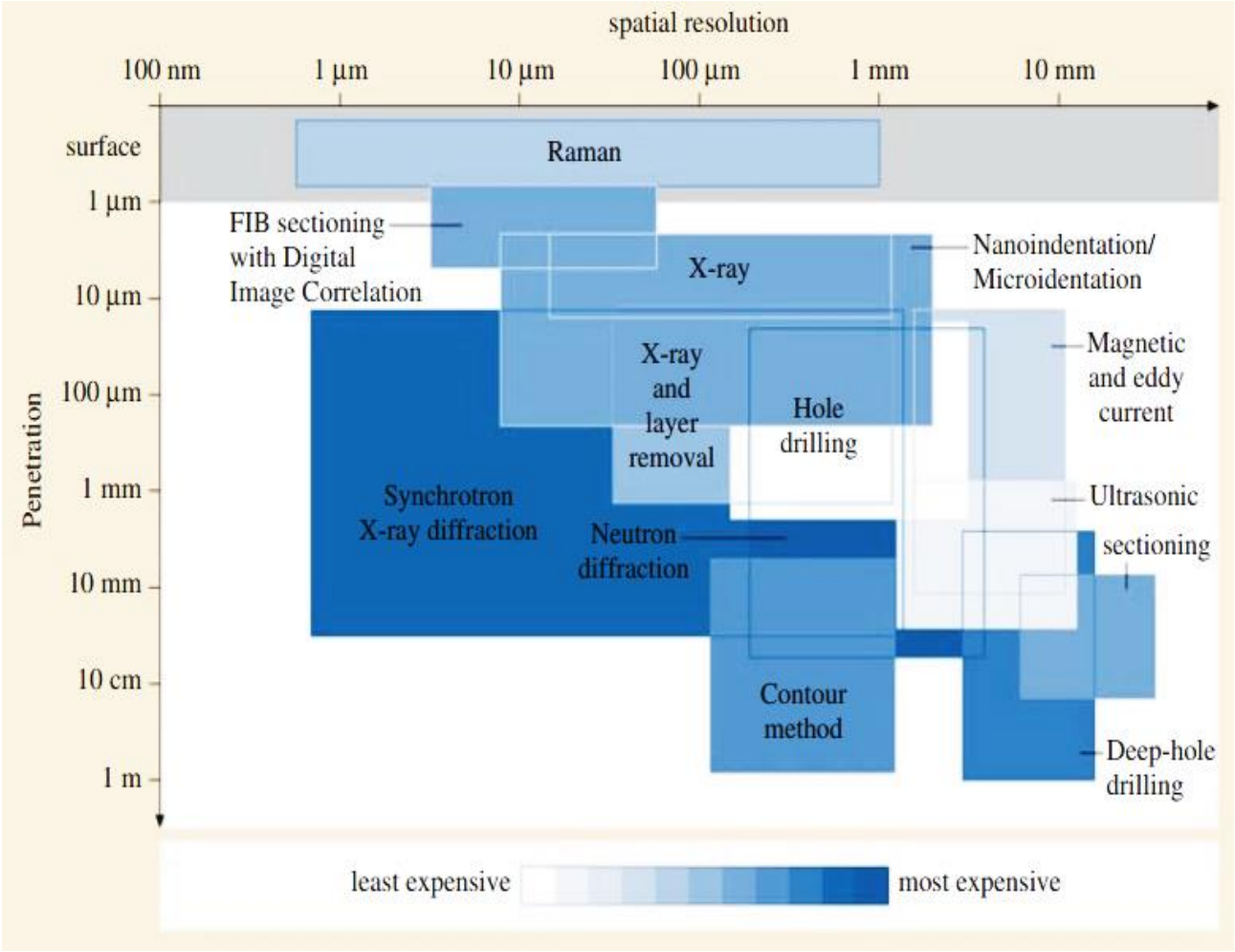

Figure 13. Shows the penetration and spatial resolution [11]

Table 2. Summary of experimental investigations carried out for determining the residual stresses in a pipe weld

Pipe diameter (mm)	Thickness (mm)	Welding Process	Heat Input KJ./mm	Max. RS, MPa	Measurement techniques	References
274	5	MMAW	-	486	ND	M. Law [44]
128.3	6	Manual GTAW	1.06	-	XRD	C.C. Silva [29]
508	25	PGMAW	0.77	250	ND	T. Neeraj [45]
406	19	PGMAW/GMAW	0.37	435	Hole Drilling	Y.-H. Zhang [46]
508	22	PGMAW/GMAW	0.33	600	Hole Drilling	Y.-H. Zhang [47]
1067	24	MMAW	1.2	348	ND	T. L. Teng [48]
1067	30	FCAW	1.2	321	ND	T. L. Teng [49]
100.5	7	MAGW	0.86	240	XRD,ND	N. Hempel [50]
355.6	19	PGMAW	0.5	204	ND	Y. Ren [51]
273	18	GMAW	Low	250	ND	E. Eren [52]
323	24	PGMAW,FCAW	0.4	590	Hole Drilling	A.Mirzaee-Sisan [53]
323	24	PGMAW, FCAW	0.4	400	Hole Drilling	A.Mirzaee-Sisan [54]

2.12 Significance of Finite Element Simulation of Arc Welding

FEM has been the critical link between theoretical mathematic and its application in science and technology for many years. Several numerical approaches exist to provide a sufficiently accurate approximation of the often quite complex problem of simulating the arc welding process, as the technique poses difficult issues to the design community. A considerable number of experimental trials are often necessary to get more data on welding-related problems. For these reasons, numerical simulation, or here the finite element method (computational modelling), has much to offer in the welded structure, mainly if the modelling strategies can predict the residual stresses in welding pipe at the different design stages. Different design configurations, material thickness, and different welding processes can be investigated in a virtual welding environment to avoid trial and error at the real welding stages.

Numerical simulation with the calculation of the thermophysical cycle and elastic-plastic strain-stress has been hampered by the complexity of welding geometry, the material properties and boundary conditions. With exponential power growth of capacities of the computers and the improvements in numerical simulation and geometric modelling, the development of the computational model such as MSC Marc software as an alternative to experiments has become more common in solving many industrial problems in pipelines, power plants and many others.

Numerical simulation models need a minimum amount of experiments for their developments and validations. The development of numerical simulation models will drastically reduce the number, time and cost of investigations. However, the value of experiments cannot be ignored. Some data for use in numerical simulation models can be obtained only by experiments. Hence, experiments and numerical simulation should be used together, where possible, to provide more knowledge about the welding problem. Of all numerical simulation models, FEM has been the most popular among the research of arc welding processes over the last few decades. FEM models are generally able to incorporate all characteristics of the material to be welded. These can include temperature dependency of material, complex shape, dissimilar joint material, filler material, or heat source moving.

Many researchers have used FEM as a numerical tool to investigate temperature distribution and residual stresses during the fusion welding process with different materials and welding pipe joints [55]–[59]. Numerical simulation of the welding process is very complicated due to the variation in temperature, thermophysical expansion and shrinkage and variation of material properties with time and space. Various researchers use software such as ANSYS, ABACUS, SYSWELD and WELDSIM. MSC Marc enhanced with user subroutines is a common choice for welding process simulation.

Numerical simulation of the welding process in the finite element method is carried out using thermo-mechanical analysis [60]. The computational process is generally split into two solution steps, such as thermophysical and mechanical analyses. The sequentially coupled thermo-mechanical analysis is used to simulate the welding process. Initially, the temperature distribution and its history in the welding model are computed. Further, the results of simulated thermophysical histories are given as an input in the successive mechanical evaluation of the residual stress field and distortion. After the creation of the FE model for the required study, the thermophysical analysis is carried out. The selection of element type, heat source model, temperature-dependent material properties and boundary conditions play a vital role in the study. The model is fine-tuned using experimental results. The model's output is used in subsequent mechanical analysis to evaluate residual stress [61] [62].

2.13 Risks and Failure in Welding of Pipe Steels

Researchers have investigated and studied failure phenomena in oil and gas pipe welding to discover their possible causes. The most common reasons for the failures are shown in Table 3.

Table 3. Pipe weld failure investigations with their causes of failure

The reason for the failure	Position	References
Corrosion	Weld metal	Majid et al., Majid and Mohsin [63]–[65]
Crack	Weld metal	Datta and Deva, [66]
Residual stress	Weld metal	Chapetti et al., [67]
Defects	Weld metal	Fazzini et al., 2005[68]
Hydrogen embrittlement	HAZ	Azevedo, [69]
Misalignment of inner and outer weld	HAZ	Fazzini et al., [70]
Thinning of the wall due to grinding of weld	Weld metal	Ahmed et al.,[71]
Mechanical damage	BM	Macdonald et al., [72]
Stress cracking	Surface Pipe	E. Sadeghi Meresht et al., [73]
Residual stress	HAZ	Al-Anezi et al., [74][75]
Residual stress	HAZ, BM	Ruibin Gou et al.,[76]

2.14 Finite Element Analysis and Simulation of Welding Residual Stress

During recent decades, many of the existing welding processes have been simulated by numerical methods, especially by the finite element method. The method is convenient and useful. A numerical simulation of a welding process is not easy because of the complexity of the welding process, which includes localized heating, the temperature dependence of material properties and moving heat source, etc., as it is a complex process involving the interaction of thermophysical, mechanical, electrical and metallurgical phenomena. There have been significant research activities on the FE simulation focusing on circumferential pipe welding and another. To confirm the finite element analysis method's accuracy, a verification experiment procedure was carried out in different studies. Besides the simulation approaches and assumptions, the accuracy of predicted residual stress (or strain) results depends on the precision of the defined heat source model, temperature, and phase transformation, which is dependent on material properties. However, most researchers have employed the rotational symmetry condition (axisymmetric condition) to reduce computational power requirements and time.

In contrast to these studies, interactions between the weld zone and the overall welded structures can also be studied, and in these cases complications arise from the elastic coupling between the weld zone and the base metal (BM). Some main topics include thermophysical stresses in welds; finite element models for welding processes analysis, thermo-elastoplastic analysis, transformation plasticity, thermo-metallurgical modelling, study of the solid-fluid transition zone; new material laws; microstructural and macrostructural analysis, computational aspects of welding processes, element library and modelling; welding of large structures; weld analysis for long welds; reliability analysis; and 2-D and 3-D model simulations [67].

Two stages can characterise the simulation of arc welding: tailoring the shape of the fusion zone (melting) and simulating the solidification process within the prescribed shape. Recent research work has been done on the analysis or simulation of the following welding processes. [29], [41], [52]–[54], [98], [122], [125]–[129], [44], [130]–[139], [45], [140]–[149], [46], [150], [47]–[51][151].

2.15 Prediction and Validation of Welding Models

Most researchers measured the thermophysical cycles at different locations on inner or outer surfaces using a thermocouple to verify the thermophysical simulation cycles and compare them with the finite element model. Another method used by some other researchers was preparing macrographs of cross-sections of the weldment to make sure that the welding pool's geometric appearance matches the geometric dimensions of the weld macrograph. Some authors have no experimental validation (e.g. [1], [7], [155]–[159], [9], [14], [18], [19], [21], [152]–[154]), and most authors who do use validation use data from thermocouples to validate the model. Experimental validation is necessary, and authors such as Zubairuddin et al. [160] used a thermocouple to measure the thermophysical cycle and predicted near the fusion zone are compared with experimentally measured thermophysical processes using SYSWELD software.3-D mesh model used to analyze residual stress and distortion in GTA welding steel. Murugan et al. [56] measured temperature distribution in stainless steel welded using thermocouples. The results showed that the temperature distributions are dependent on welding conditions. Venkata et al. [161] predicted the thermophysical history and the residual stresses and verified with the measured thermocouple recordings and the stresses, respectively. Deng and Murakawa [162] experimentally obtained temperature distributions in butt-welded pipe joints using thermocouples and compared them with numerical simulations. According to their results, it is clear that the temperature distribution around the heat source is very steady when the welding torch moves around the pipe. In another work, Deng and Murakawa [163] measured the temperature cycles and residual stresses in steel pipes incorporating solid-state phase transformation and validated welding simulation for dissimilar materials of pipes. Kermanpur et al. [164] studied the temperature cycles due to different welding sequences and welded pipes' parameters. The result showed that the volumetric heat source provides the best results for temperature cycles throughout the pipe. Kasuyaet al. [165] suggested an analytical heat conduction model for predicting temperature histories of multi-pass welding and verified the model with experimental results using thermocouples. Chukkan et al. [166] used the ultrasonic technique for measuring the residual stresses and validated the model predictions using three different position thermocouples from the weld centreline, as shown in Figure 13.

Thermocouples are measured peak values as 489, 285 and 232 °C at 4, 7 and 9 mm away from the weld centreline, respectively. The result showed disagreement between peak temperatures and FEM, which they attributed to assumed constants in the model and artificially increased thermophysical conductivity instead of considering convective heat transfer.

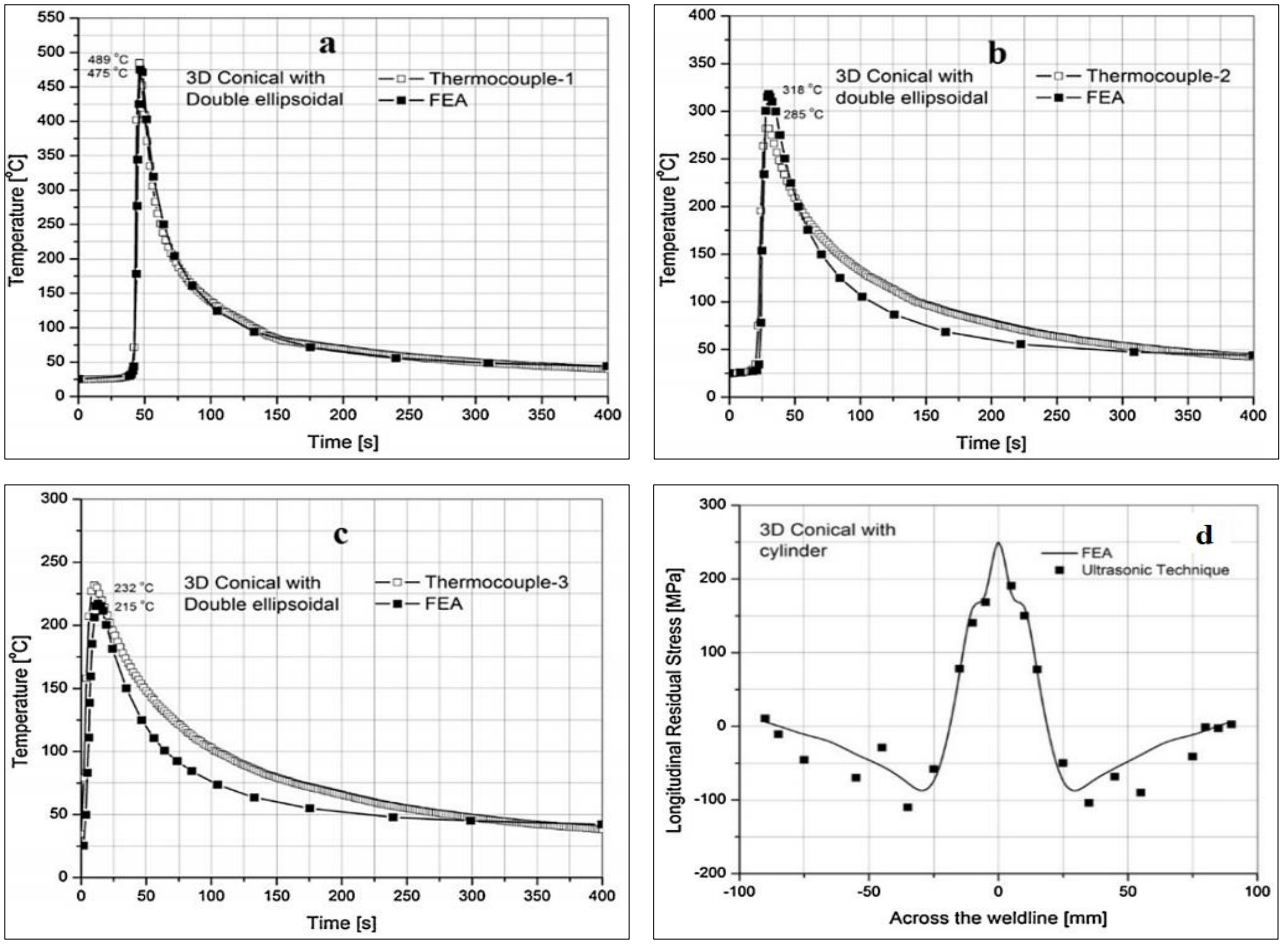

Figure 14. Thermophysical cycle comparison between measurement and FEM (a) thermocouple 1, (b) thermocouple 2, (c) thermocouple 3, (d) Comparison of longitudinal residual stresses from FEM with ultrasonic technique [166]

Pamnani et al. [19] simulated thermophysical cycles validated by thermocouple measurements at specified locations during SMAW multipass welding and autogenous double-sided welding using the GTAW process. For double-sided GTAW, both passes being symmetrical, thermocouples were used to measure temperature profiles for the second pass only. For multi-pass SMAW, with limited storage capacity for thermocouple data, the time duration between changing of electrodes and removal of slag was not logged. The simulated residual stress profiles were validated by non-destructive testing.

Aarbogh et al. [167] performed a numerical distortion analysis on austenitic stainless steels. The heat source calibration was not based on an experiment and explained the inaccuracy of using

thermocouple measurement. Attarha and Far [168] analysed similar and dissimilar plate welding by numerical modelling, validated experimentally using thermocouples. They suggested that the measurements using thermocouples should be treated with caution, as accurate measurements are not given if any junctions are present along with the thermocouple.

As shown in the literature, thermocouples are widely used by various researchers for the measurement of the temperature distribution during the welding process. Bulk residual stress measurements and the model predictions did not correlate well in some previous studies. This work addresses the mentioned gap. The model prediction was validated using the hardness test measurement and the nominal residual stress was validated by XRD in the next section. Since the thermocouple, which was used to monitor the temperature history of locations near the welding zone during the welding, was unstable for the rapidly changing temperature, a modified procedure of validation based on the new method is developed in this study. Although thermocouples can be reliable, as mentioned in different studies, temperature measurement errors can occur for various reasons when using thermocouples. For example:

- The change in the temperature during welding is speedy. The inherent slow and low spatial response of thermocouples represents a significant problem [169];
- Choosing the wrong type of thermocouple is a common error. Each has a different range, accuracy, and electrical output. Some error in thermocouple accuracy is unavoidable such as inherent variations in alloys or temperature variations around the reference junction connection. Because a thermocouple measures temperature differentials, any temperature fluctuations result in an erroneous temperature reading;
- The thermocouple should be grounded at only one location. This is likely to generate electromagnetic fields, which can lead to radio-frequency-interference-related problems that can impact measurement accuracy;
- Finally, the age of thermocouples measurements is drift with time. It cannot be predicted. The only solution is to periodically replace the thermocouple based on how long the user used it.

2.16 Prediction of Welding Residual Stresses: Phase Transformation Effects

Phase transformations occur when metal is heated or during cooling from an elevated temperature. Figure 15 (a) shows the iron-carbon phase diagram that describes the iron-carbon system of alloys containing up to 6.67% of carbon. It discloses the phase's compositions and their transformations occurring with the alloys during their cooling or heating. The phase transformation's main products are ferrite, pearlite, bainite, and martensite, and the transformation

process depends on the cooling conditions. When a base metal is heated above a lower critical temperature A1, its body-centred cubic (BCC) structure transforms into a face-centred cubic (FCC) structure, and the volume decreases. Temperature, pearlite or ferrite partly transforms into austenite. When the temperature is higher than the upper critical temperature A3, pearlite–ferrite completely changes into austenite, as shown in Figure 15(b). During rapid cooling, the austenite with FCC structure changes to martensite with a body-centred tetragonal (BCT) structure, and the volume increases.

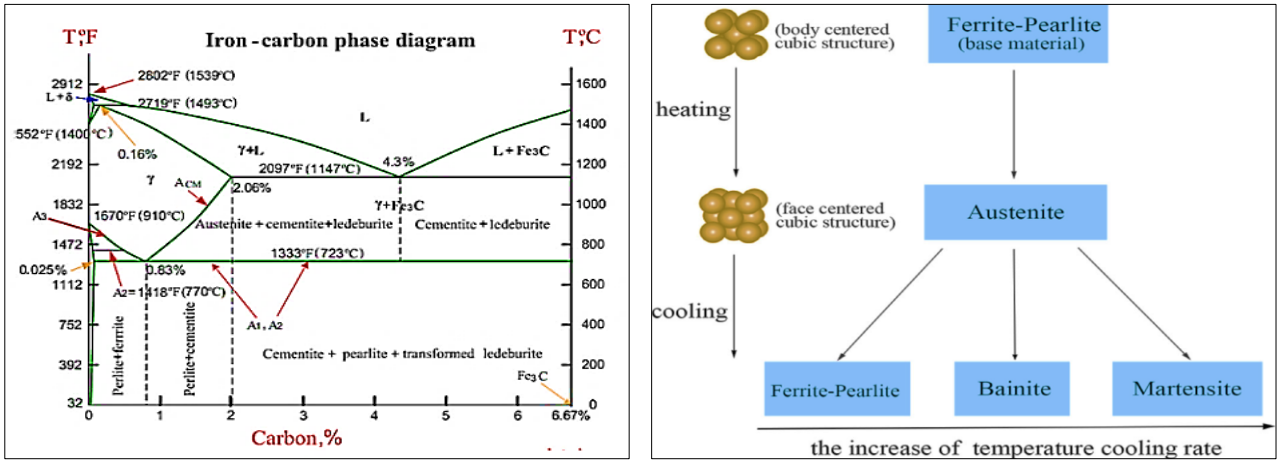

Figure 15 (a) Iron-carbon phase diagram (b) Transformation diagram related to the heating and cooling processes [137]

Keinänen et al. [170] studied the residual stress state after a weld repair using ABAQUS software and experimental measurements of residual stresses using the hole-drilling technique. Still, the material database used by the authors did not take phase transformation into account. Kimet et al. measured and simulated the residual stresses distribution for two welded plates using ABAQUS, phase transformation in the material was not considered in the material base. Yagi et al.[171] calculated residual stresses for a thick cylinder using ABAQUS, and phase transformation was neglected. Prasad and Sankaranarayanan [112] developed 2-D plane stress model of the arc welding of a steel plate without taking into account any phase transformation effects. Xia et al.[172] reported the welding simulation of residual stresses on butt welding on different thicknesses of austenitic stainless steel; however, their models analysis did not consider the effect of austenite transformation on stress states. Tall [173] used an analytical method for the calculation of residual stresses in welded plates, and did not consider the effect of phase transformation except for the anomalous linear expansion coefficient behaviour due to the change in the constitution of steel from phase and to another phase transformation. Because of this simplification, the method produced results which are totally different from the experimental data. In contrast, it gives good results when

single-phase materials are considered (i.e. stainless steels, aluminium alloys). Sarkani et al. [108] compared the residual stress fields computed by 3-D models with those computed by 2-D models for mild steel and found good correlation (for the in-plane stresses) but without taking into account phase transformations. Cai et al. [174] studied the residual stresses in flash-butt joints of steel. However, only the austenite-pearlite and austenite-martensite transformations were employed in the cooling transformation analysis [175]. Zubairuddin et al. [176] executed an FE analysis on thin steel welded plate for residual stress and distortions on ABAQUS without considering the effect of phase transformation effect phenomenon and later conducted an experiment and thermo-mechanical analysis of preheating effect on the same plate [177]. Based on their calculations, single-pass was used to investigate the welding residual stresses. It is also clearly seen that there were limited references to the finite element model considering phase transformation effects for welding; most of the studies were focused on similar and with one-pass weld joints. However, the influence of phase transformations remains a problem that is still wide open. To the best of our knowledge; there are no simulations to date (2-D and 3-D) or experimental works exploring phase transformation during dissimilar material with multi-pass weld and different thickness of pipe weld joint and its effects on the residual stresses, though these factors are very important for the residual stress value and its distribution.

2.17 Numerical Simulation of Residual Stress and Comparison with Experimental Measurements

Akbari and Sattari-Far [4] employed the FEM and the hole-drilling method to investigate residual stress. The principle of stress was calculated. The result showed axial stress (σ_x) and hoop stress ($\sigma\phi$) in the inner and outer surfaces and compared FEM results with those from the hole-drilling method. The residual stresses were measured at the surface using a destructive method (hole-drilling method).

Colegrove et al. [178] compared the residual stresses between the model and experimental predictions and reported the residual stresses were divided into three groups, the first explained with the experimental work; the second seeks to understand the experiments with a simple model that predicts the residual stress and finally compares these residual stress investigations with residual stress measurements by neutron diffraction.

Zeinoddini et al. [179] reported on the residual stress results obtained from the repetition of repair welding in the heat affect zone and near the weld centerline. They found an increase in the residual stress distribution in single/double and full/partial repairs. The residual stress was measured by

sectioning and whole drilling methods in repair welds after removing inspected defects due to welding. Limitations of both the hole drilling method and sectioning are the destruction of the specimen and lower accuracy.

Wen et al. [180] residual stresses from the forming processes may play an important key in predicting geometrical distortion. They analysed and investigated the residual stress distributions and modelled the heat transfer phenomena during multi-wire SAW using (ABAQUS) 2-D & 3-D analysis residual stresses numerically and hole drilling method experimentally.

Jang et al. [181] evaluated the distribution of welding residual stresses in API X65 pipeline weldments. They found residual stress distribution by applying a magnetic Barkhausen noise method (MBN) with a HAZ-based calibration approach. Presence of compressive residual stresses in the coarse-grained heat-affected zone, the maximum tensile residual stress found at the WLC**.**

Mochizuki et al. [182]used inherent strain analysis and thermophysical elastic-plastic analysis to predict residual stress in carbon steel pipe, and they verified their numerical models using neutron diffraction measurement.

Yan et al. [183] investigated the effect of the welding approach on residual stresses. Compared to the simultaneous welding sequence, the sequential welding sequence induced lower residual stresses and distortions. The welded joint of pipeline steel was simulated using ABAQUS software. It is found that magnitude residual stress occurs strongly in the HAZ. It has been observed as a magnitude gradient in the welding region. In this study, no residual stress measurement was mentioned.

Khalid et al. [184] studied the destructive hole drilling experimental technique for analysing the stresses in the spiral welded pipe (SWP). The distribution of residual stresses is calculated in two parts: first, through the uniform method, power series method and integral method, and the second part of this work consist of finite element modelling. The power series method gave smooth linear variation along with depth as compared to the integral method. Residual hoop stresses (tensile) were calculated at the inner and outer sides of the pipe. This was compressive close to the weld zone. Residual stresses were measured at different locations using the uniform, power and integral method and hole drilling method.

Houman et al. [185] employed the finite element simulation and neutron diffraction measurements for high strength low alloy (HSLA) steels and found an interrelationship between residual stress and microstructure in multi-pass welds. The cooling rate can change the result of residual stress. Residual stress was measured in different samples with different effects of heat input and distance from the weld centreline.

Sowards et al. 2015 [186] studied the residual stresses values in different directions in a friction stir weld of API 5L X80. The highest level of residual stress was found in the longitudinal direction of the weld. Residual stresses were relatively low compared to the yield strength of the stir zone and base metal as a result of the lower peak temperatures of the friction-stir welding process as compared to fusion welding.

Neutron diffraction was used to measure residual stress. A two-pass butt weld configuration was used to join two plates together with the friction stir welding process by Brown et al.[129]. Obeid et al. [23] studied the effect of six parametric thermophysical fields and residual stress in pipe weld to examine and appraise the influence of welding properties such as heat input on the thermophysical and residual stress fields. The measurements for residual stress were obtained using a strain gauge experimentally. The weld overlay leads to reduce the axial and hoop residual stresses at the FZ. The results obtained from numerical analysis using ABAQUS and are compared with the experimental results.

Some researchers have used XRD but only with similar materials. For instance, Silva et al. [29] presented residual stress measured on the external surface of a manually welded plate using X-ray diffraction. The residual stresses (compressive and tensile) were calculated. The residual stress profiles for the four samples with similar material were analysed for the compressive residual stresses and tensile stresses in the weld region (FZ and HAZ). The maximum stress was found in the HAZ.

Ruibin et al. [76] measured residual stress in the axial and hoop directions of the pipeline with similar material by X-ray diffraction or by the full-width methods at half maximum (FWHM) were measured. All measurements were conducted using the X-ray diffraction method before the pipeline was put into service. High WRS generally occurred in the weld seam and the HAZ.

In Hempel et al. [133], the residual stress state in girth-welded steel pipes was thoroughly investigated using both X-ray and neutron diffraction. The magnitude and direction of load stress and residual stress both lead to significant residual stress relaxation. The axial compressive stresses balance the axial tensile stresses on the FZ and HAZ's inner surface of girth welding on the outer surface. The results are shown for neutron diffraction measurements mostly agree well with the X-ray measurements on the surface. Pipes with similar materials were used in this study. Another research showed the predicted stresses even in similar welds are sensitive to the numerical modelling assumptions and boundary conditions [175].

Kolikov et al. [187] investigated the residual stress distribution in the welded pipe with similar material. Residual stress, which also depends on cooling rate, exists in the material after welded pipe manufacture. The residual stresses may cause the weld to fail prematurely. Axial and tangential

tensile stresses were present on the surface of the pipe. This tensile stress prediction and analysis are essential in predicting a pipe's lifetime and application scope, as shown by the authors in the paper.

Costa et al. [188] evaluated residual stress results by XRD, and hole drilling was used in residual stress measurement techniques. The values of maximum and minimum residual stresses were located in the FZ and HAZ. High-tension values were obtained for the residual stresses in the weld. The high-stress gradient at the surface affects the distortion and fatigue life of structures.

2.18 Numerical Simulation of Residual Stresses Using 2-D and 3-D Models

Prediction and measurement of residual stresses are not easy tasks because of the complexity of interaction between the many factors associated with pipe welding. Researchers and the welding industry accept this challenge and work in this area with full enthusiasm and make a continuous effort to come up with better solutions to new problems. Current developments in residual stress assessing methods for pipe welds demand more steps from researchers.

Andersson et al. [189] determined the residual stresses distribution in welding's inner and outer surfaces during butt SAW processes using a 2-D model. Subsequently, Nodeh et al. [190] employed FEM 2-D model predictions that captured the characteristic through the thickness weld zone and residual stress profiles measured by XRD. In Yaghi et al. [191] two parts of the steel pipe were joined together, and a 2-D finite element model based on the ABAQUS software was used to simulate welding. Ueda and Yamakawa [122] used 2-D finite element analysis (FEA) to analyse the residual stresses. They examined the effect of geometry configuration on residual stress in HAZ and compared the results with X-ray diffraction measurement. Brickstad and Josefon [128] used a 2-D axisymmetric model to simulate welding of stainless steel pipe up to 40 mm thickness. Deng and Murakawa [61] used a 2-D model to simulate residual stresses, and their reason for using 2-D was the high computational cost of 3-D models. Duranton et al. [192] highlighted that the 2-D model approach in longitudinal welding when the heat flux in the direction of the weld is ignored. Paolo et al. [193] compared residual stresses coming from a 2-D and 3-D model. It was attributed to the limitation of 2-D models to assess the residual stress field induced by welding processes correctly. Li et al. [194] developed a 2-D model for the prediction of temperature and stress distribution for in-service welding of pipe welded by manual metal arc welding. It was reported that the peak value of the transverse residual stress was higher. Wen et al. [195] also used a 2-D axisymmetric finite element (FE) model to simulate three-pass pipe girth welding with a wall thickness of 19 mm. However, none of the above works has used a fully 3D model for simulation and compared results with those of experimental pipe welding.

In 3-D simulations, various authors have tried to build a 3-D model to calculate the residual stresses and compare them with 2-D results, but still, 3-D needs reliable measurement techniques and more accurate to check the 3-D model able to calculate residual stresses. Some researchers calculated 2-D and 3-D without measurement validation or comparison. Most researchers measured residual stresses in only one position and ignored and compared the date with 2-D and 3-D, but still, investigations in other positions in circumferential welding are missing. We suggest that more experimental residual stress measurements on dissimilar pipe weldments are needed to verify the 3-D model.

Wu et al. [196] used 3-D modelling with a single pass to simulate the residual stresses on the outer and inner surface of pipe welds. The model is validated with experiment measurement using the hole drilling method. Akbari and Sattari-Far [4] used FEM to evaluate the thermo-mechanical behaviour and residual stresses in pipe welded. It was used to analyse the effects of heat input from the welding on residual stresses in pipe welds. It was reported that the welding heat input had an essential impact on residual stresses in the stainless steel side of the joints. Jiang et al. [197] used a 3-D model to predict temperature distributions in a multi-pass welded piping branch junction. However, welding residual stresses were not investigated in their research.

Duranton et al. [192] used a 3-D finite element model to simulate the welding of a stainless steel pipe. The numerical studies were carried out in SYSWELD software. The heat input was modelled by a semi-ellipsoid model. The adaptive meshing technique was used to carry out transient thermophysical analysis for the prediction of thermophysical histories. It was reported that the adaptive meshing technique highly reduced the computational time. Varma et al. [198] studied the effects of weld parameters on residual stress developed during welding of pipes. Welding was simulated, and effects of welding current and pipe thickness on residual stress were found. Feulvarch et al. [199] computed residual stress in multipass pipe welds.

A full 3-D analysis is shown to be required to predict residual stress in multi-pass circular welds, while a 2-D axisymmetric analysis is justified for a few initial welds passes only. Suman et al. [200] performed 3-D thermophysical-mechanical analysis in and around the weld areas and, subsequently, an elastic stress analysis of the entire structure by imposing the local plastic strains as boundary conditions. A significant reduction in the computational demand with very little loss in accuracy in prediction is reported. Yaghi et al. [201] [202] calculated residual stresses during welding of steel

pipes and stress-relieving during post-weld heat treatment (PWHT). Results showed a significant reduction in the residual hoop and axial stresses after PWHT.

Deng et al. [203] presented 3-D results and compared them with 2-D finite element model to predict residual stresses in welded stainless steel pipes. Dar et al. [204] developed residual stress using a 3-D model in GTA circumferential welded thin-walled cylinders. Abid et al. [205][206][207] used 3-D FE models to investigate the effect of weld zone and root gap on residual stresses in a pipe-flange joint. Deng et al. [163], [208], [209] developed a 3-D finite element approach to investigating the residual stress distribution in welding pipe. Referring to their results, it is shown that the results of 3-D finite element models provide acceptable agreement with experimental measurements, but some types of measurements are still needed to verify 3-D models. Lee and Chang [20], [55], [210]–[212] simulated residual stress distributions in a pipe model considering the 3-D effect, but the study gives little information on residual stress distribution near the weld start/stop location.

Table 4 shows the summary of pipe weld simulation studied by different researchers. However, there is very limited literature describing the prediction and measurement of welding in dissimilar material pipe welded structures, especially for multi-pass welded structures whose pipes are of different thicknesses. It is necessary to continue to carry out experiments to verify the numerical models for a multi-pass welded steel pipe. In addition, it is also necessary to compare the simulated results of a 3-D model with those of a 2-D model to confirm that the 3-D model can capture residual stress distribution in detail during multi-pass welding processes with different seam welding positions.

In the present study, based on the MARC software, a 2-D model is developed to simulate the welding residual stress fields in the pipe weld at first. Based on the characteristics of the temperature fields and the residual stress fields, a 3-D model is also created to calculate the welding residual stresses. Moreover, experiments are also carried out to verify the effectiveness of the proposed computational procedures from both 2-D and 3-D in more than one location. Previous studies, both numerical and experimental, focused exclusively on the start and stop weld location.

Table 4. Summary of pipe weld simulation studies carried out for residual stresses

Aim	Material	Finding	Author
Measurement of residual stresses in welds using Destructive technique sectioning and hole drilling methods	API 5L X52 steel (similar material)	Increased the magnitude residual stress distribution found in full and partial repairs	Zeinoddini et al. 2013 [179]
Investigate the effect of the welding approach on residual stresses	AISI316L stainless steel (similar material)	welding sequence induced less residual Stresses and distortions.	Yan et al. 2014 [213]
Using 2-D and 3-D FEM for predicting thermophysical cycle and residual stress distribution	API X65 steel (similar material)	The 2-D result compared with the 3-D model	Nezamdost et al. 2016 [214]
Investigate residual stresses and intimal temperature method	X70 strength (similar material)	Proposed the method for assessing the service life of welds	Kurkin and Ponomareva 2012 [215]
Using hole drilling experimental technique for analysing the stresses in the pipe and to simulate residual stresses through the uniform method, power series method and integral method	API 5L X70 high grade steel (similar material)	The power series method gave advantage of smooth linear variation along with depth as compared with another method. Residual stresses were found at the inner and outer surface and were compressive around the weld zone	Nasim et al. 2015 [184]
Investigated residual stresses	(API 5L grade X70) (similar material)	Low heat input in HAZ caused a high level of residual stresses	Alipooramirabad et al. 2016 [185]
Value of residual stresses in different directions in a friction stir weld	X70 pipeline steel (similar material)	The highest magnitude of residual stress was found in the y-direction of the weld	Sowards et al. 2015 [186]

2.19 Prediction of Welding Residual Stresses: Preheating Effects

Traditionally, a manufacturer required time-consuming trial and error methods for the development of methods to control welding parameters, such as preheating to obtain a good welded joint with reducing detrimental residual stress. In contrast, numerical simulation for the prediction of stress distribution is relatively quick and low cost and accurate if compared with reliable measurements, although usually it is still limited to simple geometries with several assumptions.

For these reasons, numerical simulation seems to be a valuable option. Many researchers have tried to estimate the effect of preheating temperatures on residual stress behaviour. Charkhi et al. investigated the residual stresses of single-pass similar material pipe welded joints and the effect of the preheating of the sample on the magnitude and distribution of the residual stress by using numerical simulation and hole drilling measurements. Hsiang and Liang [6] compared the residual stresses of single-pass plate welded joints by using numerical and hole drilling methods. They also studied the effect of preheating of the sample on the magnitude and distribution of the residual stress. The influence of preheating and inter-pass temperature on welding-induced residual stresses was investigated in similar material weld by Heinze et al. [28]. Teng and Lin [49] discussed the changes in residual stress magnitude due to different preheating temperatures in steel plates. Also, Fu et al. [216] employed a 2-D numerical model for investigating preheating temperatures on cooling time, the temperature field and residual stresses. In the studies mentioned above, it is important to note that the authors used similar material of pipe weld and non-destructive method as well. Asadi et al. [217] investigated the effects of base material and preheating temperature on the pipe's inner and outer surface stresses. The stress magnitude is reduced by raising the preheating temperature but with more intensity in the pipe's inner surface. Zubairuddin et al. [177] executed FE analysis on single thin pass steel welded plate for residual stress and distortions on ABAQUS. They conducted the experiment and thermo-mechanical study of preheating effect on a similar material plate. They found the preheating procedure before welding can significantly reduce welding distortions. Fu et al. [218] investigated the preheat temperature during the welding process in a T-joint welded structure, finding that preheating during welding significantly reduces deformations, while its influence on the longitudinal and tensile residual stresses is much smaller. Influences of different preheat temperatures and the inter-pass time on the longitudinal residual stress fields and structure deflections were also investigated. In the frame of the numerical investigations, two thermo-mechanical finite element models in a T-joint welded structure were analysed by Peric et al. [219]. Zhang et al. [220] introduced a multi-beam preheating method in a thin plate to reduce structure deformation. They concluded that a multi-beam preheating method could successfully reduce the compressive stress in the welding area. In Sepe et al. [221], a coupled thermo-mechanical non-linear transient analysis was performed to determine the influence of preheating treatment both on temperature and residual stress distribution in welding. A finite element model was used to evaluate temperature and residual stress distribution in single-pass butt weld joints. Weld residual stress was found to decrease with increasing preheating temperature in Fallahi et al. [222]. Suman et al. [223] employed a 3-D numerical model plate for investigating preheating temperatures, as shown in Figure 16, and observed that preheating effectively reduced the edge

deflection and angular deformation values and exhibited a favourable effect on longitudinal residual stress distribution by reducing the values.

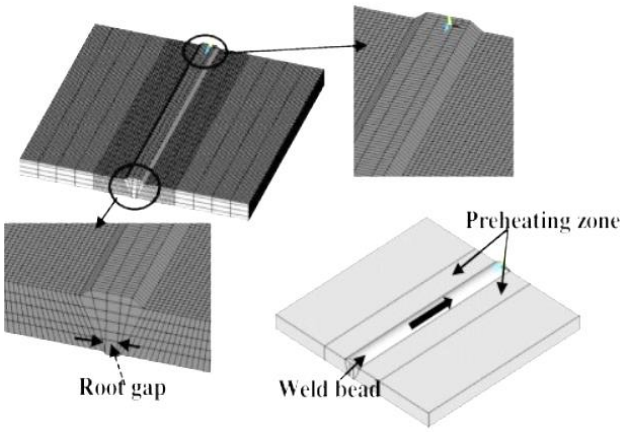

Figure 16. Modelling and meshing of single pass square butt weld joint

Most studies are confined to single-pass welding for thick pipes or plates; very few studies were found on the effect of preheating on multi-pass pipe welds. Studies show that preheating can have a significant effect on the residual stress in the welded samples. In spite of that, the effect of the pre-heating parameter on the magnitude and distribution of residual stresses of the dissimilar pipe welding has been the focus of very limited research so far. So, in this present study, the effects of preheating in the modification of the residual stresses in the internal and external surfaces meshed models pipe welding are investigated.

2.20 Effect of Welding Conditions on Residual Stresses

Weld quality is influenced by various welding parameters such as heat input, welding current, voltage, and welding speed. In the last decade, and regarding the researchers who worked on welding in different fields, further studies are required to evaluate residual stresses of the weldment, particularly under different welding conditions. Some welding conditions or parameters that are used before and during welding can also play an important role in increase or decrease welding residual stress. Researchers have studied the effects of some of the mentioned parameters on the welding temperature history. Choi and Mazumder [224] analysed the solidification and the residual stresses in plate welding. They found that residual stresses in plate welding increase with the increase in welding speed. Ranjbarnodeh et al. (2011) [225]studied the relation between the heat input and residual stresses. The result shows an increase in heat input with increased current, and keeping the weld travel speed constant in welding plate lead to reduce the residual stresses. Teng and Lin 1998 [49] investigated the effects of welding speed, plate size and mechanical constraint on

residual stresses. They predicted the residual stresses during one-pass arc welding in a steel plate. Hsiang and Liang [6] investigated the residual stresses of welded joints using numerical and experimental methods. They also studied the effects of the weld velocity and size of the sample on the magnitude and distribution of the residual stress. Results of their work show that the tensile longitudinal and transverse stresses were created near the welding line. Xu and Wang [226] estimated the residual stress and used 2-D axisymmetric thermophysical and mechanical models to investigate the effects of the tubes and heat input gap. They found that the highest residual stress takes place in the base metal far away from the weld zone. Sattari-Far and Farahani [4] studied a 3-D FEM of welding residual stresses in similar steel pipes to investigate the effects of the weld groove shape. Abid et al. [205] presented a three-dimensional sequentially coupled non-linear transient thermo-mechanical analysis to investigate the effect of tack weld positions in single-pass MIG welding for a single 'V' butt-weld joint and root gap on welding distortions. Jang et al. [227] investigated the effects of root opening on mechanical properties, preheating and welding deformation. Obeid et al. [228] proposed models based on the ABAQUS and studied the effects of different parameters, including girth welding materials, geometric parameters, and heat input on the thermophysical and residual stress fields.

So far, few researchers have focused on some of the effects of welding parameters on residual stresses in multi-pass dissimilar material pipe welds in arc welding operations, and several effects have been neglected. It is also not clear whether or not the preheating temperature, root gap pipes, and heat input include the current and voltage have an effect on residual stress. This present work aims to provide a basis for optimizing multi-pass welding for dissimilar materials numerically. Estimating the residual stress of welded joints can be complex, costly and time-consuming, owing to the complex joint geometry, the number of stress concentration points and the heterogeneous material properties. Although residual stresses of welded joints have been widely investigated, no complete study has considered the combined effects of all the important parameters on residual stresses.

2.21 Investigation of the Accuracy of Heat Source Models

Goldak's model et al. (1984) [229] proposed a non-axisymmetric three-dimensional heat source model called the double ellipsoidal model suited for simulating shallow and deep, wide and narrow fusion zones of conventional welding processes made by arc welding processes and deep penetration. The heat source model parameters have a significant effect on the temperature field and the residual stress field. Depending on the welding process, an adequate, accurate heat source model

must be defined for the numerical simulation. The model geometry is actualised after metal deposition and for a moving heat source according to the assumed welding speed for each time step.

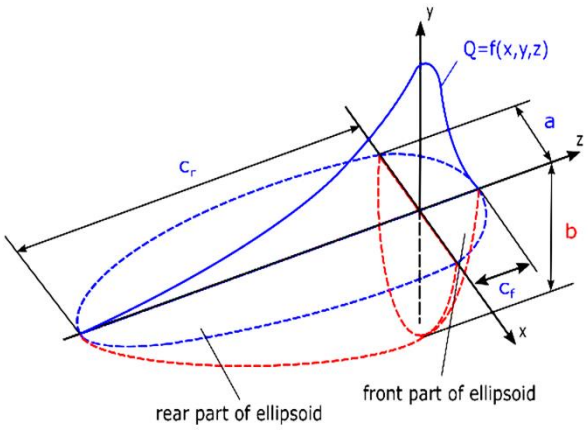

Figure 17. Goldak or double ellipsoidal heat source model distribution shape

Goldak's 1984 model [229] was used with the front and rear areas of the arc with dimensions, which were based on the observation of the weld bead and some approaches suggested by Wentz (2008) [230]. Therefore, Goldak's model became a welding heat source model, combining two half ellipses into an ellipsoid of the heat source distribution, as shown in Figure 17. The modified equations are

$$\boldsymbol{Q = \eta UI/v} \tag{3}$$

$$\boldsymbol{q_f(x,y,z) = \frac{6\sqrt{3}\, f_f Q}{abc_f \pi\sqrt{\pi}} e^{-3\left(\frac{x}{a}\right)^2} e^{-3\left(\frac{y}{b}\right)^2} e^{-3\left(\frac{z}{c}\right)^2}} \tag{4}$$

$$\boldsymbol{q_r(x,y,z) = \frac{6\sqrt{3}\, f_r Q}{abc_r \pi\sqrt{\pi}} e^{-3\left(\frac{x}{a}\right)^2} e^{-3\left(\frac{y}{b}\right)^2} e^{-3\left(\frac{z}{c}\right)^2}} \tag{5}$$

where x, y, and z are the coordinates of the Goldak's model double ellipsoid model, π is the fraction of heat deposited in the weld region, the heat input rate is calculated by welding operational parameters current (I), voltage (U) and η is the arc efficiency for the welding process, v is the welding speed of torch travel in mm/s, and t is the time in seconds. The factors f_f and f_r refer to the fraction of the heat deposited in the front and rear quadrant, respectively, which are presented as $f_f + f_r = 2$. The parameters a, b and c are the characteristics of the welding heat source. Goldak's model double ellipsoid model of the heat source model entirely deals with the weaknesses of the 2-D Gaussian distribution heat source model.

Gaussian heat source model is a more recent formulation in small thickness. Geometrically, it can be explained as a 2-D Gaussian distribution in the x-y plane that decays linearly in the z-axis (i.e., the penetration axis). It is, therefore, the linear decay along the penetration axis that sets this

model apart from Goldak's model ellipsoidal model. Figure 18 shows the Gaussian heat source model, in which heat flux distribution occurs according to the Gaussian curve

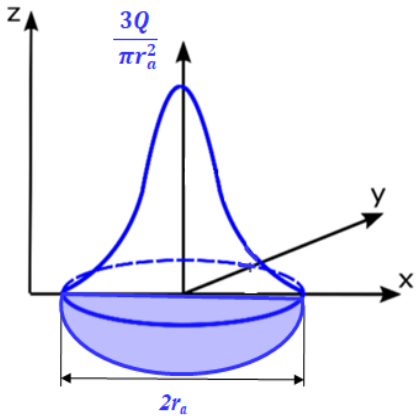

Figure 18. Gaussian heat source distribution shape

This model geometry is represented by several different formulations in the literature. The modified equations for Gaussian heat source distribution shape are

$$q(x,y) = \frac{3\,Q}{\pi r_a^2} e^{\left(\frac{-3r^2}{{r_a}^2}\right)} \tag{6}$$

It is generally used in numerical simulation of welding such as laser, electron beam and welding plasma arc welding. A lack of generalised solutions to the heat source model with arc welding of dissimilar pipes led to the investigation. The heat source models are constrained in specific geometries, and their general form is that two-dimensional Gaussian distribution is on the top surface but double heat source. The effective heat source models were presented and compared to the experimental results, but a computationally efficient and accurate comparison is not found in the literature. To more accurately simulate the shape of melt weld pool dimensions, modelling of heat source model is the vital component in the prediction of pipe welds induced temperature distribution and residual stress. Researchers should supply the width, height, forward, and rear length of the heat source shape. Therefore, the entire welding process is strongly influenced by the movement of heat, and simulation using numerical simulation analysis is crucial for obtaining accurate data. Depending on the welding processes and weld bead profiles, volumetric heat sources of double ellipsoidal [231] semi-spherical As known, a two-dimensional Gaussian intensity distribution [232] [233] and other approaches [198]–[207], [208]–[215], [191]–[197] have been used for conduction mode welding simulation. The movement of heat source through time and

space is the major characteristic of welding pipes. The 3-D conical model is a source used for the correct design of a welding simulation using a laser [235] or arc welding by high power density [256] as shown in Figure 19. From a parametric point of view, the model is determined by the power of the heat source, its radius, and the depth of penetration.

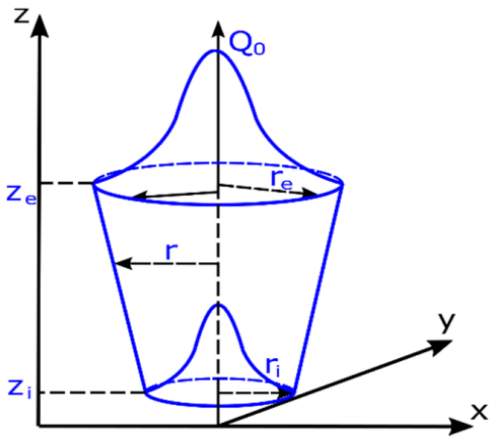

Figure 19. Conical heat source distribution shape

$$q(x,y,z) = q_o e\left(-\frac{x^2+y^2}{r_o^2(z)}\right) \tag{7}$$

$$r_o^2(z) = r_e + \frac{r_i - r_e}{z_i - z_e}(z - z_e) \tag{8}$$

Where q_0 is the heat flux density, r_e, r_i are the 3-D cone radius dimension parameters, and z_e, z_i are the 3-D cone length parameters. Different types of heat source models have been employed by researchers for their studies to accurate prediction of weld induced effects with different types of software. A heat source model for describing the temperature distribution on a thin moving sheet heated was developed by Brockmann et al. [236]. A 3-D finite element model using SYSWELD has been developed for simulating and predicting distortion welding of shipbuilding steel by Tsirkas et al. [257] result showed a good agreement between the simulated and measured. Jin and Li [235] proposed a cylindrical surface heat source for full penetration welding. Hashemzadeh et al. [254] investigated the effect of three different heat sources in a 3-D finite element model on an elastic-plastic analysis of welded plates, confirming that the double ellipsoidal heat source can provide a good agreement with the results Wu et al. [250] investigated a new heat source model for welding in numerical simulation of the temperature profile weld. The results showed that the melt lines predicting location and locus in the PAW weld cross-section are in good agreement with

experimental measurement. Bruna-Rosso et al. [245] implemented a semi-ellipsoid heat source model. Nguyen et al. [237] used an analytical solution to obtain the temperature field induced by a heat source distributed through a double ellipsoidal. Balasubramanian and Shanmugam [242] carried out finite element analysis using SYSWELD for simulating thermophysical cycles, weld pool dimensions, depth and width of penetration. Kazemi and Goldak's model [253] have proposed parametric design capabilities of the finite element code ANSYS to simulate full penetration welding. Siva et al. [248] employed a 3-D conical Gaussian heat source model for developing a finite element model to analyse the temperature distribution in a T-joint weld. Nélias et al. [234] employed the FE model ABAQUS using laser welding using conical heat source with Gaussian volumetric distribution. A sequentially coupled thermophysical and mechanical analysis has been carried out using SYSWELD to model TIG welding of AISI 316LN stainless steel by Ganesh et al. [255]. Several studies have been developed through numerical simulation models that correlate with heat source models. Basically, there are two possibilities commonly found and used in the international literature, as shown below. The most popular heat source model shape currently used in numerical simulation and analysis of welding processes is Goldak's model's double ellipsoidal heat source model (Figure 17). It is typically used for arc welding and was utilised for the weld pool's geometrical shape and the distribution of the moving heat source

The present study summarises and compares the heat source models commonly used by researchers in the literature. It is necessary to investigate appropriate good welding heat source models of welding simulations because the heat source will influence the geometries of melt pools to predict temperature distribution and thermophysical cycles accurately during welding. The combination of a double ellipsoidal heat source with a 3-D conical model was considered next to be incorporated in the numerical models, which provides the same geometric characteristics. Three different heat sources, including 3-D semi-spherical shape, 3-D double ellipsoidal and 3-D conical, were compared for carrying out the simulation utilising MSC Marc software.

2.22 Knowledge Gaps

The literature in the prediction of residual stresses has been reviewed. The significant research areas such as the finite element method (numerical simulation), heat source models, residual stress measurement techniques and phase transformation have been briefly discussed, and salient points are highlighted. The inferences and the research gap have also been identified and presented.

- **Validation of numerical simulation model using hardness testing**

It was concluded based on the literature review that the commonly used validation processes are limited almost exclusively to the thermocouple measurement technique. Residual stress measurements and the model predictions did not correlate well in some previous studies. This work addresses to find a viable approach for the validation of pipe welding with dissimilar metals.

- **Validation of numerical simulation model using XRD**

In spite of though experimental measurements of the residual weld stress are widely applied by researchers using destructive and non-destructive techniques, there are still limitations and inaccurate analysis of these residual so far. Because of its high accuracy and practicability, XRD was chosen as a non-destructive technique to measure residual welding stresses. X-ray diffraction equipment was provided with an ideal method for measuring these small areas without modifying the sample and possibly changing the stresses present. After that, we used the numerical simulation to develop and establish the FE model's reliability for the interpretation of residual stress in dissimilar weld joints. However, most of the research focused on deformations or residual stresses induced by welding in welded joints or structures whose thickness and pipe size are small. Limited research paid attention to the residual stress calculation behaviour in dissimilar materials of the welded structure. The experimental study of residual stresses distribution is very complex due to the 3-D stress state in the multi-pass welds. Experimental methods to determine residual stresses, such as non-destructive (XRD) or another technique, are not always suitable or practical, and are often insufficient for this purpose because they provide results only on the surface or near the specimen's surface. For this reason, numerical simulation 2-D and 3-D models were chosen, which allow for the investigation of residual stress distribution to depths of several centimetres with different angles of the weld circumferential due to highly accurate results for outer and inner surfaces.

- **Prediction of the effect of welding parameters on residual stresses**

There are very limited studies on characterising the effect of welding parameters on residual stresses in dissimilar pipe arc welded joints and the approach to reduce the residual stress such as heat input, groove shape, arc welding travel speed, specimen thickness, external mechanical constraints, phase transformation and preheating.

- **Investigation of the accuracy of heat source models**

Although there are many papers in the literature that used different types of heat source models, these studies are focused only on the two-dimensional model and mostly the Goldak model. The

Goldak model is generally agreed to be the most suitable for modelling arc welding; since arc welding is modelled at the highest rate, this model is used the most. A systematic study on the accuracy of these models such as the effect of heat source parameters, is missing and needs to be investigated.

2.23 Scientific Goals

The present work's need is to contribute to understanding finite element simulation of welding induced residual stresses in dissimilar welding pipe by manual metal arc welding (MMAW) process. Despite many research works that have been carried out about finite element simulation of the welding process in general, only a few researchers have attempted simulation of welding pipes of dissimilar materials. The study focuses on 2-D and 3-D finite element simulations of residual stresses and validation of the model through experimental investigation, residual stress evaluation. The thermo-mechanical analysis of the model is developed and carried out. Numerical simulation of dissimilar steel welding processes is generally more challenging than that of similar steel welding because of the differences in the physical, mechanical and metallurgical properties of the materials to be joined. The works published in the literature review tend to validate the FE models using a thermocouple, despite the difficulties involved in accurate measurement with a thermocouple. Thus, a different choice of validation data, XRD, was used to measure residual stresses.

After a careful literature review and identification of the knowledge gap, the following research questions emerged:

- What alternative method can be used for validation of finite element model for pipe arc welding with dissimilar material?

- Is it allowable only to use a two-dimensional model (2-D) for the prediction of residual stresses data for pipe arc welding with dissimilar material?

- What is the effect of different welding parameters on residual stresses in dissimilar pipe arc welded joints, and which have the most significant influence on residual stresses?

- What is the most accurate heat source model for the prediction of pipe arc welding of dissimilar materials?

DOI: 10.14750/ME.2022.004

3. MATERIAL AND METHOD

3.1 Pipe Weld Geometry and Specifications

The pipe was prepared and welded at the University of Miskolc, Miskolc, Hungary. Pipe with dissimilar material was welded with the MMAW process and with filler material. The pipes are also dissimilar in thickness: both pipes have an outer diameter of 133 mm, with different thicknesses of 8 mm and 11mm, and a total length of 450 mm, as shown in Figure 20.

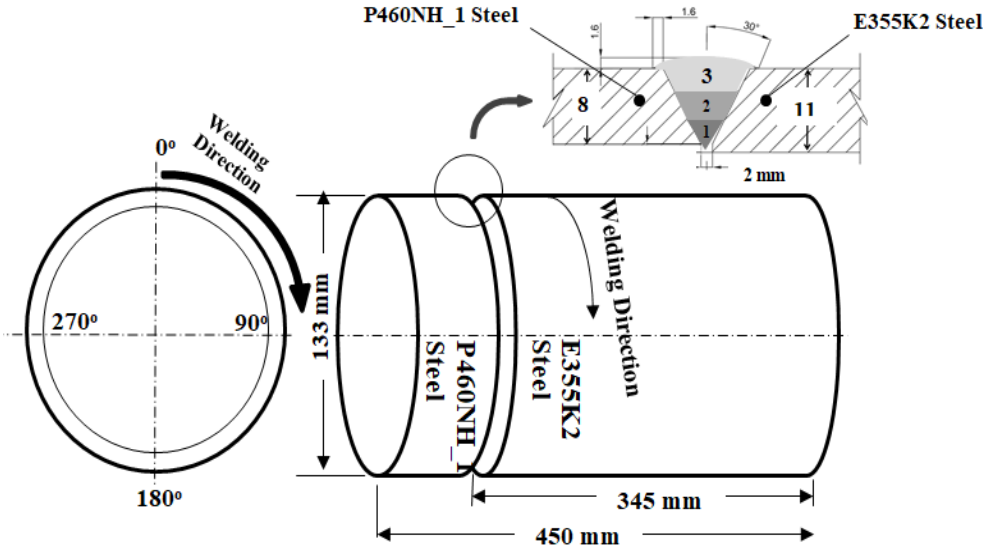

Figure 20. Schematic sketches of the welded pipe with the welding direction for three passes, dimensions in mm

Pipe materials P460NH_1 steel, E355K2 steel and the fillers for the first pass (A5.1-04: E6010) and the second and third passes (A5.5-96: E6010) were welded. The chemical compositions for the parent and weld materials are shown in Table 5. Welding with dissimilar material pipe welds was used in this work. The standard single V-groove design was employed for butt joints, with an included angle of 60º used for dissimilar joints. The pipe was joined with a manual circumferential weld.

Table 5. Chemical composition (wt%)

Materials	C	S	P	Mn	Si	Mo	Ni	Nb	V	Cr	Cu	Fe
P460NH_1 (BM-1)	0.2	0.001	0.02	1.4	0.33	0.1	0.01	0.05	0.2	0.01	0.03	95.23
E355K2 (BM-2)	0.1	0.01	0.86	0.8	0.01	-	-	0.02	0.058	0.02	0.02	-
Filler metal A5.1-04: E6010	0.1	-	0.02	0.4	0.14	0.5	0.15	-	-	0.1	0.17	-
Filler metal A5.5-96: E6010	0.1	0.01	0.01	0.63	0.36	0.01	0.02	-	-	0.03	-	-

Welding parameters utilised in this study are given in Table 6. Usually, the welding efficiency used is between 65% and 88% [27], [258]. Table 7 shows the welding pool parameters, which present a Godack model shape.

Table 6. Welding parameters and heat source

Pass No.	Current (A)	Voltage (V)	Speed mm/s	Efficiency
1	80	23.2	3	0.8
2	90	23.6	3	0.8
3	100	24	3	0.8

Table 7. Welding pool parameters

Pass No.	Welding pool parameters			
	2a (mm)	b (mm)	c_f (mm)	c_r (mm)
1	5.6	4	5.3	8.3
2	11.5	3.8	5.2	8.3
3	13.8	4.7	5.3	8.2

3.2 Numerical Simulation Procedure

Complex numerical approaches are required to accurately model the welding process in 2-D, with finer mesh (small element size) and materials region used to simulate welding instead of 3-D to save the CPU time of computation. To validate the accuracy of FE model simulation, experimental results of the welded specimen are used to compare with the simulation results of FEM. During the welding cycle process, coupled thermo-metallurgical and mechanical calculations were carried out by considering the effect of the different chemical compositions of steel and with phase transformation. Numerical calculations were performed with the commercial finite element software package MSCMarc. The problem was solved numerically in a cylindrical coordinate system due to the geometry's axial symmetry. Four-node axisymmetric elements were used to model the specimens. The fillers' model was built with the birth and death technique using 8,466 elements to calculate and analyse phase transformation distribution. In numerical simulation analysis, the accuracy of the results and required computing time are determined by the finite element size (mesh density). According to numerical analysis theory, the model with a fine mesh yields highly accurate results but requires longer computing time. On the other hand, a model with coarse mesh (large element size) may lead to less accurate results but not take much computing time. Figure 21 shows the procedure for the 2-D FE model calculation.

DOI: 10.14750/ME.2022.004

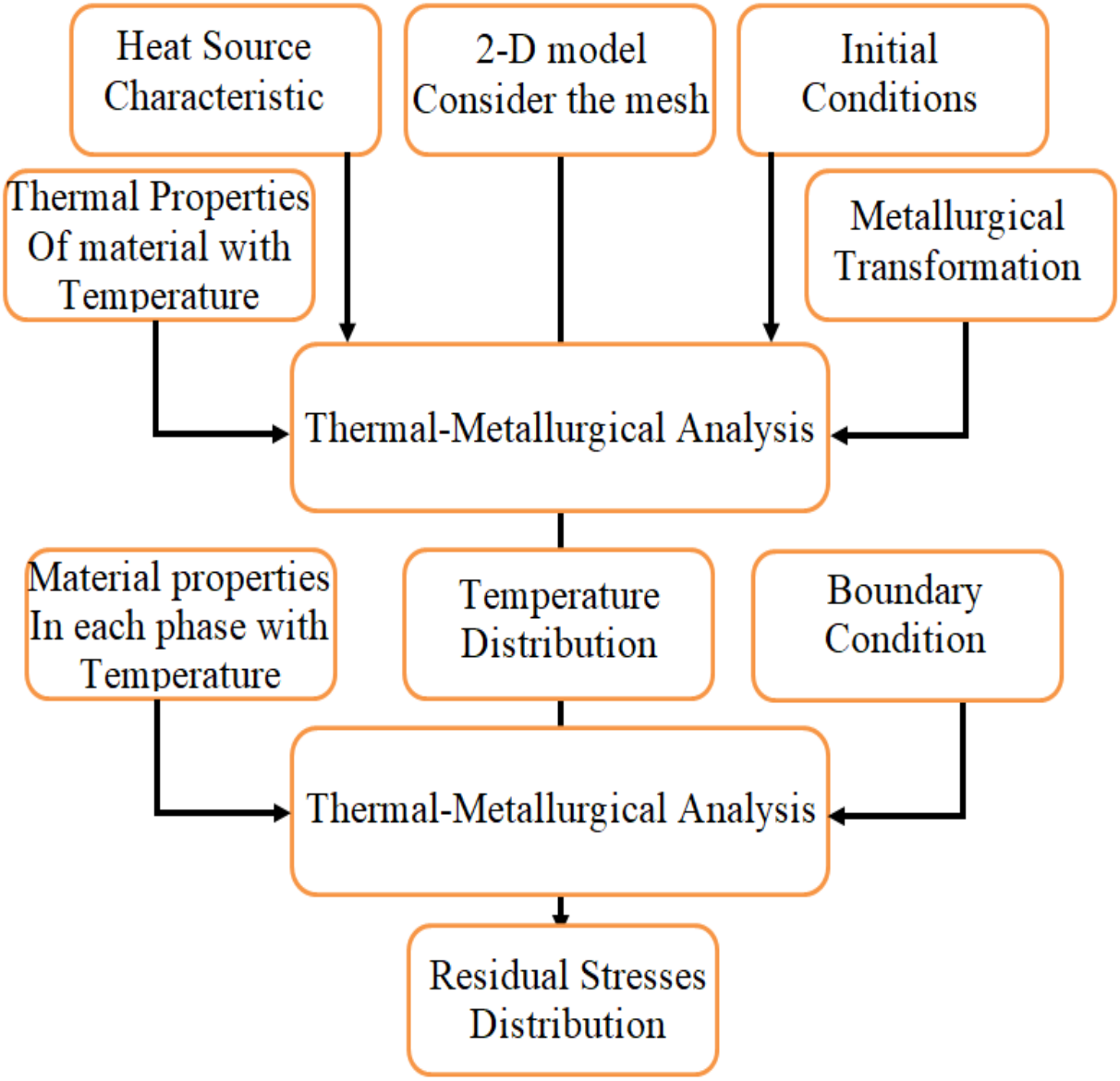

Figure 21. Flow chart of the welding simulation procedure

3.3 Two-Dimensional Model (2-D)

Figure 22 shows the 2-D model. The X-axis is pipe length direction, Y-axis is pipe thickness direction, and the Z-axis is pipe welding direction. The dimensions of the finite element model are the same as those of the experimental specimen. In this model, to minimise CPU time and calculation accuracy fine mesh was used for the weld and HAZ, and a coarse mesh was used in the region further from the weld. The software used for the welding simulations is MSC Marc. The three materials used are Base material P460NH_1, Base material E355K2, and filler metal, shown in Figure 23. Due to the symmetry, an axisymmetric FE model with linear four-node finite elements was developed to simulate the welding temperature field and residual stress distribution on the dissimilar welded joint.

DOI: 10.14750/ME.2022.004

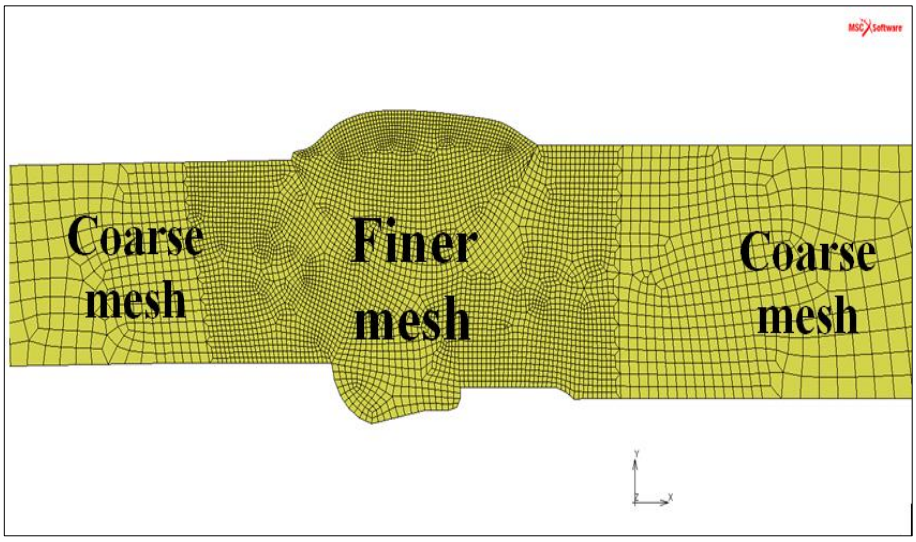

Figure 22. 2-D finite element model of pipe

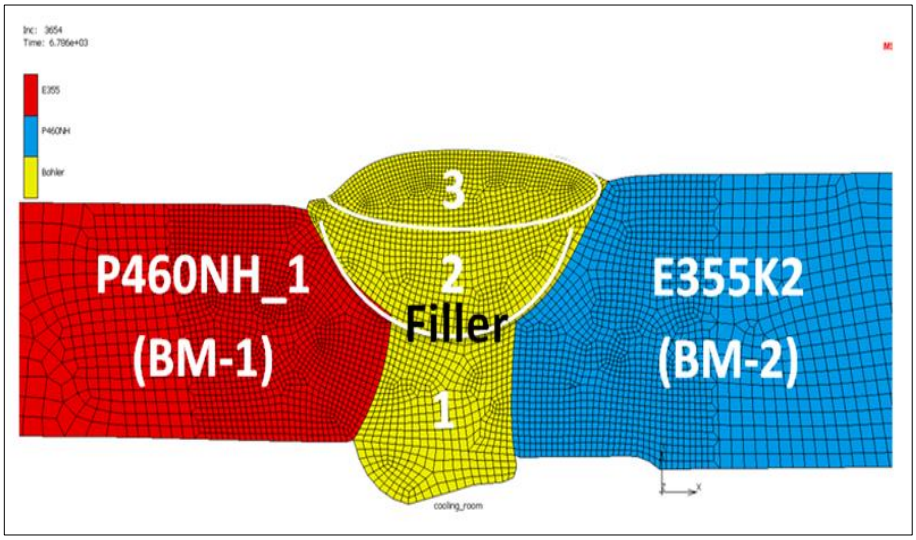

Figure 23. 2-D model with fine and coarse mesh and materials of the dissimilar welded joint

3.4 Three-Dimensional Model (3-D)

The whole length of the pipe is 450 mm; the inside diameter is 133 mm, and the groove shape is shown in Figure 24(a). In this section, the 3-D FE model based on MSC-Marc code is developed to accurately obtain the temperature fields and the residual stresses during the circumferential welding process, as shown in Figure 24(b). As mentioned with the 2-D model and considering that the temperature gradient was larger near the welding zone, the non-uniform mesh was used. More refined mesh elements were designed at the weld zone, and a relatively coarser grid was used further away from the weld bead. The length of each element in the welding direction is 2 mm, so the number of divisions in the longitudinal direction is 150. In the thickness direction, the number of divisions is 4. The total number of nodes is 21,202, and that of the element is 15,720. Figure 25 shows the 3-D FE model simulation process.

DOI: 10.14750/ME.2022.004

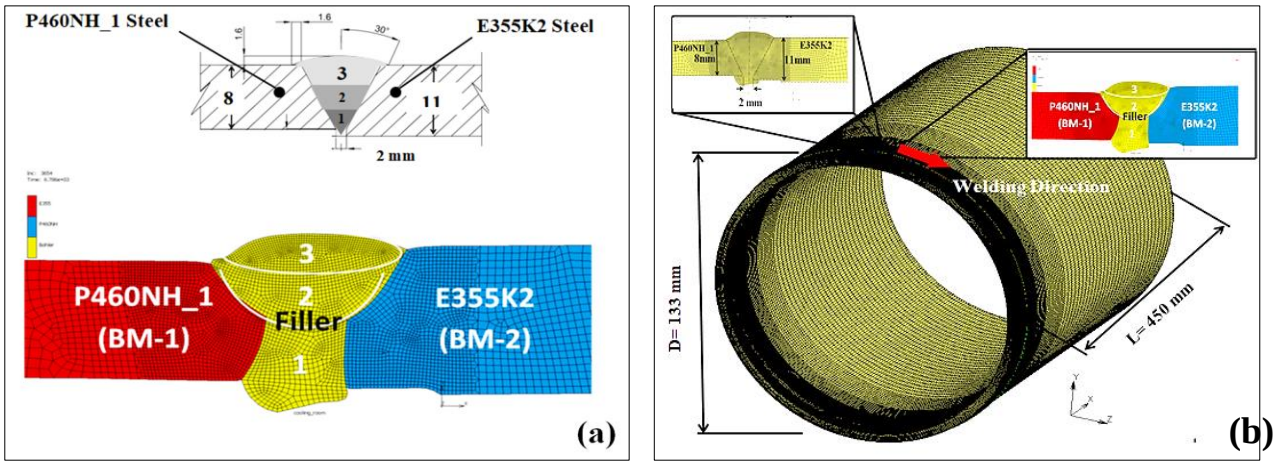

Figure 24. (a) Groove schematic with dimension (b) 3-D finite element model of pipe

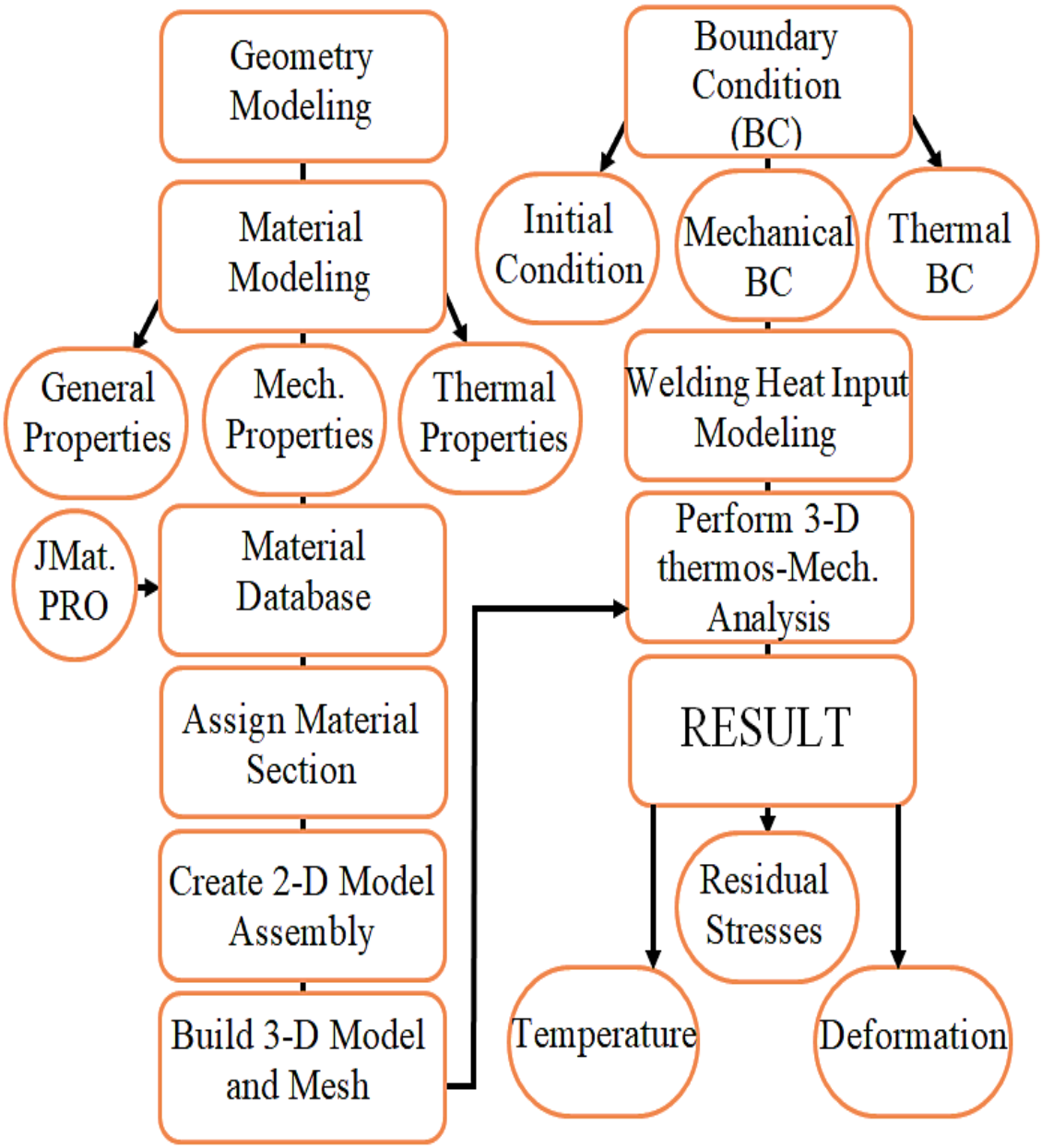

Figure 25. 3-D FE model simulation process

DOI: 10.14750/ME.2022.004

3.5 Material Properties

3.5.1 *Thermophysical properties, mechanical analyses and CCT diagram for the filler*

Figure 26 shows Thermal conductivity, specific heat capacity coefficient, while Figure 27 shows thermophysical expansion and Young's modulus. Figure 28 shows Poisson's ratio and density. The continuous cooling transformation diagram for the filler is shown in (Appendix B).

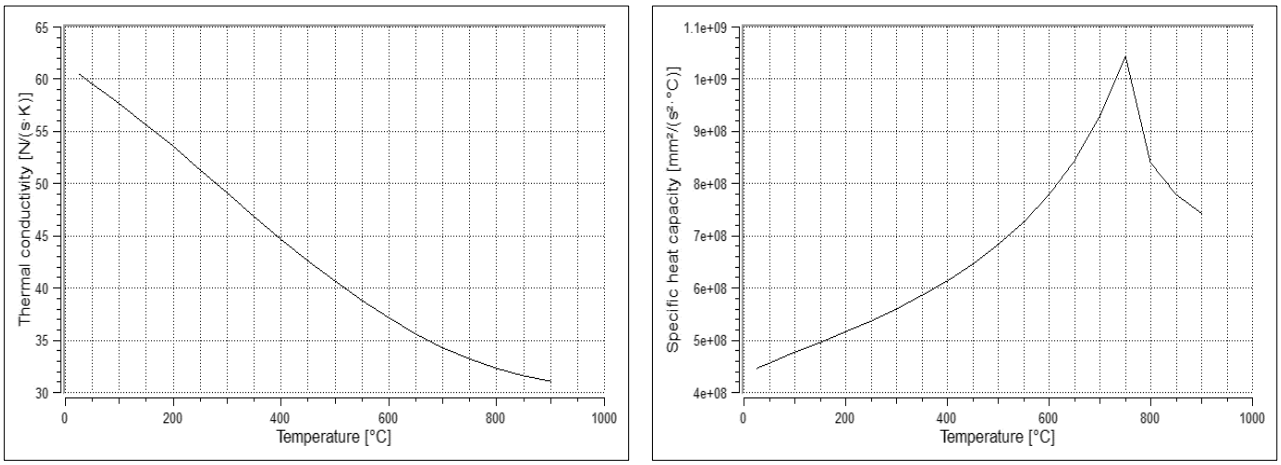

Figure 26. (a) Thermophysical conductivity (b) Specific heat capacity

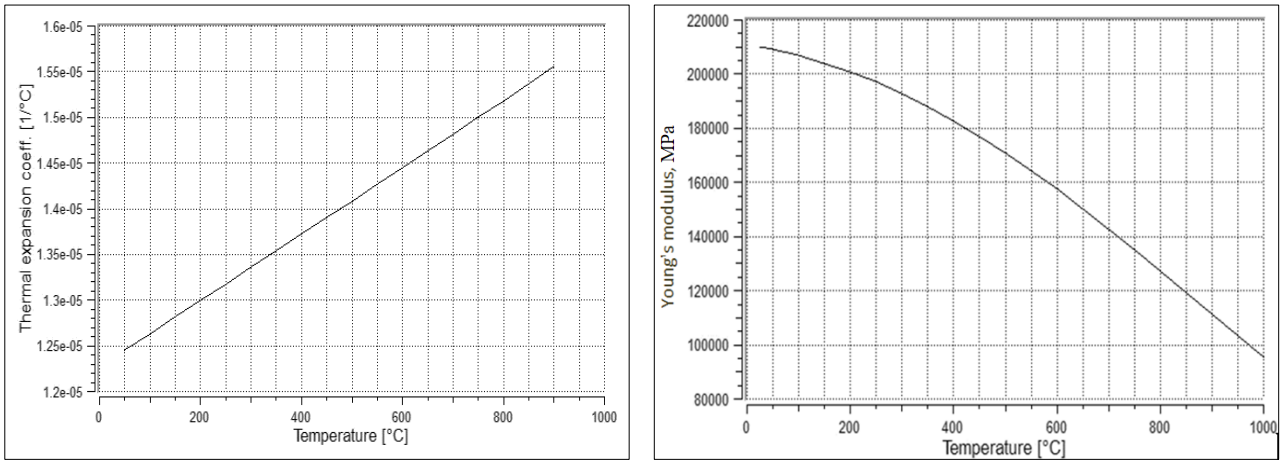

Figure 27. (a) Thermal expansion coefficient (b) Young's modulus

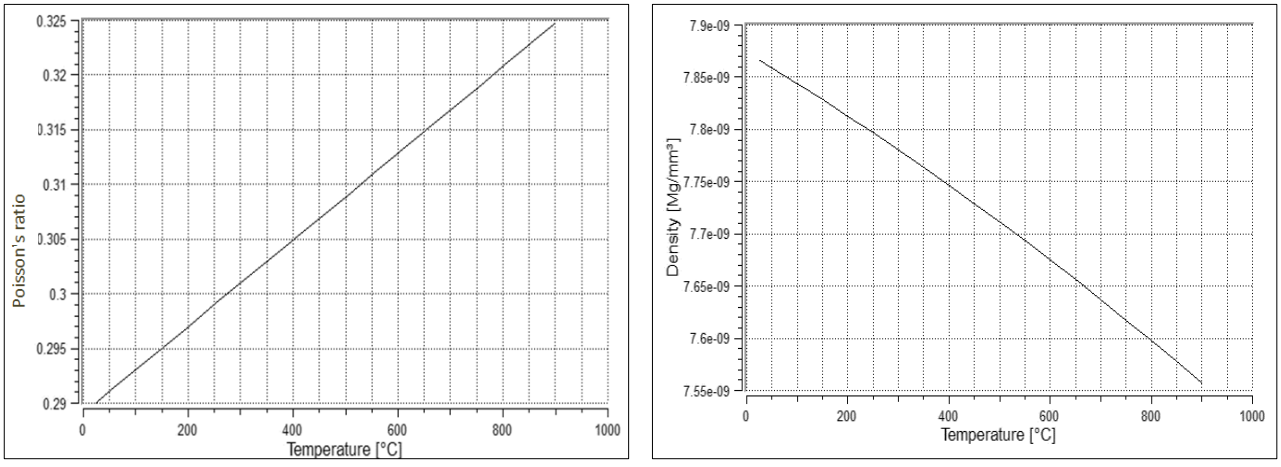

Figure 28. (a) Poisson's ratio and (b) Density for the filler materials

DOI: 10.14750/ME.2022.004

3.5.2 *Thermophysical properties, mechanical analyses and CCT diagram for E355K2*

Figure 29 shows Thermal conductivity, specific heat capacity coefficient, while Figure 30 shows thermophysical expansion and Young's modulus. Figure 31 shows Poisson's ratio and density. The continuous cooling transformation diagram for E355K2 showed in (Appendix B).

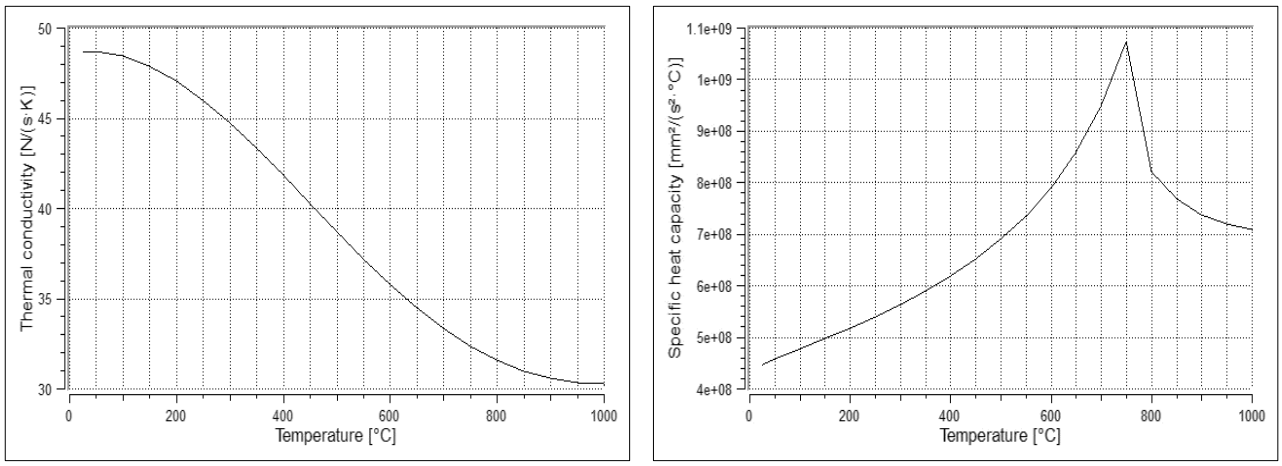

Figure 29. (a) Thermal conductivity (b) Specific heat capacity for E355K2

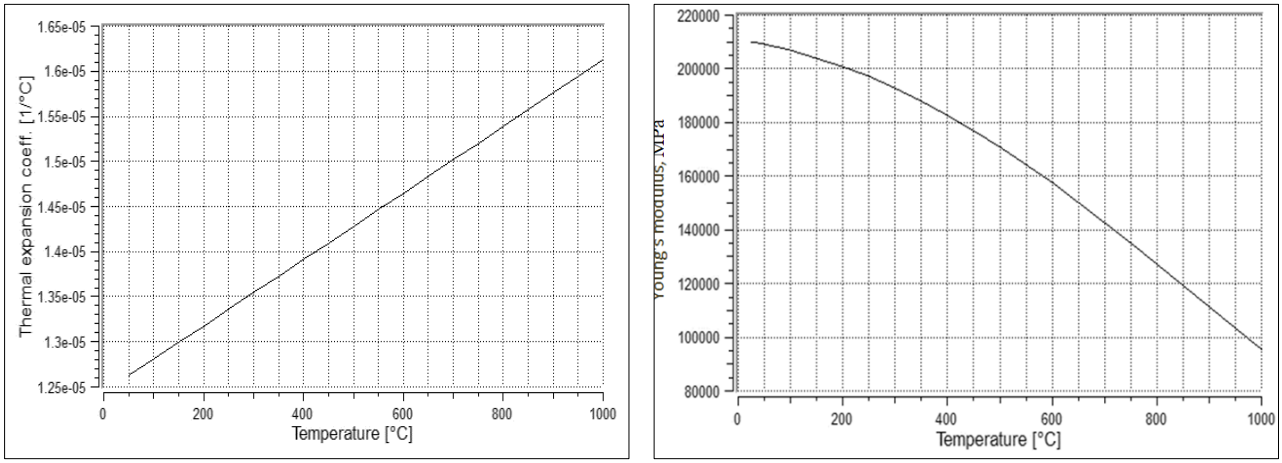

Figure 30. (a) Thermal expansion coefficient (b) Young's modulus for E355K2

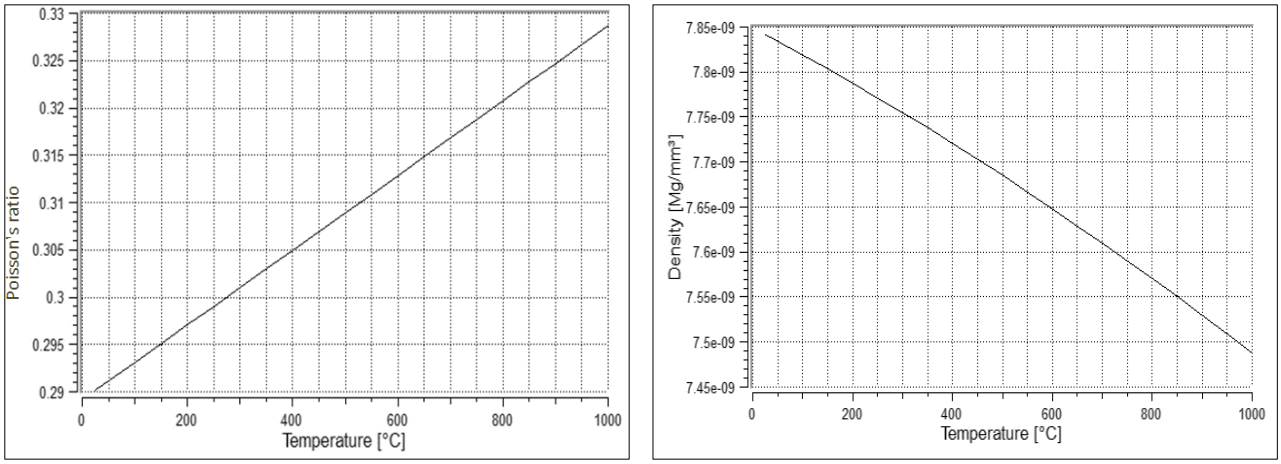

Figure 31. (a) Poisson's ratio and (b) Density for E355K2

DOI: 10.14750/ME.2022.004

3.5.3 *Thermophysical properties, Mechanical properties and CCT diagram for P460NH_1*

Figure 32 shows Thermal conductivity, specific heat capacity coefficient, while Figure 33 shows thermophysical expansion and Young's modulus. Figure 34 shows Poisson's ratio and density. The continuous cooling transformation diagram for P460NH_1 is shown in (Appendix B).

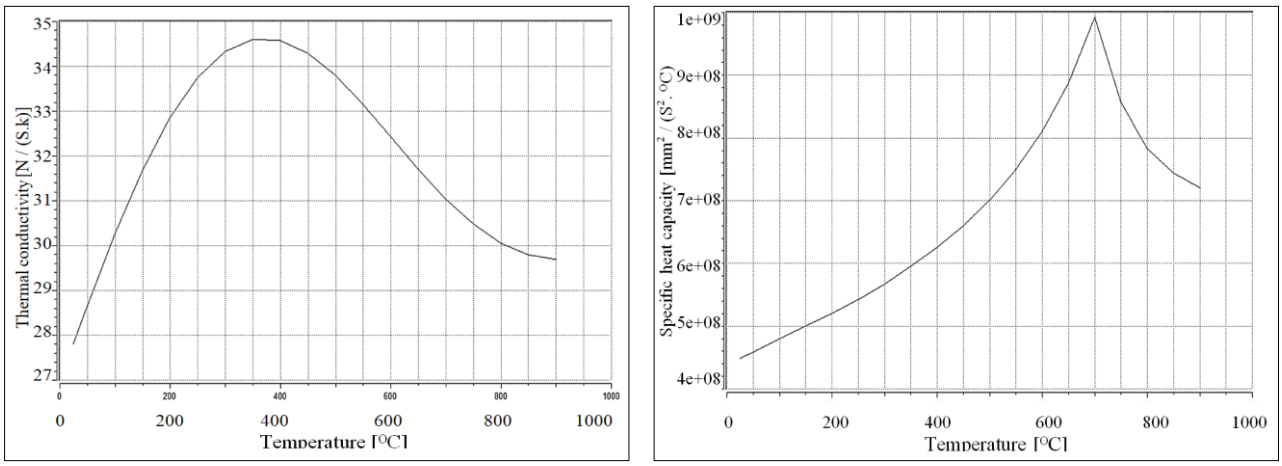

Figure 32. (a) Thermal conductivity (b) Specific heat capacity for P460NH_1

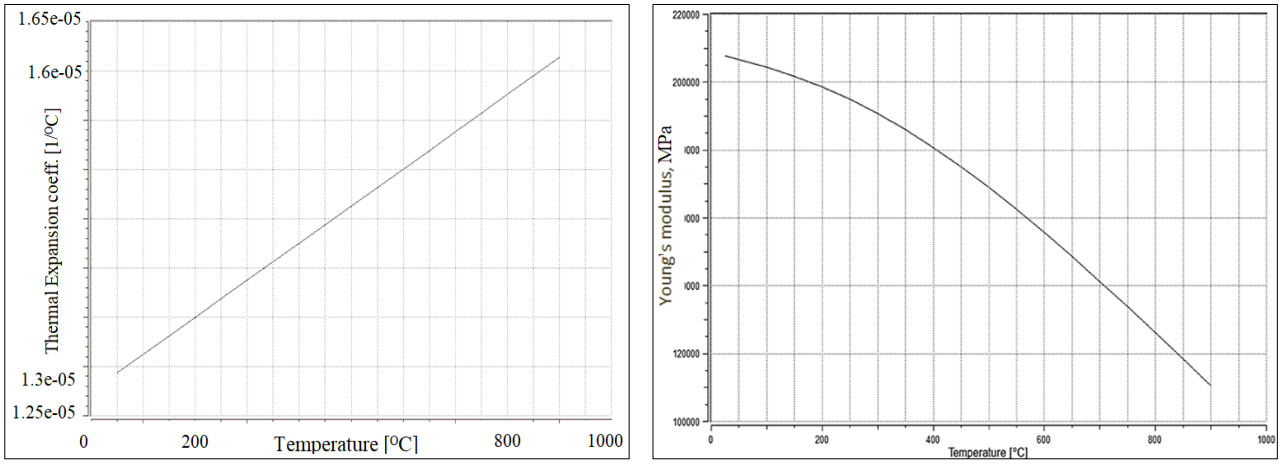

Figure 33. (a) Thermal expansion coefficient (b) Young's modulus for P460NH_1

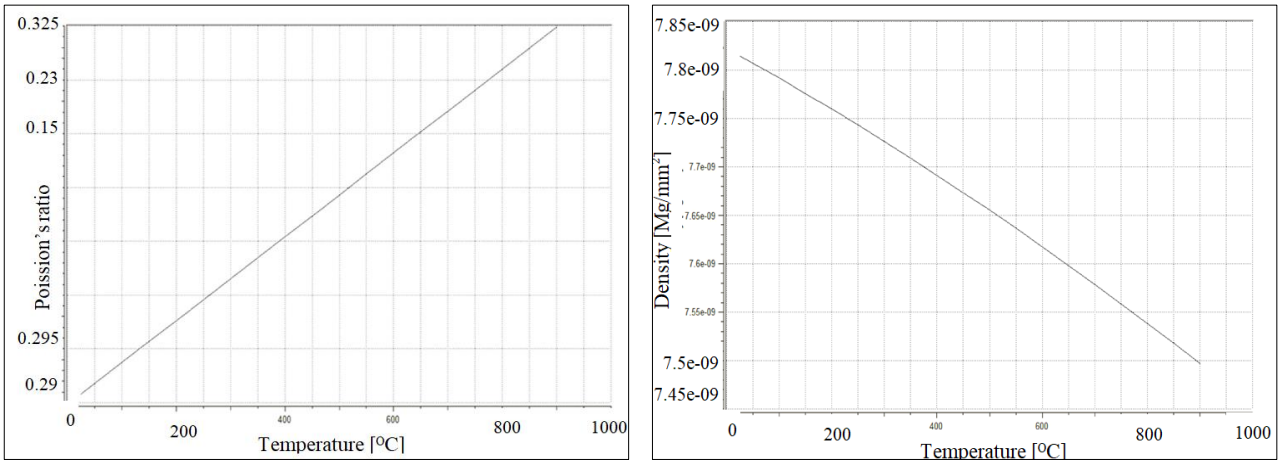

Figure 34. (a) Poisson's ratio and (b) Density for P460NH_1

DOI: 10.14750/ME.2022.004

3.6 Experimental Procedure

3.6.1 *Non-destructive method of residual stresses measurement*

X-ray diffraction is the most important non-destructive method to determine and analyse residual stress fields within crystalline materials in the welding pipe and other components. The x-ray method does not measure stress directly but measures strain, from which residual stress values are calculated. The principle is simple. The XRD technique uses the distance between crystallographic planes or measuring the inter-atomic lattice spacing, i.e. d-spacing, like an atomic strain gauge. Figure 35 shows the basic principle of XRD. When the material is in tension, the interplanar space d increases and when the material is in compression, the interplanar space d decreases.

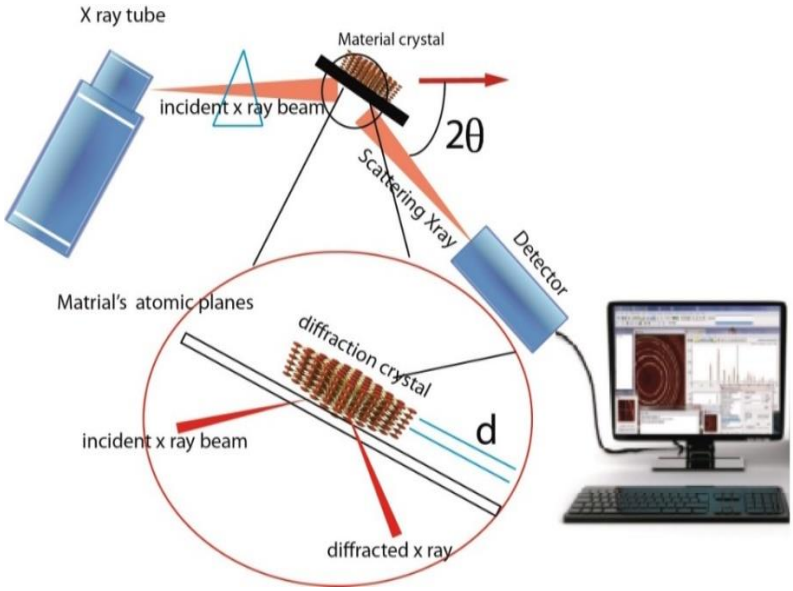

Figure 35. Schematic diagram of the basic principle of XRD

Stresses can be determined from the measured distance between the atoms' planes, dependent upon the material and the strains present in the material. X-rays diffract from crystalline materials at known angles such as diffraction angle θ for a given x-ray wavelength λ can be used to determine the material d spacing using Bragg's law. Bragg's law is one of the most useful and instructive relations for diffraction from the material. Bragg's principle describes the determination of residual stresses in the material based on diffraction theory. Figure 36 shows an illustration of Bragg's law. In this method, the alteration of inter-planar lattice spacing is employed to determine any deformation in the crystal lattice. Bragg's law is formulated as follows:

$$\boldsymbol{n\,\lambda = 2\,d\,sin\,\theta} \tag{9}$$

DOI: 10.14750/ME.2022.004

Where λ is the wavelength of the X-rays, θ is the diffraction angle and d is interplanar space, the distance between atomic planes.

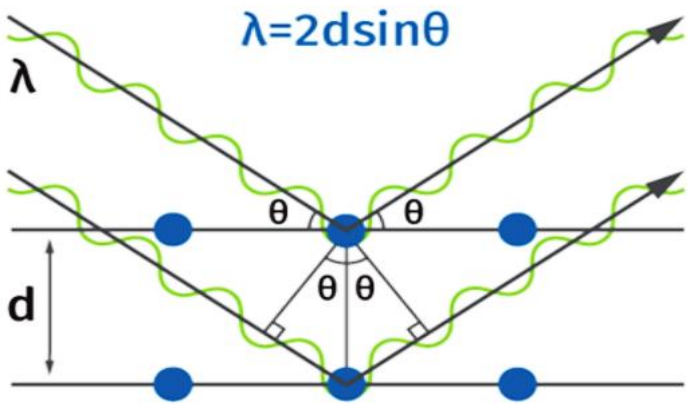

Figure 36. Illustration of Bragg's law

3.7 Sin^2 Ψ Method of X-Ray

The sin^2 ψ x-ray method of stress determination has been used for over 30 years [259]. In essence, measurements are made over a range of inclination angles (ψ) using a high scattering angle (2θ). Using the X-ray sin^2 ψ method, the plane strain can be determined from the atomic lattice spacing variation as the ψ angle is increased (see Figure 36 (a)). Though it describes the strain corresponding to this diffraction vector as $\varepsilon_{\varphi\psi}^{hkl}$, the scattered X-rays are recorded for a specific family of planes {hkl} and will use ∈ for simplicity. The elastic strain could be determined as follows:

$$\mathrm{Ɛ} = (\boldsymbol{d} - \boldsymbol{do})/\boldsymbol{do} \tag{10}$$

Three measured strain components ε, in combination with the elastic constants E and ν, are then used to calculate the stresses in the material using Hooke's law. Once the lattice d-spacings are measured for the unstressed (d_o) and stressed (d) material conditions, the atomic lattice strain can then be calculated by the following relationship. The degree of diffracted X-rays depends on arranging the materials atomic planes within the crystal lattice.

$$\boldsymbol{\sigma} = \boldsymbol{E}\varepsilon \tag{11}$$

For isotropic materials, strains can be changed to stress values, with the sin^2 ψ method, the traditional equation for X-ray stress measurement is used as:

DOI: 10.14750/ME.2022.004

$$\boldsymbol{\sigma = \frac{d_{\varphi} - d_o}{d_o} \left(\frac{E}{1+\upsilon}\right) \frac{1}{sin^2 \psi}} \tag{12}$$

The residual stress is calculated by using the relation here to strain-free interplanar spacing. The calculated strain and angle Ψ is the angle between the surface normal and the strain measurement direction. The stress distribution by principal stresses σ_1 and σ_2 exist in the surface plane, and no stress is assumed vertical to the surface σ_3=0 (see Figure 37). High accuracy is necessary, which requires accurate sample alignment and precise methods of diffraction peak location. For XRD to occur, i.e., constructive wave interference, the path difference travelled by the diffracted beam through the material is compared to a non-diffracted beam.

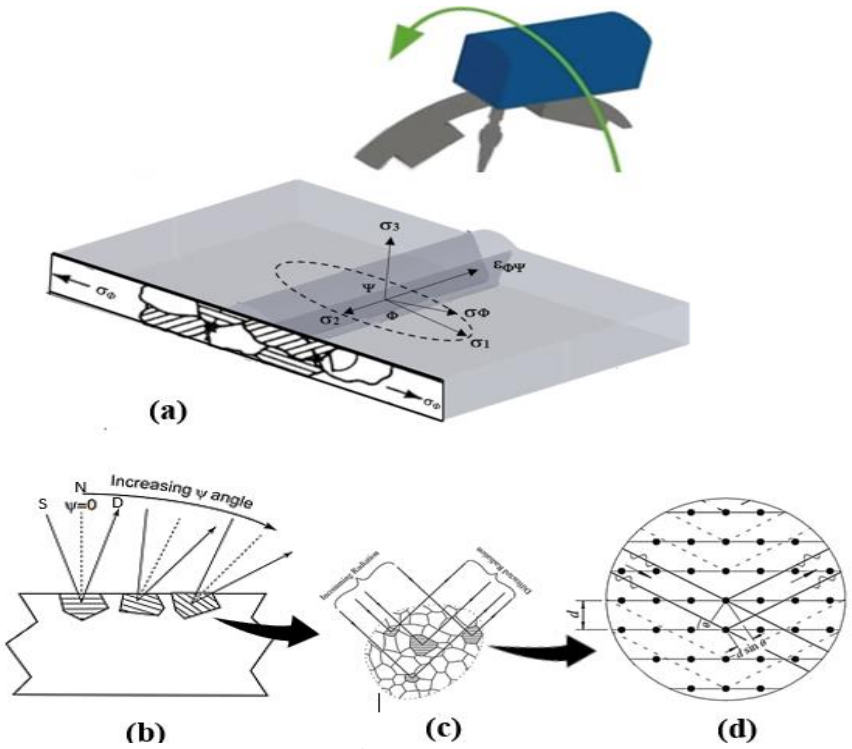

Figure 37. Schematic illustrating: (a) the $\sin^2 \psi$ method (b) the stress can be deduced from the variation in atomic lattice spacing as the ψ angle is increased D, x-ray detector: S, x-ray source; N, normal to the surface; (c) A schematic showing how the Bragg diffraction of X-ray beam selects; (d) crystals with planes of the correct spacing oriented to satisfy Bragg's law.

3.8 Robotised Solutions for Measuring Residual Stresses by X-Ray Diffraction

The most common problem encountered in using XRD techniques is the high precision required for measurement of the diffraction angles, which requires accurate sample alignment and precise diffraction peak location methods. It is currently possible to measure residual stresses by various methods, but the accurate measurement is difficult. XRD is also one of the non-destructive techniques that can measure residual stresses with high resolution and accuracy. In many

DOI: 10.14750/ME.2022.004

circumstances, the determination of the stress-free lattice parameter is the most challenging. One of the major disadvantages and limitations of XRD technique is the test workpiece size and geometry. XRD equipment with goniometer mounted on a robotic arm makes stress measurements by Stresstech Xstress Robot easy and flexible on large and/or complex surface parts. Figure 38 shows a close-up of the setup, and measurement directions are shown in Figure 39 (a) and (b). In this setup, a robot makes the movements, enabling measuring residual stresses of virtually any shape or size piece.

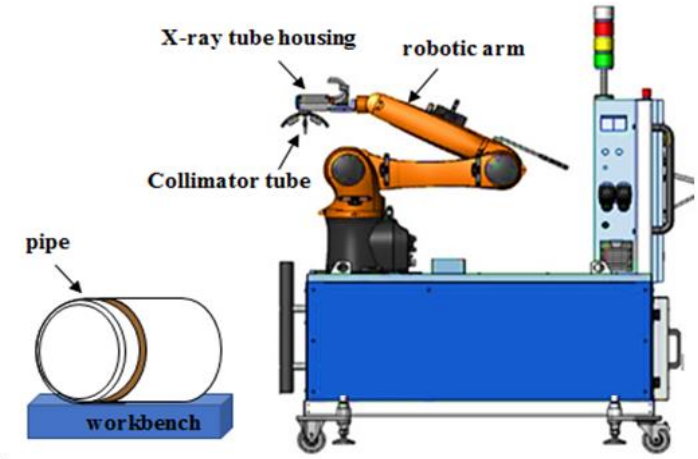

Figure 38. Xstress Robot

The residual stresses were measured at the post-processed surface using X-ray diffraction with equipment from Stresstech, XStress Robot X-ray Diffractometer. This diffractometer was equipped with a chromium X-ray tube (λ: 0.229 nm) and 30 kV and 7 mA settings. The lattice plane (2 1 1) was measured with a 2θ diffraction peak located at approximately 156, 4°. The modified $\sin^2\psi$ measurement strategy was used with 17 psi angles from (−45° to +45°). The residual stress was calculated assuming elastic strain theory, according to Hook's law.

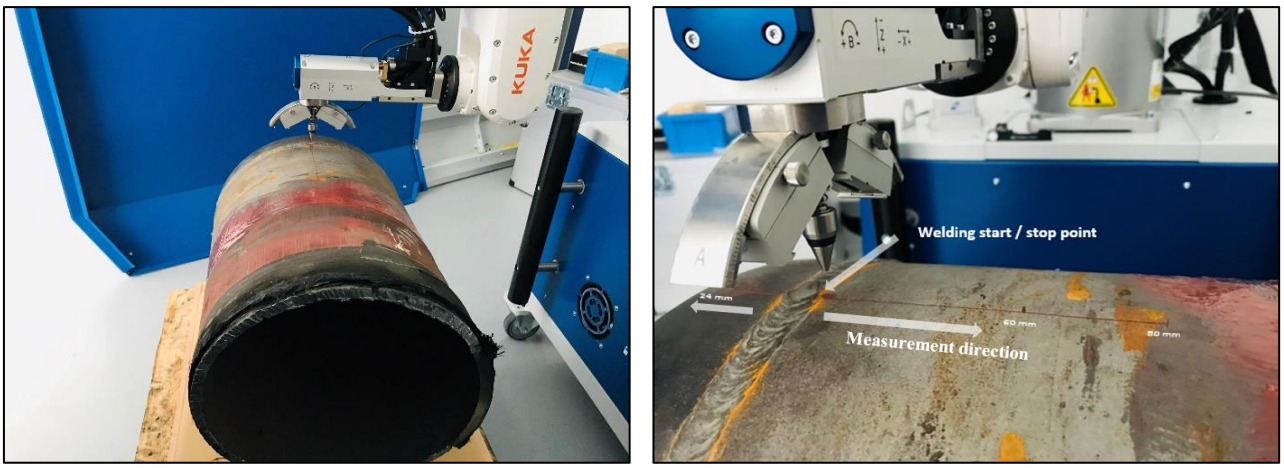

Figure 39. The examined positions of residual stress measurements by X-ray diffraction: (a) XRD measurement (b) Close-up of the setup and measurement directions

DOI: 10.14750/ME.2022.004

4. VALIDATION OF 2-D/3-D MODEL: NEW STRATEGIES

Validation is the essential procedure required to assess the accuracy and credibility of welding numerical model simulation analyses. We need to verify the numerical simulation model using experimental results to ensure that the developed model is correct. After that, we need to validate ways to ensure that the model can simulate pipe welding under different conditions. The researcher's primary responsibility is to create an FE model representing the real physical model by adopting appropriate shapes, boundary conditions, elements, etc. Only then can we be sure that the numerical solution is a good approximation and can make good predictions. Four strategies were followed to analyse welding interaction. Therefore, strategies for validation and qualification of simulation models are essential, and the following research question was formulated:

How should modelling and validation of welding be carried out to provide adequate accuracy to calculate residual stresses?

The study presented in this work is limited to models with multi-passes using arc welding and related phenomena such as weld pool geometry and phase transformation etc. The welding macrographs were obtained to confirm the width and depth of penetration for the numerical simulation's obtained welding parameters. The heat source fitting was carried out to define Godlak's model parameters. During this, heat source parameters were adjusted such that the simulated molten weld pool size should match with the macrograph's cross-section. Finally, a calibrated heat source is used in thermos-metallurgical-mechanical numerical simulation. The flow chart for validation of the welding simulation procedure used MSC Marc is described in Figure 39.

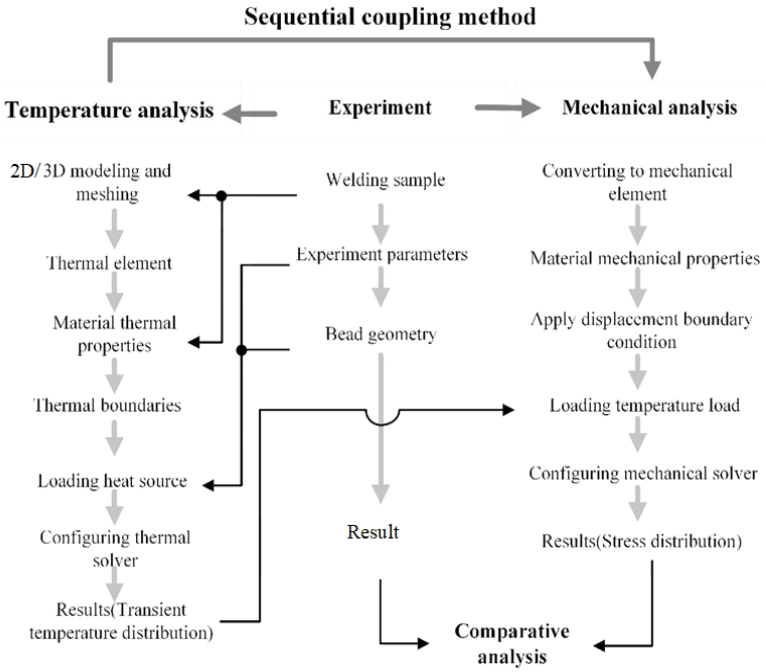

Figure 40. Flow chart of validation of the welding simulation procedure

DOI: 10.14750/ME.2022.004

4.1 Validation of Heat Source Model

The essential thing in the thermophysical and mechanical analysis is the heat source model. Usually in the literature, the effect of the heat source model is neglected by the researchers. In this study, an accurate model of the heat source of pipe welding is proposed. The validation of the heat source model is done by observing the temperature histories of measured nodes and comparing the predicted and measured weld-pool shapes. The comparison between weld shape pool and heat source by the numerical model is presented in Figure 41 (a) and (b).

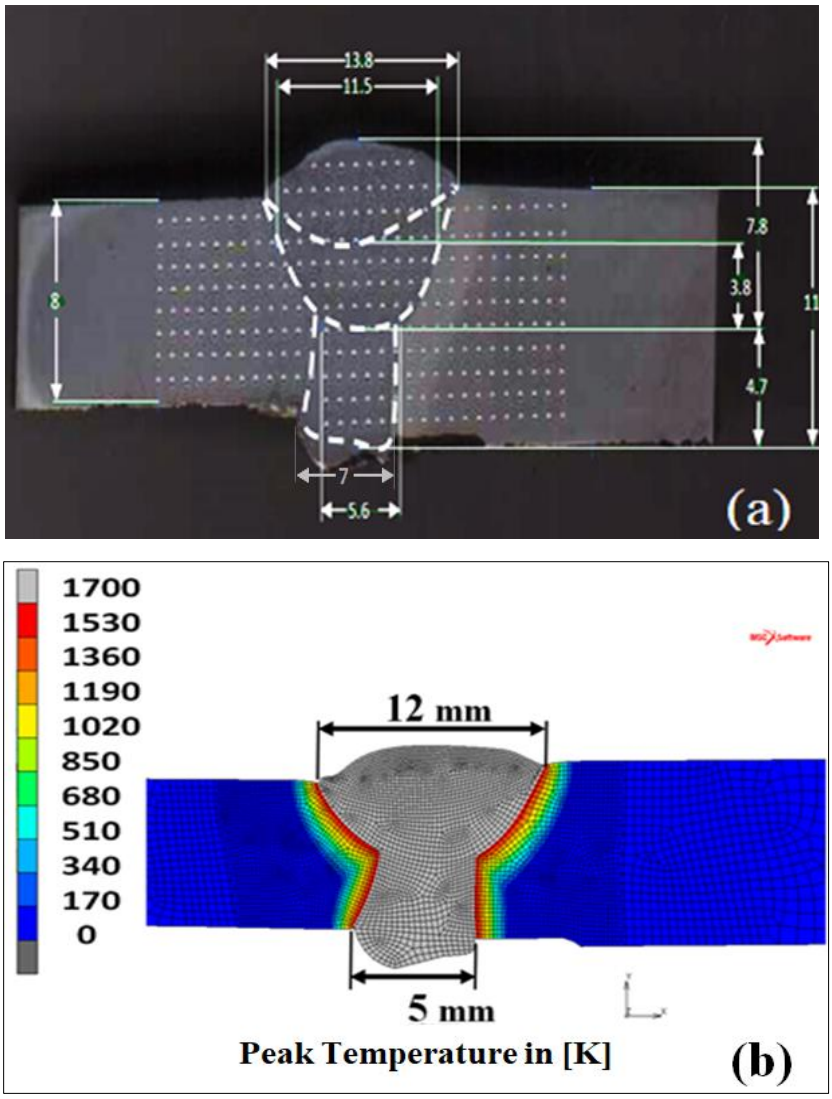

Figure 41. Weld pool profile obtained from (a) the specimen, (b) simulation, all dimensions in mm

4.2 Hardness Measurement

The hardness test was measured and compared with the simulation results to verify the accuracy of the simulation. The validation of welding simulation procedures is carried out on a multi-pass pipe weld. To set up the numerical model's accuracy, validation of the model is necessary to predict the residual stress. The sample was polished and etched weld through a multi-pass weld with HNO_3 (nitric acid) 2% solution (nitrate etching agent) to show the passes and HAZ.

DOI: 10.14750/ME.2022.004

Figure 42. The specimen after hardness measurement

Vickers hardness measurement (HV_{10}) was carried out from top to bottom with 12 lines (see Figure 42). The validation of the welding simulation procedure is carried out on a multi-pass butt weld with eight tracks. Maynier et al. [260] developed a useful method to predict hardness.

The results are compared with the experimental hardness test. Figure 42 shows measurements with a microscope-mounted camera showing an average of the measurement distance from the surface at a given point. The distances are in millimetres, and the hardness values are in HV_{10}. The hardness distribution from the simulation at the weld of the investigated dissimilar material with welding was calculated by using the rule of mixtures. The total hardness of steel is calculated dependent on the volume fractions of the constituents of the microstructure:

$$\boldsymbol{HV = (FP\% * HV_{F-P} + B\% * HV_B + M\% * HV_M)/100} \quad (12)$$

The hardness of the microstructures produced is given by:

$$\boldsymbol{HV_M = 127 + 949C\% + 27Si\% + 11Mn\% + 16Cr\% \, Ni\% + 21logv_R,} \quad (13)$$

$$\boldsymbol{HV_B = -323 + 185C\% + 330Si\% + 153Mn\% + 144Cr\% + 191Mo\% + 65Ni\% + (logv_R)(89 + 53C\% - 55Si\% - 2Mn\% - 20Cr\% - 33Mo\% - 10Ni\%)} \quad (14)$$

$$\boldsymbol{HV_{F-P} = 42 + 223C\% + 53S\%i + 30Mn\% + 7Cr\% + 9Mo\% + 12.6N\%i + (logv_R)(10 - 19Si\% + 8Cr\% + 4Ni\% + 130V\%)} \quad (15)$$

where: V_R is the cooling rate in K/h; Hv is the hardness (Vickers); X_M, X_B, X_F and X_P are the volume fractions of martensite, bainite, ferrite and pearlite, respectively; and HV_M, HV_B and HV_{F+P} are the hardness of martensite, bainite and the mixture of ferrite and pearlite, respectively. The calculating of HV_M, HV_B and HV_{F+P} were used in the formulae developed by Maynier et al. [260][261].

DOI: 10.14750/ME.2022.004

4.2.1 *Methodology for validation of the welding simulation procedure*

The validation simulation procedure performed with the MSC Marc software is shown in Figure 43. The following steps were adopted during this study:

Step 1: Build up the FE model of the weld joint, choose the element type, and define the thermophysical and mechanical properties;

Step 2: Choose the meshing type

Step 3: Define the boundary condition;

Step 4: Birth the element at the weld zone and start loading heat input;

Step 5: Inactivate all elements, especially those located at the weld zone;

Step 6: Rezone meshing and shape of weld bead, then checking numerical simulation result.

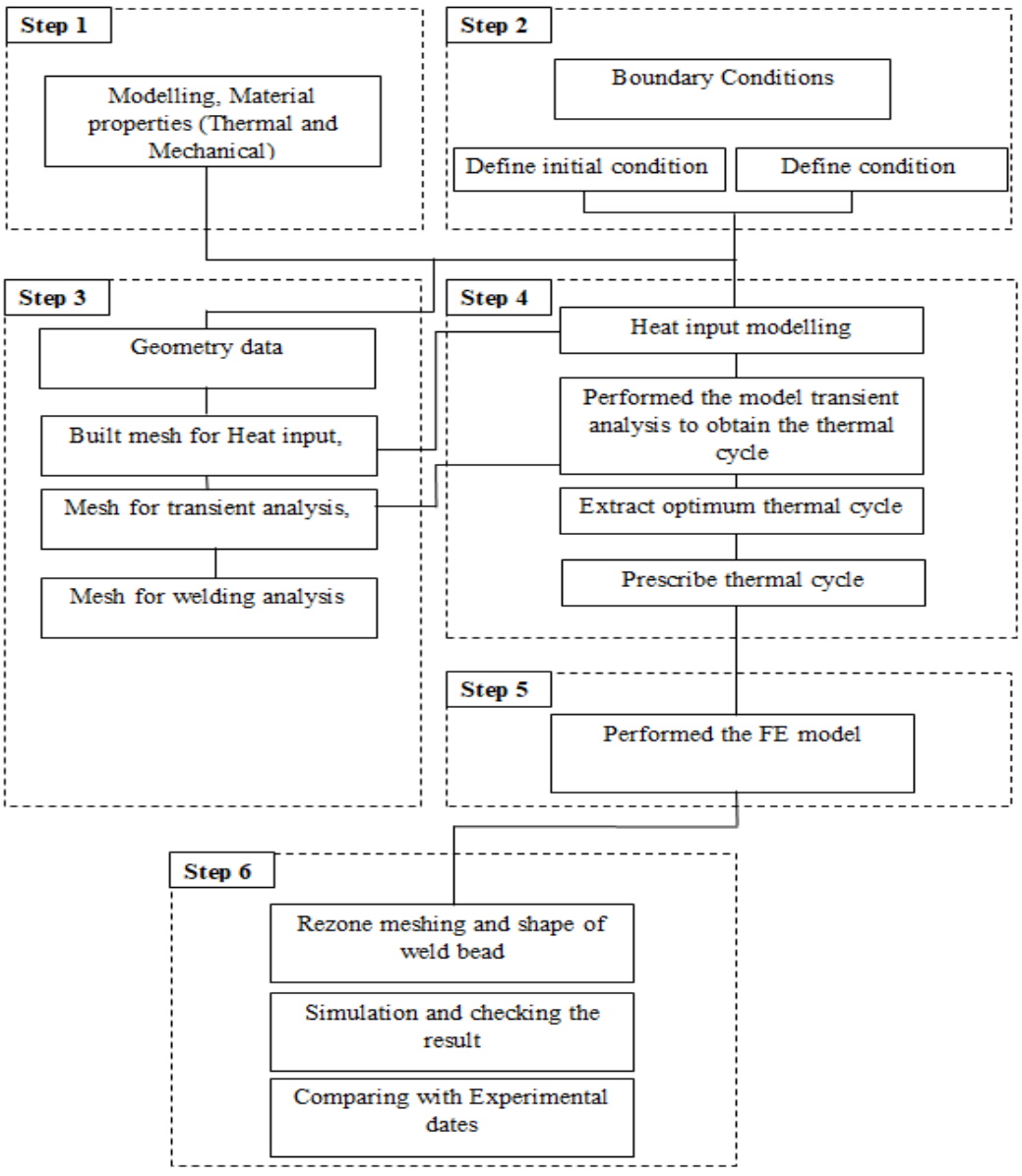

Figure 43. Flow chart of validation of the welding simulation procedure

DOI: 10.14750/ME.2022.004

This work was validated using a numerical trial and error strategy. The first phase consists of simulating a model with all steps mentioned above after checking the welding parameters effects, including model dimension, material properties, boundary condition, power, and heat source parameters.

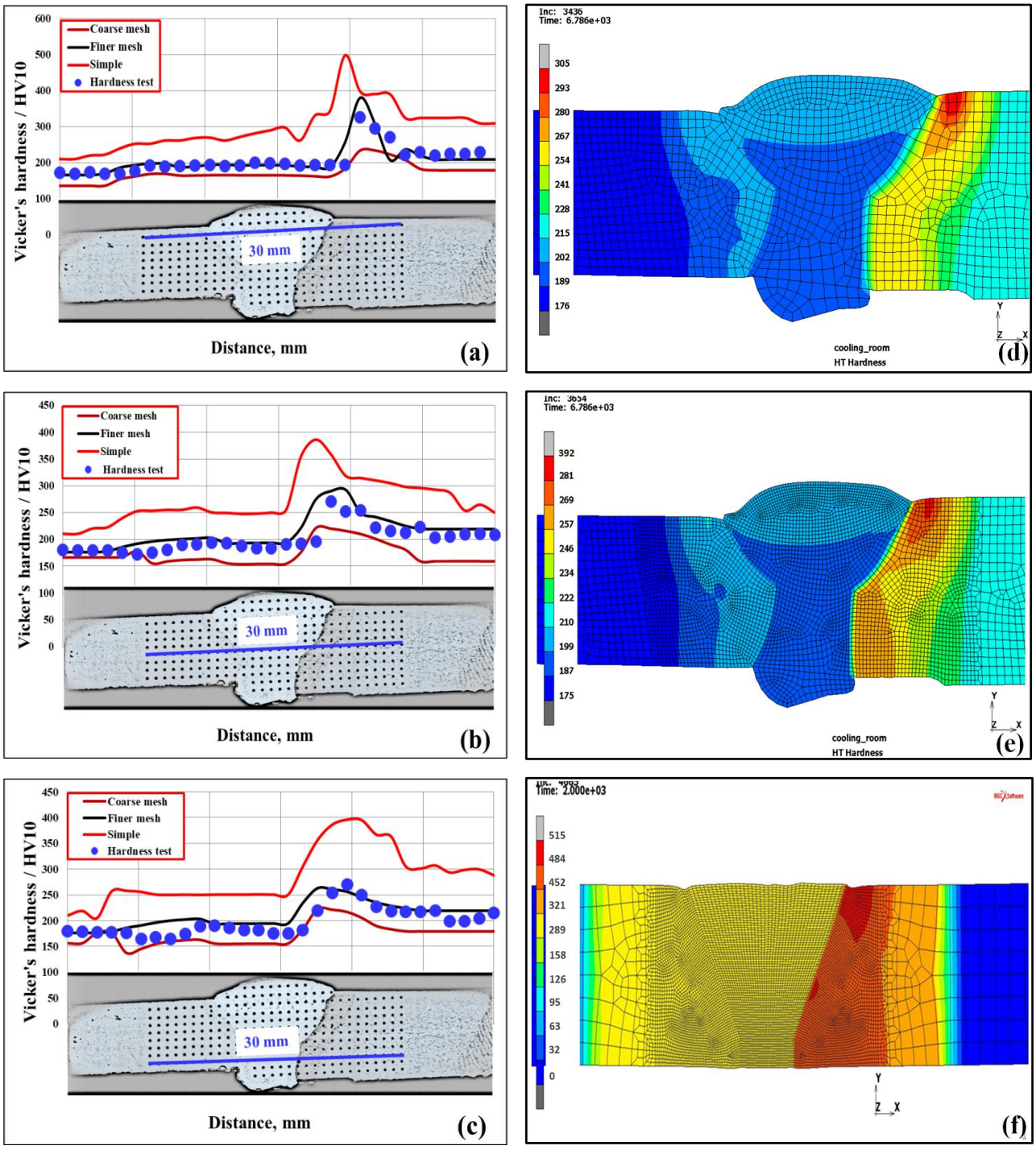

Figure 44. Three FEM models and comparison hardness test using (a) Finer mesh (b) Coarse mesh model (c) Simple model (d) Model with finer mesh (e) Model with coarse mesh (f) Simple model

DOI: 10.14750/ME.2022.004

The purpose of changing the weld bead profile shape was to improve agreement between simulated and experimental data. The sensitivity of the mesh was also analysed in my work. Figure 44 shows three models (simple shape, coarse mesh and finer mesh model) that were used to compare with the hardness measurement. The second phase is to minimise the error simulation related to representing changing weld-bead joint shape geometry to create similarity with the real weld shape; this was undertaken using an optical microscope. The measurement and capture of weld bead geometry were performed with a microscope. Four micrographs samples were measured the area of weld bead, and each micrograph coming from different samples in different angles. The strategy of the validation the model is based on a numerical trial and error method in which the area of the modelled weld-bead joint shape geometry is changed in multi-step iterative calculations to minimize the difference between the calculated and the measured hardness data and to create similarity of the phases corresponding to the heat-affected zone and the fusion zones that were identified by metallurgical optical measurement. The weld beads geometry found for the welded series is shown in Figure 45 (a-b) with profiles captured with micrographs of the cross-section.

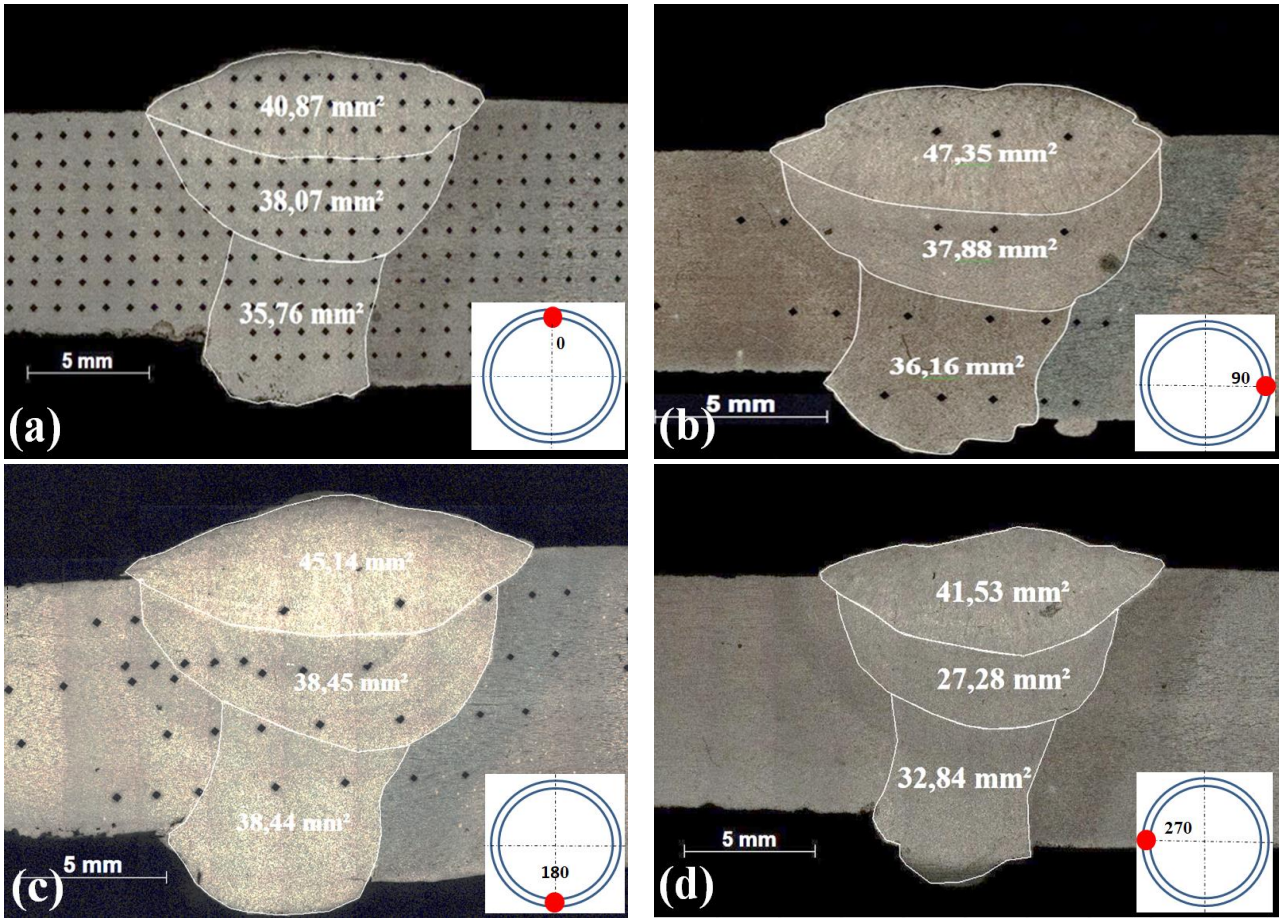

Figure 45. Weld bead profile at different poistion (a) 0^{O} (b) 90^{O} (c) 180^{O} (d) 270^{O}

DOI: 10.14750/ME.2022.004

The model with finer mesh is expected to be more accurate than the sample model and coarse model. The meshes that are fine density can be difficult to solve accurately but also take longer computational time to solve; thus, the good strategy was to do simulation with coarse mesh after that start simulation until to achieve great accuracy. The predicted (finer mesh model) simulation results are shown to be in good agreement with the measurement results, meaning high accuracy.With the recent developments in the 3-D simulation of welding, it is now possible to expand the numerical analysis of welding to include hardness measurement testing. The area of the weld-bead joint applied in computations varies between the values of the optically measured minimum and maximum area, as shown in Figure 46 a. Figure 46 b, c and d show the comparison between the prediction and hardness test measurement and show good agreement.

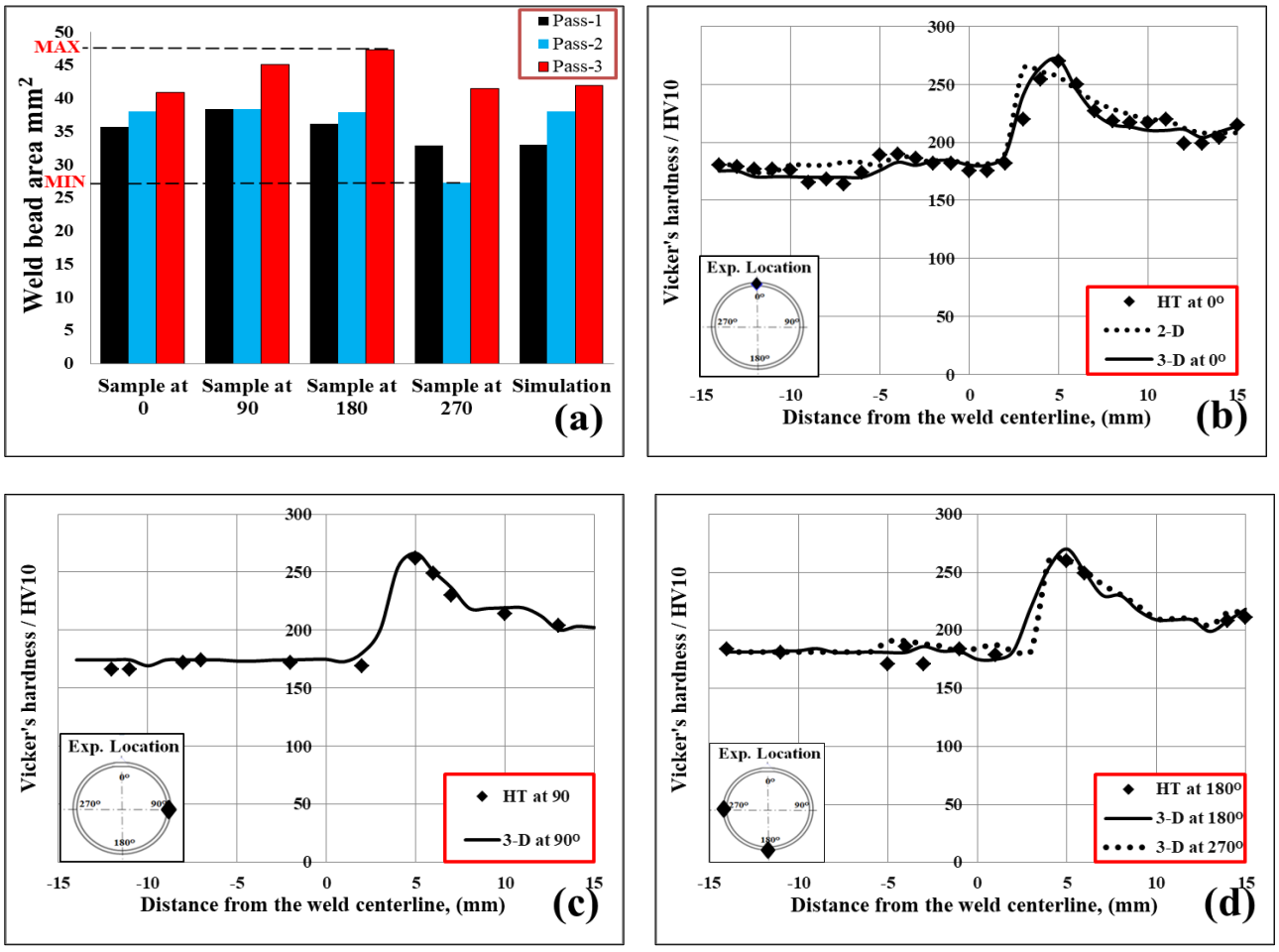

Figure 46. (a) Weld bead profile at different poistion with simualtion (b) Comparsion 2-D, 3-D with HT at 0^O (b) 3-D with HT at 90^O (c) 3-D with HT at 180^O and 270^O

4.3 Validation of the numerical model using phase distribution

A metallographic test on the linear cross-sections of the pipe welded sample is carried out to study the microstructures of the sample's welded zones. The samples are thoroughly polished and then etched with 5% Nital reagent (HNO_3 (5ml) + ethyl alcohol (100 ml)). An optical image

analyser (Leica) is used for microstructure analysis. Microstructure analysis revealed the grain size of the welded sample. After cleaning the surface of the sample, it was burnished by a mechanical grinding machine and polished by a polishing machine. The metal surface was soaked in a mixed solution of HNO_3 and alcohol to reveal the microstructures of various zones under an optical microscope. Microstructures of the welded joint, HAZ-1, HAZ-2, the base metal of dissimilar material and fusion zone are shown in Figure 47. Differences in the microstructures between the welded joint, HAZ, base metal, and fusion line of the welded structures were observed because of the high temperature during welding and subsequent rapid cooling. During the specimen weld, the welded joint, whose microstructure is made of ferrite, and pearlite, is formed through the solidification of the welding pool. Large amounts of pearlite were distributed in the space between granular ferrite and acicular ferrite, making the microstructure of the welded joint finer. Crystal expansion and bulk ferrites of large size appear in HAZ-2 due to the heat input in the weld zone, and a small amount of bainite is generated. Therefore, the microstructure of HAZ is mainly composed of ferrite, with a small amount of pearlite. Each base material (BM-1 and BM-2) has different microstructure before welding: for the region close to HAZ, welding is a heat treatment process that leads to macrostructure change in and around HAZ-1 and HAZ-2. The volume of metal crystal between HAZ and the welded joint increases as more heat is absorbed; moreover, the temperature gradient change of the metal in the fusion line is higher while cooling, leading to the creation of Widmänstatten in some areas of welding.

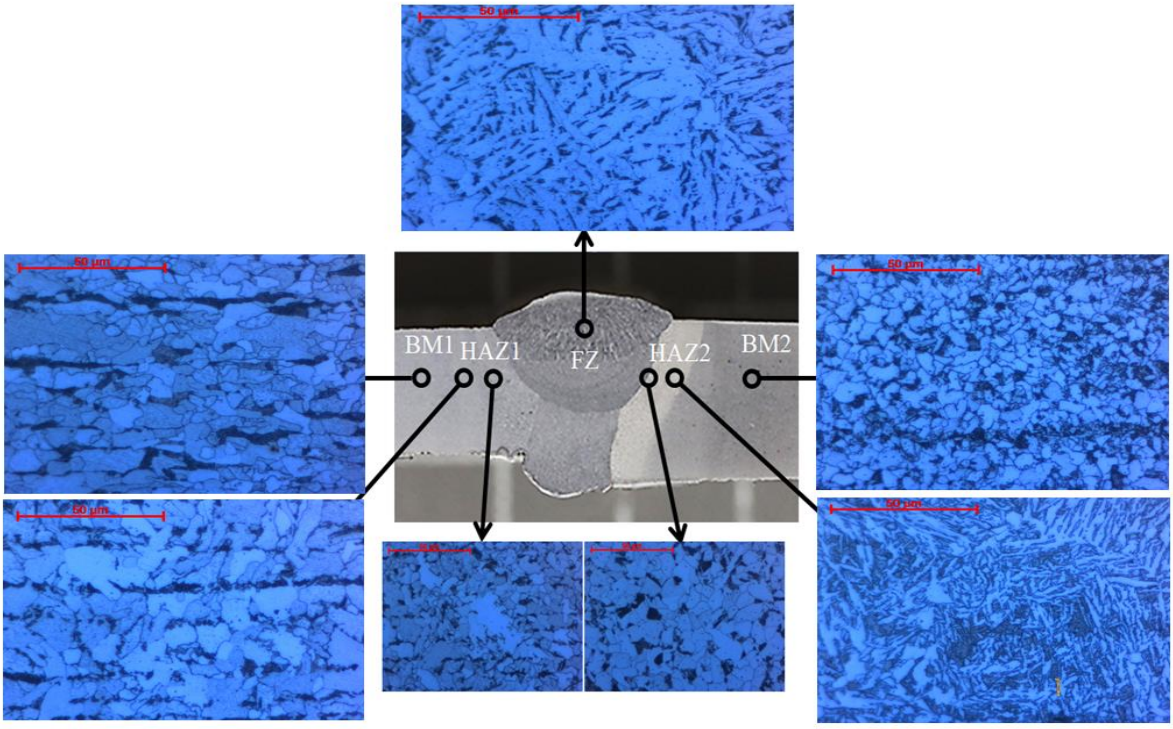

Figure 47. Microstructures of different areas of the welded structure: Microstructure in HAZ-1 and HAZ-2 observation

DOI: 10.14750/ME.2022.004

It is challenging to control metal microstructures between the heat-affected zone (HAZ) and base metal in the weld. Particularly, the control of HAZ is considered a challenge for welding engineers. The differences between the weld metals and base metals are connected with mechanical and metallurgical properties. For example, the weld metal thermophysical coefficient is different from base metals, leading to high stresses that promote service failures because of the thermophysical cycles from low-temperature zones to high-temperature zones. Besides, differences in composition and microstructure may be the leading cause of local variations of the residual stresses in either the weld metal or the transition region.

The HAZ in the multipass weld also shows an interesting evolution of the microstructure; where the HAZ next to the first bead is explained as follow. The HAZ showed higher ferrite fractions in the as-welded condition compared with the base and weld metal. It starts at the beginning of cooling regions as the phase transformations start. Austenite cools down at different rates at different regions. An internal stress state is developed due to the differences in thermal contraction rates and rates of variation of thermo-mechanical properties, Fast cooling regions are loaded in tension, whereas slow cooling regions are loaded in compression transformation plasticity. This leads to unloading and reverse loading on transforming regions while the untransformed regions react to balance those stresses. Transforming regions are loaded in compression whereas the untransformed regions are loaded in tension.

Normally, the weld of pipe using multi-pass welding methods aims to ensure the strength and the homogeneity of the microstructure between weld metals and base metals. Generally, the multi-pass weld characteristics are so complex compared to a one-pass weld because of the thermophysical cycles of subsequent passes that impact the mechanical properties (such as hardness, tensile strength, the microstructure, and the residual stresses after cooling ambient temperature).

Figures 48 and 49 show the HAZ-1 and HAZ-2. It is clear that the HAZ-2 is larger than HAZ-1. In terms of multi-pass welding, the HAZ-2 in the low-carbon steel might correspond to the Fe-C phase diagram. It can be seen that the gradual change in the grain size occurred from the fusion line to BM-2. In the next fusion line, in location (D), the average grain size was the largest, and this grain size decreased at BM-2 in location A. Widmanstatten ferrite phases were thought to be formed along grain boundaries and in and around the HAZ-2. Furthermore, this is thought to be due to the variations in peak temperature, as well as the cooling rate. In the case of weld material, the temperature was relatively high (near the melting point). This temperature allows the austenite phase to be fully formed. Austenite phases were transformed into ferrite and pearlite phases or bainite phases.

DOI: 10.14750/ME.2022.004

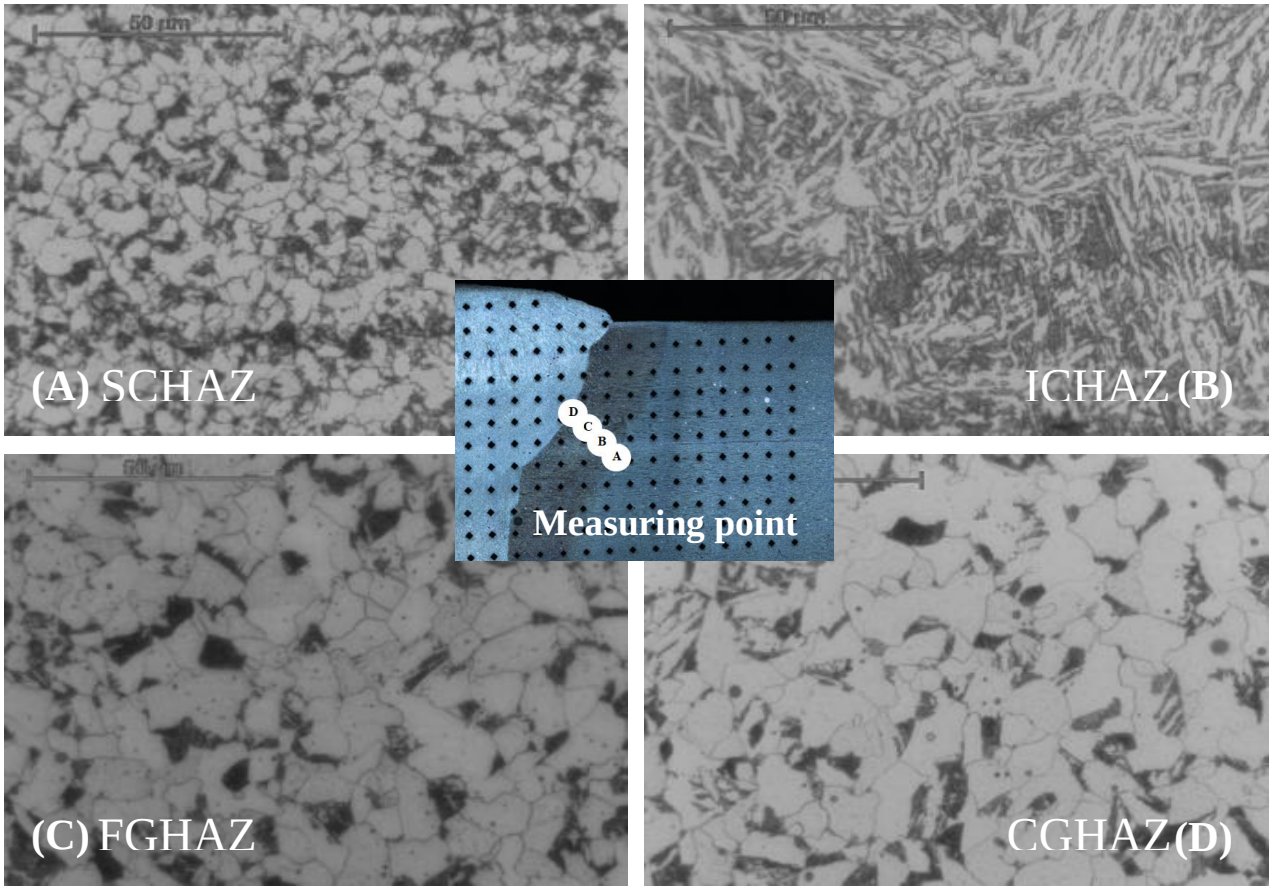

Figure 48. Microstructure of HAZ-2

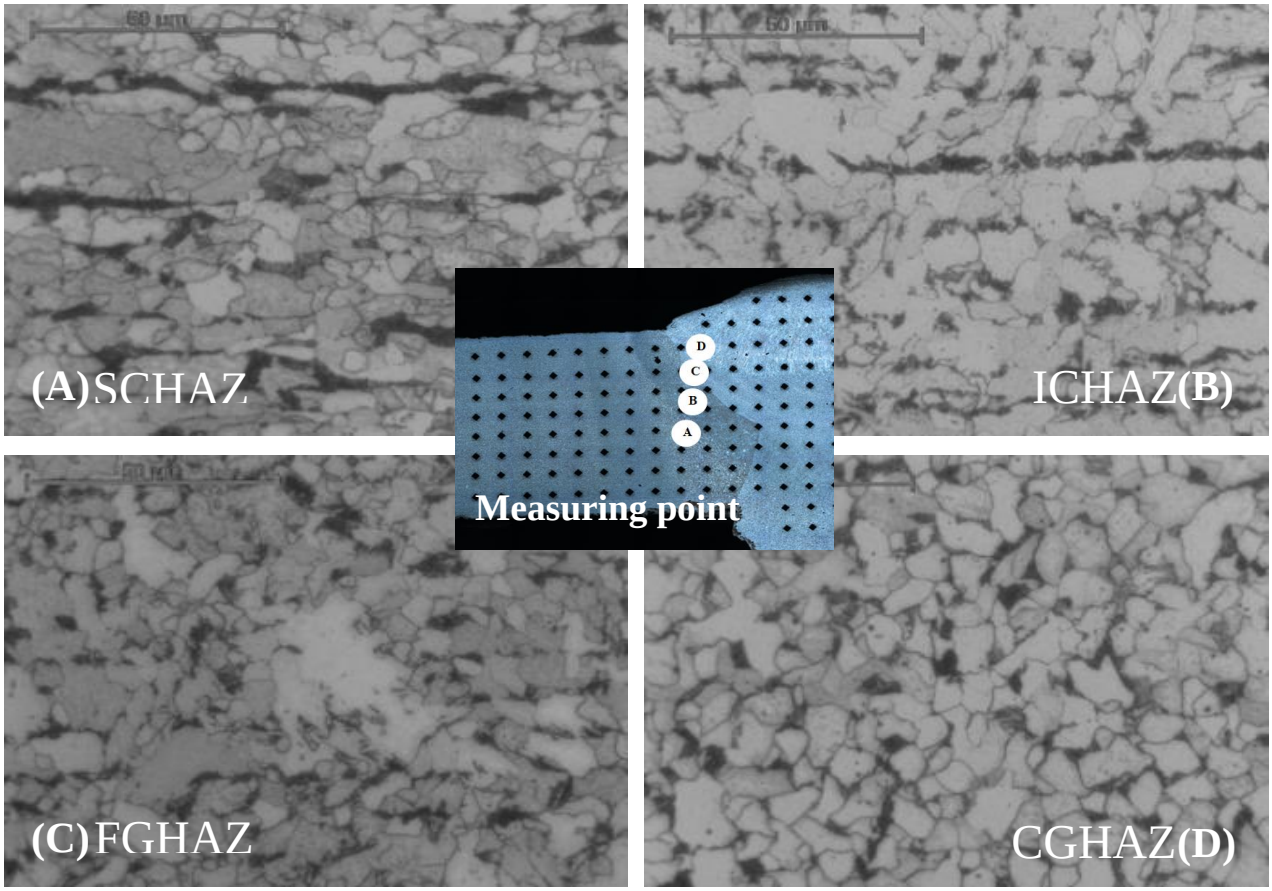

Figure 49. Microstructure of HAZ-1

DOI: 10.14750/ME.2022.004

Figure 50 shows the predicted microstructure constituent distributions in the simulated weld specimen. In the simulation of phase transformation, the thermo-metallurgical model allows calculation not only of the magnitude of temperature distribution but also ofeach metallurgical phase in the weld zone. The distribution of the phases, which it is possible to calculate, gives information about the dissimilar welding material that undergoes metallurgical changes due to the interaction of the welding. Information on phase distribution is provided by the shape of the distribution. Analysis of the calculated metallurgical phases indicates that the amount of martensite was nearly 0%, and the maximum amount of fraction of ferrite was in BM-1, which was about 16%. It ranges between 4% and 9% in the middle portion (the area between BM-1 and BM-2) and BM-2, respectively. The maximum amount of pearlite was about 75% in BM-2, and in the middle of the joint and BM-1, it was about 17% and 50%, respectively.

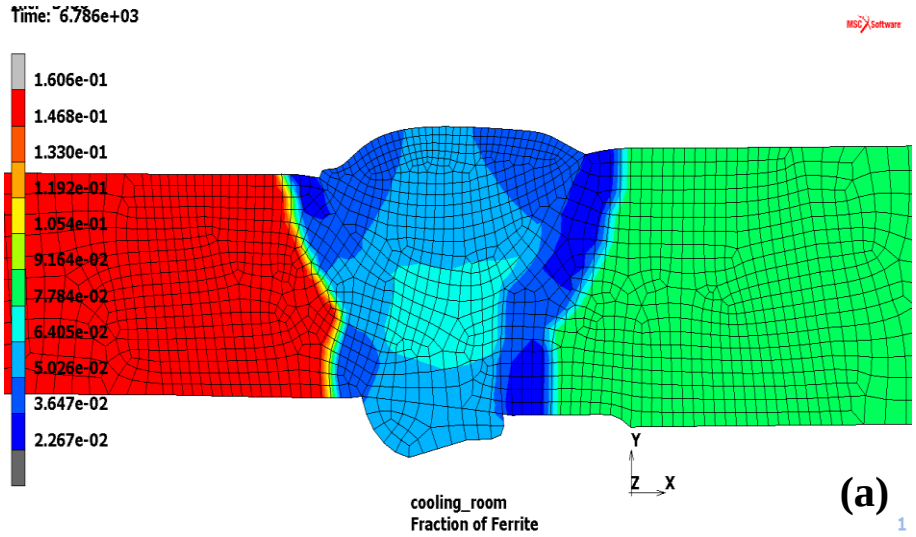

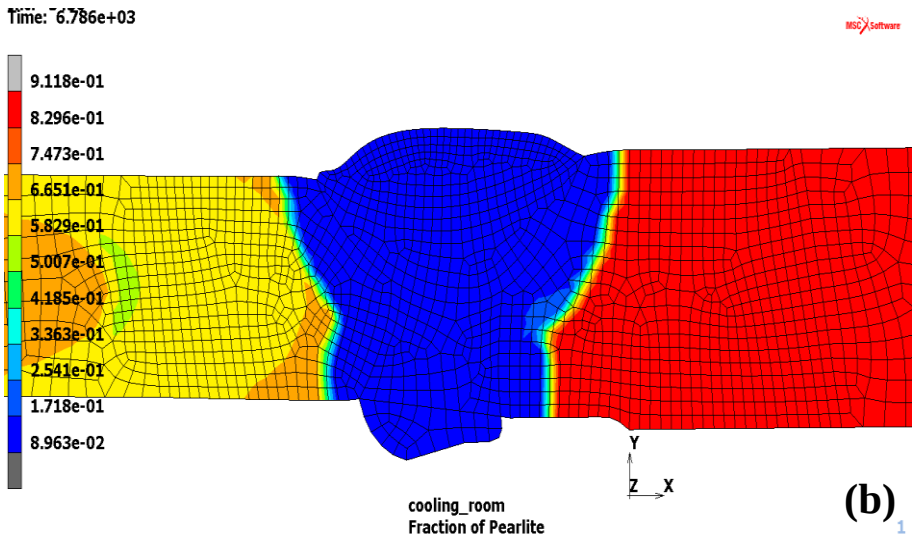

DOI: 10.14750/ME.2022.004

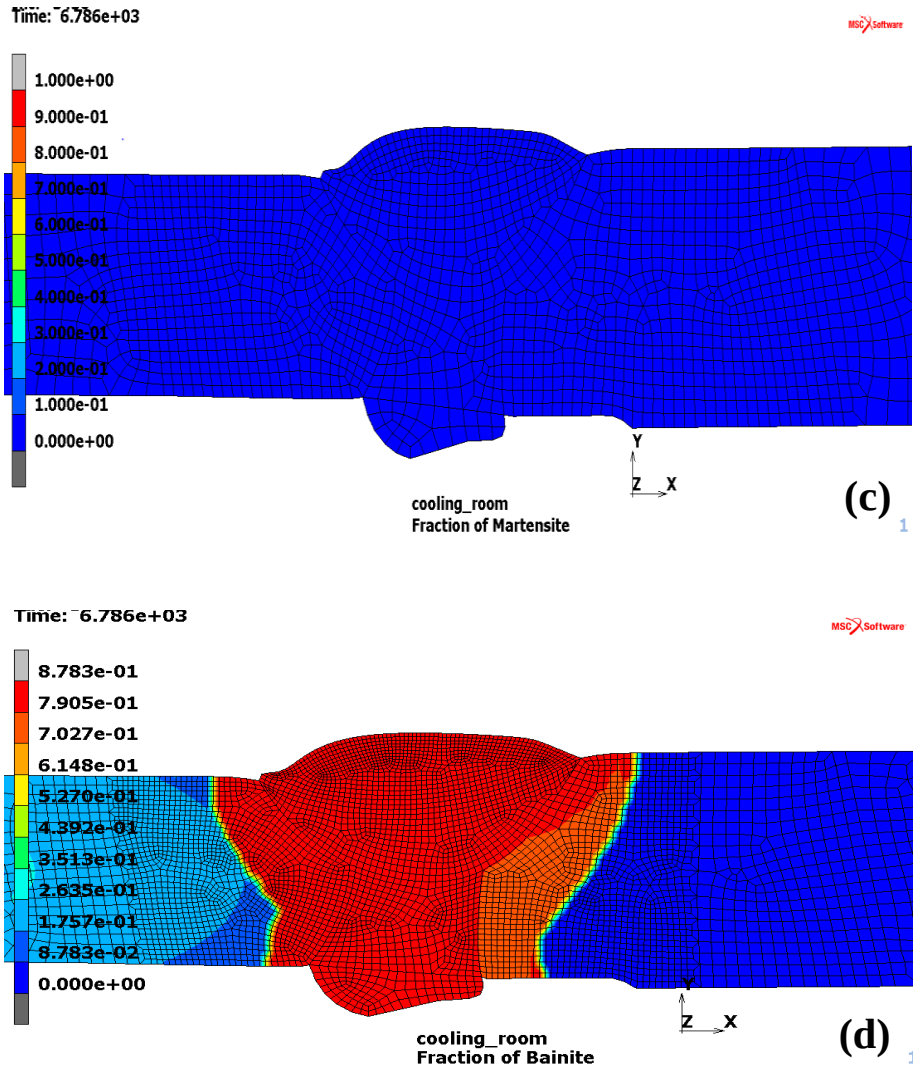

Figure 50. Distribution of (a) ferrite (b) pearlite (c) martensite (d) bainite phases of the simulation weld zone

4.4 Validation using the comparison of sectional morphology

MSC Marc software can predict fusion-zone profiles with reasonable accuracy over all three passes. The resulting final fusion zone is indicated by the region with the temperature above 1650 °C. The heat affective zone (HAZ1) and (HAZ2) are outlined approximately by the temperature interval between about 1000 K and 1700 K. The temperature-dependent mechanical and thermophysical properties were taken into account in the calculation, as shown in Figure 51. The equilibrium transformation temperatures for the formation of austenite from an initial microstructure and the decomposition of austenite into ferrite/perlite, bainite and martensite are required. Material properties, based on their chemical composition, were determined using JMatPro software. The temperature-dependent, elastic-plastic phase-dependent material model was used in the simulation.

DOI: 10.14750/ME.2022.004

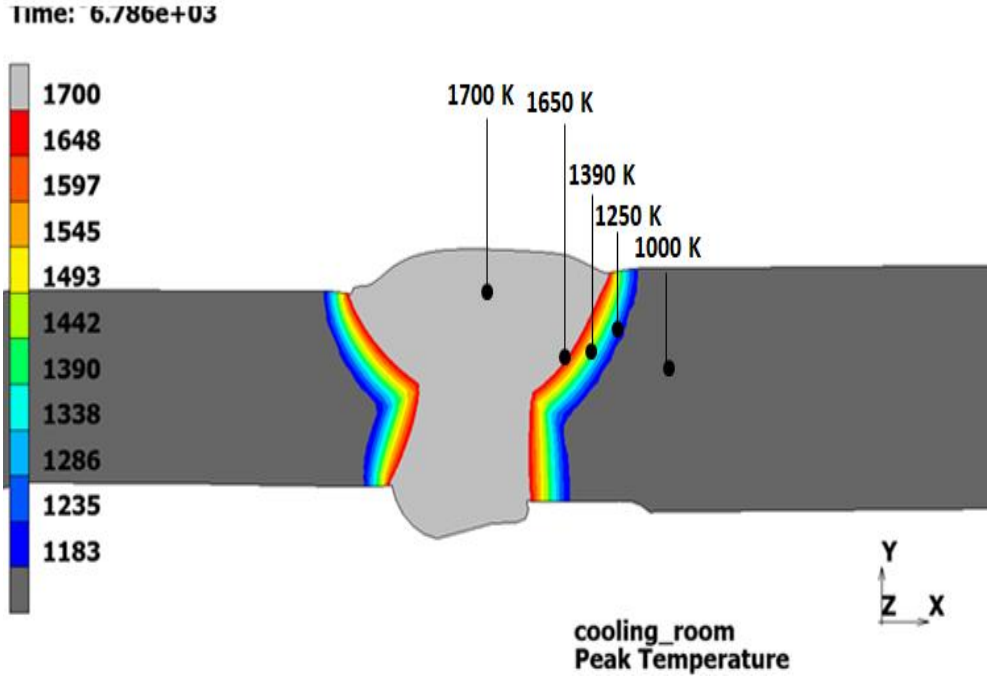

Figure 51. The temperature profile in the dissimilar weld joint in [K]

From Figure 52, it was demonstrated that numerical results and experimental data under the same parameters were in good correspondence. The top of the third layer weld presented a smooth arc-shape. The double ellipsoid heat source models were used for all passes to successfully simulate the shape of full-penetration weld. Thus, it was verified that the heat source model was valid and could be used to simulate the weld morphology and temperature field accurately.

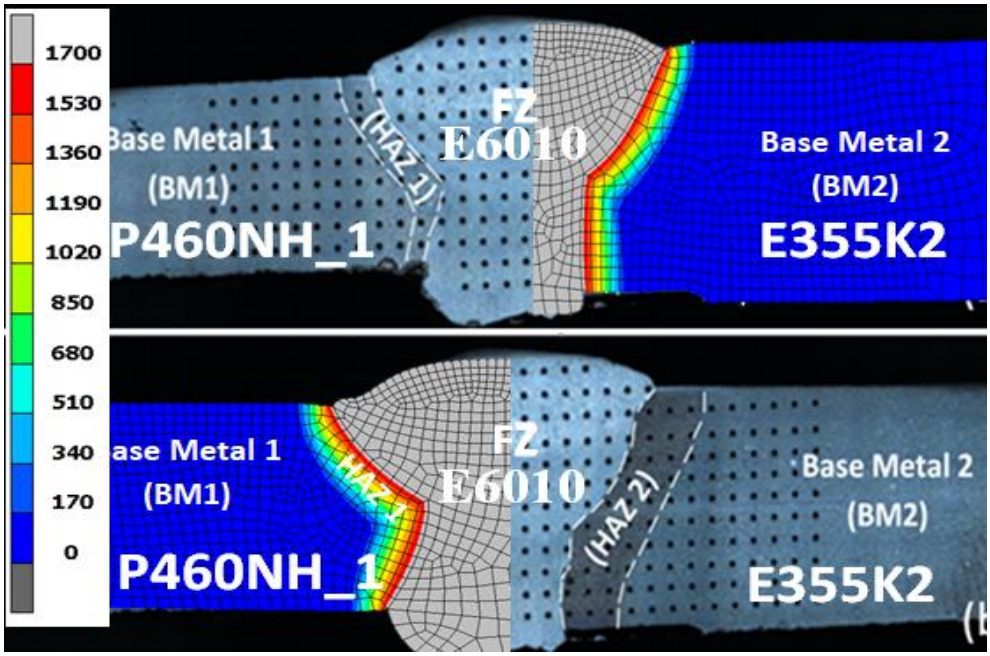

Figure 52. Simulated temperature distributions in the cross-section in [K]

DOI: 10.14750/ME.2022.004

Figure 53 shows the temperature histories at the weld centreline and further from the weld zone. From this figure, it can be seen that the peak temperature at the centre of the weld pool is about 1700 °C. In the same figure, it can also be observed that the difference between the peak temperature at the HAZ-1 and HAZ-2 is not significant. The thermophysical effects due to solidification in the weld zone are considered in the FE model, so these two cooling curves reflect the weld pool's solidification phenomena. Except for the peak temperature, the temperature history curves in the fusion zone have no difference.

The temperature histories in the middle of the cross-section of weld through and along the heat-affected zone (HAZ-1 and HAZ-2) of the mid-section were simulated. The distance between different positions and the weld centerline is 7 mm. This figure indicates that both HAZ-1 and HAZ-2 have almost the same peak temperature and an identical cooling rate. In the FE model, the fusion zone's pipe thickness is less than 11 mm, and the pipe thickness is only 8 mm in the other parts. The materials were well chosen, which resulted in an even temperature distribution through thickness during welding.

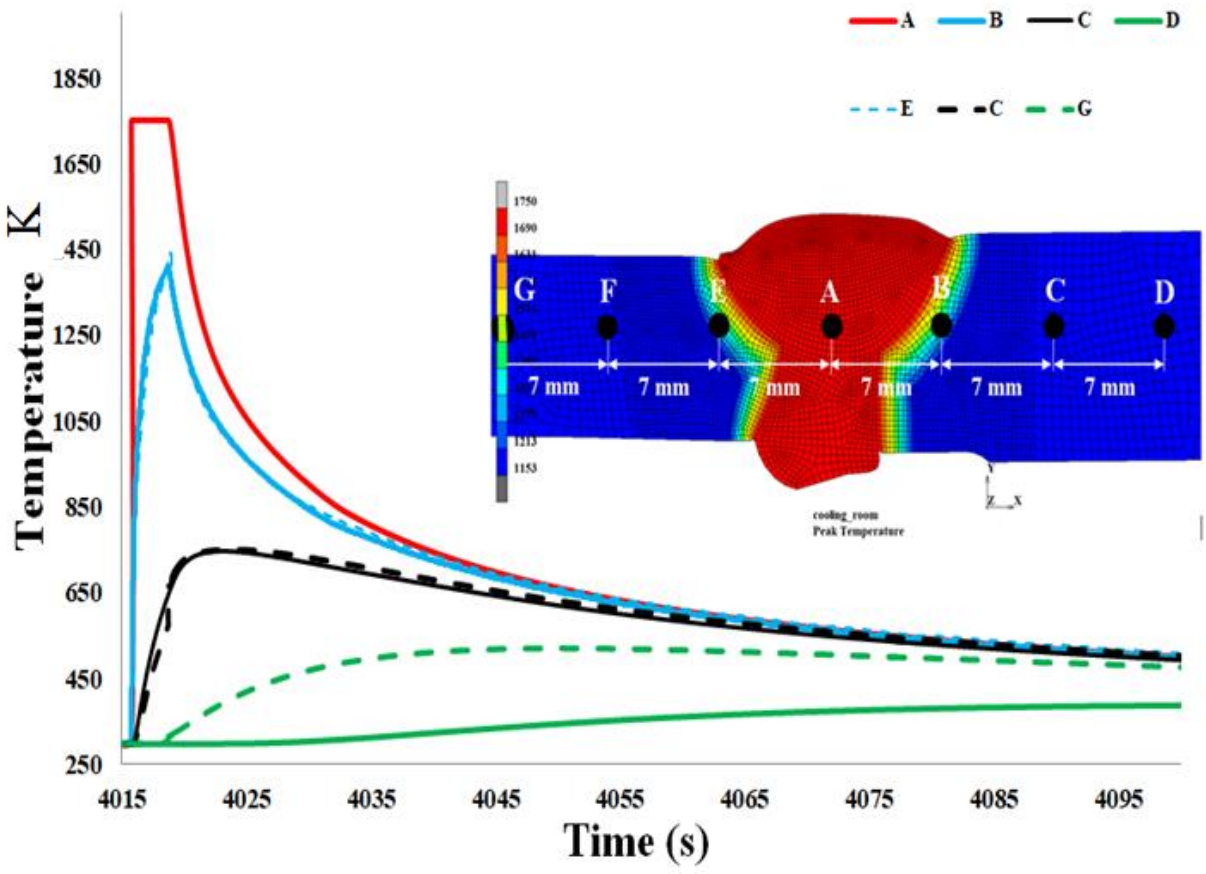

Figure 53. Temperature histories [K]

DOI: 10.14750/ME.2022.004

5. RESULTS AND DISCUSSION

5.1 Prediction of Numerical simulation model and comparison of the residual stress using XRD: accuracy data

XRD residual stress measurements were performed near the weld zone rather than on the distorted superficial layer cap weld pass because the weld metal was not clear enough. To avoid error and to receive more accurate results, a weld bead sample for XRD measurement should have a smooth flat surface. If the surface is not smooth and flat, X-ray absorption may reduce the intensity of low angle peaks. Therefore we measure the residual stresses in the heat-affected zone; residual stresses were measured at several locations and the base metal pipe as well. Figure 54(a) shows the XRD measurement setup, and the directions of the paths of XRD measurement of residual stresses (Figure 53(b)) were calculated using the robotized solution for measuring stresses.

The $\sin^2 \psi$ X-ray methodology for stress determination was used.In this work, residual stresses were analysed in a steel pipe joint, with 133 mm (5.236 inches) outside diameter with the different thickness that was the girth welded with MMAW (all weld passes). Residual stresses were measured using XRD on both sides on the outside surfaces near weld start and stop positions at 0° and 90° degrees, as shown in Figures 55(a) and (b). Transverse residual stress (axial, σ_x) and circumferential residual stress or (hoop stress) (σ_ϕ) were measured by XRD at 0 and 90 locations, and the magnitudes of residual stress are different among them, both show compressive. In this study, it was assumed that the stress component in the radial direction (σ_r) could be neglected.

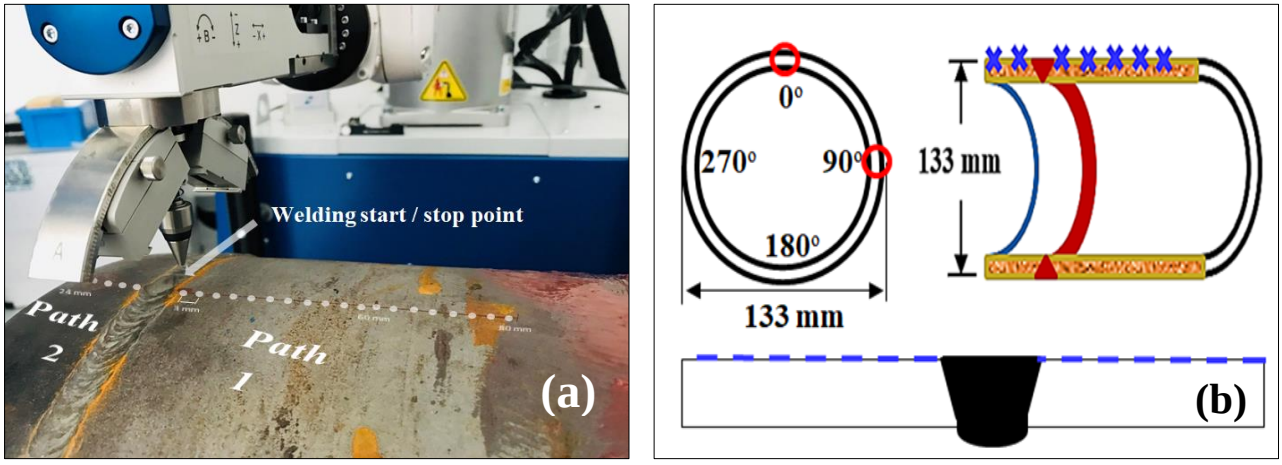

Figure 54. The XRD measurement: (a) welding start/stop point and paths (b) locations of residual stress measurements

DOI: 10.14750/ME.2022.004

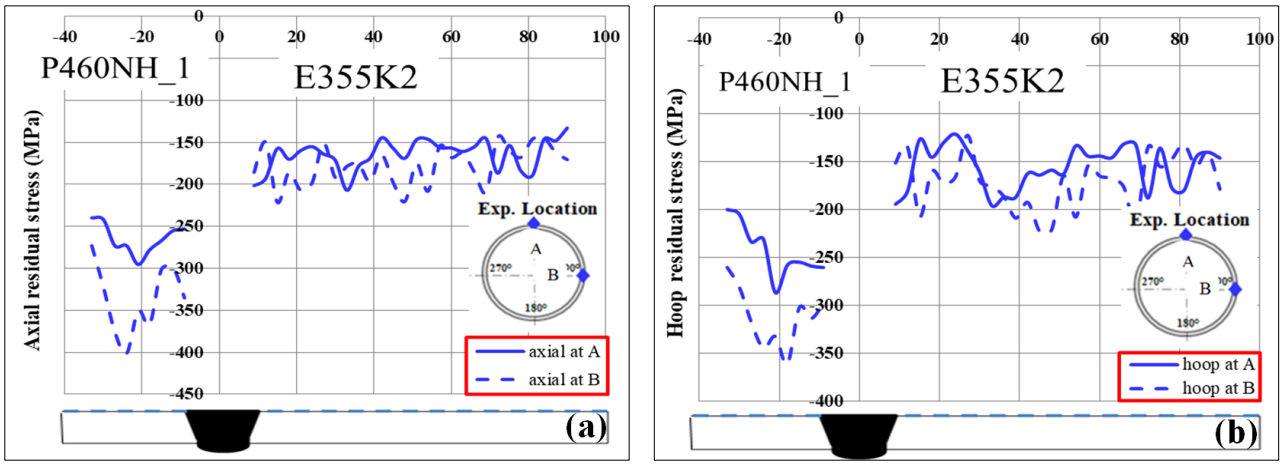

Figure 55. RS measurement results from XRD (a) axial stresses (b) hoop stresses

5.2 Comparison of the Numerical and Measured Residual Stress using 2-D model

To investigate the detailed local axial and hoop residual stress distributions, the 2-D element model with a fine mesh (see Fig. 56(a), (b)) was used to verify the developed model computational approach's prediction accuracy based on MSC Marc software. The axial and hoop residual stress distributions on both sides' outer surfaces measured by experiment used XRD and simulated by FEM were compared.

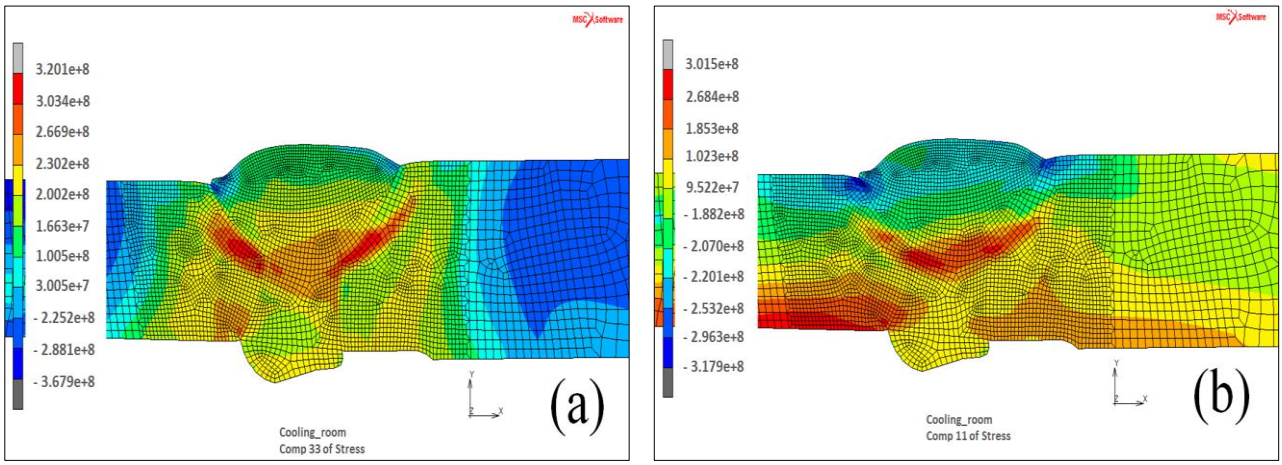

Figure 56. RS calculation results achieved by 2-D numerical simulation model (a) axial residual stress; (b) hoop residual stress [Pa]

Figure 57(a) shows that the maximum axial residual stress under compression is located at the interface on the outer surface and has a magnitude of 160 MPa on the E355K2 side and 290 MPa P460NH_1 side. Figure 57 (b) also indicates the hoop residual stress distributions on outer surfaces, and compressive hoop residual stresses are generated on the outer surface, the weld in HAZ-1 and HAZ-2 and stresses were increased sharply and reach maximum compressive stress of

DOI: 10.14750/ME.2022.004

about 200 MPa, which is seen near weld centreline. By comparing numerical simulation predictions and the XRD measurements, it is concluded that the 2-D model developed by the present work gives acceptable results for hoop residual stress distributions. Still, there are some slight discrepancies between the numerical results and measured data in the axial residual stress in the dissimilar pipe joint, that we can use further to change some welding parameters. In other words, the computational approach developed by the present study has been verified through the experiment. In the next section, we will discuss the influence of different parameters on the final residual stress distribution only based on the simulation results.

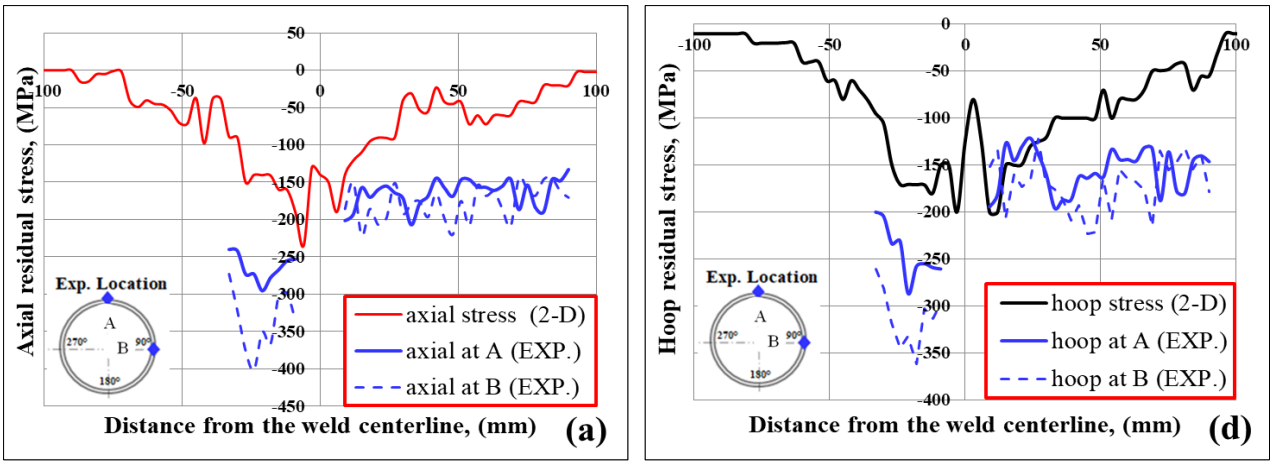

Figure 57. Comparison of finite element model residual stresses simulation and X-ray diffraction measurements outer surface of pipe: (a) axial residual stresses on the outer surface; (b) hoop residual stresses on the outer surface

5.3 Residual Stresses through the Thickness

Figure 58 (a) shows that the axial stresses are compressive at the outer pipe surface and stay compressive to about 4 mm from the outer surface into the thickness. These stresses become tensile at the inner surface in FZ. In Figure 58 (b), the hoop or circumferential stresses are tensile but decrease to compressive far away from the weld centerline.

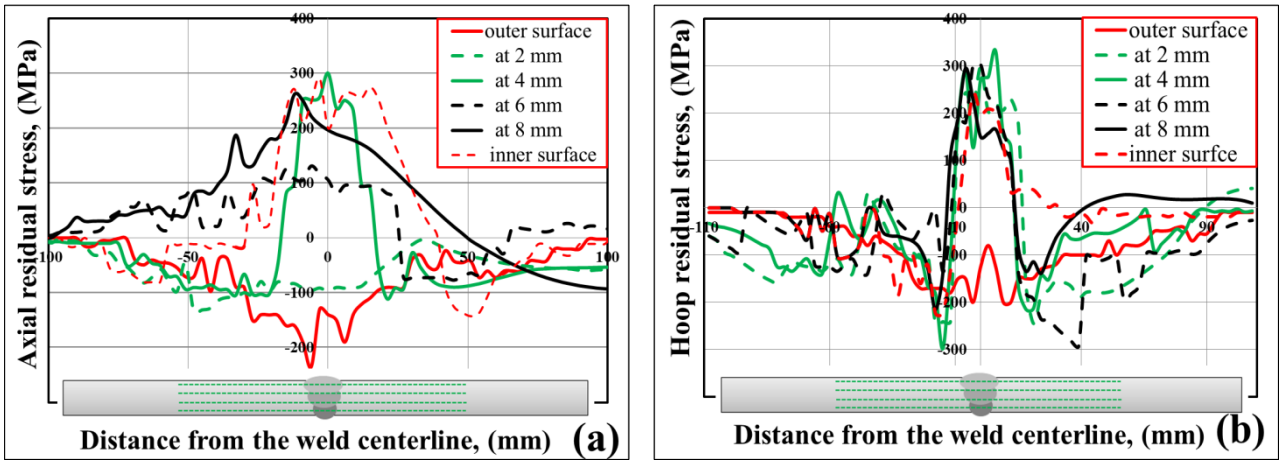

Figure 58. (a) Axial residual stress; (b) hoop residual stress distribution through the thickness

DOI: 10.14750/ME.2022.004

5.4 Prediction of residual stress generated by dissimilar pipe manual arc welding considering the phase transformation

Figure 59 shows the case of the comparison between 2-D models in the same condition of thermophysical and mechanical analysis, the model that predicted axial residual stresses and hoop residual stresses in the outer surface using phase transformation properties in the material database showed an acceptable agreement with experimental results, whereas, in another FE model considered without phase transformation in the outer surface, there is large difference in numerical simulation predictions.

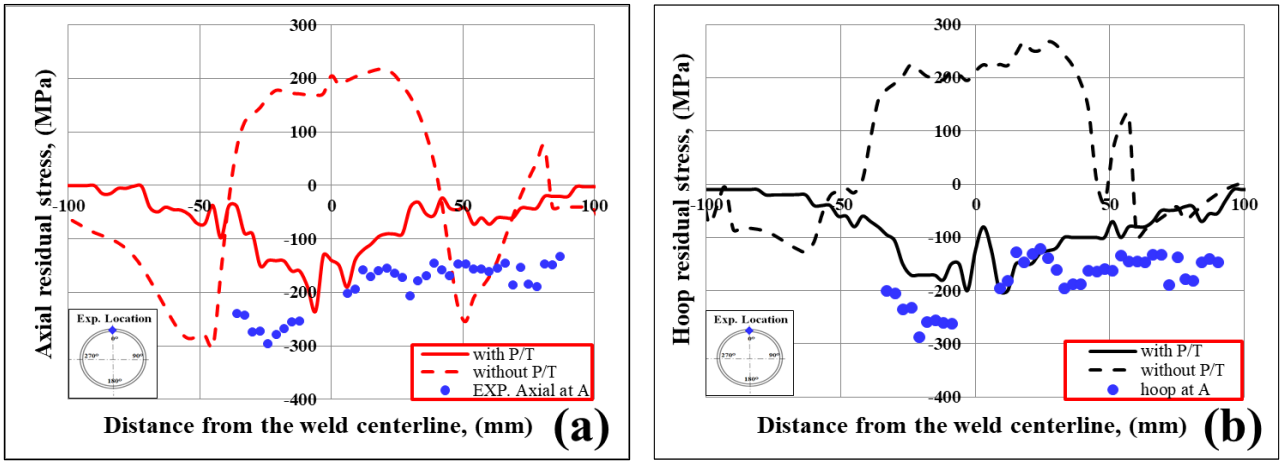

Figure 59. Predicted residual stress distributions using 2-D model on the outer surface with and without phase transformation: (a) axial residual stress; (b) hoop residual stress

5.5 Effect of Welding Parameters on Residual Stresses

5.5.1 *Effect of Heat Input on Residual Stresses*

The models with different heat input cases were established to discuss the influence of heat input effect on residual stresses, as shown in Table 8.

Table 8. Cases of changing the heat input

Cases	Pass No.	Current (A)	Voltage (V)	Speed mm/s	Heat input KJ/mm
Case-1 (low)	Pass 1	64	18.56	2	28.508
	Pass 2	72	18.88	2	32.625
	Pass 3	80	19.2	2	36.864
Case-2 (Medium)	Pass 1	80	23.2	3	29.696
	Pass 2	90	23.6	3	33.984
	Pass 3	100	24	3	38.4
Case-3 (High)	Pass 1	96	27.84	4	32.072
	Pass 2	108	28.32	4	36.703
	Pass 3	120	28.8	4	41.472

Figure 60 (a) and (b) shows the influence of heat input on the residual stresses on the outer surface. It is shown the residual stress distribution is increased for the entire peak with almost the same heat input increasing. Figure 61 shows the effect of heat input on residual stress on the inner surface. It is also observed that the heat input did not affect the hoop residual stress distribution law. The hoop residual stresses distributions follow almost the same trend.

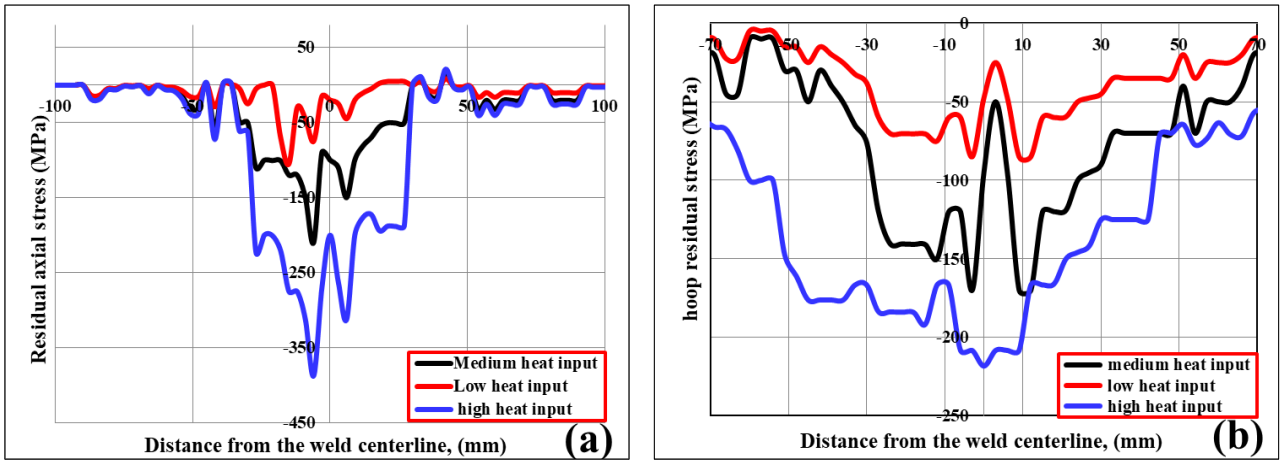

Figure 60. Effect of heat input on (a) axial residual stress; (b) hoop residual stress distribution along the outer surface

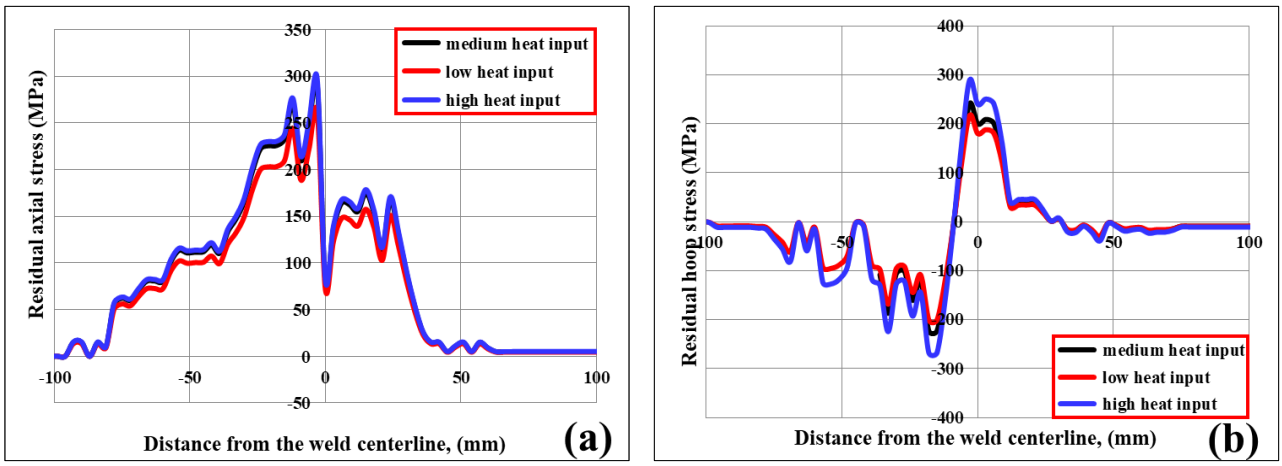

Figure 61. Effect of heat input on (a) axial residual stress; (b) hoop residual stress distribution along the inner surface

5.5.2 *Effect of Current on Residual Stress*

The residual stress calculation of weld pipe and weld distance and three cases (70 A, 80 A and 100 A) with the same heat source model are shown in Table 9. From both Figures 62 (a) and (b), it can be observed that the range of stress becomes wider with increasing welding currents. To clarify the influences of welding current change on welding residual stress, stresses at the outer and inner surfaces from the weld start point are considered for various welding current combinations in multi-pass welding. Three main regions on the inner weld surface (HAZ, FZ and BM) of the axial residual

DOI: 10.14750/ME.2022.004

stress in the weld are shown in Figure 63 (a) compressive stress (regions BM-1, BM-2, HAZ-1, HAZ-2 and FZ) and tensile stress (region FZ) in case B. For welding currents (case A) with current 70 A, the limit of stress is about 455 MPa in tension and 213 MPa in compression on the outer and inner weld surface. But for the 100 A case, the maximum stress range is 800 MPa and in tension and 650 MPa in compression. The same is true for the pipe's inner surface stress plot, shown in Figure 63 (b).

Table 9. Cases of changing the current

Cases	Pass No.	Current (A)	Voltage (V)	Speed mm/s	Heat input Kj/mm
Case A	1	70	10	3	11.2
	2	70	12	3	13.44
	3	70	10	3	11.2
Case B	1	80	12	3	15.36
	2	80	15	3	19.2
	3	80	12	3	15.36
Case C	1	100	10	3	16
	2	100	12	3	19.2
	3	100	10	3	16

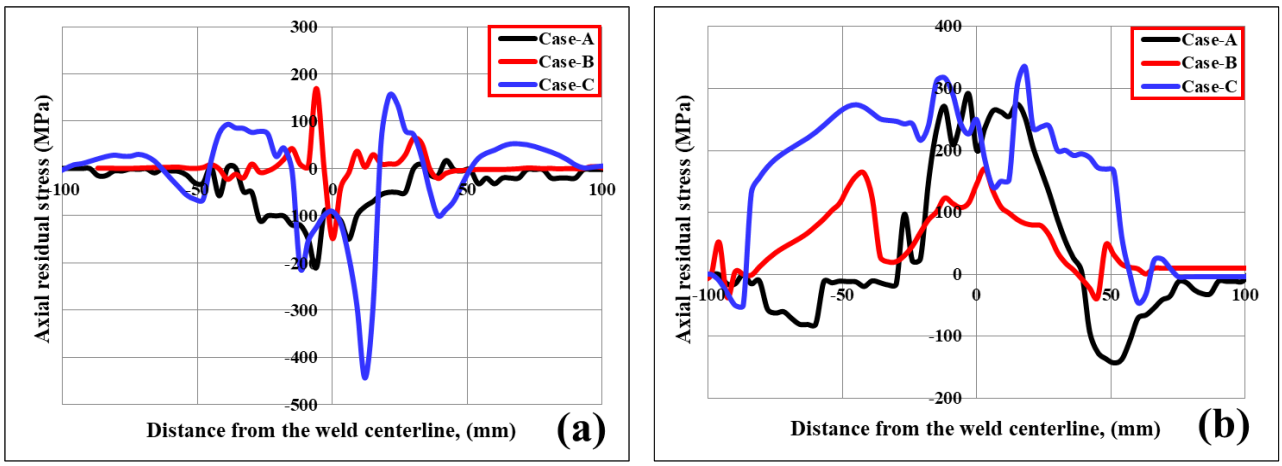

Figure 62. Variations of axial residual stress with welding current (a) outer surface (b) inner surface

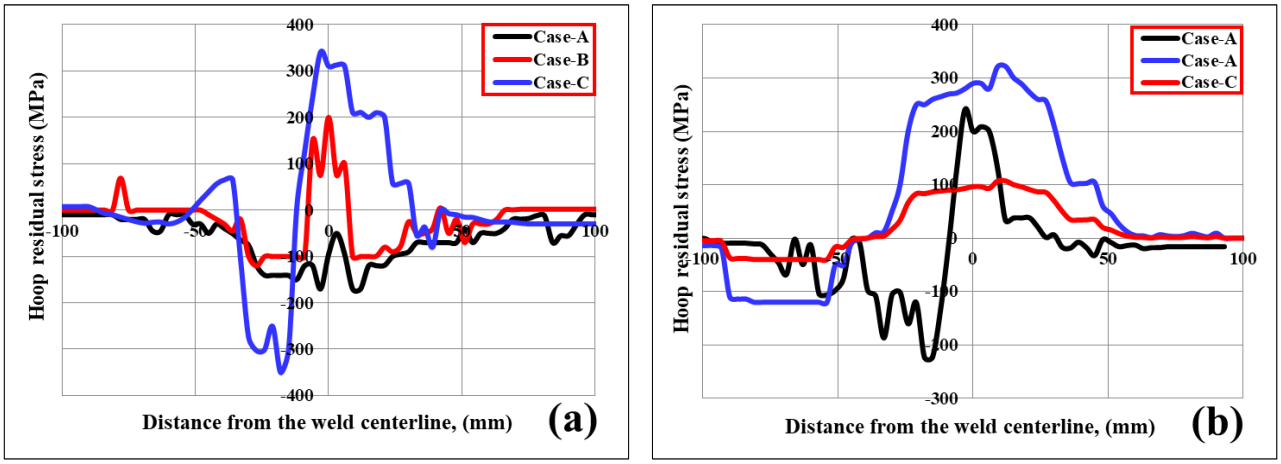

Figure 63. Variations of hoop residual stress with welding current (a) outer surface (b) inner surface

DOI: 10.14750/ME.2022.004

5.5.3 *Effects of Travel Speed Arc Welding on Residual Stresses*

Approximately the same weld size was produced with various arc travel speeds of 2 mm/s, 4 mm/s (average) and 10 mm/s and for all cases the heat inputs are constant. A higher welding speed not only affects the amount of adjacent material affected by the heat of the arc, but also progressively decreases the hoop residual stresses, the difference lies in the fact that the higher travel speed welding technique produced a slightly narrower isotherm. This leads to the weld zone's shrinkage, accounting for why faster welding speeds generally result in less residual stresses. The distribution of axial and hoop residual stresses for the three cases along the line on the outer and inner surface is shown in Figure 62 and 63. It can be seen from Figure 63 (b) that the peaks of axial stress in the three cases do not display significant differences. Figure 64 (b) shows the distributions of hoop stress; it can be seen that they have the same trend at different welding speeds. Peaks of the tensile hoop stress increase from 300 MPa to 390 MPa at weld centreline when the arc travelling speed increases from 2 mm/s to 10 mm/s, and 450 near the WCL.

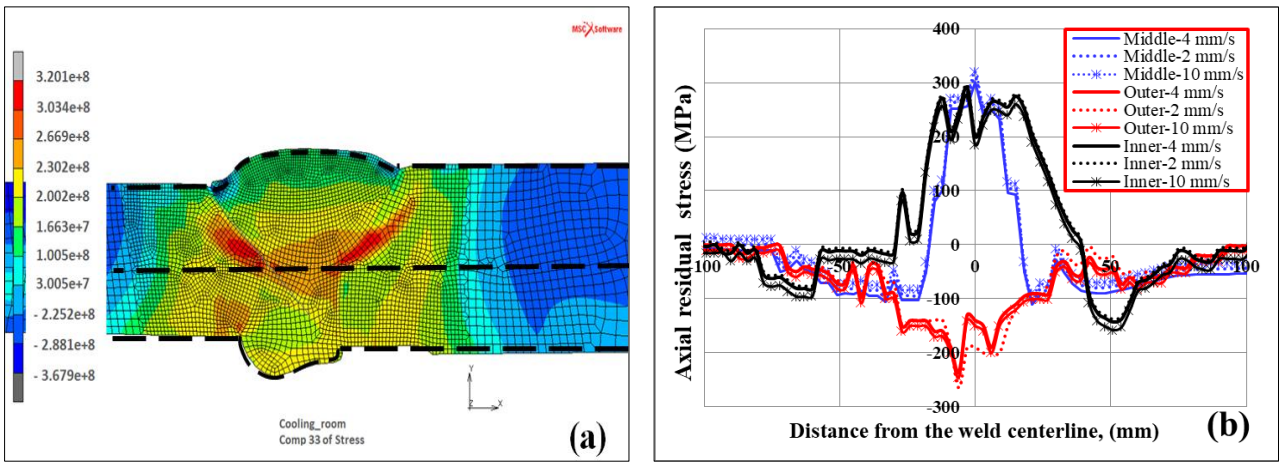

Figure 64. (a) The line to investigate the axial stresses [Pa] (b) axial stress distributions at different arc travelling speed distributions along the cross-section weld line

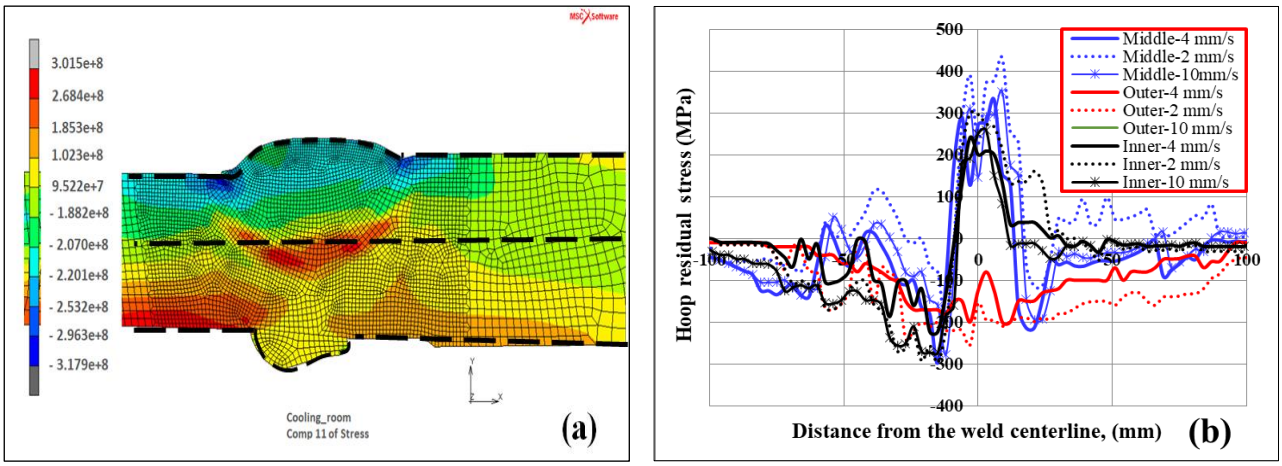

Figure 65. (a) The line to investigate the hoop stresses [Pa] (b) hoop stress distributions at different arc travelling speed distributions along the cross-section weld line

DOI: 10.14750/ME.2022.004

5.5.4 *Effects of External Mechanical Constraints on Residual Stresses*

The thermophysical and mechanical behaviour of weldments could be readily manipulated through external constraints. For a circumstance in which an external constraint restrains the lateral joints contraction, Figure 65 depicts the distribution of transverse residual stresses. Moreover, the fact that the degree of the transverse shrinkage of a restrained joint is reduced accounts for the magnitude of the residual stresses with a restrained joint being larger than that estimated with an unrestrained joint.

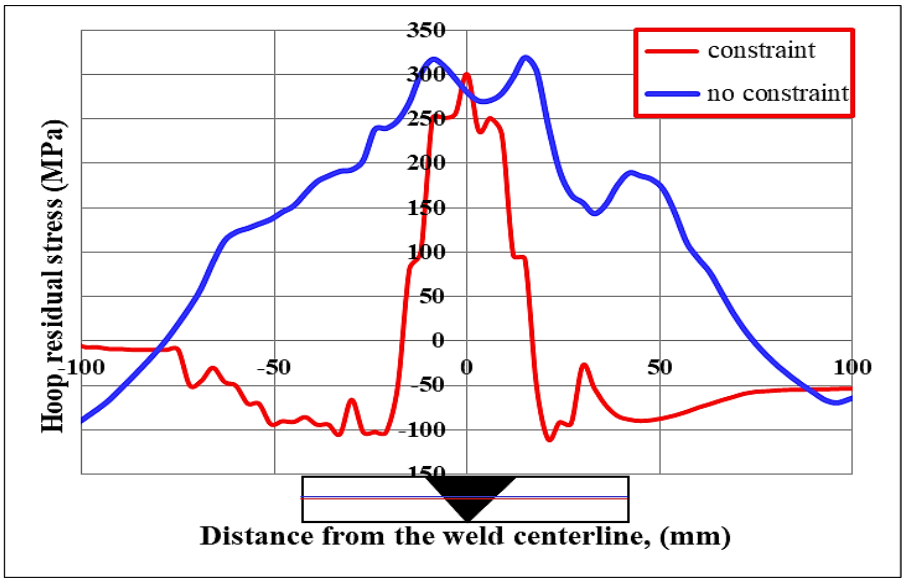

Figure 66. The effect of mechanical constraint on hoop residual stresses

5.5.5 *Effect number of passes on Residual Stresses*

The conditions for different passes of welding are listed in Table 10. The parameters for each case are mentioned separately for different passes. The amount of voltage and welding speed in all welding passes were 14.5 V and 10 mm/s. The axial and hoop residual stresses on the middle of the thickness of pipes were influenced by the pass number. As shown in Figure 67 (a) the peaks of axial stress were the highest in the case of using three-pass welding. While the residual stress is tensile with the amount of 310 MPa, in contrast, the areas far from the weld centre are compressive with 300 MPa (for two passes weld showing). The six-pass weld has the lowest residual stress, as it is the tensile maximum (200 MPa) and compressive (110MPa). As shown in Figure 67(b), peaks of tensile hoop stress were the lowest for six-pass weld with the amounts of 201 MPa. The tensile hoop stress's highest values were achieved using a two-pass weld with the amounts of 413 MPa. Generally, by comparing between (a) and (b), it can be deduced that the pass number (compared to pipe metal type) has no significant effect on residual stresses besides producing a bit more variations with two-pass welds.

DOI: 10.14750/ME.2022.004

Table 10. Parameter of multi-pass welding on dissimilar material pipes Parameter of multi-pass welding on dissimilar material pipes

Cases	Pass No.	Current (A)	Voltage (V)	Speed (mm/s)	Heat input (KJ/mm)
Two-pass welds	Pass 1	125	25	5	30
	Pass 2	124	25	5	29.79
Three-pass welds	Pass 1	80	23.2	5	17.818
	Pass 2	90	23.6	5	20.39
	Pass 3	100	24	5	23.04
Five-pass welds	Pass 1	70	19	5	12.7
	Pass 2	70	19.2	5	12.76
	Pass 3	70	19	5	12.768
	Pass 4	70	19.1	5	12.768
	Pass 5	70	19	5	12.7

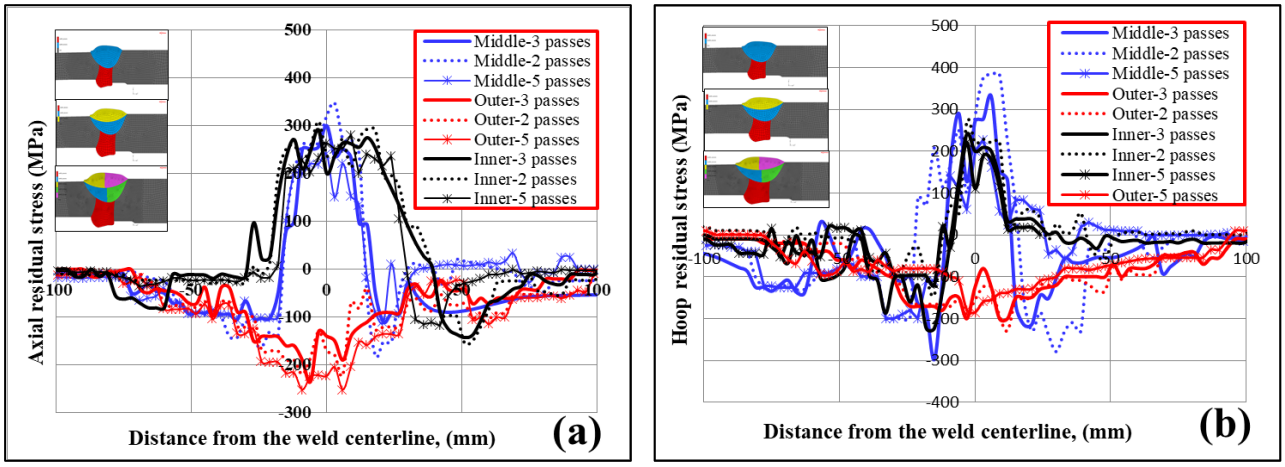

Figure 67. Effect number of passes on residual stresses: (a) Axial stresses and (b) Hoop stresses

5.5.6 *Effect of root gap on residual stresses*

The gap between the two metals to be welded should not be too small to enhance proper welding operation. Otherwise, the root would be inadequately fused during welding, and the weld would be reduced. On the other hand, the gap should be not set too large because the weld metal would simply pass through it. The function of the gap between adjoining root faces is to increase the depth of penetration down to the root of the weld. The effect of the gap welding shape joint on residual stress was investigated by keeping the rest of the welding parameters constant. Three sample models with a gap of 1 mm, 2 mm, and 4 mm were used to discuss the influence of gap root. It can see that the gap slight affects residual stress, as shown in Figure 68 (a) and (b). The distributions of all the residual radial stresses have a slight difference. The predicted residual stress distributions in the axial and hoop direction resulting from outer and inner surface or through thickness show same trend.

DOI: 10.14750/ME.2022.004

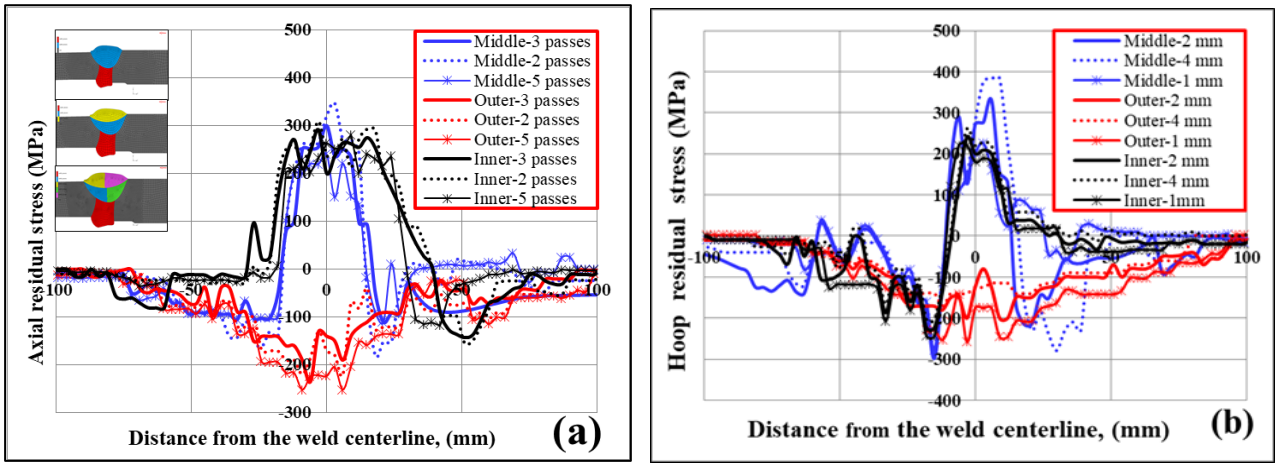

Figure 68. Effect of the root gap on residual stress: (a) axial stress (b) hoop stress

5.5.7 *Effect of the weld groove shape*

Three mock-ups sample models with different groove types (V-groove, J-groove and U-groove) are studied. The different groove shapes have a significant effect on temperature history and the shape of HAZ. The influences of groove type on residual stress of pipe weld joint were investigated by numerical simulation. Welding temperature cycles, residual stress distributions in V, J and U groove joints were calculated by using the proposed computational procedure. The simulation results show that the groove type no significantly affects the magnitude and distribution of residual stresses in welded pipes. The numerical simulation results showed that the axial stress in the V-groove joint is the same as in the other two joints, while the hoop stress in the U-groove joint is significantly wider than that in the V-groove or J-groove joint. Also, the peak value of hoop tensile stress of the V-groove joint is much higher than that of the other two joints, as shown in Figure 69 (a) and (b).

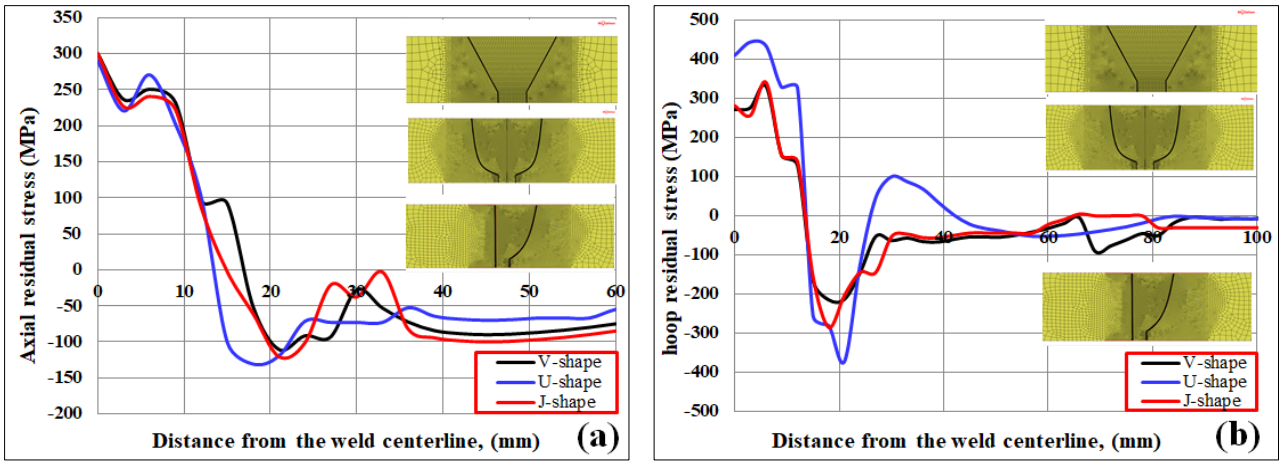

Figure 69. Distribution of the residual stress in the axial direction of three different weld groove shapes studied here (a) axial stresses (b) hoop stresses

DOI: 10.14750/ME.2022.004

5.5.8 *Effects of Thickness on Residual Stresses*

Another characteristic of the residual stress results is shown in Figure 70, related to pipe thickness. Results show a pipe with 11 mm thickness has a larger zone of influence of the residual stresses. Figure 70 (a) and (b) presents the distributions of residual axial stresses at the top surface with various model thicknesses, i.e. 5 mm, 8 mm, and 11 mm, in the weld metal joint. The tensile stress always appears only in the areas in the FZ. The reason for increasing residual stresses with increasing thickness is that absorption energy per unit volume in a thin weldment exceeds that in thick weldments, accounting for why the residual stresses increased with decreasing model thickness.

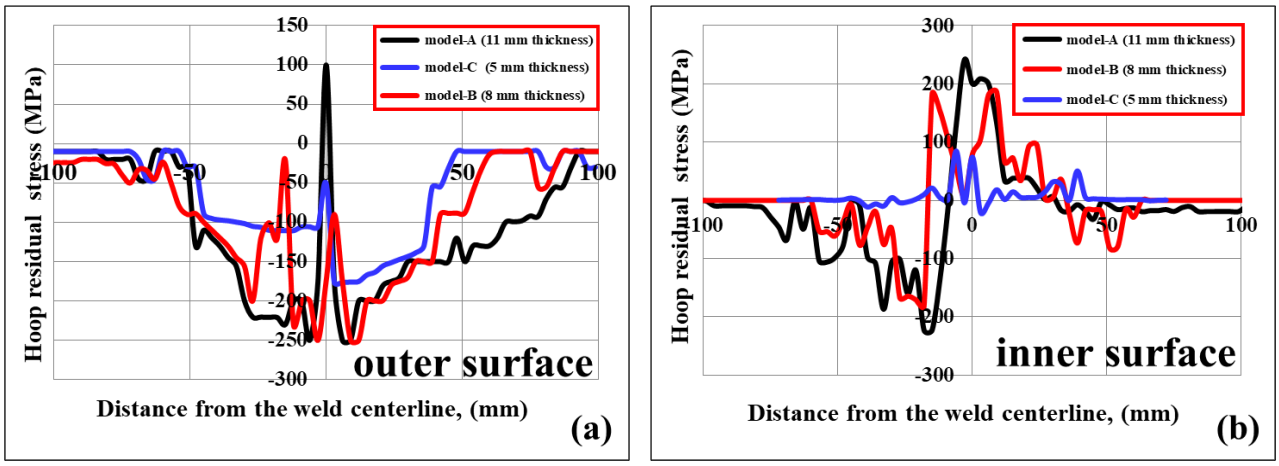

Figure 70. The distributions of residual hoop stresses: (a) outer (b) inner surface

5.5.9 *Prediction of Residual Stress in Welding Two Similar Material Pipes*

Numerical simulation of residual stresses in the welding of two similar pipes is obtained. This analysis includes the 2-D model for the thermophysical and mechanical welding simulation. It also includes a moving heat source, material deposit, temperature-dependent material properties, metal plasticity and elasticity, transient heat transfer and mechanical analysis. This simulation aims to see if there is any effect of residual stress with a similar weld and compare this with a dissimilar weld joint. The welding simulation was considered as a sequential coupled thermo-mechanical analysis, and the element birth and death technique was employed for the simulation of filler metal and base metal. The residual stress distribution and magnitude in the axial direction was predicted. Figure 71 (a) and (b) shows the hoop residual stress with similar and dissimilar material of pipe (E355K2). The axial stresses and hoop stresses were compared with dissimilar material and showed slightly different curves between both models in the outer and inner surface, as shown in Figure 72 (a) and (b). Axial stress with similar material of pipe (E355K2) and with dissimilar material of pipe in (Appendix C)

DOI: 10.14750/ME.2022.004

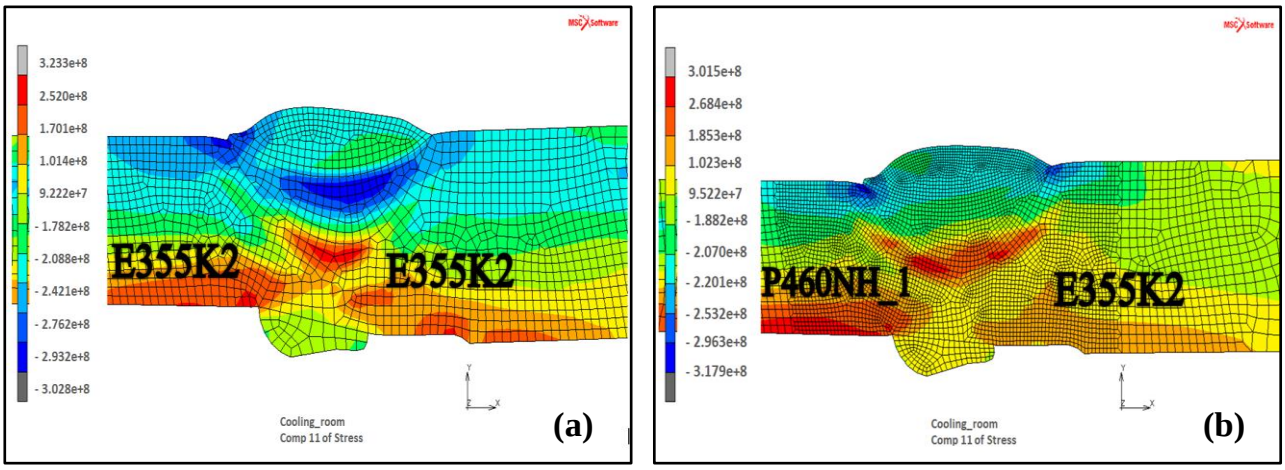

Figure 71. Axial stress with similar material of pipe (b) with dissimilar material of pipe [Pa]

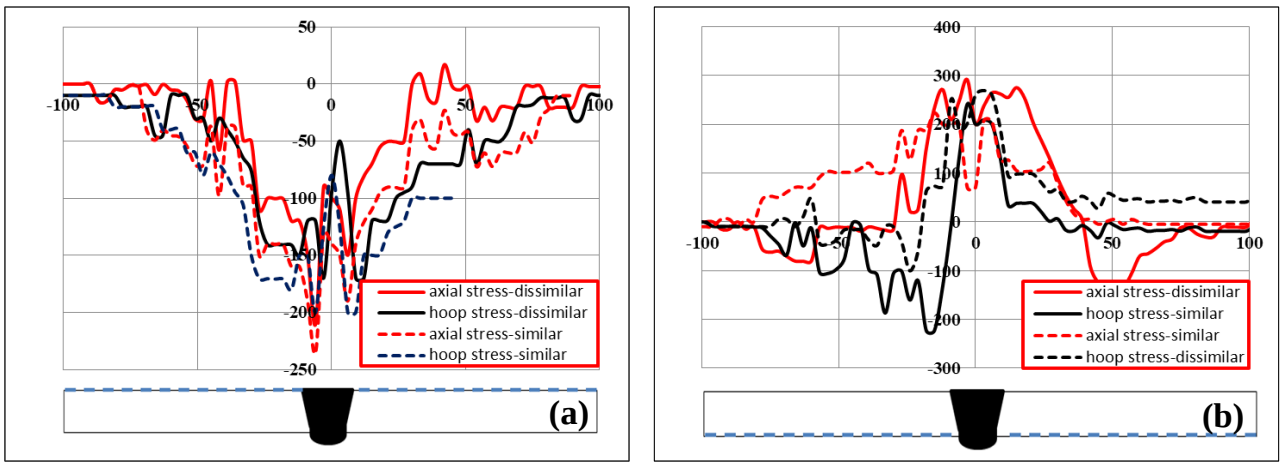

Figure 72. (a) Axial and hoop residual stress distribution on the outer surface, (b) axial and hoop residual stress distribution on the inner surface

5.5.10 *Prediction of Residual Stress Generated by Dissimilar Pipe Manual Arc Welding: Preheating*

To study the effect of preheating temperature on residual stress, which depends on the final equilibrium, temperature stress cycle temperature, and the rest of the welding parameters are kept constant. Preheating is used primarily between 100 – 200^{O}C to effect cooling rates in the weld, thereby reducing the residual stresses. At the location near the weld centreline, the axial stresses were observed to be tensile under preheating and no-preheat conditions. Figure 73 shows that axial residual stresses are significantly reduced after applying the preheating treatment. This trend can be explained in terms of shrinkage of hot metal in the fusion zone against the constraint of the cooler metal in base metal, which shrinks less. The results indicate the importance of including preheating in the simulation of residual stresses during the welding.

DOI: 10.14750/ME.2022.004

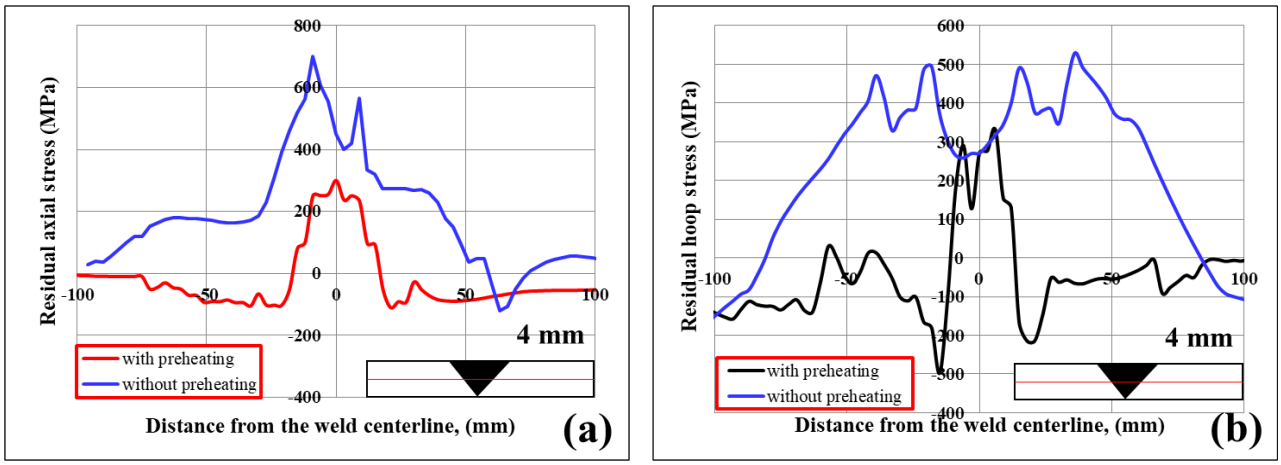

Figure 73. The effect of preheating treatment on (a) axial stress (b) hoop residual stress

DOI: 10.14750/ME.2022.004

6. RESIDUAL STRESS ANALYSES USING 3-D MODEL

6.1 3-D Model Strategies Simulation

6.1.1 *3-D Model using 5° expand*

The residual stresses of 3-D models were average values of one concerned position because the computation time the element expands 5 degrees, as shown in Figure 74 (a) and (b). Although the heat source was moved within a short time and distance, residual stress was compared between 2-D/3-D models under the same peak temperature conditions shown in Figure 75 (a) and (b). It presents the residual stress distribution (axial stress, radial and hoop stress) at 0° in a 3-D pipe along the outer surface. It can be seen that the model shared a similar residual stress distribution with the 2-D model. At the same time, a significant difference in stress values for those two models can be observed. Figure 76 (a) shows axial and hoop distributions in the model and (b) shows the comparison of residual axial, radial and hoop stress distribution for 2D/3D models on the inner surface.

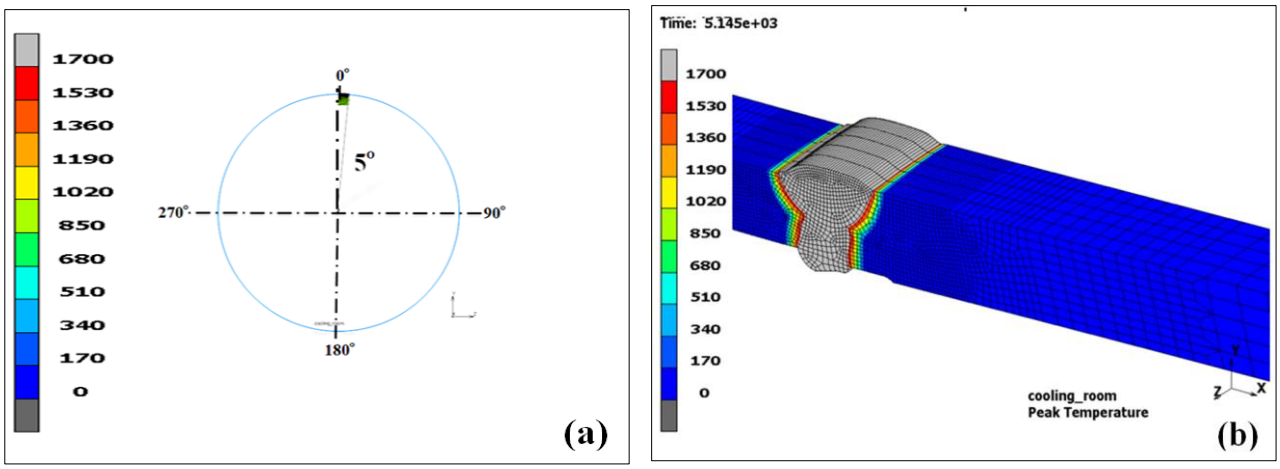

Figure 74. (a) 3-D model with 5° (b) Temperature distribution [K]

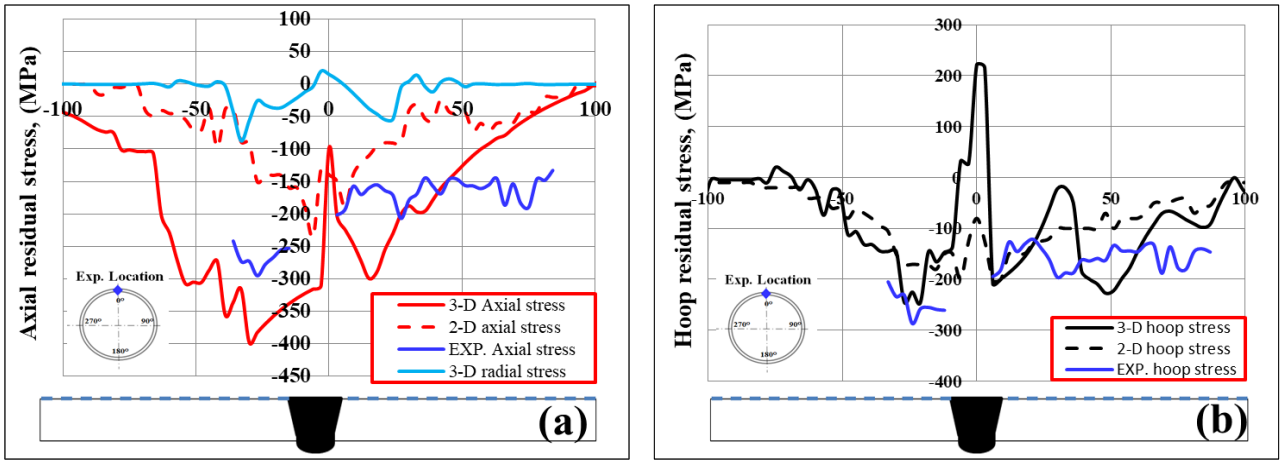

Figure 75. Comparison of residual stresses distribution for 2D/3D models with XRD measurement on the outer surface: (a) axial residual stress; (b) hoop residual stress

DOI: 10.14750/ME.2022.004

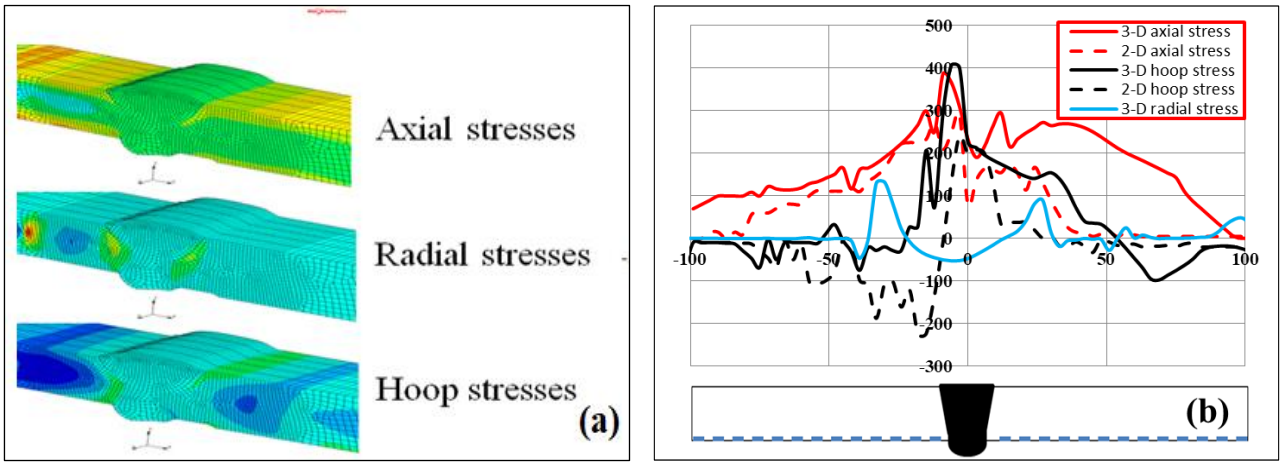

Figure 76. (a) Axial, radial and hoop stresses distribution; (b) Comparison of residual axial, radial and hoop stress distribution for 2D/3D models on the inner surface

6.1.2 *3-D Model with using the quarter axisymmetric model expand*

Figure 76 shows the temperature distributions with 3-D quarter model was used to save the calculation of time and for investigating the heat source model. Figure 77 (a) and (b) presented the residual stress distribution (axial stress and hoop stress) at the positions of 0°and 90°, in the 3-D pipe along the outer surface path with 90° expand 2-D model.

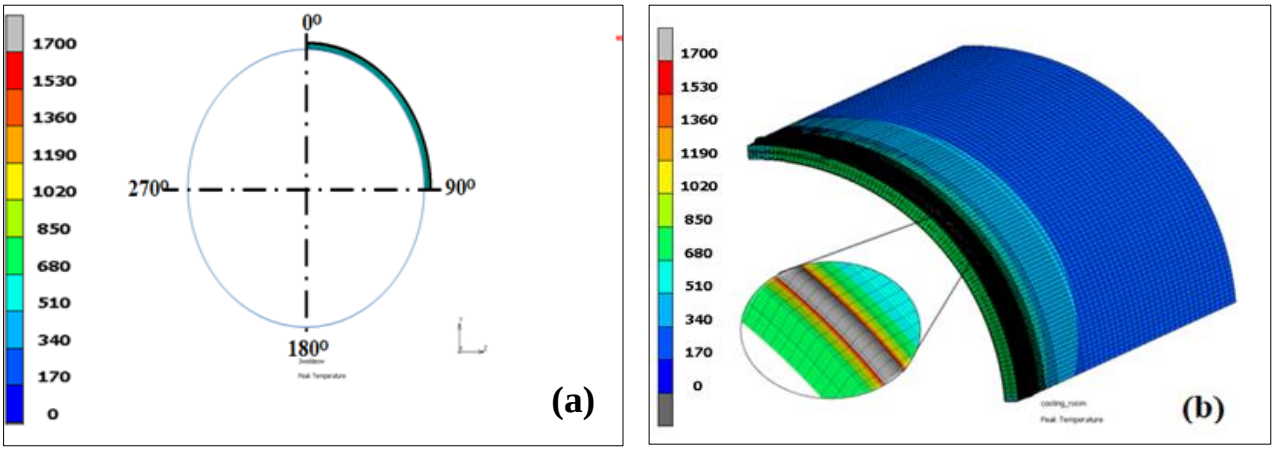

Figure 77. (a) 3-D quarter axisymmetric model expand [K] (b) temperature distribution [K]

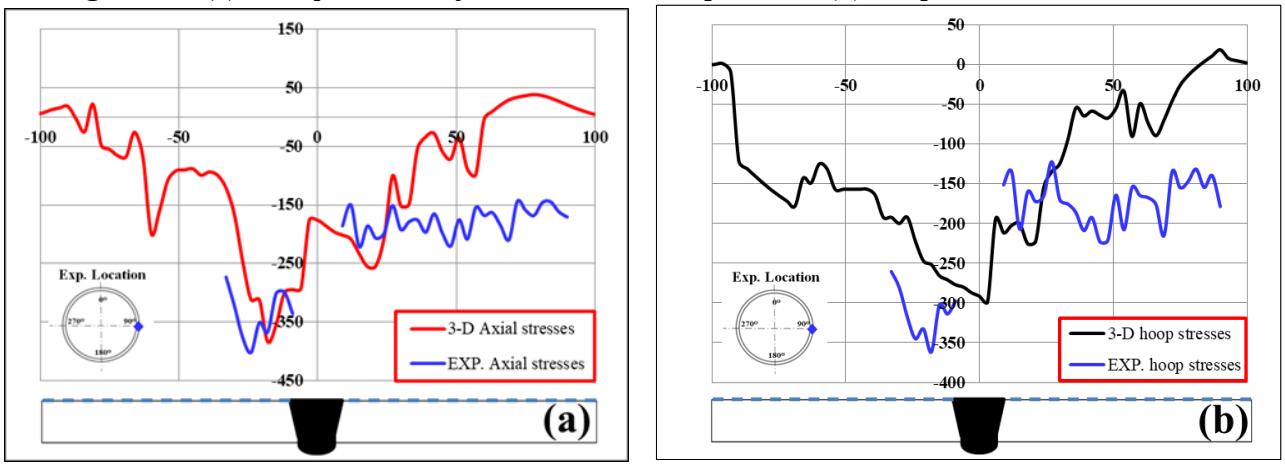

Figure 78. Comparison of residual stresses distribution for the 3-D quarter axisymmetric model with XRD measurement on the outer surface: (a) axial stresses; (b) hoop stresses

DOI: 10.14750/ME.2022.004

6.1.3 *3-D Model with full model expand*

The 3-D finite element model is shown in Figure 79 (a) and (b) shows the welding temperature field during the welding. From this figure, it can be observed that the maximum temperature at the weld pool is 1700 ^{o}C. The main purpose of creating 3-D model is because XRD measured the axial and hoop residual stresses at 0 and 90 degree locations. The magnitudes of residual stress are different among them. The residual stresses (axial and hoop) on the outer surface with a 180^{o} and 270^{o} central angles were not measured in the experiment, so values for this location and inner surface locations (0^{o}, 90^{o}, 180^{o}, and 270^{o}) were predicted. In this study, it was assumed that the stress component in the radial direction could be neglected. Figures 80 (a) and (b) show the comparison of axial and hoop residual stresses distribution for the full 3-D model with XRD measurement on the outer surface. It is obvious that the distribution of axial and hoop residual stress is sensitive to the change of different angle positions. This figure shows that the predictions generally match the measurements well at the weld zone.

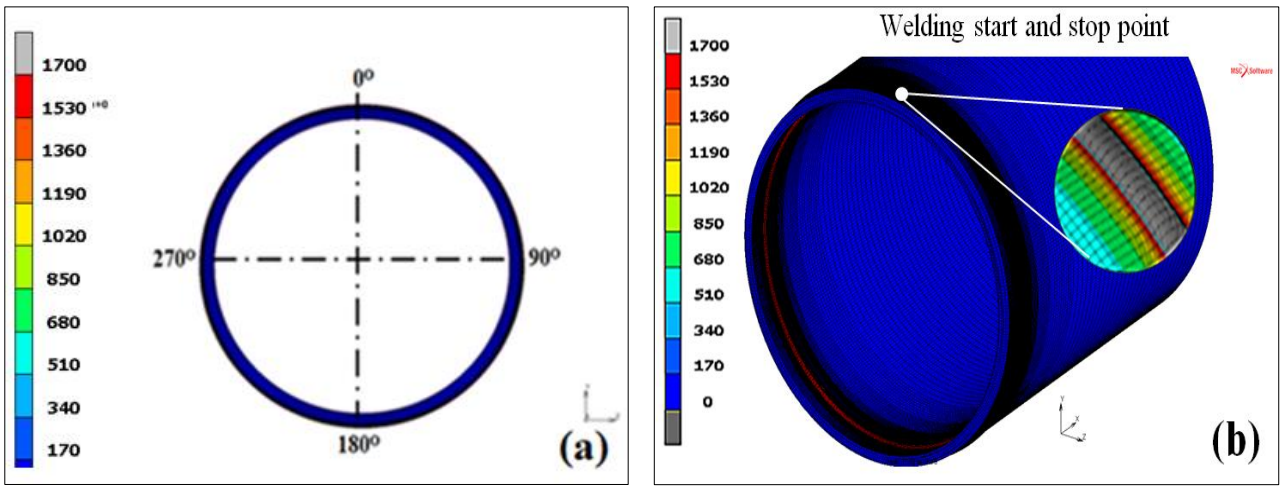

Figure 79. (a) 3-D model with full expand (middle section) [K] (b) temperature distribution [K]

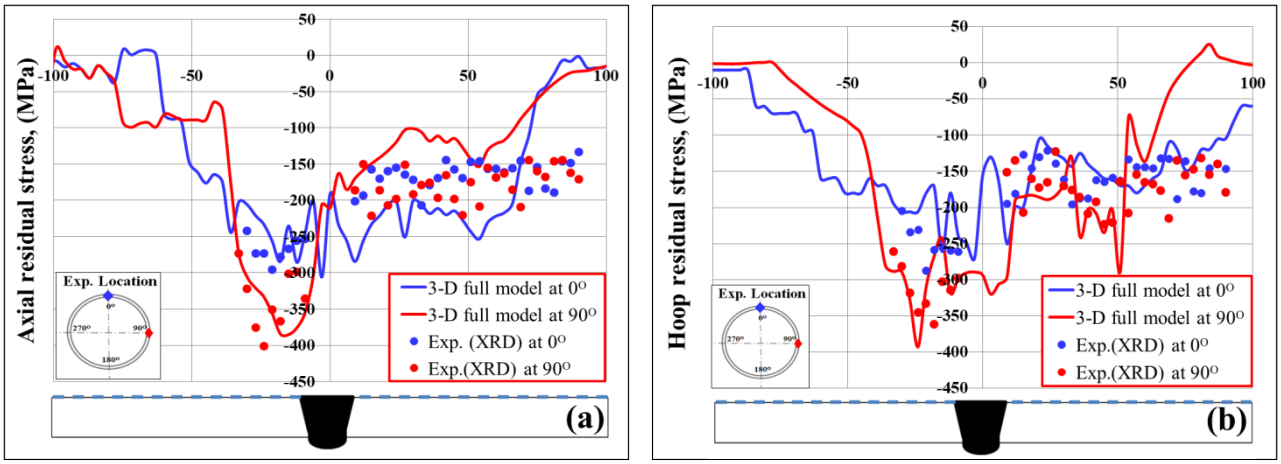

Figure 80. Comparison of residual stresses distribution for 3-D full model with XRD measurement on the outer surface: (a) axial stresses; (b) hoop stresses

DOI: 10.14750/ME.2022.004

6.1.4 *Comparison of residual stresses distribution for 3-D and 2-D models with XRD*

Figure 81 presented the axial residual stress distribution at the positions of 0°/360°and 90°in 3-D pipe model along the outer surface path and compared with 2-D and XRD measurement. It can be seen that the axial stresses for positions at the outer surface welding center line were compressive stresses. While the hoop stresses were compressive stress at all positions, as shown in Figure 82. However, both the hoop and axial residual stresses near start/end region (at 0°/360°) shown shape gradients and significantly different from those in 2-D model. A comparison of residual stress was also carried out between 2D/3D models under the conditions of the same peak temperature and the same heat source shape parameters. At the same time, a significant difference in stress values for those two models can be observed. However, this should not mean that the results of 2-D model were unacceptable.

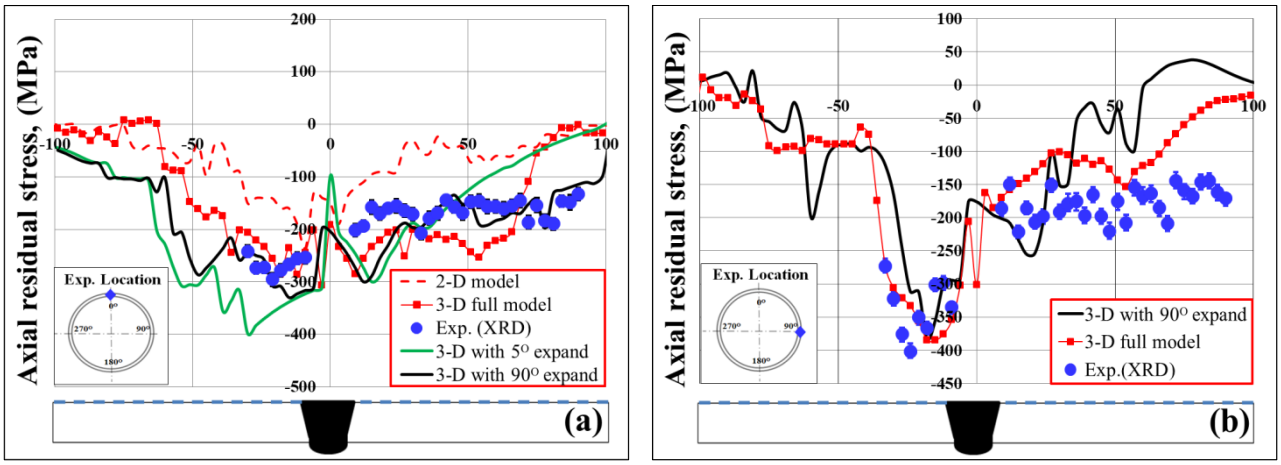

Figure 81. Comparison of axial residual stresses distribution for 3-D (5°, 90° expand and full) and 2-D models with XRD measurement on the outer surface: (a) predicted and measured RS distributions at 0°, (b) predicted and measured RS distributions at 90°

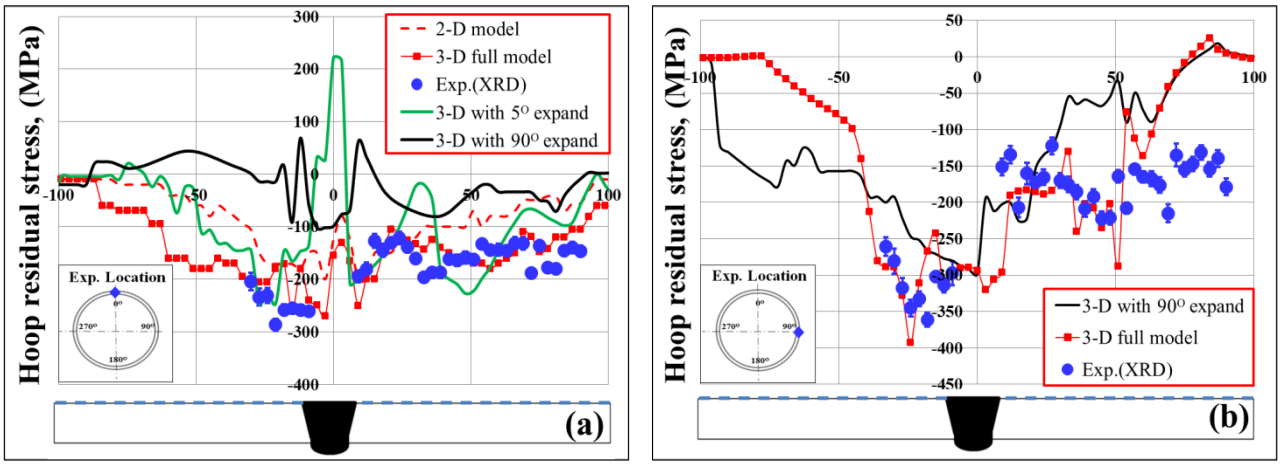

Figure 82. Comparison of hoop residual stresses distribution for 3-D (5°, 90° expand and full) and 2-D models with XRD measurement on the outer surface: (a) predicted and measured RS distributions at 0°, (b) predicted and measured RS distributions at 90°

Calculation of the normalized root-mean-square deviation or error (NRMSD) is shown in Table 11, this table presents (NRMSD) between all models. It shows that 3-D is more accurate comparing with 2-D model.

Table 11. Calculation of the normalized root-mean-square deviation or error (NRMSD)

Model	Axial RS at 0° (NRMSD)	Axial RS 90° (NRMSD)	Hoop RS at 0° (NRMSD)	Hoop RS 90° (NRMSD)
2-D	1.987	-	2.090	-
3-D (5°)	1.839	-	1.459	-
3-D (90°)	1.096	1.963	3.781	2.192
3-D	1.2767	1.432	1.02	1.731

6.1.5 *Residual stress distribution at different positions*

The explored RS is located at a position where the circumferential angle is 0 and 90 degrees from the welding start point by XRD that necessarily leads to investigate the stresses in another position or another circumferential angle by numerical simulation. Figures (83 and 84) shows the axial stresses and hoop stresses with different angles on the outer and inner surface. In Figures 83 (a) and 83(a), the axial stress distribution seems not to be sensitive with different positions on the inner surface and vice versa with the outer surface the axial stress distribution in the weld zone at 90^{o} central angle, and its vicinity is slightly higher from that of the other three locations (0^{o}, 180^{o}, and 270^{o}). In Figure 84 (b) and 84 (b), the hoop stress distribution also seems not to be sensitive to the angle except when is 270 degree on the inner surface in the weld zone. Its vicinity is slightly higher than that of the other three locations (0^{o}, 90^{o}, and 180^{o}) because the end of the effect shows the compressive stress along the weld zone.

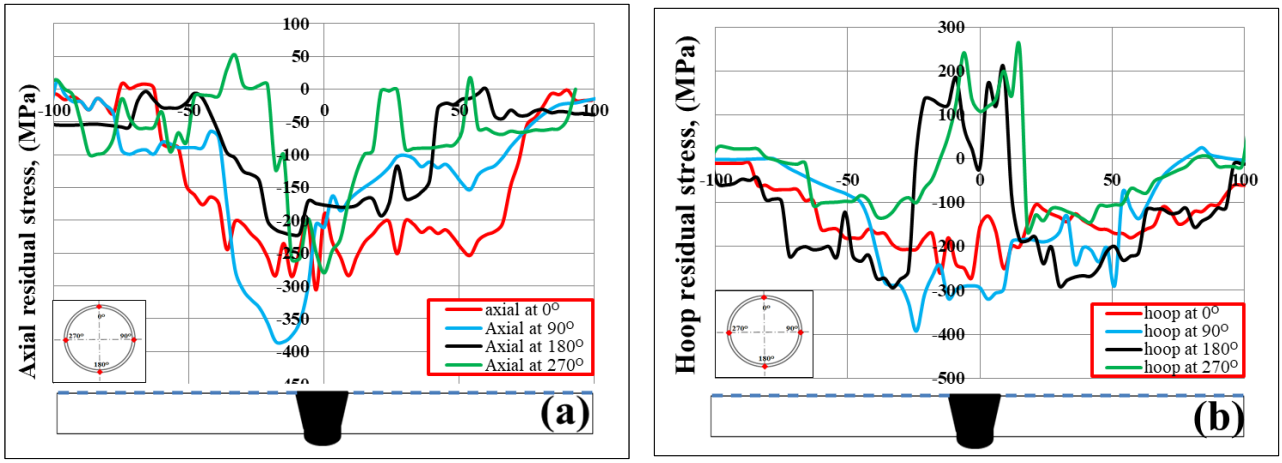

Figure 83. RS profiles at different circumferential angles: (a) axial residual stress on the outer surface; (b) hoop residual stress on the outer surface

DOI: 10.14750/ME.2022.004

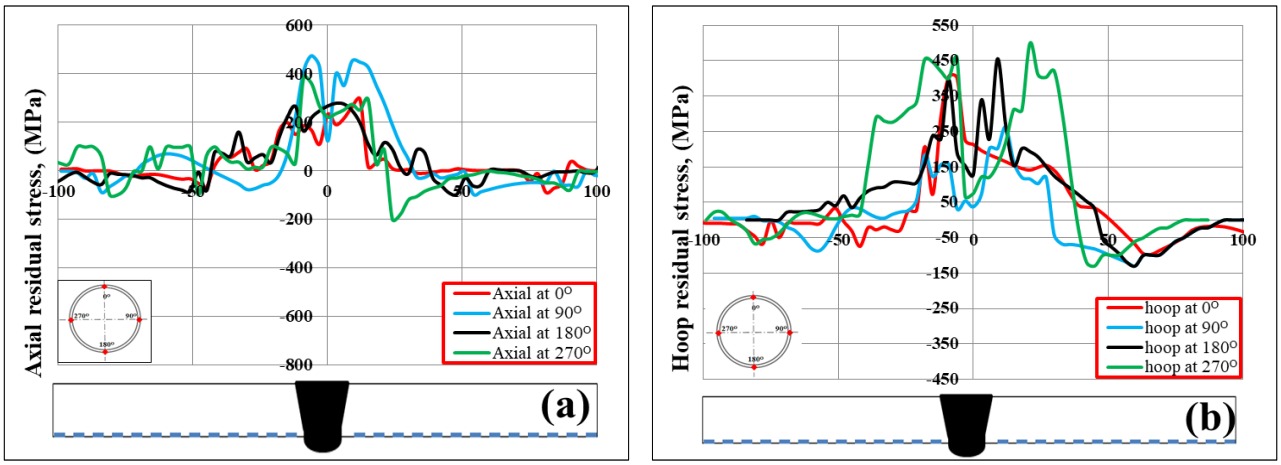

Figure 84. RS profiles at different circumferential angles: (a) axial residual stress on the inner surface, (b) hoop residual stress on the inner surface

With regard to the axial and hoop residual stress distributions, which act normal to the weld line at the four locations on the inner and outer surfaces in Figure 85 with maximum and minimum stresses region, their magnitudes are affected by the axial residual stresses. The residual hoop stresses are tensile on the FZ's inner surface and the area adjacent to it. For the self-equilibrating purpose, stress reversal from compressive to tensile and vice versa is noticed on the outer and inner surfaces away from the WCL, at 180^{o} and 270^{o}, respectively.

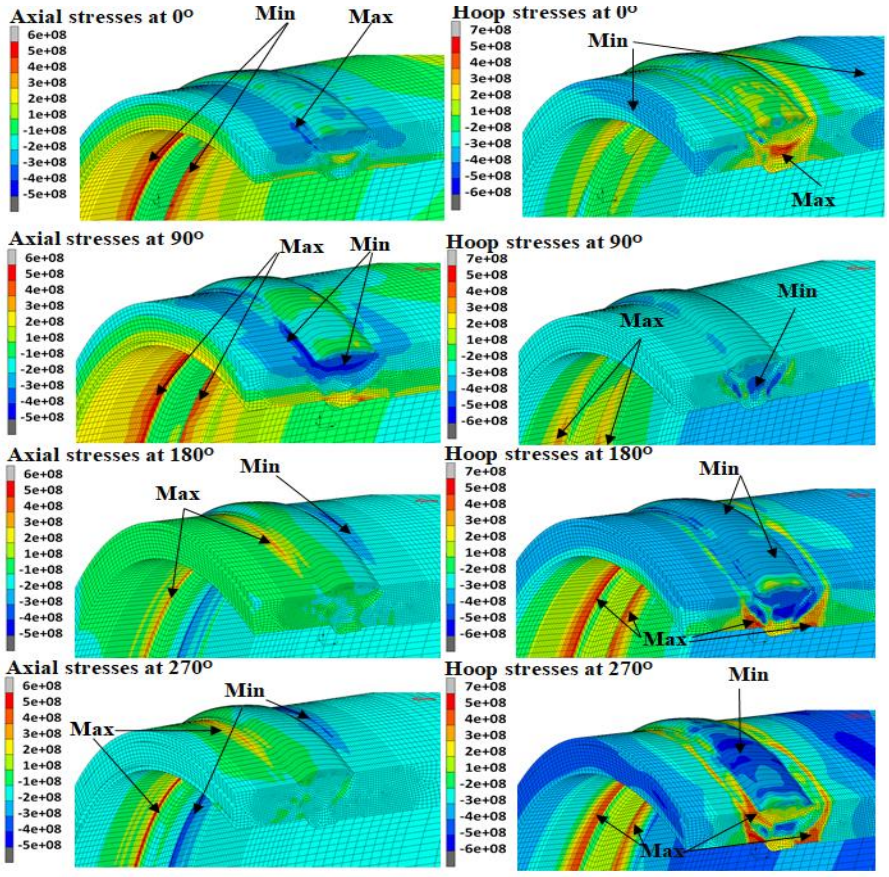

Figure 85. Axial and hoop residual stresses distributions with a cross-section of full 3-D model pipe weld at 0°, 90°, 180° and 270° [Pa]

DOI: 10.14750/ME.2022.004

6.2 Investigating the Accuracy of Different and Combinations Heat Source Models

It should be stated that the implemented models of heat sources for the numerical simulation of welding processes are one of the solutions to the prediction problems. The possibility of often introducing simple changes or modifications to the built heat source models allows them to be adapted in a much better way to the real experimental results. Otherwise, the results of numerical analyses may lead to erroneous conclusions. 3-D model with four different heat source models (Goldak, Gaussian, conical and combined (Goldak and conical)) have been used, which are shown in Figure 86. Figure 87 (a) shows combined model has been used, and the purpose of using the combined model is the shape of the weld cross-section in the root or the first pass. This is because of the narrow groove pipe welding, as shown in Figure 87 (b). An adaptive model of the heat source in numerical simulation of the arc welding requires that the model takes into consideration the larger aspect ratio of welds and the volumetric distribution characteristic of heat intensity along the direction of the pipe thickness.

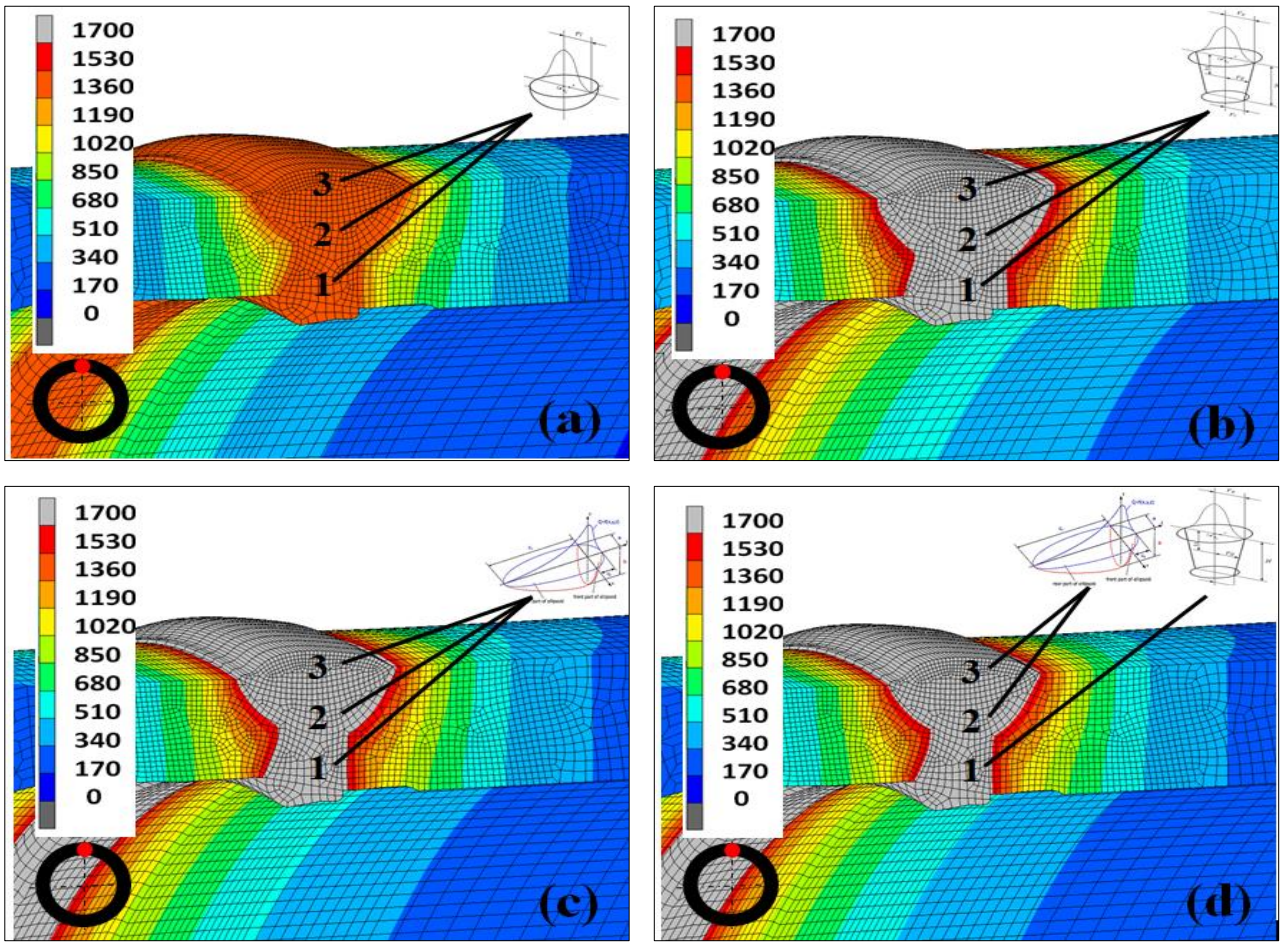

Figure 86. Comparison of the view of the molten pool surface and cross-sections the quarter axisymmetric when using the models: (a) Gaussian (b) Conical (c) Goldak (d) Combined heat source model [K]

DOI: 10.14750/ME.2022.004

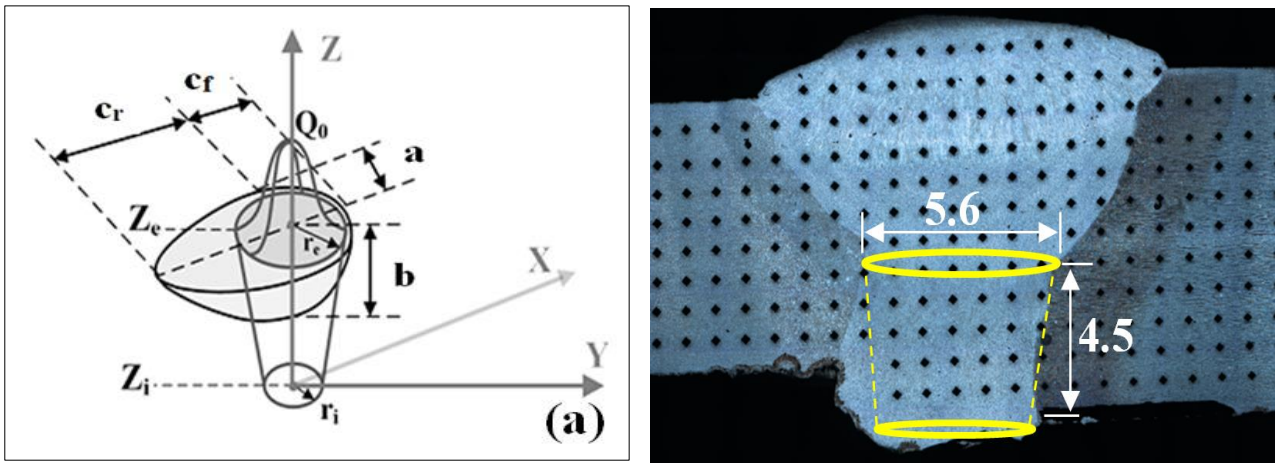

Figure 87. (a) Combined heat source model (b) Schematic illustration of first pass weld (dimensions in mm)

A combined heat source model is proposed for the numerical analysis of temperature fields. With this adaptive heat source model, finite-element analysis of temperature profile and the weld geometry is determined. The results show that the results of the combined model for predicting the geometry and locus of the fusion line weld cross-section are in best agreement with the experimental measurements, as shown in Figures 88 and 89. Moreover, the overall shape of the weld pool matches exactly when using the combined method. The penetration depth and fusion width of the welding pool increased with the moving of the combined heat source, the penetration of FZ in depth and width direction was increased much more obvious than for the other models. This lays a solid foundation for process optimisation, metallurgical analysis and residual stress simulation. The combined heat source model is able to provide a faster calculation of penetration depth and fusion width of the welding pool shape and acceptable agreement, making it a good choice for the simulation of pipe arc welding with dissimilar materials.

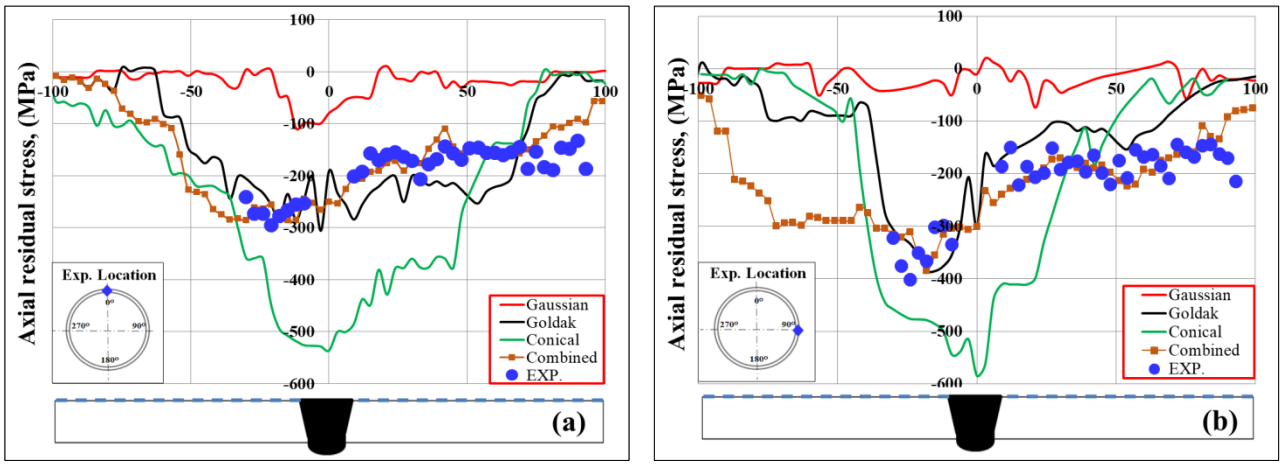

Figure 88. Comparison of axial residual stresses when using different heat source models with XRD measurements: Goldak; Gaussian; Conical; Combined heat source model (a) 0° (b) 90°

DOI: 10.14750/ME.2022.004

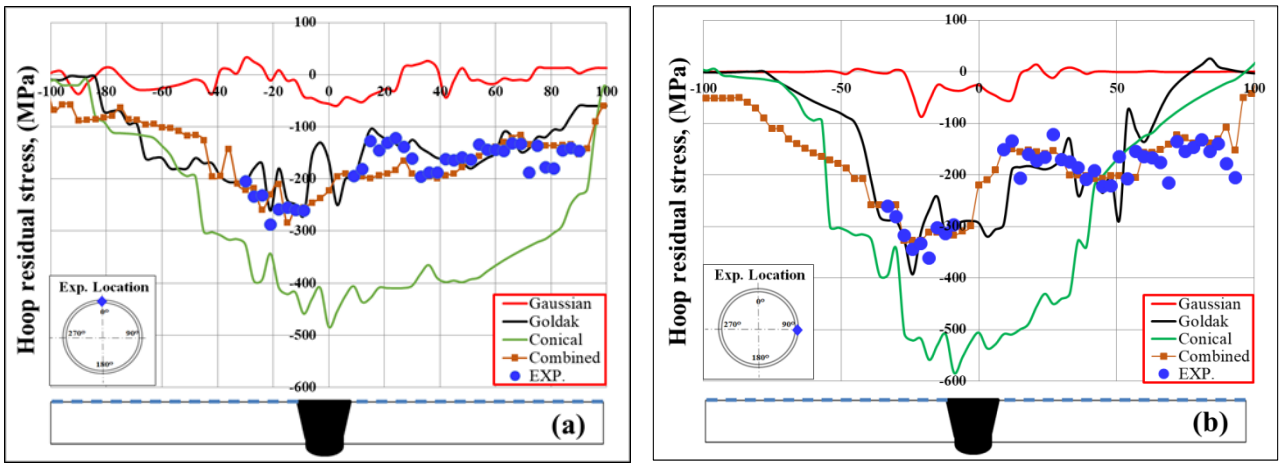

Figure 89. Comparison of hoop residual stresses when using different heat source models with XRD measurements: Goldak; Gaussian; Conical; Combined heat source model (a) 0° (b) 90°

The calculation of the normalized root-mean-square deviation or error (NRMSD) is shown in Table 12, this table presents (NRMSD) between all models. A combined heat source model form using the ellipsoid heat source (Goldak) as the upper part and the conical heat source as the lower part is more suitable in numerical simulation of welding.

Table 12. Calculation of the normalized root-mean-square deviation or error (NRMSD)

Heat source model	Axial RS at 0^O (NRMSD)	Axial RS 90^O (NRMSD)	Hoop RS at 0^O (NRMSD)	Hoop RS 90^O (NRMSD)
Gaussian	3.678	5.4	5.3	5.86
Goldak	1.2767	1.4322	1.02	1.731
Conical	4.8399	4.8019	5.677	3.64
Combined	0.3103	0.192	0.169	0.27

Figure 90 and 91 a–d displays the 3-D mapping of circumferential welding residual stresses in the middle cross-section computed by the numerical simulation axial and hoop residual stresses when using Gaussian heat source model at 0^O, 90^O, 180^O and 270^O.

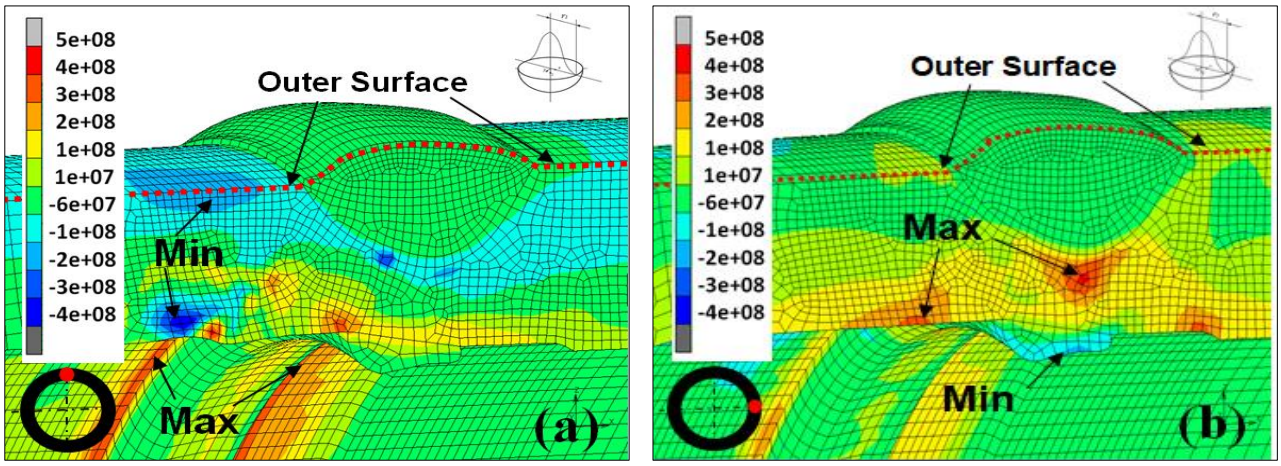

DOI: 10.14750/ME.2022.004

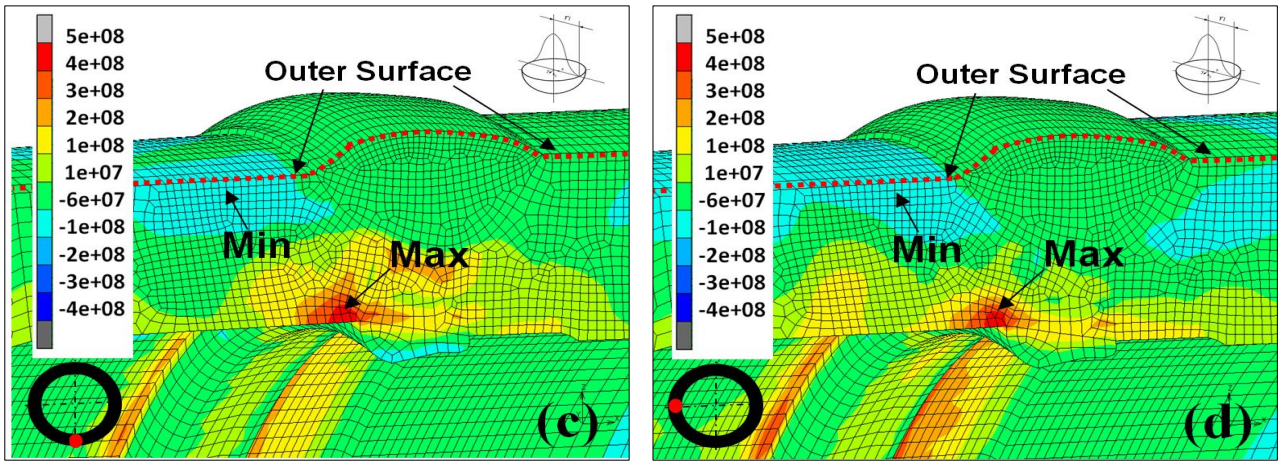

Figure 90. Axial residual stresses when using Gaussian heat source model in [P] at (a) 0^{O} (b) 90^{O} (c) 180^{O} (d) 270^{O}

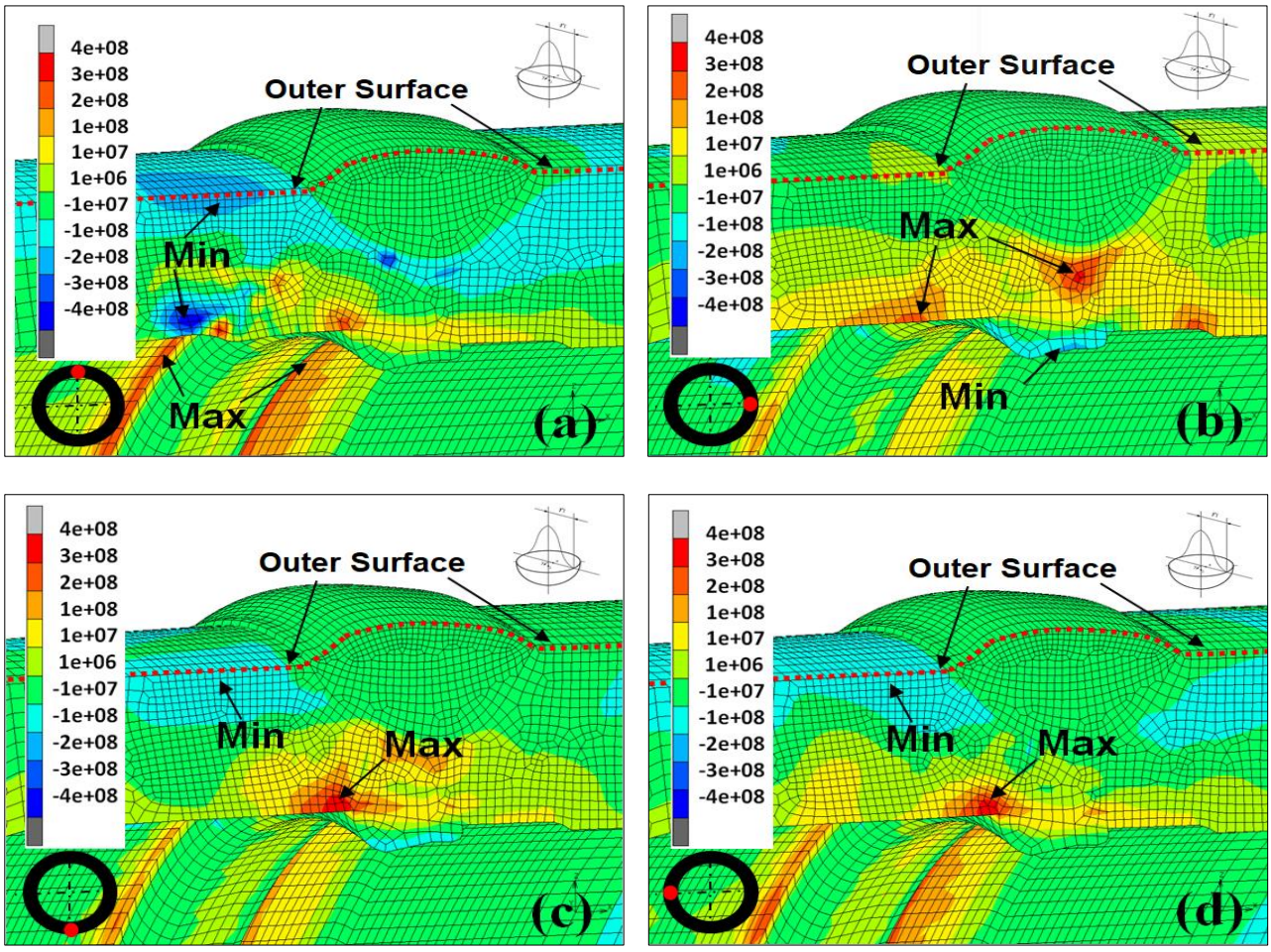

Figure 91. Hoop residual stresses when using Gaussian heat source model in [P] at (a) 0^{O} (b) 90^{O} (c) 180^{O} (d) 270^{O}

Figure 92 and 93 a–d displays the 3-D mapping of circumferential welding residual stresses in the middle cross-section computed by the numerical simulation axial and hoop residual stresses when using conical heat source model at 0^{O}, 90^{O}, 180^{O} and 270^{O}. As it is shown, the axial and hoop residual stresses at different angles change from tensile stresses in the inner surface to compressive

DOI: 10.14750/ME.2022.004

stresses in the outer surface. The axial and hoop residual stresses at the base metal near the weld regions in the pipe sides on the inner surface are higher than those in steel pipe sides outer surface. Moreover, the range subjected to tensile hoop stress adjacent to the weld area is wider on the pipe's inner surface in weld zone.

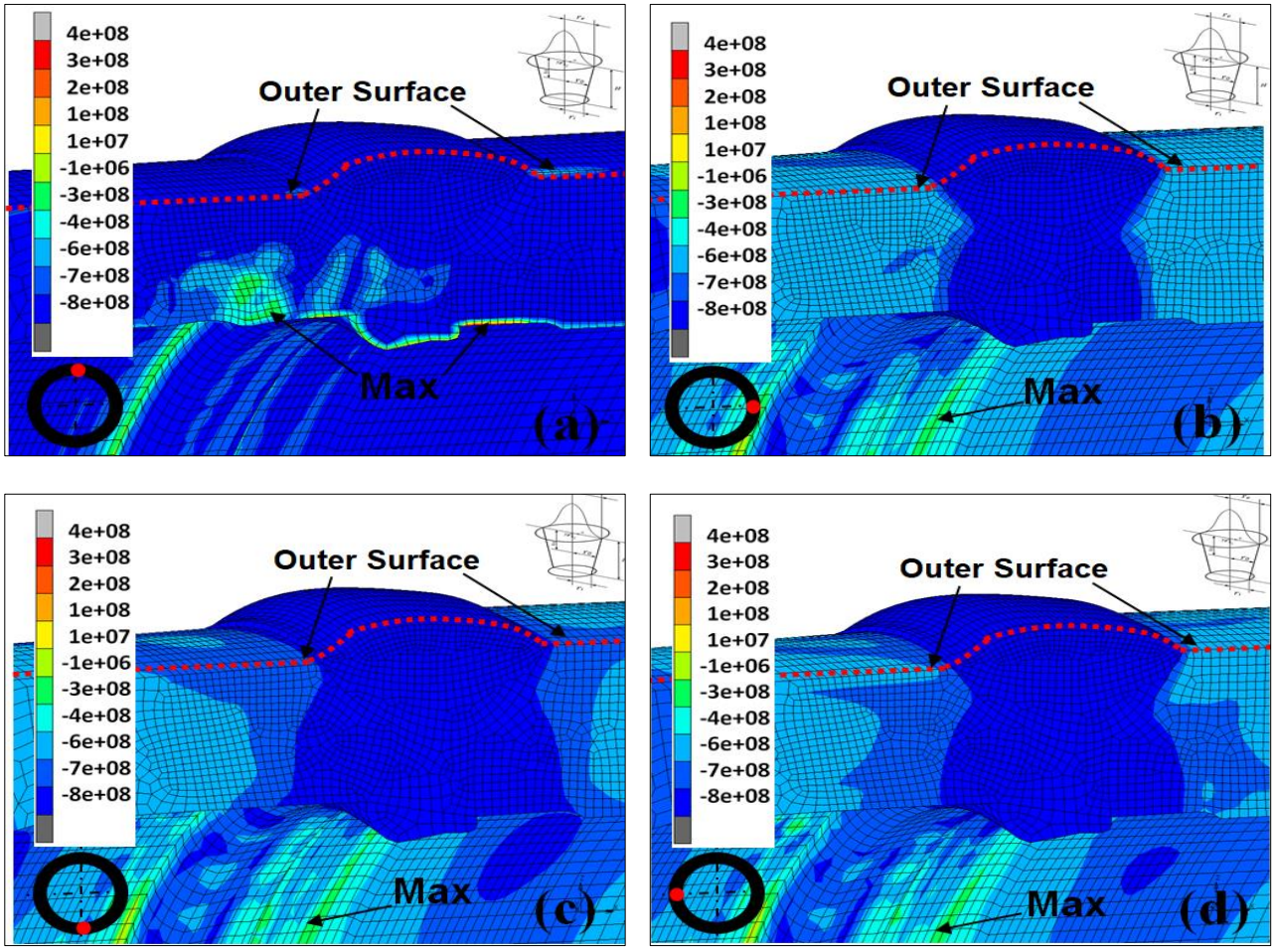

Figure 92. Axial residual stresses when using conical heat source model in [P] at (a) 0^{O} (b) 90^{O} (c) 180^{O} (d) 270^{O}

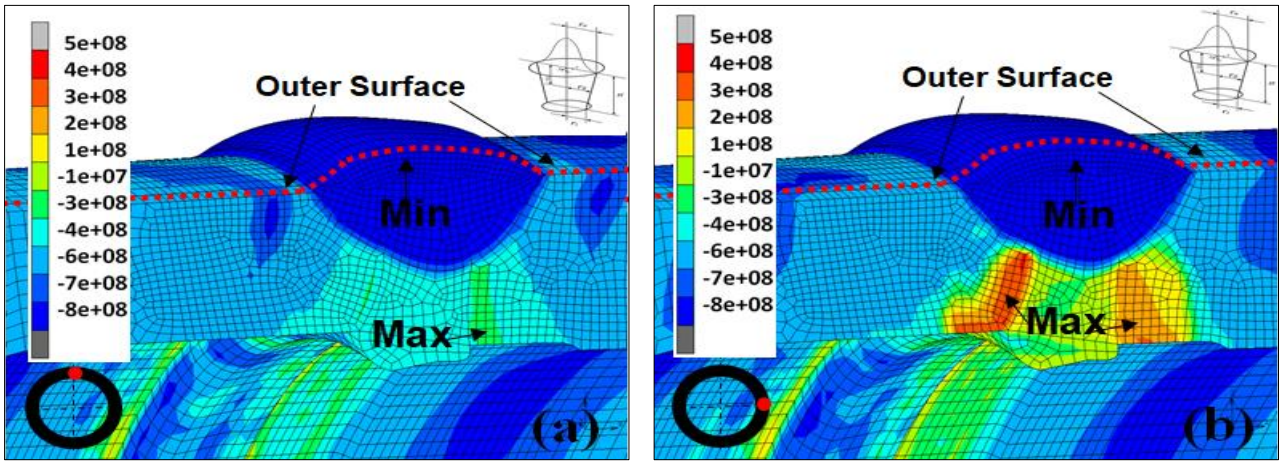

DOI: 10.14750/ME.2022.004

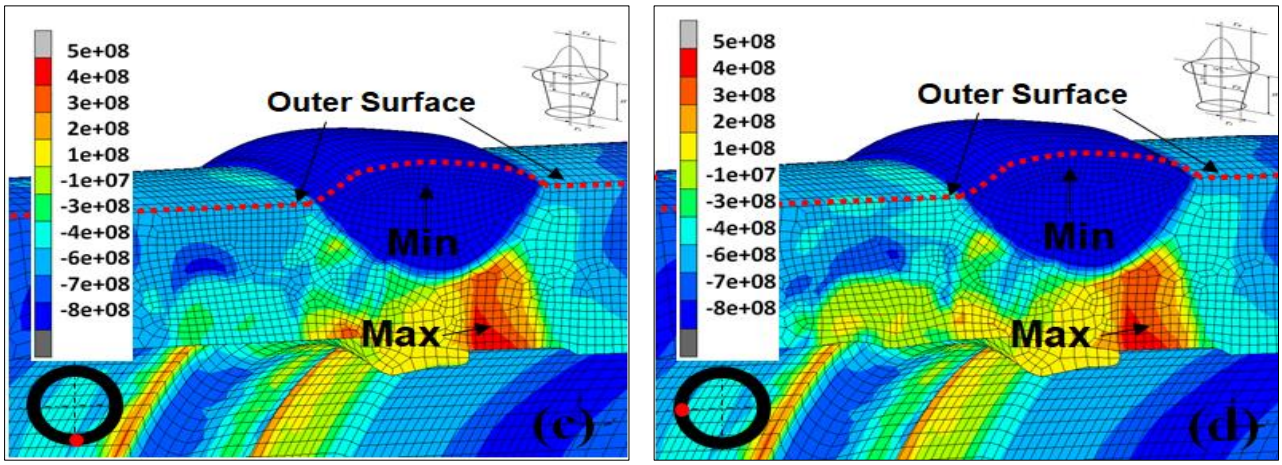

Figure 93. Hoop residual stresses when using Conical heat source model in [P] at (a) 0^{O} (b) 90^{O} (c) 180^{O} (d) 270^{O}

Figure 94 and 95 a–d displays the 3-D mapping of circumferential welding residual stresses in the middle cross-section computed by the numerical simulation axial and hoop residual stresses when using Goldak heat source model at 0^{O}, 90^{O}, 180^{O} and 270^{O}. As shown, the axial and hoop residual stresses at different angles change from tensile stresses in the inner surface to compressive stresses in the outer surface at 0 and 90 degrees when using the Goldak heat source model.

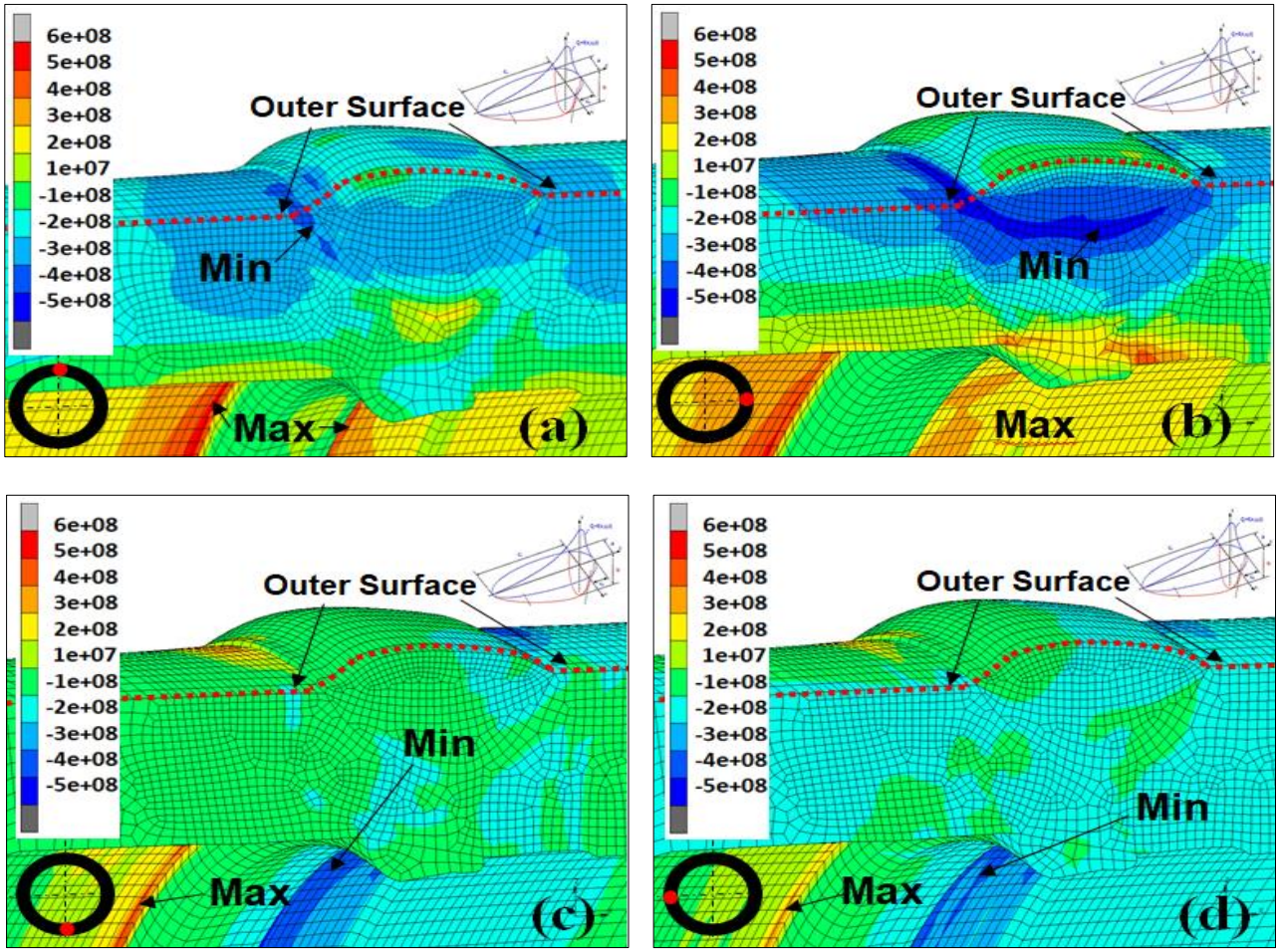

Figure 94. Axial residual stresses when using Goldak heat source model in [P] at (a) 0^{O} (b) 90^{O} (c) 180^{O} (d) 270^{O}

DOI: 10.14750/ME.2022.004

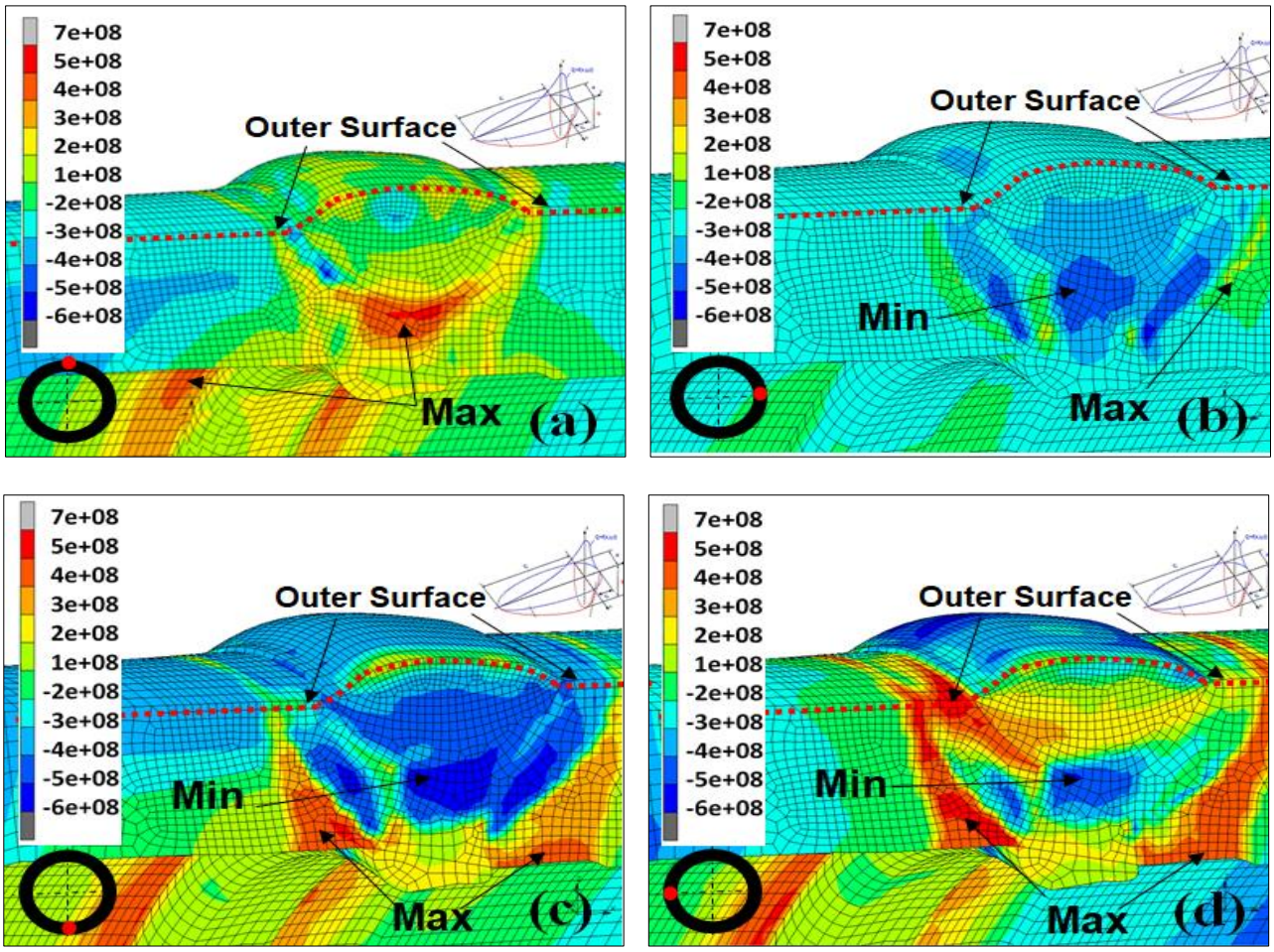

Figure 95. Hoop residual stresses when using Goldak heat source model in [P] at (a) 0^{O} (b) 90^{O} (c) 180^{O} (d) 270^{O}

Figures 96 and 97 a–d display the 3-D mapping of circumferential welding residual stresses in the middle cross-section computed by the numerical simulation axial and hoop residual stresses when using a combined heat source model at 0^{O}, 90^{O}, 180^{O} and 270^{O} when using combined heat source model.

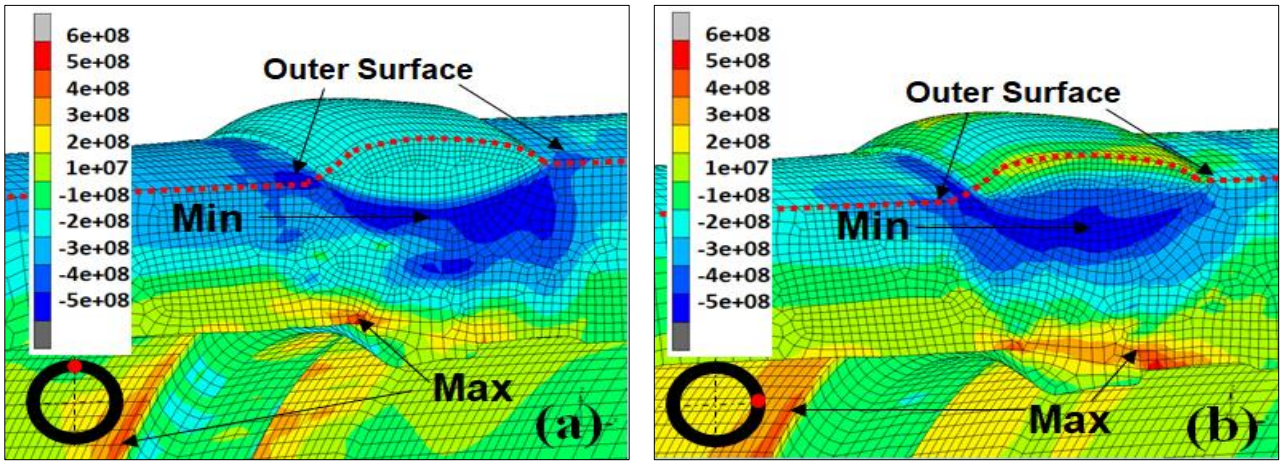

DOI: 10.14750/ME.2022.004

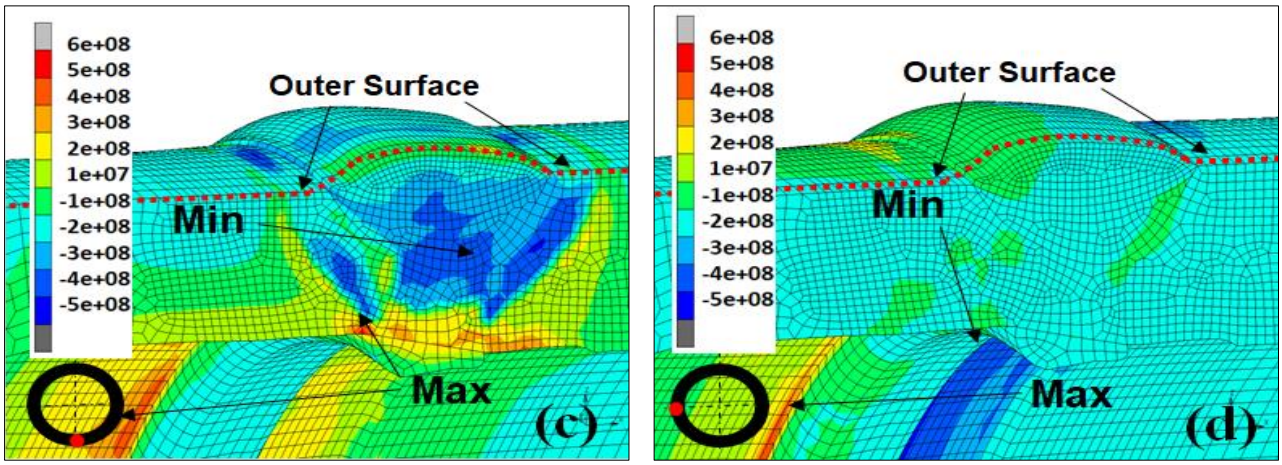

Figure 96. Axial residual stresses when using combined heat source model in [P] at (a) 0^{O} (b) 90^{O} (c) 180^{O} (d) 270^{O}

The hoop residual stresses distribution are concentrated in HAZ. In the weld zone and its vicinity, a tensile hoop residual stress is produced on the inside surface and compressive hoop stress at the outside surface.

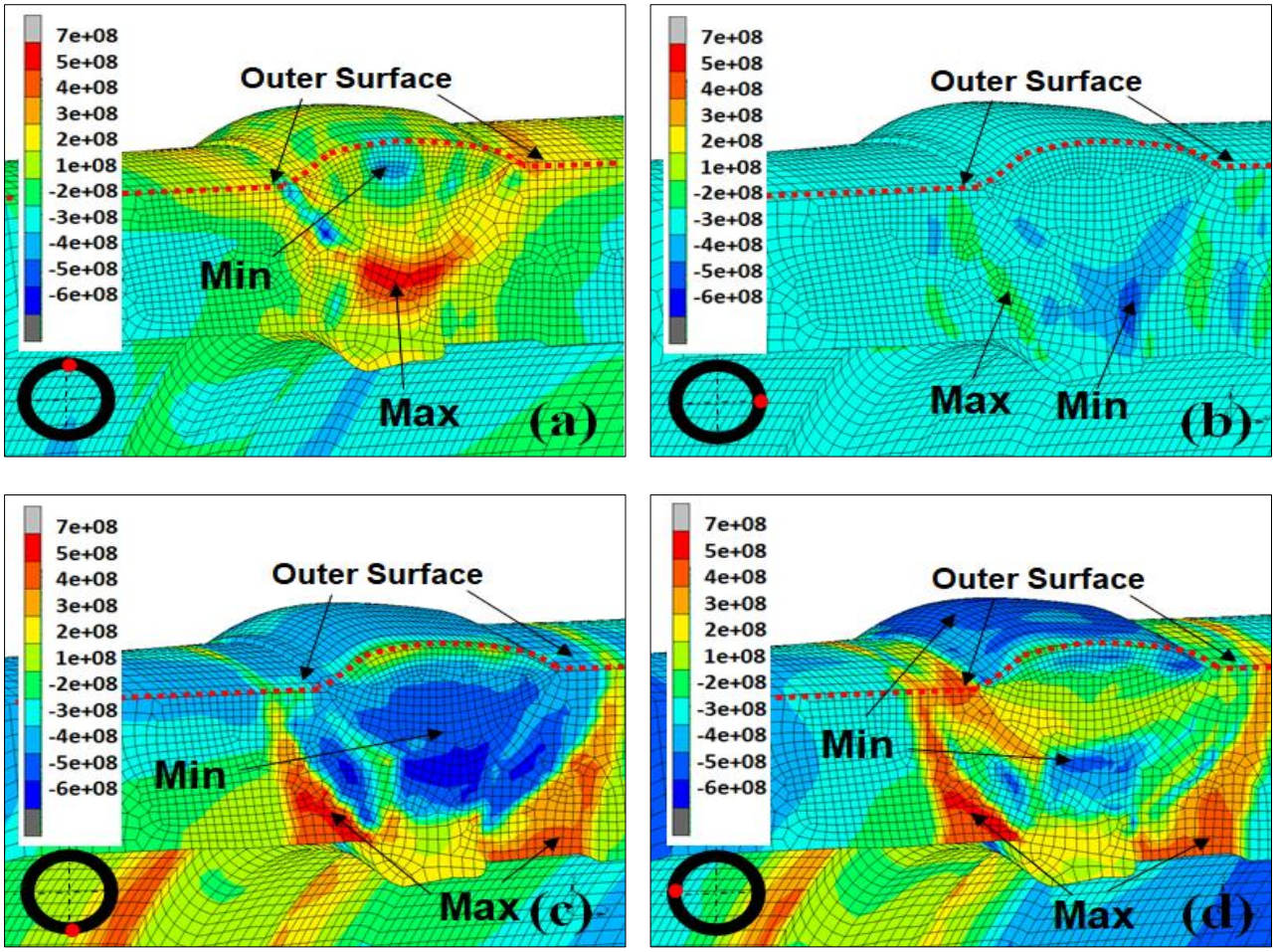

Figure 97. Hoop residual stresses when using combined heat source model in [P] at (a) 0^{O} (b) 90^{O} (c) 180^{O} (d) 270^{O}

DOI: 10.14750/ME.2022.004

6.2.1 *Investigating the accuracy of the heat source model parameter*

To investigate the double ellipsoidal heat source parameters for numerical welding, simulations in fillet joints were proposed. A parametric study analysed the influence of Goldak's parameters on the weld bead size for 2-D and 3-D numerical models. It was found that parameters a and b had a strong influence on the model's penetration and prediction melting weld pool. On the other hand, parameters c_r and c_f had less influence on wide penetration using 2-D. By changing these parameters, the advantage of greater flexibility in the modeling of a heat source shape. It was increasing b lead to increase deep penetration and reduced validation of heat source model. Table 13 shows a comparison of geometric dimensions of welding pool parameters. Using the same Goldak parameters for both models (2-D and 3-D) with the same conditions shows some error, because the heat source model moved with a non-uniform shape in the weld path, showing that the 3-D model (combined) produced a more accurate prediction of the heat source model than the 2-D model and 3-D model when using Goldak heat source model. However, the combination of two volumetric heat sources is sometimes required to obtain accurate thermal fields. Figure 98 and 99 shows the weld bead size after using the Goldak model and combined with the same parameters in the 2-D model and 3-D model.

Table 13. Comparison of geometric dimensions of welding pool parameters with change values (values in brackets)

FE Model	Pass No	Current (A)	Voltage (V)	Speed mm/s	Effic-iency	Welding pool parameters (mm)						
						2a	b	c_f	c_r	r_e	r_i	z_e
2-D (Goldak)	1	80	23.2	2	0.8	5.6 (6.7)	4.5 (5)	5.3 (5.8)	8.3 (9.4)	-	-	-
	2	90	23.6	2	0.8	11.5 (12)	3.8 (4.3)	5.2 (5.5)	8.3 (9.4)	-	-	-
	3	100	24	2	0.8	13.8 (14.3)	4.7 (5.2)	5.3 (5.8)	8.2 (9.3)	-	-	-
3-D (Goldak)	1	80	23.2	2	0.8	5.6	4.5	5.3	8.3	-	-	-
	2	90	23.6	2	0.8	11.5	3.8	5.2	8.3	-	-	-
	3	100	24	2	0.8	13.8	4.7	5.3	8.2	-	-	-
2-D (Combined)	1	80	23.2	2	0.8	-	-	-	-	2.8	2.5	4.5
	2	90	23.6	2	0.8	11.5	3.8	5.2	8.3	-	-	-
	3	100	24	2	0.8	13.8	4.7	5.3	8.2	-	-	-
3-D (Combined)	1	80	23.2	2	0.8	-	-	-	-	2.8	2.5	4.5
	2	90	23.6	2	0.8	11.5	3.8	5.2	8.3	-	-	-
	3	100	24	2	0.8	13.8	4.7	5.3	8.2	-	-	-

DOI: 10.14750/ME.2022.004

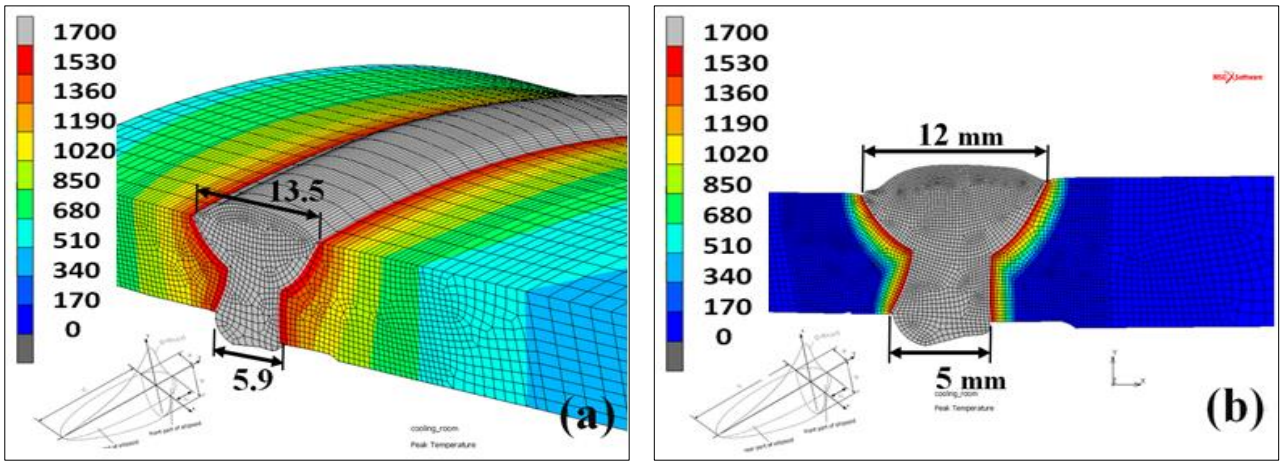

Figure 98. Weld bead size of Goldak model: (a) 3-D model; (b) 2-D model in [K]

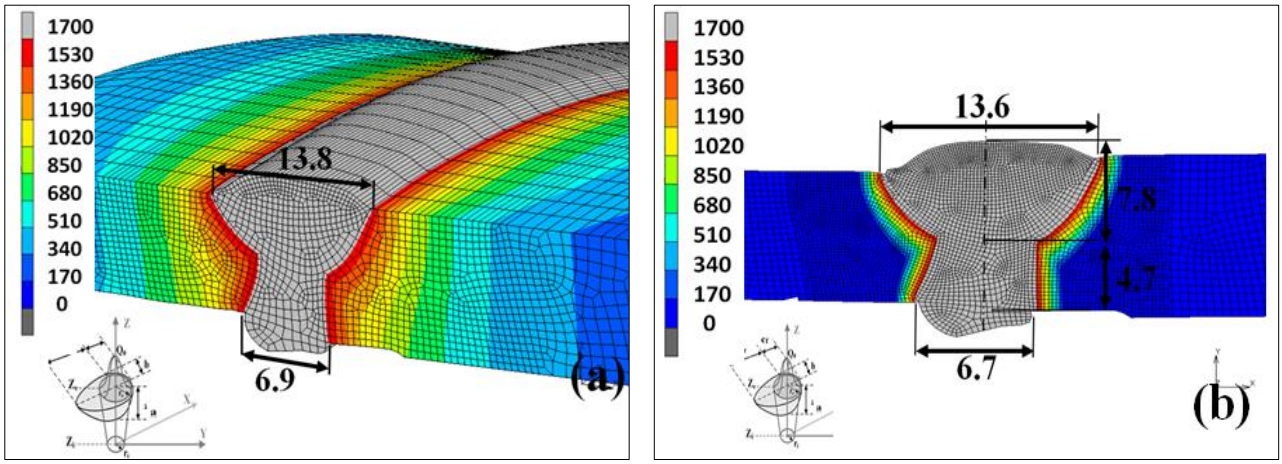

Figure 99. Weld bead size of combined model: (a) 3-D model; (b) 2-D model in [K]

6.3 Finite element mesh (Death and Birth Method)

In this study, the type of element was used in 2-D quad element, quad4 linear element and in 3D brick element type hex8 linear thermal-mechanical element. The element of birth and death technique is used to move Goldak's ellipsoidal heat source model. The models used the birth and death elements technique to simulate the weld variation with time in multi-pass welded joints. All elements must be created, including those weld pass fillers to be born in later for the temperature and residual stresses analysis. The method proposed herein does not remove elements to achieve the "element death" effect. Instead, the technique deactivates them. Similarly, when elements are "born", they are not added to the model but are reactivated, as shown in Figure 100. The eight-node three-dimensional thermophysical element SOLID70 with a single degree of freedom (temperature) is used for modelling, and four-node elements are presented in the two-dimensional model. In the weld zone and its vicinity, a fine mesh is adopted to predict the thermophysical histories very precisely, and the meshes are gradually coarser away from the weld zone. The minimum size of the

DOI: 10.14750/ME.2022.004

element was 0.24 mm × 1 mm × 0.5 mm. In the weld direction, the element size is kept constant at 1 mm. The finite element model consists of 52,850 nodes, and 44,100 elements represent the weld.

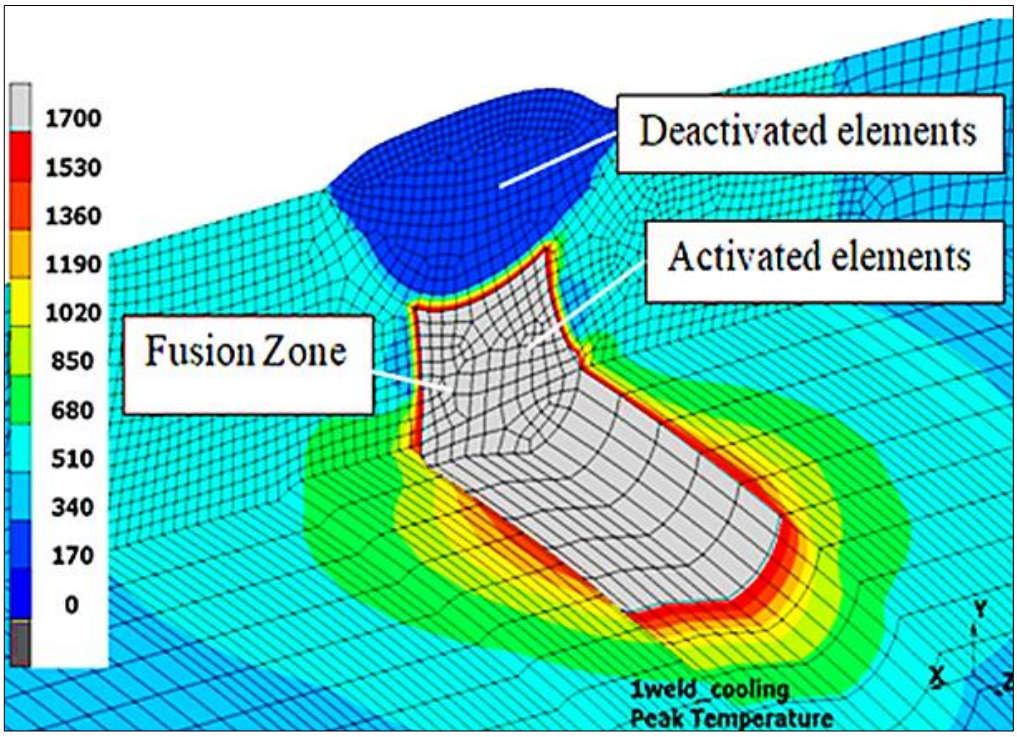

Figure 100. Schematic representation of element birth and death technique with heat source moving in 3-D model and the temperature at start and stop welding in [K]

6.4 CPU time of models for analysis and comparison

The simulations are conducted on a personal computer with double 2.2 GHz CPUs and a 2.21 GB memory. The central processing unit (CPU) time and the number of increments needed for 2-D, 3-D and sample model to simulate the welding process are presented in Table 14. If the 2-D model can be replaced by a reasonable and reliable 3-D model, it is meaningful that a large amount of computational time can be saved. From the analysis in the present study, it can be concluded that the 3-D model cannot only predict the residual stress accurately in the welding process but also improve the computational efficiency. The residual stress axial, radial and hoop predictions in the 3-D model show good agreement with the measurements. For residual stresses distribution analysis, it is important to have a finer mesh to be able to resolve the stress gradients at the critical weld zones. Therefore, simplified 2-D welding simulations for the prediction of residual welding stresses are required, especially for multi-pass joints to reduce computational and modeling time. In spite of the simplification of welding simulation by excluding various effects, welding simulations are still a challenge in terms of CPU time needs; simplified 2-D welding residual stresses simulation

DOI: 10.14750/ME.2022.004

procedures are required to reduce the complexity and thus maintain the accuracy of predictions. Therefore, it is very important to develop time effective computational approaches for welding residual stresses analysis. Although the personal computer's capability has been largely improved, simulating thermo-mechanical behaviour based on a full 3-D model with a multi-pass pipe welded joint is still time-consuming work, and it is not possible to have as fine a mesh in the 3-D model as in a 2-D model.

Table 14. CPU time of models for analysis and comparison

MSC.Marc (simulated model)	2-D (fine mesh) model	2-D (coarse mesh) model	3-D model	Simple model
Computational time (hr)	~16	~ 12	~ 27.5 (5^o) ~ 48 (90^o) ~ 170 (Full)	~ 8
Number of Element	8,466	5,916	12,360 (5^o) 222,480 (90^o) 889,920 (Full)	2,482
Accuracy	Acceptable	Acceptable	Good	Poor

DOI: 10.14750/ME.2022.004

7. CLAIMS AND FUTURE DIRECTIONS

7.1 Claims

Claim 1:

A complex method was designed to validate the finite-element model for the process of manual arc welding of a pipe with dissimilar steels P460NH_1 steel, E355K2 steel and the fillers for the first pass (A5.1-04: E6010) and the second and third passes (A5.5-96: E6010) were welded. I established a method for validation using hardness data and optical metallographic analysis of the heat-affected zone and the fusion zone. The area of the modelled weld-bead joint shape geometry is changed in multi-step iterative calculations to minimize the difference between the calculated and the measured hardness data and to create similarity of the phases identified by metallurgical optical measurement. The area of the weld-bead joint applied in computations varies between the values of the optically measured minimum and maximum area. Predicted results show good agreement with experimental results. The hardness measurement test results are not dependent on the angle of measurement.

Claim 2:

I developed a two-dimensional (2-D) and three-dimensional (3-D) finite element model to simulate and predict the central angle-dependent welding residual stress distribution in a multi-pass girth-welded pipe model for the dissimilar steels (P460NH_1 steel, E355K2 steel) and for the fillers used ((A5.1-04: E6010) for the first pass and the second and third passes (A5.5-96: E6010)). The 3-D model allows calculation results for axial and hoop residual stresses to be obtained with relatively good agreement to the measured data for both angles investigated. The comparison of calculated and measured data confirms that the 3-D model estimates the residual stresses more accurately than the 2-D model, even if the prediction of residual stresses is required at different angles around the longitudinal axis of the pipe welds. The angle dependency of residual stresses was observed by X-ray diffraction measurement for 0° and 90°, and the same trend was predicted by the 3-D finite-element model of pipe welding. This confirms that the only useful and permissible model to predict the residual stresses is the three dimensional one. Figures A-1 and A-2 show the comparison of axial and hoop residual stresses distribution for 3-D and 2-D models with XRD measurement on the outer surface. The measurement in depth is difficult to perform by X-ray diffraction or other means, but the 3-D model actually gives more extra information along the circumferential direction that can be considered as an alternative way to complete and describe the total stress state in the non-

measurable parts of the heat-affected and the fusion zone. Calculation of the normalized root-mean-square deviation or error (NRMSD) is shown in Table A, this table presents (NRMSD) between all models. It shows that 3-D is more accurate comparing with 2-D model.

Table A. Calculation of the normalized root-mean-square deviation or error (NRMSD)

Model	Axial RS at 0° (NRMSD)	Axial RS 90° (NRMSD)	Hoop RS at 0° (NRMSD)	Hoop RS 90° (NRMSD)
2-D	1.987	-	2.090	-
3-D (5°)	1.839	-	1.459	-
3-D (90°)	1.096	1.963	3.781	2.192
3-D	1.2767	1.432	1.02	1.731

Claim 3:

For axial and hoop residual stresses in V-groove arc welding pipe with dissimilar material that used (P460NH_1 steel, E355K2 steel) and for the fillers used ((A5.1-04: E6010) for the first pass and the second and third passes (A5.5-96: E6010)) distribution increases for the entire peak with almost the same heat input and current increase on the outer surface and through the thickness. However, the heat input and current have a relatively small effect on residual stresses on the inner surface. The axial residual stress distribution on the welded joint does not significantly change, but residual hoop stress shows some changes for both surfaces and through the thickness in case of weld speed effect. Although the number of passes is generally thought to have effect on residual stresses (fewer passes leading to higher stresses), the numerical results revealed that the hoop and axial stresses in the dissimilar welded joint do not change on the outer or inner surface related to the number of passes; two passes increase the residual stress distribution slightly in the middle of the weld. The root gap has no significant effect on residual stress distribution through the thickness and the outer and inner surface of weld dissimilar joints. In order to enhance the reliability of the joints, smaller heat input should be employed to decrease the residual stress.

Claim 4:

In the three-dimensional finite element simulation of the welding process, the applied heat source model is the combination of Goldak and conical types that provides a good agreement with the experimental results and the most accurate prediction for axial and hoop residual stresses in V-groove arc welding pipe with dissimilar material that used (P460NH_1 steel, E355K2 steel) and for the fillers used ((A5.1-04: E6010) for the first pass and the second and third passes (A5.5-96: E6010)). Based on the results of the Normalized Root Mean Square Error (NRMSE) implemented models analysis, the minimum deviation was obtained by the combined model-independent on the

DOI: 10.14750/ME.2022.004

circumferential angle (0 and 90 degrees) and the residual stress in the axial and circumferential directions. Table B presents (NRMSD) between all models. It shows that combined heat source model is more accurate comparing with other models.

Table B. Calculation of the normalized root-mean-square deviation or error (NRMSD)

Heat source model	Axial RS at 0^O (NRMSD)	Axial RS 90^O (NRMSD)	Hoop RS at 0^O (NRMSD)	Hoop RS 90^O (NRMSD)
Gaussian	3.678	5.4	5.3	5.86
Goldak	1.2767	1.4322	1.02	1.731
Conical	4.8399	4.8019	5.677	3.64
Combined	0.3103	0.192	0.169	0.27

DOI: 10.14750/ME.2022.004

7.2 Future Directions

The ultimate goal of the current effort is to produce a weld simulation and residual stress prediction tool, attractive to the industry due to its cost-effectiveness, ease of use, robustness and applicability that will not compromise reliability in favour of simplicity. Further parametric investigation of the significance of other problem variables, like material model complexity, phase change, metallurgical transformations, solid model analysis, etc., is necessary to evaluate and validate an already promising fusion welding simulation residual stress prediction technique. Further researchers are needed for residual stress to obtain adequate accuracy with different welding and techniques measurements. The interaction between phase transformation and residual stresses needs further investigation. In future work, more investigates are needed to make a guideline for designing reasonable variable heat sources model in various multi-pass joints.

Furthermore, a validation procedure for the welding would be preferable. This should be based on knowledge of the initial state of stresses and deformations. The current work focuses on stresses in welding. However, cracking is another important issue, and the development of techniques to predict cracking would be of significant industrial interest. Both destructive and non-destructive methods are particularly useful in this regard, especially those that can be made on the component in situ, as better models for predicting residual stress evolution. If these challenges can be met then, residual stresses can bring significant safety and economic benefits to new designs in the future.

DOI: 10.14750/ME.2022.004

ACKNOWLEDGEMENTS

This work has been carried out at the Institute of Physical Metallurgy, Metal Forming, and Nanotechnology, University of Miskolc (ME), Hungary, during the period 2016-2021. The work was supervised by Professor György Krállics at the University of Miskolc.

I would like to express my gratitude to Prof. György Krállics, who regrettably and very suddenly passed away. He was my supervisor for my dissertation. His teaching capabilities were great and he was a great professor, always helping out with everything he could and very supportive of my work. I have very fond memories of him.

I would like to thank the head of Doctoral school Prof. Zoltán Gácsi, the head of my department, Prof. Dr. Valéria Mertinger, the Dean of the faculty Prof. Dr. Árpád Palotás

I would thank Dr. Márton Benke, and all my colleagues in my department.

A special thanks to Mr.Máté Sepsi and Mr. Peter Szobota for helping with measurements (XRD) throughout the duration of my PhD.

Also, thanks to Dr. Máté Szűcs for his support, discussions, and critical review of my work and for his great enthusiasm. Special thanks to Dr. Sándor Kovács for the help, advises, encouragement and discussions about this work.
I am indebted to Mr. Zoltán Bézi who showed me interesting undiscovered fields and helped give birth to new ideas during our inspiring discussions.

A special thanks to Mrs. Anikó Márkus and Mrs. Napsugár Bodnár for helping with sample preparation throughout the duration of my PhD. I would like to thanks Mrs. Judit Szabó, Mrs. Ágnes Solczi, Dr. Mária Svéda, and Mrs. Éva Stumpf for their continued and valuable support in the administrative work at the university.

I would like to thank Ms Robin L. Nagano for her help and encouragement.

I would like to thank my colleagues, former and present, at the department and office for the excellent working environment and for sharing their knowledge in many different areas. Ali Al-Azzawi, Hamid Lahmaidi, Manoj Kumar Pal, Dheeraj Varanasi, Végh Ádám, Korózs József and

DOI: 10.14750/ME.2022.004

Ei Khine for everything for numerous discussions and other fascinating issues and not least, thanks for all the laughs!

To HÖOK Stipendium Hungaricum Mentor Network, I would like to thank you for the most wonderful organisation. This program was a fruitful, amazing and great experience time for me.

I would finally like to thank my wife Adrienn for the love, patience, perseverance and encouragement that helped me to undertake and complete this work and my son Adam, also my friends, teachers, my parents and my brothers and sisters for always supporting and believing and in me during my study. I express my gratitude to Judit Kollárné Tóth and Kollár József for letting me live in their house during my stay in Miskolc.

My study was financially supported by Stipendium Hungaricum (SH). The contribution of this organization is much appreciated.

Mahmood Hasan Dakhil ALHAFADHI
University of Miskolc

8. REFERENCES

[1] F. Kong, J. Ma, and R. Kovacevic, “Numerical and experimental study of thermally induced residual stress in the hybrid laser-GMA welding process,” *J. Mater. Process. Technol.*, vol. 211, no. 6, pp. 1102–1111, 2011, doi: 10.1016/j.jmatprotec.2011.01.012.

[2] J. N. Siddall, “Welding, Brazing, and Soldering,” *Mech. Des.*, pp. 155–155, 2019, doi: 10.3138/9781487579890-121.

[3] C. H. Lee and K. H. Chang, “Numerical analysis of residual stresses in welds of similar or dissimilar steel weldments under superimposed tensile loads,” *Comput. Mater. Sci.*, vol. 40, no. 4, pp. 548–556, 2007, doi: 10.1016/j.commatsci.2007.02.005.

[4] D. Akbari and I. Sattari-Far, “Effect of the welding heat input on residual stresses in butt-welds of dissimilar pipe joints,” *Int. J. Press. Vessel. Pip.*, vol. 86, no. 11, pp. 769–776, 2009, doi: 10.1016/j.ijpvp.2009.07.005.

[5] A. Joseph, S. K. Rai, T. Jayakumar, and N. Murugan, “Evaluation of residual stresses in dissimilar weld joints,” *Int. J. Press. Vessel. Pip.*, vol. 82, no. 9, pp. 700–705, 2005, doi: 10.1016/j.ijpvp.2005.03.006.

[6] P. H. Chang and T. L. Teng, “Numerical and experimental investigations on the residual stresses of the butt-welded joints,” *Comput. Mater. Sci.*, vol. 29, no. 4, pp. 511–522, 2004, doi: 10.1016/j.commatsci.2003.12.005.

[7] D. F. Almeida, R. F. Martins, and J. B. Cardoso, “Numerical simulation of residual stresses induced by TIG butt-welding of thin plates made of AISI 316L stainless steel,” *Procedia Struct. Integr.*, vol. 5, pp. 633–639, 2017, doi: 10.1016/j.prostr.2017.07.032.

[8] A. M. Paradowska, J. W. H. Price, R. Ibrahim, and T. R. Finlayson, “The effect of heat input on residual stress distribution of steel welds measured by neutron diffraction,” vol. 17, no. 1, pp. 385–388, 2006.

[9] H. Vemanaboina, S. Akella, and R. K. Buddu, “Welding Process Simulation Model for Temperature and Residual Stress Analysis,” *Procedia Mater. Sci.*, vol. 6, no. Icmpc, pp. 1539–1546, 2014, doi: 10.1016/j.mspro.2014.07.135.

[10] S. Li, S. Ren, Y. Zhang, D. Deng, and H. Murakawa, “Numerical investigation of formation mechanism of welding residual stress in P92 steel multi-pass joints,” *J. Mater. Process. Technol.*, vol. 244, pp. 240–252, 2017, doi: 10.1016/j.jmatprotec.2017.01.033.

[11] G. S. Schajer, *Practical Residual Stress Measurement Methods*. 2013.

[12] H. Muneel Syed, “Modeling of residual stresses and distortion due to welding in fillet welds,” *Master’s thesis*, 2013.

[13] H. Liu and F. Liou, “Residual Stress Modeling and Deformation Measurement in Laser Metal Deposition Process,” *New Challenges Residual Stress Meas. Eval.*, pp. 1–20, 2020, doi: 10.5772/intechopen.90539.

[14] K. Hemmesi, M. Farajian, and M. Boin, “Numerical studies of welding residual stresses in tubular joints and experimental validations by means of x-ray and neutron diffraction analysis,” *Mater. Des.*, vol. 126, pp. 339–350, 2017, doi: 10.1016/j.matdes.2017.03.088.

[15] P. J. Withers and H. K. D. H. Bhadeshia, “Residual stress part 2 - Nature and origins,” *Mater. Sci. Technol.*, vol. 17, no. 4, pp. 366–375, 2001, doi: 10.1179/026708301101510087.

[16] K. Hemmesi, M. Farajian, and M. Boin, “Numerical studies of welding residual stresses in tubular joints and experimental validations by means of x-ray and neutron diffraction analysis,” *Mater. Des.*, vol. 126, no. March, pp. 339–350, 2017, doi: 10.1016/j.matdes.2017.03.088.

[17] C. Paper and T. Ropar, “Numerical Simulation of Multi-pass Laser Bending Processes using Finite Element Method,” no. December 2013, pp. 1–7, 2015.

[18] G. I. Mahiskar, R. B. Chadge, S. P. Ambade, and A. P. Patil, “Thermo-mechanical Analysis of Multi-pass Bead-on-Plate Welding,” *Procedia Mater. Sci.*, vol. 5, pp. 2522–2531, 2014, doi: 10.1016/j.mspro.2014.07.504.

[19] R. Pamnani, M. Vasudevan, T. Jayakumar, P. Vasantharaja, and K. C. Ganesh, “Numerical simulation and experimental validation of arc welding of DMR-249A steel,” *Def. Technol.*, vol. 12, no. 4, pp. 305–315, 2016, doi: 10.1016/j.dt.2016.01.012.

[20] C. H. Lee, K. H. Chang, and J. U. Park, “Three-dimensional finite element analysis of residual stresses in dissimilar steel pipe welds,” *Nucl. Eng. Des.*, vol. 256, pp. 160–168, 2013, doi: 10.1016/j.nucengdes.2012.12.016.

[21] G. Genchev, N. Doynov, R. Ossenbrink, V. Michailov, G. Bokuchava, and P. Petrov, “Residual stresses formation in multi-pass weldment: A numerical and experimental study,” *J. Constr. Steel Res.*, vol. 138, pp. 633–641, 2017, doi: 10.1016/j.jcsr.2017.08.017.

[22] M. Zubairuddin, S. K. Albert, M. Vasudevan, S. Mahadevan, V. Chaudhari, and V. K. Suri, “Numerical simulation of multi-pass GTA welding of grade 91 steel,” *J. Manuf. Process.*, vol. 27, pp. 87–97, 2017, doi: 10.1016/j.jmapro.2017.04.031.

[23] O. Obeid, G. Alfano, H. Bahai, and H. Jouhara, “Numerical simulation of thermal and residual stress fields induced by lined pipe welding,” *Therm. Sci. Eng. Prog.*, vol. 5, no. August 2017, pp. 1–14, 2018, doi: 10.1016/j.tsep.2017.10.005.

[24] Z. Barsoum and A. Lundbäck, “Simplified FE welding simulation of fillet welds - 3D effects on the formation residual stresses,” *Eng. Fail. Anal.*, vol. 16, no. 7, pp. 2281–2289, 2009, doi: 10.1016/j.engfailanal.2009.03.018.

[25] C. Heinze, C. Schwenk, and M. Rethmeier, “Influences of mesh density and transformation behavior on the result quality of numerical calculation of welding induced distortion,” *Simul. Model. Pract. Theory*, vol. 19, no. 9, pp. 1847–1859, 2011, doi: 10.1016/j.simpat.2011.05.001.

[26] N. K. Babu, M. Kumar, S. Zheng, P. Dayou, S. Jerome, and V. Muthupandi, “Handbook of Manufacturing Engineering and Technology,” *Handb. Manuf. Eng. Technol.*, pp. 1–19, 2013, doi: 10.1007/978-1-4471-4976-7.

[27] P. Ramakrishnan, *Welding Metallurgy*, vol. 4, no. 3. 1972.

[28] C. Heinze, C. Schwenk, and M. Rethmeier, “Numerical calculation of residual stress development of multi-pass gas metal arc welding,” *J. Constr. Steel Res.*, vol. 72, pp. 12–19, 2012, doi: 10.1016/j.jcsr.2011.08.011.

[29] C. C. Silva and J. P. Farias, “Non-uniformity of residual stress profiles in butt-welded pipes

in manual arc welding," *J. Mater. Process. Technol.*, vol. 199, no. 1, pp. 452–455, 2008, doi: 10.1016/j.jmatprotec.2007.08.026.

[30] L. Y. Bai, L. Gao, and K. B. Jiang, "Influence of Residual Stress on the Corrosion Behaviors of Welded Structures in the Nature Seawater," *IOP Conf. Ser. Mater. Sci. Eng.*, vol. 392, no. 4, 2018, doi: 10.1088/1757-899X/392/4/042009.

[31] M. H. Cho, Y. C. Lim, and D. F. Farson, "Simulation of Weld Pool Dynamics in the Stationary Pulsed Gas Metal Arc Welding Process and Final Weld Shape A computer simulation accurately predicts weld pool fluid flow convection and final weld shape," *Weld. J.*, vol. 85, no. 12, pp. 271–283, 2006.

[32] J.-M. Wang, Y. Liu, K. Wang, and Y. Liu, "Research on Welding Heat Affected Zone of Pipeline Steel in High Heat Input Welding," no. Icmsa, pp. 906–910, 2015, doi: 10.2991/icmsa-15.2015.168.

[33] P. Dai, Y. Wang, S. Li, S. Lu, G. Feng, and D. Deng, "FEM analysis of residual stress induced by repair welding in SUS304 stainless steel pipe butt-welded joint," *J. Manuf. Process.*, vol. 58, no. September, pp. 975–983, 2020, doi: 10.1016/j.jmapro.2020.09.006.

[34] "physical-metallurgy-of-welding.pdf." .

[35] A. R. Shahani, I. Shakeri, and C. D. Rans, "Effect of residual stress redistribution and weld reinforcement geometry on fatigue crack growth of butt welded joints," *Int. J. Fatigue*, vol. 139, no. March, p. 105780, 2020, doi: 10.1016/j.ijfatigue.2020.105780.

[36] M. J. Park, H. N. Yang, D. Y. Jang, J. S. Kim, and T. E. Jin, "Residual stress measurement on welded specimen by neutron diffraction," *J. Mater. Process. Technol.*, vol. 155–156, no. 1–3, pp. 1171–1177, 2004, doi: 10.1016/j.jmatprotec.2004.04.393.

[37] S. Wen, H. O. Ox, L. Le, A. Bannister, and T. S. R, "Omae2013-11257 Neutron Diffraction Measurement of Weld Residual Stresses in an," *Omae*, pp. 1–8, 2013.

[38] H. Dai, J. A. Francis, H. J. Stone, H. K. D. H. Bhadeshia, and P. J. Withers, "Characterizing phase transformations and their effects on ferritic weld residual stresses with X-rays and neutrons," *Metall. Mater. Trans. A Phys. Metall. Mater. Sci.*, vol. 39, no. 13, pp. 3070–3078, 2008, doi: 10.1007/s11661-008-9616-0.

[39] P. Ferro, H. Porzner, A. Tiziani, and F. Bonollo, "The influence of phase transformations on residual stresses induced by the welding process-3D and 2D numerical models," *Model. Simul. Mater. Sci. Eng.*, vol. 14, no. 2, pp. 117–136, 2006, doi: 10.1088/0965-0393/14/2/001.

[40] E. Salvati and A. M. Korsunsky, "An analysis of macro- and micro-scale residual stresses of Type I, II and III using FIB-DIC micro-ring-core milling and crystal plasticity FE modelling," *Int. J. Plast.*, vol. 98, pp. 123–138, 2017, doi: 10.1016/j.ijplas.2017.07.004.

[41] J. GUO, H. FU, B. PAN, and R. KANG, "Recent progress of residual stress measurement methods: A review," *Chinese J. Aeronaut.*, 2020, doi: 10.1016/j.cja.2019.10.010.

[42] N. S. Rossini, M. Dassisti, K. Y. Benyounis, and A. G. Olabi, "Methods of measuring residual stresses in components," *Mater. Des.*, vol. 35, pp. 572–588, 2012, doi: 10.1016/j.matdes.2011.08.022.

[43] J. Xu, X. Jia, Y. Fan, A. Liu, and C. Zhang, "Residual Stress Analyses in a Pipe Welding Simulation: 3D Pipe Versus Axi-symmetric Models," *Procedia Mater. Sci.*, vol. 3, pp. 511–

516, 2014, doi: 10.1016/j.mspro.2014.06.085.

[44] M. Law, H. Prask, V. Luzin, and T. Gnaeupel-Herold, “Residual stress measurements in coil, linepipe and girth welded pipe,” *Mater. Sci. Eng. A*, vol. 437, no. 1, pp. 60–63, 2006, doi: 10.1016/j.msea.2006.04.062.

[45] T. Neeraj, T. Gnäupel-Herold, H. J. Prask, and R. Ayer, “Residual stresses in girth welds of carbon steel pipes: Neutron diffraction analysis,” *Sci. Technol. Weld. Join.*, vol. 16, no. 3, pp. 249–253, 2011, doi: 10.1179/1362171810Y.0000000028.

[46] S. Smith, A. Stacey, and C. Johnston, “OMAE2013-10234,” pp. 1–11, 2017.

[47] Y.-H. Zhang, S. Smith, W. Liwu, and C. Johnston, “Residual stress measurements and modelling,” *Fatigue Fract. Eng. Mater. Struct.*, no. 40, pp. 1868–1881, 2017.

[48] T. L. Teng and P. H. Chang, “A study of residual stresses in multi-pass girth-butt welded pipes,” *Int. J. Press. Vessel. Pip.*, vol. 74, no. 1, pp. 59–70, 1997, doi: 10.1016/S0308-0161(97)00091-4.

[49] T. L. Teng and C. C. Lin, “Effect of welding conditions on residual stresses due to butt welds,” *Int. J. Press. Vessel. Pip.*, vol. 75, no. 12, pp. 857–864, 1998, doi: 10.1016/S0308-0161(98)00084-2.

[50] “ResidualStressAnalysisbySimplifiedInherentStrainatWeldedPipeJuncturesinaPressureVessel1999JPVT.pdf.” .

[51] Y. Ren, A. Paradowska, B. Wang, E. Eren, and Y. Jin Janin, “Residual Stress State of X65 Pipeline Girth Welds before and after Local and Furnace Post Weld Heat Treatment,” *J. Press. Vessel Technol. Trans. ASME*, vol. 139, no. 4, pp. 1–8, 2017, doi: 10.1115/1.4035884.

[52] A. E. Eren, S. Zhang, and T. London, “Industrial Member Report Summary – Key Findings for Industry Examination of Residual Stress State in a Girth Welded Pipe Spool Subject to High Plastic Deformation TWI Core Research Programme Industrial need How to benefit from this work :,” vol. 44, no. 0, p. 899000, 2017.

[53] A. Mirzaee-Sisan and A. Bastola, “Redistribution of welding residual stress following high plastic deformation in seamless pipes,” *Int. J. Press. Vessel. Pip.*, vol. 158, no. October, pp. 37–50, 2017, doi: 10.1016/j.ijpvp.2017.10.004.

[54] A. Mirzaee-Sisan, “Welding residual stresses in a strip of a pipe,” *Int. J. Press. Vessel. Pip.*, vol. 159, no. August 2017, pp. 28–34, 2018, doi: 10.1016/j.ijpvp.2017.11.007.

[55] C. H. Lee and K. H. Chang, “Prediction of residual stresses in high strength carbon steel pipe weld considering solid-state phase transformation effects,” *Comput. Struct.*, vol. 89, no. 1–2, pp. 256–265, 2011, doi: 10.1016/j.compstruc.2010.10.005.

[56] S. K. Velaga, G. Rajput, S. Murugan, A. Ravisankar, and S. Venugopal, “Comparison of weld characteristics between longitudinal seam and circumferential butt weld joints of cylindrical components,” *J. Manuf. Process.*, vol. 18, pp. 1–11, 2015, doi: 10.1016/j.jmapro.2014.11.002.

[57] L. Zhao, J. Liang, Q. Zhong, C. Yang, B. Sun, and J. Du, “Numerical simulation on the effect of welding parameters on welding residual stresses in T92/S30432 dissimilar welded pipe,” *Adv. Eng. Softw.*, vol. 68, pp. 70–79, 2014, doi: 10.1016/j.advengsoft.2013.12.004.

[58] O. Obeid, G. Alfano, H. Bahai, and H. Jouhara, “Experimental and numerical thermo-mechanical analysis of welding in a lined pipe,” *J. Manuf. Process.*, vol. 32, no. February, pp. 857–872, 2018, doi: 10.1016/j.jmapro.2018.04.009.

[59] A. S. Ahmad, Y. Wu, H. Gong, and L. Liu, “Numerical Simulation of Thermal and Residual Stress Field Induced by Three-Pass TIG Welding of Al 2219 Considering the Effect of Interpass Cooling,” *Int. J. Precis. Eng. Manuf.*, vol. 21, no. 8, pp. 1501–1518, 2020, doi: 10.1007/s12541-020-00357-1.

[60] A. H. Yaghi, T. H. Hyde, A. A. Becker, and W. Sun, “Finite element simulation of residual stresses induced by the dissimilar welding of a P92 steel pipe with weld metal IN625,” *Int. J. Press. Vessel. Pip.*, vol. 111–112, pp. 173–186, 2013, doi: 10.1016/j.ijpvp.2013.07.002.

[61] D. Deng and S. Kiyoshima, “FEM prediction of welding residual stresses in a SUS304 girth-welded pipe with emphasis on stress distribution near weld start/end location,” *Comput. Mater. Sci.*, vol. 50, no. 2, pp. 612–621, 2010, doi: 10.1016/j.commatsci.2010.09.025.

[62] C. Wu and J. W. Kim, “Analysis of welding residual stress formation behavior during circumferential TIG welding of a pipe,” *Thin-Walled Struct.*, vol. 132, no. September, pp. 421–430, 2018, doi: 10.1016/j.tws.2018.09.020.

[63] Z. A. Majid and R. Mohsin, “Failure Investigation of Natural Gas Pipeline,” *Arab. J. Sci. Eng.*, vol. 37, no. 4, pp. 1083–1088, 2012, doi: 10.1007/s13369-012-0236-z.

[64] Z. A. Majid, R. Mohsin, and M. Z. Yusof, “Experimental and computational failure analysis of natural gas pipe,” *Eng. Fail. Anal.*, vol. 19, no. 1, pp. 32–42, 2012, doi: 10.1016/j.engfailanal.2011.09.004.

[65] Z. A. Majid, R. Mohsin, Z. Yaacob, and Z. Hassan, “Failure analysis of natural gas pipes,” *Eng. Fail. Anal.*, vol. 17, no. 4, pp. 818–837, 2010, doi: 10.1016/j.engfailanal.2009.10.016.

[66] R. Datta and A. Deva, “An investigation into the failure of API 5L X-46 grade ERW linepipes,” *J. Fail. Anal. Prev.*, vol. 2, no. 2, pp. 59–62, 2002, doi: 10.1007/BF02715420.

[67] M. D. Chapetti, J. L. Otegui, and J. Motylicki, “Fatigue assessment of an electrical resistance welded oil pipeline,” *Int. J. Fatigue*, vol. 24, no. 1, pp. 21–28, 2002, doi: 10.1016/S0142-1123(01)00111-6.

[68] P. G. Fazzini, A. P. Cisilino, and J. L. Otegui, “Experimental validation of the influence of lamination defects in electrical resistance seam welded pipelines,” *Int. J. Press. Vessel. Pip.*, vol. 82, no. 12, pp. 896–904, 2005, doi: 10.1016/j.ijpvp.2005.07.006.

[69] C. R. F. Azevedo, “Failure analysis of a crude oil pipeline,” *Eng. Fail. Anal.*, vol. 14, no. 6 SPEC. ISS., pp. 978–994, 2007, doi: 10.1016/j.engfailanal.2006.12.001.

[70] P. G. Fazzini, J. C. Belmonte, M. D. Chapetti, and J. L. Otegui, “Fatigue assessment of a double submerged arc welded gas pipeline,” *Int. J. Fatigue*, vol. 29, no. 6, pp. 1115–1124, 2007, doi: 10.1016/j.ijfatigue.2006.09.013.

[71] F. Ahmed, L. Ali, J. Iqbal, and F. Hasan, “Failure of pipe joints during hydrostatic testing,” *Eng. Fail. Anal.*, vol. 15, no. 6, pp. 766–773, 2008, doi: 10.1016/j.engfailanal.2007.06.008.

[72] K. A. Macdonald, A. Cosham, C. R. Alexander, and P. Hopkins, “Assessing mechanical damage in offshore pipelines - Two case studies,” *Eng. Fail. Anal.*, vol. 14, no. 8 SPEC. ISS., pp. 1667–1679, 2007, doi: 10.1016/j.engfailanal.2006.11.074.

[73] E. Sadeghi Meresht, T. Shahrabi Farahani, and J. Neshati, “Failure analysis of stress corrosion cracking occurred in a gas transmission steel pipeline,” *Eng. Fail. Anal.*, vol. 18, no. 3, pp. 963–970, 2011, doi: 10.1016/j.engfailanal.2010.11.014.

[74] M. A. Al-Anezi, S. Rao, and G. R. Lobley, “Pipeline failure by transit fatigue,” *J. Fail. Anal. Prev.*, vol. 9, no. 1, pp. 35–38, 2009, doi: 10.1007/s11668-008-9201-2.

[75] M. A. Al-Anezi, T. A. Al-Ghamdi, W. L. Al-Otaibi, and S. M. Al-Muaili, “Prevention of Hydrogen Assisted Damage in Sour Service,” *J. Fail. Anal. Prev.*, vol. 14, no. 6, pp. 736–745, 2014, doi: 10.1007/s11668-014-9877-4.

[76] R. Gou, Y. Zhang, X. Xu, L. Sun, and Y. Yang, “Residual stress measurement of new and in-service X70 pipelines by X-ray diffraction method,” *NDT E Int.*, vol. 44, no. 5, pp. 387–393, 2011, doi: 10.1016/j.ndteint.2011.03.003.

[77] K. Abdel-Tawab and A. K. Noor, “Uncertainty analysis of welding residual stress fields,” *Comput. Methods Appl. Mech. Eng.*, vol. 179, no. 3–4, pp. 327–344, 1999, doi: 10.1016/S0045-7825(99)00045-6.

[78] V. Akrivos *et al.*, “Neutron diffraction measurements of weld residual stresses in three-pass slot weld (Alloy 600/82) and assessment of the measurement uncertainty,” *J. Appl. Crystallogr.*, vol. 53, pp. 1181–1194, 2020, doi: 10.1107/S1600576720009140.

[79] H. (Lulea U. of T. Alberg, “Simulation of Welding and Heat Treatment Modelling and Validation,” *Sci. Technol.*, 2005.

[80] C. R. Arganis Juárez, R. Hernández Callejas, and A. L. Medina Almazán, “Crack growth rate in core shroud horizontal welds using two models for a BWR,” *J. Nucl. Mater.*, vol. 460, pp. 166–173, 2015, doi: 10.1016/j.jnucmat.2015.02.019.

[81] A. A. Bhatti and Z. Barsoum, “Development of efficient three-dimensional welding simulation approach for residual stress estimation in different welded joints,” *J. Strain Anal. Eng. Des.*, vol. 47, no. 8, pp. 539–552, 2012, doi: 10.1177/0309324712463866.

[82] J. Cañas, R. Picón, F. Paris, A. Blazquez, and J. C. Marin, “A simplified numerical analysis of residual stresses in aluminum welded plates,” *Comput. Struct.*, vol. 58, no. 1, pp. 59–69, 1996, doi: 10.1016/0045-7949(95)00112-T.

[83] J. Cañas, R. Picón, F. París, J. C. Marín, and A. Bermejo, “Experimental and numerical analysis of residual stresses in welded AI-5083-O aluminium plates,” *Weld. Int.*, vol. 8, no. 1, pp. 30–35, 1994, doi: 10.1080/09507119409548539.

[84] X. Cao, M. Jahazi, J. P. Immarigeon, and W. Wallace, “A review of laser welding techniques for magnesium alloys,” *J. Mater. Process. Technol.*, vol. 171, no. 2, pp. 188–204, 2006, doi: 10.1016/j.jmatprotec.2005.06.068.

[85] W. Dc, “On the Effects of W e t U n d e r w a t e r W e l d i n g on the Fracture B e h a v i o u r of Welds,” no. August, 2001.

[86] T. L. Dickson, B. R. Bass, and W. J. Mcafee, “THE INCLUSION OF WELD RESIDUAL STRESS IN FRACTURE ColvF- q l0708--,” pp. 0–25.

[87] U. Dilthey, U. Reisgen, and M. Kretschmer, “Comparison of FEM simulations to measurements of residual stresses for the example of a welded plate: a state-of-the-art report,” *Model. Simul. Mater. Sci. Eng.*, vol. 8, no. 6, pp. 911–926, 2000, doi: 10.1088/0965-

0393/8/6/311.

[88] P. Dong, J. K. Hong, and P. Rogers, “Analysis of residual stresses in Al-Li repair welds and mitigation techniques,” *Weld. J. (Miami, Fla)*, vol. 77, no. 11, pp. 439–445, 1998.

[89] P. Dong and J. Zhang, “Residual stresses in strength-mismatched welds and implications on fracture behavior,” *Eng. Fract. Mech.*, vol. 64, no. 4, pp. 485–505, 1999, doi: 10.1016/S0013-7944(99)00088-0.

[90] T. W. Fan, “Simulation of welding residual stress to the fracture strength of steel moment-resist frame connection,” *Adv. Mater. Res.*, vol. 250–253, pp. 3682–3687, 2011, doi: 10.4028/www.scientific.net/AMR.250-253.3682.

[91] S. Fricke, E. Keim, and J. Schmidt, “Numerical weld modeling - A method for calculating weld-induced residual stresses,” *Nucl. Eng. Des.*, vol. 206, no. 2–3, pp. 139–150, 2001, doi: 10.1016/S0029-5493(00)00414-3.

[92] R. Gadallah, S. Tsutsumi, S. Tanaka, and N. Osawa, “Accurate evaluation of fracture parameters for a surface-cracked tubular T-joint taking welding residual stress into account,” *Mar. Struct.*, vol. 71, no. January, p. 102733, 2020, doi: 10.1016/j.marstruc.2020.102733.

[93] D. George, D. J. Smith, and P. J. Bouchard, “Evaluation of through wall residual stresses in stainless steel weld repairs,” *Mater. Sci. Forum*, vol. 347, pp. 646–651, 2000, doi: 10.4028/www.scientific.net/msf.347-349.646.

[94] T. Gnäupel-Herold *et al.*, “Measurement of residual stress in materials using neutrons Proceedings of a technical meeting held in Vienna 13-17 October, 2003,” *Int. At. Energy Agency*, no. June, pp. 1–99, 2005.

[95] J. Hensel, T. Nitschke-Pagel, and K. Dilger, “Effects of residual stresses and compressive mean stresses on the fatigue strength of longitudinal fillet-welded gussets,” *Weld. World*, vol. 60, no. 2, pp. 267–281, 2016, doi: 10.1007/s40194-015-0284-6.

[96] M. R. Hill and D. V. Nelson, “A Simplified Eigenstrain Approach for Determination of Sub-surface Triaxial Residual Stress in Welds,” *Citeseer*, no. 1970, pp. 1–8, 1987.

[97] M. R. Hill and D. V. Nelson, “Determining residual stress through the thickness of a welded plate,” *Am. Soc. Mech. Eng. Press. Vessel. Pip. Div. PVP*, vol. 327, pp. 29–36, 1996.

[98] J. K. Hong, J. Zhang, P. Rogers, J. Bynum, and S. Shah, “o :,” vol. 120, no. June 1997, pp. 122–128, 2015.

[99] J. K. Hong, C. L. Tsai, and P. Dong, “Assessment of numerical procedures for residual stress analysis of multipass welds,” *Weld. J. (Miami, Fla)*, vol. 77, no. 9, pp. 372-s, 1998.

[100] K. Hong, D. C. Weckman, and A. B. Strong, “The Influence of Thermofluids Phenomena in Gas Tungsten ARC Welds in High and Low Thermal Conductivity Metals,” *Can. Metall. Q.*, vol. 37, no. 3–4, pp. 293–303, 1998, doi: 10.1179/cmq.1998.37.3-4.293.

[101] J. J. Jaeger and J. A. Padula, “Estimation of residual stresses in thick section weldments,” *Struct. Congr. - Proc.*, vol. 2, no. September, pp. 1260–1264, 1997.

[102] W. Jiang, J. M. Gong, W. Woo, Y. F. Wang, and S. T. Tu, “Control of welding residual stress and deformation of the butt welded ultrathick tube-sheet: Effect of applied load,” *J. Press. Vessel Technol. Trans. ASME*, vol. 134, no. 6, pp. 61406-1-61406–8, 2012, doi:

10.1115/1.4007037.

[103] H. Kockelmann, J. Schreiber, Y. V. Taran, and J. S. Wright, “Investigation of residual stresses in a shape welded steel tube by the time-of-flight neutron diffraction technique,” *Mater. Sci. Forum*, vol. 321, pp. 726–731, 2000, doi: 10.4028/www.scientific.net/msf.321-324.726.

[104] B. P. Marquis, D. Y. Jeong, and A. B. Perlman, “Residual stresses in tank car shells in the vicinity,” pp. 157–164, 1995.

[105] P. Michaleris, J. Dantzig, and D. Tortorelli, “Minimization of welding residual stress and distortion in large structures,” *Weld. J. (Miami, Fla)*, vol. 78, no. 11, pp. 361-s, 1999.

[106] K. Nakacho, “A simple estimating method for reduction of welding residual stresses in thick welded joint from stress-relief annealing - Part IV: Applicability of the simple estimating method for stress-relief annealing of thick welded joint,” *J. Press. Vessel Technol. Trans. ASME*, vol. 124, no. 2, pp. 207–214, 2002, doi: 10.1115/1.1398285.

[107] P. G. Rao, P. S. Rao, and A. G. Krishna, “R Eview on R Esidual S Tresses in W Elded J Oints P Repared Under the I Nfluence of M Echanical V Ibrations,” vol. 6, no. 1, p. 8095, 1943.

[108] S. Sarkani, V. Tritchkov, and G. Michaelov, “Efficient approach for computing residual stresses in welded joints,” *Finite Elem. Anal. Des.*, vol. 35, no. 3, pp. 247–268, 2000, doi: 10.1016/S0168-874X(99)00068-2.

[109] S. M. Schlögl and E. Van Der Giessen, “Influence of residual stresses in a welded vessel on the hydrogen attack lifetime,” *Mater. Sci. Forum*, vol. 347, pp. 628–633, 2000, doi: 10.4028/www.scientific.net/msf.347-349.628.

[110] D. Schroepfer, A. Kromm, and T. Kannengiesser, “Engineering approach to assess residual stresses in welded components,” *Weld. World*, vol. 61, no. 1, pp. 91–106, 2017, doi: 10.1007/s40194-016-0394-9.

[111] X. Shen, K. Gao, and S. Dong, “Simulation and analysis of electron beam welding residual stress in thin-walled high-temperature alloy aeroengine structures,” *Int. J. Adv. Manuf. Technol.*, vol. 107, no. 9–10, pp. 3953–3966, 2020, doi: 10.1007/s00170-020-05276-z.

[112] N. Siva Prasad and T. K. Sankaranarayanan, “Estimation of residual stresses in weldments using adaptive grids,” *Comput. Struct.*, vol. 60, no. 6, pp. 1037–1045, 1996, doi: 10.1016/0045-7949(96)00006-5.

[113] D. J. Smith, P. J. Bouchard, and D. George, “Measurement and prediction of residual stresses in thick-section steel welds,” *J. Strain Anal. Eng. Des.*, vol. 35, no. 4, pp. 287–305, 2000, doi: 10.1243/0309324001514422.

[114] I. Starcevic and F. Werner, “Determination of Residual Stresses in Steel Constructions Due To the Welding,” no. January, pp. 1487–1496, 2006.

[115] M. Sutton and A. P. Reynolds, “Erratum to: A Study of Residual Stresses and Microstructure in 2024-T3 Aluminum Friction Stir Butt Welds, ASME J. Eng. Mater. Technol., 124, No. 2, pp. 215-222,” *J. Eng. Mater. Technol. Trans. ASME*, vol. 124, no. 4, p. 451, 2002, doi: 10.1115/1.1511521.

[116] B. Taljat *et al.*, “Numerical analysis of residual stress distribution in tubes with spiral weld

cladding," *Weld. J. (Miami, Fla)*, vol. 77, no. 8, pp. 328–335, 1998.

[117] B. Taljat, T. Zacharia, X. L. Wang, J. R. Keiser, Z. Feng, and M. J. Jirinec, "Residual stresses in weld overlay tubes: A finite element study," *American Society of Mechanical Engineers, Pressure Vessels and Piping Division (Publication) PVP*, vol. 347. pp. 83–89, 1997.

[118] L. Tao, S. Yaowu, and J. Lipei, "Residual stress distributions and plastic zones in heterogeneous welded plates with a transverse crack," *Int. J. Press. Vessel. Pip.*, vol. 77, no. 9, pp. 549–553, 2000, doi: 10.1016/S0308-0161(00)00053-3.

[119] T. L. Teng, C. P. Fung, P. H. Chang, and W. C. Yang, "Analysis of residual stresses and distortions in T-joint fillet welds," *Int. J. Press. Vessel. Pip.*, vol. 78, no. 8, pp. 523–538, 2001, doi: 10.1016/S0308-0161(01)00074-6.

[120] C. L. Tsai, M. L. Liaw, and J. I. Teng, "Effect of residual stresses on design assessment of partial penetration laser welds in a pressure valve component," *Weld. J. (Miami, Fla)*, vol. 77, no. 10, pp. 403–410, 1998.

[121] R. Weiss, "Residual stresses and strength of friction welded ceramic/metal joints," *Weld. J. (Miami, Fla)*, vol. 77, no. 6, pp. 115-s, 1998.

[122] T. Yamashita, T. Hattori, K. lida, T. Nomoto, and M. Sato, "Effects of residual stress on fatigue strength of small- diameter welded pipe joint," *J. Press. Vessel Technol. Trans. ASME*, vol. 119, no. 4, pp. 428–434, 1997, doi: 10.1115/1.2842326.

[123] M. G. Yuan and Y. Ueda, "Prediction of residual stresses in welded T- and I-joints using inherent strains," *J. Eng. Mater. Technol. Trans. ASME*, vol. 118, no. 2, pp. 229–234, 1996, doi: 10.1115/1.2804892.

[124] J. Zhang, P. Dong, F. W. Brust, W. J. Shack, M. E. Mayfield, and M. McNeil, "Modeling of weld residual stresses in core shroud structures," *Nucl. Eng. Des.*, vol. 195, no. 2, pp. 171–187, 2000, doi: 10.1016/S0029-5493(99)00251-4.

[125] "mesuerment and modeling residual stresees in offrshoe.pdf." .

[126] "ASME_PVP1996_Feng_fem for R.S. repair welds.pdf." .

[127] S. BERRY, "Los Alamos," *Don't Leave Hungry*, pp. 176–177, 2017, doi: 10.2307/j.ctt1ffjgnb.124.

[128] B. Brickstad and B. L. Josefson, "A parametric study of residual stresses in multi-pass butt-welded stainless steel pipes," *Int. J. Press. Vessel. Pip.*, vol. 75, no. 1, pp. 11–25, 1998, doi: 10.1016/S0308-0161(97)00117-8.

[129] D. W. Brown, J. D. Bernardin, J. S. Carpenter, B. Clausen, D. Spernjak, and J. M. Thompson, "Neutron diffraction measurements of residual stress in additively manufactured stainless steel," *Mater. Sci. Eng. A*, vol. 678, no. August, pp. 291–298, 2016, doi: 10.1016/j.msea.2016.09.086.

[130] N. R. Commission, "50 years of INIS International Nuclear Information System," pp. 5–6, 2000.

[131] P. Dong, "Residual stress analyses of a multi-pass girth weld: 3-D special shell versus axisymmetric models," *J. Press. Vessel Technol. Trans. ASME*, vol. 123, no. 2, pp. 207–213,

2001, doi: 10.1115/1.1359527.

[132] P. Dong and F. W. Brust, “Welding residual stresses and effects on fracture in pressure vessel and piping components: a millennium review and beyond,” *J. Press. Vessel Technol. Trans. ASME*, vol. 122, no. 3, pp. 329–338, 2000, doi: 10.1115/1.556189.

[133] N. Hempel, J. R. Bunn, O. Ridge, T. N. Nitschke-pagel, E. A. Payzant, and O. Ridge, “Residual Stress Analysis in Girth-welded Ferritic and Austenitic Steel Pipes Using Neutron and X-Ray Diffraction,” *Residual Stress. 2016*, vol. 2, no. July, pp. 229–234, 2017, doi: 10.21741/9781945291173-39.

[134] M. R. Hill and D. V. Nelson, “Inherent strain method for residual stress determination and its application to a long welded joint,” *Am. Soc. Mech. Eng. Press. Vessel. Pip. Div. PVP*, vol. 318, no. June, pp. 343–352, 1995.

[135] R. Iwahori, A., Hirota, Y., Sampe, “NII-Electronic Library Service,” *Chem. Pharm. Bull.*, no. 43, p. 2091, 1970.

[136] F. A. Kandil, J. D. Lord, A. T. Fry, and P. V Grant, “A review of residual stress measurement methods,” *A Guid. to Tech. Sel. NPL, Rep. MATC*, vol. 4, no. November 2015, pp. 1–42, 2001.

[137] C. H. Kim, D. H. Bae, S. Y. Cho, and B. K. Kim, “Welding residual stress analysis and fatigue crack growth characteristics of multi-pass welded pipe weldment,” *Key Eng. Mater.*, vol. 187, no. 187 PART 2, pp. 1345–1350, 2000, doi: 10.4028/www.scientific.net/kem.183-187.1345.

[138] R. Konar and M. Mician, “Numerical simulation of residual stresses and distortions in butt weld in simulation programme sysweld,” *Komunikacie*, vol. 14, no. 3, pp. 49–54, 2012.

[139] J. Kusnick, M. Benson, and S. Lyons, “Finite Element Analysis of Weld Residual Stresses in Austenitic Stainless Steel Dry Cask Storage System Canisters,” no. December, p. 32, 2013.

[140] M. Law and V. Luzin, “Measured residual stresses and integrity of pipeline girth welds,” *Sci. Technol. Weld. Join.*, vol. 17, no. 8, pp. 694–698, 2012, doi: 10.1179/1362171812Y.0000000064.

[141] P. Michaleris, L. Zhang, S. R. Bhide, and P. Marugabandhu, “Evaluation of 2D, 3D and applied plastic strain methods for predicting buckling welding distortion and residual stress,” *Sci. Technol. Weld. Join.*, vol. 11, no. 6, pp. 707–716, 2006, doi: 10.1179/174329306X147724.

[142] P. Michaleris, “Residual stress distributions for multi-pass welds in pressure vessel and piping components,” *Am. Soc. Mech. Eng. Press. Vessel. Pip. Div. PVP*, vol. 327, pp. 17–20, 1996.

[143] M. Mochizuki, M. Hayashi, and T. Hattori, “Residual stress analysis by simplified inherent strain at welded pipe junctures in a pressure vessel,” *J. Press. Vessel Technol. Trans. ASME*, vol. 121, no. 4, pp. 353–357, 1999, doi: 10.1115/1.2883714.

[144] M. Mochizuki, M. Hayashi, M. Nakagawa, N. Tada, and S. Shimizu, “Residual stress estimation at welded joint of a pipe penetrating a thick plate,” *Nippon Kikai Gakkai Ronbunshu, A Hen/Transactions of the Japan Society of Mechanical Engineers, Part A*, vol. 62, no. 597. pp. 1250–1255, 1996, doi: 10.1299/kikaia.62.1250.

[145] A. J. Pinkerton *et al.*, “THE EFFECT OF PROCESS PARAMETERS ON RESIDUAL STRESSES WITHIN AN Paper 1402.”

[146] Y. Ren, “Investigation of Residual Stresses in X65 Narrow-Gap Pipe Girth Welds,” no. March, 2018.

[147] C. S. Seok, M. W. Suh, and J. H. Park, “Investigation of welding residual stress of high tensile steel by finite element method and experiment,” *KSME Int. J.*, vol. 13, no. 12, pp. 879–885, 1999, doi: 10.1007/BF03184755.

[148] S. Song and P. Dong, “Residual stresses in weld repairs and mitigation by design,” *Proc. Int. Conf. Offshore Mech. Arct. Eng. - OMAE*, vol. 5, no. June, 2014, doi: 10.1115/OMAE2014-24547.

[149] Y. Wu, X. Zhan, H. Yu, X. Feng, and P. Xia, “FE analysis of the residual stresses for the laser welded T-joint of Al-Li alloy under service loads,” *Mater. Res. Express*, vol. 6, no. 9, 2019, doi: 10.1088/2053-1591/ab2c4d.

[150] J. Xu, X. Jia, Y. Fan, A. Liu, and C. Zhang, “Residual Stress Analyses in a Pipe Welding Simulation: 3D Pipe Versus Axi-symmetric Models,” *Procedia Mater. Sci.*, vol. 3, pp. 511–516, 2014, doi: 10.1016/j.mspro.2014.06.085.

[151] S. Szávai, Z. Bezi, and C. Ohms, “Numerical simulation of dissimilar metal welding and its verification for determination of residual stresses,” *Frat. ed Integrita Strutt.*, vol. 10, no. 36, pp. 36–45, 2016, doi: 10.3221/IGF-ESIS.36.04.

[152] H. Moshayedi and I. Sattari-Far, “The effect of welding residual stresses on brittle fracture in an internal surface cracked pipe,” *Int. J. Press. Vessel. Pip.*, vol. 126, pp. 29–36, 2015, doi: 10.1016/j.ijpvp.2015.01.003.

[153] A. S. Ahmad, Y. Wu, H. Gong, and L. Nie, “Finite element prediction of residual stress and deformation induced by double-pass TIG welding of Al 2219 plate,” *Materials (Basel).*, vol. 12, no. 14, 2019, doi: 10.3390/ma12142251.

[154] M. Hamdi, H. A. Benhorma, A. Hadjaj, and A. Benchatti, “Residual stresses measurement in the weld seam of X70 steel, analyzed by XRD,” *Acta Phys. Pol. A*, vol. 132, no. 3, pp. 866–868, 2017, doi: 10.12693/APhysPolA.132.866.

[155] K. Hsu, B. Tsai, and L. Kang, “Experimental Measurements and Numerical Simulation of Welding Residual Stress on A240 Metal in Multi-Pass Welding Process,” pp. 1–5.

[156] F. Kong and R. Kovacevic, “3D finite element modeling of the thermally induced residual stress in the hybrid laser/arc welding of lap joint,” *J. Mater. Process. Technol.*, vol. 210, no. 6–7, pp. 941–950, 2010, doi: 10.1016/j.jmatprotec.2010.02.006.

[157] G. Salerno *et al.*, “On the interaction between welding residual stresses: A numerical and experimental investigation,” *Int. J. Mech. Sci.*, vol. 144, pp. 654–667, 2018, doi: 10.1016/j.ijmecsci.2018.04.055.

[158] M. S. Yi, S. H. Noh, D. H. Lee, D. H. Seo, and J. K. Paik, “Direct measurements, numerical predictions and simple formula estimations of welding-induced biaxial residual stresses in a full-scale steel stiffened plate structure,” *Structures*, vol. 29, no. June 2020, pp. 2094–2105, 2021, doi: 10.1016/j.istruc.2020.05.030.

[159] D. Deng, Y. Zhou, T. Bi, and X. Liu, “Experimental and numerical investigations of welding

distortion induced by CO2 gas arc welding in thin-plate bead-on joints," *Mater. Des.*, vol. 52, pp. 720–729, 2013, doi: 10.1016/j.matdes.2013.06.013.

[160] M. Zubairuddin, S. K. Albert, V. Chaudhari, and V. K. Suri, "Influence of Phase Transformation on Thermo-mechanical Analysis of Modified 9Cr-1Mo Steel," *Procedia Mater. Sci.*, vol. 5, pp. 832–840, 2014, doi: 10.1016/j.mspro.2014.07.368.

[161] K. Abburi Venkata, C. E. Truman, R. C. Wimpory, and T. Pirling, "Numerical simulation of a three-pass TIG welding using finite element method with validation from measurements," *Int. J. Press. Vessel. Pip.*, vol. 164, pp. 68–79, 2018, doi: 10.1016/j.ijpvp.2017.05.014.

[162] D. Deng and H. Murakawa, "Finite element analysis of temperature field, microstructure and residual stress in multi-pass butt-welded 2.25Cr-1Mo steel pipes," *Comput. Mater. Sci.*, vol. 43, no. 4, pp. 681–695, 2008, doi: 10.1016/j.commatsci.2008.01.025.

[163] D. Deng and H. Murakawa, "Numerical simulation of temperature field and residual stress in multi-pass welds in stainless steel pipe and comparison with experimental measurements," *Comput. Mater. Sci.*, vol. 37, no. 3, pp. 269–277, 2006, doi: 10.1016/j.commatsci.2005.07.007.

[164] A. Kermanpur, M. Shamanian, and V. E. Yeganeh, "Three-dimensional thermal simulation and experimental investigation of GTAW circumferentially butt-welded Incoloy 800 pipes," *J. Mater. Process. Technol.*, vol. 199, no. 1, pp. 295–303, 2008, doi: 10.1016/j.jmatprotec.2007.08.009.

[165] T. Kasuya, Y. Hashiba, S. Ohkita, and M. Fuji, "Heat conduction analysis of bidirectional multipass welding with short bead lengths," *Sci. Technol. Weld. Join.*, vol. 5, no. 4, pp. 215–220, 2000, doi: 10.1179/136217100101538236.

[166] J. Rahman Chukkan, M. Vasudevan, S. Muthukumaran, R. Ravi Kumar, and N. Chandrasekhar, "Simulation of laser butt welding of AISI 316L stainless steel sheet using various heat sources and experimental validation," *J. Mater. Process. Technol.*, vol. 219, pp. 48–59, 2015, doi: 10.1016/j.jmatprotec.2014.12.008.

[167] H. M. Aarbogh, M. Hamide, H. G. Fjær, A. Mo, and M. Bellet, "Experimental validation of finite element codes for welding deformations," *J. Mater. Process. Technol.*, vol. 210, no. 13, pp. 1681–1689, 2010, doi: 10.1016/j.jmatprotec.2010.05.014.

[168] M. J. Attarha and I. Sattari-Far, "Study on welding temperature distribution in thin welded plates through experimental measurements and finite element simulation," *J. Mater. Process. Technol.*, vol. 211, no. 4, pp. 688–694, 2011, doi: 10.1016/j.jmatprotec.2010.12.003.

[169] M. Perić *et al.*, "Numerical analysis and experimental investigation of welding residual stresses and distortions in a T-joint fillet weld," *Mater. Des.*, vol. 53, pp. 1052–1063, 2014, doi: 10.1016/j.matdes.2013.08.011.

[170] H. Keinänen, "Computation of residual stresses for a repair weld case," *Weld. World*, vol. 60, no. 3, pp. 507–513, 2016, doi: 10.1007/s40194-016-0323-y.

[171] A. H. Yaghi, T. H. Hyde, A. A. Becker, and W. Sun, "Thermomechanical modelling of weld microstructure and residual stresses in P91 steel pipe," *Energy Mater. Mater. Sci. Eng. Energy Syst.*, vol. 4, no. 3, pp. 113–123, 2009, doi: 10.1179/174892310X12779109287084.

[172] J. Xia and H. Jin, "Numerical study of welding simulation and residual stress on butt welding

of dissimilar thickness of austenitic stainless steel," *Int. J. Adv. Manuf. Technol.*, vol. 91, no. 1–4, pp. 227–235, 2017, doi: 10.1007/s00170-016-9738-2.

[173] R. Bjorhovde, J. Brozzetti, G. A. Alpsten, and L. Tall, "Residual Stresses in Thick Welded Plates - A study of the cooling and welding residual stresses in heavy plates provides a method for estimating the residual stresses in welded built-up structural shapes," *Weld. Journal, res. Supl.*, pp. 392–405, 1972.

[174] C. a I. Zhipeng, N. Masashi, M. a Ninshu, Q. U. Yuebo, and C. a O. Bin, "Residual Stresses in Flash Butt Welded Rail," *Trans. JWRI*, vol. 40, no. 1, pp. 79–87, 2011.

[175] N. Ma, Z. Cai, H. Huang, D. Deng, H. Murakawa, and J. Pan, "Investigation of welding residual stress in flash-butt joint of U71Mn rail steel by numerical simulation and experiment," *Mater. Des.*, vol. 88, pp. 1296–1309, 2015, doi: 10.1016/j.matdes.2015.08.124.

[176] M. Zubairuddin, S. K. Albert, S. Mahadevan, M. Vasudevan, V. Chaudhari, and V. K. Suri, "Experimental and finite element analysis of residual stress and distortion in GTA welding of modified 9Cr-1Mo steel," *J. Mech. Sci. Technol.*, vol. 28, no. 12, pp. 5095–5105, 2014, doi: 10.1007/s12206-014-1132-0.

[177] M. Zubairuddin, S. K. Albert, M. Vasudevan, S. Mahadevan, V. Chaudhri, and V. K. Suri, "Thermomechanical analysis of preheat effect on grade P91 steel during GTA welding," *Mater. Manuf. Process.*, vol. 31, no. 3, pp. 366–371, 2016, doi: 10.1080/10426914.2015.1025964.

[178] P. Colegrove *et al.*, "Welding process impact on residual stress and distortion," *Sci. Technol. Weld. Join.*, vol. 14, no. 8, pp. 717–725, 2009, doi: 10.1179/136217109X406938.

[179] M. Zeinoddini, S. Arnavaz, A. P. Zandi, and Y. A. Vaghasloo, "Repair welding influence on offshore pipelines residual stress fields: An experimental study," *J. Constr. Steel Res.*, vol. 86, pp. 31–41, 2013, doi: 10.1016/j.jcsr.2013.03.010.

[180] O. Culha, "Finite element modelling of submerged arc welding process for a symmetric T-beam," *Mater. Tehnol.*, vol. 48, no. 2, pp. 243–248, 2014.

[181] J. B. Ju, J. S. Lee, J. il Jang, W. S. Kim, and D. Kwon, "Determination of welding residual stress distribution in API X65 pipeline using a modified magnetic Barkhausen noise method," *Int. J. Press. Vessel. Pip.*, vol. 80, no. 9, pp. 641–646, 2003, doi: 10.1016/S0308-0161(03)00131-5.

[182] M. Mochizuki, M. Hayashi, and T. Hattori, "Numerical analysis of welding residual stress and its verification using neutron diffraction measurement," *J. Eng. Mater. Technol. Trans. ASME*, vol. 122, no. 1, pp. 98–103, 2000, doi: 10.1115/1.482772.

[183] C. yan Yan, C. ying Liu, and G. yuan Zhang, "Simulation of hydrogen diffusion in welded joint of X80 pipeline steel," *J. Cent. South Univ.*, vol. 21, no. 12, pp. 4432–4437, 2014, doi: 10.1007/s11771-014-2445-y.

[184] K. Nasim, A. F. M. Arif, Y. N. Al-Nassar, and M. Anis, "Investigation of residual stress development in spiral welded pipe," *J. Mater. Process. Technol.*, vol. 215, no. 1, pp. 225–238, 2015, doi: 10.1016/j.jmatprotec.2014.08.009.

[185] H. Alipooramirabad, R. Ghomashchi, A. Paradowska, and M. Reid, "Residual stress-microstructure- mechanical property interrelationships in multipass HSLA steel welds," *J.*

Mater. Process. Technol., vol. 231, pp. 456–467, 2016, doi: 10.1016/j.jmatprotec.2016.01.020.

[186] J. W. Sowards, T. Gnäupel-Herold, J. David McColskey, V. F. Pereira, and A. J. Ramirez, "Characterization of mechanical properties, fatigue-crack propagation, and residual stresses in a microalloyed pipeline-steel friction-stir weld," *Mater. Des.*, vol. 88, pp. 632–642, 2015, doi: 10.1016/j.matdes.2015.09.049.

[187] A. P. Kolikov, A. S. Leletko, D. B. Matveev, S. A. Kulyutin, and S. V. Kadil'nikov, "Residual stress in welded pipe," *Steel Transl.*, vol. 44, no. 11, pp. 808–812, 2014, doi: 10.3103/S0967091214110096.

[188] E. S. Costa, P. D. C. Assunção, E. B. F. Dos Santos, L. G. Feio, M. S. Q. Bittencourt, and E. M. Braga, "Residual stresses in cold-wire gas metal arc welding," *Sci. Technol. Weld. Join.*, vol. 22, no. 8, pp. 706–713, 2017, doi: 10.1080/13621718.2017.1306014.

[189] B. A. B. Andersson, "Thermal stresses in a submerged-arc welded joint considering phase transformations," *J. Eng. Mater. Technol. Trans. ASME*, vol. 100, no. 4, pp. 356–362, 1978, doi: 10.1115/1.3443504.

[190] I. R. Nodeh, S. Serajzadeh, and A. H. Kokabi, "Simulation of welding residual stresses in resistance spot welding, FE modeling and X-ray verification," *J. Mater. Process. Technol.*, vol. 205, no. 1–3, pp. 60–69, 2008, doi: 10.1016/j.jmatprotec.2007.11.104.

[191] A. H. Yaghi, T. H. Hyde, A. A. Becker, and W. Sun, "Numerical simulation of P91 pipe welding including the effects of solid-state phase transformation on residual stresses," *Proc. Inst. Mech. Eng. Part L J. Mater. Des. Appl.*, vol. 221, no. 4, pp. 213–224, 2007, doi: 10.1243/14644207JMDA152.

[192] P. Duranton, J. Devaux, V. Robin, P. Gilles, and J. M. Bergheau, "3D modelling of multipass welding of a 316L stainless steel pipe," *J. Mater. Process. Technol.*, vol. 153–154, no. 1–3, pp. 457–463, 2004, doi: 10.1016/j.jmatprotec.2004.04.128.

[193] P. Ferro, F. Berto, and G. Meneghetti, "Calculation of 3D residual notch stress intensity factors by means of the peak stress method," *Theor. Appl. Fract. Mech.*, vol. 100, no. December 2018, pp. 377–382, 2019, doi: 10.1016/j.tafmec.2019.01.032.

[194] C. Li and Y. Wang, "Three-dimensional finite element analysis of temperature and stress distributions for in-service welding process," *Mater. Des.*, vol. 52, pp. 1052–1057, 2013, doi: 10.1016/j.matdes.2013.06.042.

[195] S. W. Wen and D. C. J. Farrugia, "Finite element modelling of residual stress in pipe welds," *Strain*, vol. 37, no. 1, pp. 15–18, 2001, doi: 10.1111/j.1475-1305.2001.tb01215.x.

[196] C. Wu and J. W. Kim, "Analysis of welding residual stress formation behavior during circumferential TIG welding of a pipe," *Thin-Walled Struct.*, vol. 132, no. August, pp. 421–430, 2018, doi: 10.1016/j.tws.2018.09.020.

[197] W. Jiang, K. Yahiaoui, and F. R. Hall, "Finite element predictions of temperature distributions in a multipass welded piping branch junction," *J. Press. Vessel Technol. Trans. ASME*, vol. 127, no. 1, pp. 7–12, 2005, doi: 10.1115/1.1845450.

[198] V. M. Varma Prasad, V. M. Joy Varghese, M. R. Suresh, and D. Siva Kumar, "3D Simulation of Residual Stress Developed During TIG Welding of Stainless Steel Pipes,"

Procedia Technol., vol. 24, pp. 364–371, 2016, doi: 10.1016/j.protcy.2016.05.049.

[199] E. Feulvarch, V. Robin, and J. M. Bergheau, "Thermometallurgical and mechanical modelling of welding - application to multipass dissimilar metal girth welds," *Sci. Technol. Weld. Join.*, vol. 16, no. 3, pp. 221–226, 2011, doi: 10.1179/1362171811Y.0000000008.

[200] S. Suman, P. Biswas, S. K. Patel, V. P. Singh, A. Kumar, and B. Kuriachen, "Measurement of residual stresses in submerged arc welded P91 steel using surface deformation," *Mater. Today Proc.*, vol. 21, pp. 1707–1712, 2020, doi: 10.1016/j.matpr.2019.12.049.

[201] A. H. Yaghi, T. H. Hyde, A. A. Becker, J. A. Williams, and W. Sun, "Residual stress simulation in welded sections of P91 pipes," *J. Mater. Process. Technol.*, vol. 167, no. 2–3, pp. 480–487, 2005, doi: 10.1016/j.jmatprotec.2005.05.036.

[202] A. H. Yaghi, T. H. Hyde, A. A. Becker, and W. Sun, "Finite element simulation of welding and residual stresses in a P91 steel pipe incorporating solid-state phase transformation and post-weld heat treatment," *J. Strain Anal. Eng. Des.*, vol. 43, no. 5, pp. 275–293, 2008, doi: 10.1243/03093247JSA372.

[203] D. Deng, S. Kiyoshima, K. Ogawa, N. Yanagida, and K. Saito, "Predicting welding residual stresses in a dissimilar metal girth welded pipe using 3D finite element model with a simplified heat source," *Nucl. Eng. Des.*, vol. 241, no. 1, pp. 46–54, 2011, doi: 10.1016/j.nucengdes.2010.11.010.

[204] N. U. Dar, E. M. Qureshi, and M. M. I. Hammouda, "Analysis of weld-induced residual stresses and distortions in thin-walled cylinders," *J. Mech. Sci. Technol.*, vol. 23, no. 4, pp. 1118–1131, 2009, doi: 10.1007/s12206-008-1012-6.

[205] M. Abid and M. Siddique, "Numerical simulation to study the effect of tack welds and root gap on welding deformations and residual stresses of a pipe-flange joint," *Int. J. Press. Vessel. Pip.*, vol. 82, no. 11, pp. 860–871, 2005, doi: 10.1016/j.ijpvp.2005.06.008.

[206] M. Abid, M. Siddique, and R. A. Mufti, "Prediction of welding distortions and residual stresses in a pipe-flange joint using the finite element technique," *Model. Simul. Mater. Sci. Eng.*, vol. 13, no. 3, pp. 455–470, 2005, doi: 10.1088/0965-0393/13/3/013.

[207] M. Abid and M. Siddique, "Numerical simulation of the effect of constraints on welding deformations and residual stresses in a pipe-flange joint," *Model. Simul. Mater. Sci. Eng.*, vol. 13, no. 6, pp. 919–933, 2005, doi: 10.1088/0965-0393/13/6/010.

[208] D. Deng, H. Murakawa, and W. Liang, "Numerical and experimental investigations on welding residual stress in multi-pass butt-welded austenitic stainless steel pipe," *Comput. Mater. Sci.*, vol. 42, no. 2, pp. 234–244, 2008, doi: 10.1016/j.commatsci.2007.07.009.

[209] D. Deng, "FEM prediction of welding residual stress and distortion in carbon steel considering phase transformation effects," *Mater. Des.*, vol. 30, no. 2, pp. 359–366, 2009, doi: 10.1016/j.matdes.2008.04.052.

[210] K. H. Chang and C. H. Lee, "Finite element analysis of the residual stresses in T-joint fillet welds made of similar and dissimilar steels," *Int. J. Adv. Manuf. Technol.*, vol. 41, no. 3–4, pp. 250–258, 2009, doi: 10.1007/s00170-008-1487-4.

[211] C. H. Lee and K. H. Chang, "Temperature fields and residual stress distributions in dissimilar steel butt welds between carbon and stainless steels," *Appl. Therm. Eng.*, vol. 45–46, pp. 33–

41, 2012, doi: 10.1016/j.applthermaleng.2012.04.007.

[212] C. H. Lee and K. H. Chang, “Three-dimensional finite element simulation of residual stresses in circumferential welds of steel pipe including pipe diameter effects,” *Mater. Sci. Eng. A*, vol. 487, no. 1–2, pp. 210–218, 2008, doi: 10.1016/j.msea.2007.10.011.

[213] C. Yan, C. Liu, and B. Yan, “3D modeling of the hydrogen distribution in X80 pipeline steel welded joints,” *Comput. Mater. Sci.*, vol. 83, pp. 158–163, 2014, doi: 10.1016/j.commatsci.2013.11.007.

[214] M. R. Nezamdost, M. R. N. Esfahani, S. H. Hashemi, and S. A. Mirbozorgi, “Investigation of temperature and residual stresses field of submerged arc welding by finite element method and experiments,” *Int. J. Adv. Manuf. Technol.*, vol. 87, no. 1–4, pp. 615–624, 2016, doi: 10.1007/s00170-016-8509-4.

[215] A. S. Kurkin and I. N. Ponomareva, “Method of equivalent initial temperatures to account for welding stresses in strength analysis,” *Inorg. Mater.*, vol. 48, no. 14, pp. 1309–1313, 2012, doi: 10.10.1134/S0020168512140105.

[216] H. Fu *et al.*, “Effect of preheating temperature on post-weld residual stress of dissimilar steel plates,” *Metalurgija*, vol. 59, no. 2, pp. 150–152, 2020.

[217] P. Asadi, S. Alimohammadi, O. Kohantorabi, A. Fazli, and M. Akbari, “Effects of material type, preheating and weld pass number on residual stress of welded steel pipes by multi-pass TIG welding (C-Mn, SUS304, SUS316),” *Therm. Sci. Eng. Prog.*, vol. 16, no. July 2019, p. 100462, 2020, doi: 10.1016/j.tsep.2019.100462.

[218] G. Fu and M. I. Lourenço, “Omae2014-23514 Effects of Preheat and Interpass Temperature on the Residual,” *Proc. ASME 2014 33rd Int. Conf. Ocean. Offshore Arct. Eng.*, pp. 1–8, 2014.

[219] M. Perić, I. Garašić, S. Nižetić, and H. Dedić-Jandrek, “Numerical Analysis of Longitudinal Residual Stresses and Deflections in a T-joint Welded Structure Using a Local Preheating Technique,” *Energies*, vol. 11, no. 12, 2018, doi: 10.3390/en11123487.

[220] W. Zhang *et al.*, “Influence of multi-beam preheating temperature and stress on the buckling distortion in electron beam welding,” *Mater. Des.*, vol. 139, pp. 439–446, 2018, doi: 10.1016/j.matdes.2017.11.016.

[221] R. Sepe, E. Armentani, G. Lamanna, and F. Caputo, “Evaluation by FEM of the influence of the preheating and post-heating treatments on residual stresses in welding,” *Key Eng. Mater.*, vol. 627, pp. 93–96, 2015, doi: 10.4028/www.scientific.net/KEM.627.93.

[222] K. Jafarpur and M. R. Nami, “Analysis of welding conditions based on induced thermal irreversibilities in welded structures: Cases of welding sequences and preheating treatment,” *Sci. Iran.*, vol. 18, no. 3 B, pp. 398–406, 2011, doi: 10.1016/j.scient.2011.05.030.

[223] S. Suman and P. Biswas, “Comparative study on SAW welding induced distortion and residual stresses of CSEF steel considering solid state phase transformation and preheating,” *J. Manuf. Process.*, vol. 51, no. October 2019, pp. 19–30, 2020, doi: 10.1016/j.jmapro.2020.01.012.

[224] J. Choi and J. Mazumder, “Numerical and experimental analysis for solidification and residual stress in the GMAW process for AISI 304 stainless steel,” *J. Mater. Sci.*, vol. 37, no.

10, pp. 2143–2158, 2002, doi: 10.1023/A:1015258322780.

[225] E. Ranjbarnodeh, S. Serajzadeh, A. H. Kokabi, and A. Fischer, “Effect of welding parameters on residual stresses in dissimilar joint of stainless steel to carbon steel,” *J. Mater. Sci.*, vol. 46, no. 9, pp. 3225–3232, 2011, doi: 10.1007/s10853-010-5207-8.

[226] S. Xu and W. Wang, “Numerical investigation on weld residual stresses in tube to tube sheet joint of a heat exchanger,” *Int. J. Press. Vessel. Pip.*, vol. 101, pp. 37–44, 2013, doi: 10.1016/j.ijpvp.2012.10.004.

[227] A. B. S. T. R. A. C. T. In, “Experimental Procedure and Welding Conditions Finite Element Analysis Finite Element Modeling and Mesh Generation,” no. March, pp. 80–89, 2001.

[228] O. Obeid, G. Alfano, H. Bahai, and H. Jouhara, “A parametric study of thermal and residual stress fields in lined pipe welding,” *Therm. Sci. Eng. Prog.*, vol. 4, pp. 205–218, 2017, doi: 10.1016/j.tsep.2017.10.011.

[229] J. A. Becker, K. D. Berg, M. A. Røder, K. Brasso, and P. Iversen, “Cytoreductive prostatectomy in metastatic prostate cancer: a systematic review,” *Scand. J. Urol.*, vol. 52, no. 1, pp. 1–7, 2018, doi: 10.1080/21681805.2017.1363816.

[230] P. Li, Y. Fan, C. Zhang, Z. Zhu, W. Tian, and A. Liu, “Research on Heat Source Model and Weld Profile for Fiber Laser Welding of A304 Stainless Steel Thin Sheet,” *Adv. Mater. Sci. Eng.*, vol. 2018, 2018, doi: 10.1155/2018/5895027.

[231] A. Ravisankar, S. K. Velaga, G. Rajput, and S. Venugopal, “Influence of welding speed and power on residual stress during gas tungsten arc welding (GTAW) of thin sections with constant heat input: A study using numerical simulation and experimental validation,” *J. Manuf. Process.*, vol. 16, no. 2, pp. 200–211, 2014, doi: 10.1016/j.jmapro.2013.11.002.

[232] P. Roberto de Freitas Teixeira, D. Bezerra de Araújo, and L. Antônio Bragança da Cunha, “Study of the Gaussian Distribution Heat Source Model Applied To Numerical Thermal Simulations of Tig Welding Processes Estudo Do Modelo De Fonte De Calor De Distribuição Gaussiana Na Aplicação De Simulações Térmicas Numéricas Dos Processos De Soldagem Tig,” vol. 23, no. 1, pp. 115–122, 2014.

[233] I. A. Roberts, C. J. Wang, R. Esterlein, M. Stanford, and D. J. Mynors, “A three-dimensional finite element analysis of the temperature field during laser melting of metal powders in additive layer manufacturing,” *Int. J. Mach. Tools Manuf.*, vol. 49, no. 12–13, pp. 916–923, 2009, doi: 10.1016/j.ijmachtools.2009.07.004.

[234] M. Zain-ul-abdein, D. Nélias, J. F. Jullien, and D. Deloison, “Experimental investigation and finite element simulation of laser beam welding induced residual stresses and distortions in thin sheets of AA 6056-T4,” *Mater. Sci. Eng. A*, vol. 527, no. 12, pp. 3025–3039, 2010, doi: 10.1016/j.msea.2010.01.054.

[235] X. Jin, L. Li, and Y. Zhang, “A heat transfer model for deep penetration laser welding based on an actual keyhole,” *Int. J. Heat Mass Transf.*, vol. 46, no. 1, pp. 15–22, 2003, doi: 10.1016/S0017-9310(02)00255-7.

[236] R. Brockmann, K. Dickmann, P. Geshev, and K. J. Matthes, “Calculation of laser-induced temperature field on moving thin metal foils in consideration of Stefan problem,” *Opt. Laser Technol.*, vol. 35, no. 2, pp. 115–122, 2003, doi: 10.1016/S0030-3992(02)00157-3.

[237] N. T. Nguyen, Y. W. Mai, and A. Ohta, “Analytical solution for a new hybrid double-ellipsoidal heat source in semi-infinite body,” *Proc. Int. Conf. Adv. Compos. Mater. Struct. VII*, pp. 207–217, 2000.

[238] J. Winczek, “Modeling of temperature field during multi-pass gmaw surfacing or rebuilding of steel elements taking into account the heat of the deposit metal,” *Appl. Sci.*, vol. 7, no. 1, 2017, doi: 10.3390/app7010006.

[239] F. Clain, D. Araujo, and P. Teixeira, “a Heat Source Model To Simulate Welding Processes With Magnetic Deflection,” vol. 22, no. 1, pp. 99–113, 2018, doi: 10.26678/abcm.encit2016.cit2016-0514.

[240] A. Ghosh, S. Hloch, and S. Chattopadhyaya, “Critical analysis of moving heat source shape for arc welding process of high deposition rate,” *Teh. Vjesn.*, vol. 21, no. 1, pp. 95–98, 2014.

[241] A. Ghosh and S. Chattopadhyaya, “Analytical solution for transient temperature distribution of semi -infinite body subjected to 3-D moving heat source of submerged arc welding process,” *ICMET 2010 - 2010 Int. Conf. Mech. Electr. Technol. Proc.*, no. Icmet, pp. 733–737, 2010, doi: 10.1109/ICMET.2010.5598459.

[242] K. Sankaranarayanasamy, “Numerical and Experimental Investigation of Laser Beam Welding of Aisi 304 Stainless Steel Sheet,” *Maja.Uni-Mb.Si*, vol. 3, pp. 93–105, 2008.

[243] N. R. Roshyara, G. Wilhelm, U. Semmler, and A. Meyer, “Approximate analytical solution for the temperature field in welding,” *Metall. Mater. Trans. B Process Metall. Mater. Process. Sci.*, vol. 42, no. 6, pp. 1253–1273, 2011, doi: 10.1007/s11663-011-9543-0.

[244] N. T. Nguyen, A. Ohta, K. Matsuoka, N. Suzuki, and Y. Maeda, “Analytical Solutions for Transient Temperature of Semi-Infinite Body Subjected to 3-D Moving Heat Sources,” *Weld. J. (Miami, Fla)*, vol. 78, no. 8, 1999.

[245] C. Bruna-Rosso, A. G. Demir, and B. Previtali, “Selective laser melting finite element modeling: Validation with high-speed imaging and lack of fusion defects prediction,” *Mater. Des.*, vol. 156, pp. 143–153, 2018, doi: 10.1016/j.matdes.2018.06.037.

[246] R. Derpsch *et al.*, “Why do we need to standardize no-tillage research?,” *Soil Tillage Res.*, vol. 137, pp. 16–22, 2014, doi: 10.1016/j.still.2013.10.002.

[247] J. Winczek, G. Rygal, and T. Skrzypczak, “The model of temporary temperature field during multi-pass arc weld surfacing. Part I: Analitycal description,” *J. Appl. Math. Comput. Mech.*, vol. 14, no. 2, pp. 123–130, 2015, doi: 10.17512/jamcm.2015.2.13.

[248] N. S. Shanmugam, G. Buvanashekaran, K. Sankaranarayanasamy, and S. Ramesh Kumar, “A transient finite element simulation of the temperature and bead profiles of T-joint laser welds,” *Mater. Des.*, vol. 31, no. 9, pp. 4528–4542, 2010, doi: 10.1016/j.matdes.2010.03.057.

[249] P. Xia *et al.*, “Prediction of weld shape for fiber laser keyhole welding based on finite element analysis,” *Int. J. Adv. Manuf. Technol.*, vol. 75, no. 1–4, pp. 363–372, 2014, doi: 10.1007/s00170-014-6129-4.

[250] C. S. Wu, H. G. Wang, and Y. M. Zhang, “A new heat source model for keyhole plasma arc welding in FEM analysis of the temperature profile,” *Weld. J. (Miami, Fla)*, vol. 85, no. 12, 2006.

[251] A. Blood, “(I + [K ’]) 13 (I) K- concentration,” vol. 39, pp. 536–538, 1983.

[252] G. Ziervogel *et al.*, “Climate change and adaptation in African agriculture,” *Training*, vol. 4179, no. September 2009, p. 53, 2008, doi: 10.1002/cnm.

[253] K. Kazemi and J. A. Goldak, “Numerical simulation of laser full penetration welding,” *Comput. Mater. Sci.*, vol. 44, no. 3, pp. 841–849, 2009, doi: 10.1016/j.commatsci.2008.01.002.

[254] M. Hashemzadeh, B. Q. Chen, and C. G. Soares, “Comparison between different heat sources types in thin-plate welding simulation,” *Dev. Marit. Transp. Exploit. Sea Resour.*, no. 2010, pp. 329–336, 2013, doi: 10.1201/b15813-42.

[255] K. C. Ganesh, M. Vasudevan, K. R. Balasubramanian, N. Chandrasekhar, and P. Vasantharaja, “Thermo-mechanical analysis of TIG welding of AISI 316LN stainless steel,” *Mater. Manuf. Process.*, vol. 29, no. 8, pp. 903–909, 2014, doi: 10.1080/10426914.2013.872266.

[256] V. Dhinakaran, N. S. Shanmugam, and K. Sankaranarayanasamy, “Some studies on temperature field during plasma arc welding of thin titanium alloy sheets using parabolic Gaussian heat source model,” *Proc. Inst. Mech. Eng. Part C J. Mech. Eng. Sci.*, vol. 231, no. 4, pp. 695–711, 2017, doi: 10.1177/0954406215623574.

[257] S. A. Tsirkas, P. Papanikos, and T. Kermanidis, “Numerical simulation of the laser welding process in butt-joint specimens,” *J. Mater. Process. Technol.*, vol. 134, no. 1, pp. 59–69, 2003, doi: 10.1016/S0924-0136(02)00921-4.

[258] D. B. Darmadi, A. K. Tieu, and J. Norrish, “A validated thermal model of bead-on-plate welding,” *Heat Mass Transf. und Stoffuebertragung*, vol. 48, no. 7, pp. 1219–1230, 2012, doi: 10.1007/s00231-012-0970-5.

[259] M. R. James and J. B. Cohen, *Measurement of Residual Stresses By X-Ray Diffraction Techniques.*, vol. 19, no. pt A. ACADEMIC PRESS, INC., 1980.

[260] H. M. Tensi, B. Liščić, and T. Filetin, “Prediction of Hardness Profile in Workpiece Based on Characteristic Cooling Parameters and Material Behaviour During Cooling,” *Theory Technol. Quenching*, vol. 1992, pp. 390–476, 1992, doi: 10.1007/978-3-662-01596-4_11.

[261] S. Szávaia, Z. Bézi, and P. Rózsahegyi, “Material Characterization and Numerical Simulation of a Dissimilar Metal Weld,” *Procedia Struct. Integr.*, vol. 2, pp. 1023–1030, 2016, doi: 10.1016/j.prostr.2016.06.131.

List of Publications

1. Alhafadhi, mahmood hasan, and Gyorgy krallics. "Simulation of the residual stress in a multi-pass oil and gas pipe weld joint." *journal of physics: conference series*. vol. 1527. no. 1. 2020.
2. Alhafadhi, mahmood hasan, and Gyorgy krallics. "Numerically simulated prediction of residual stresses in welding considering phase transformation effects." *journal of physics: conference series*. vol. 1527. no. 1. iop publishing, 2020.
3. Alhafadhi, mahmood, and György krállics. "Effect of the welding parameters on residual stresses in pipe weld using numerical simulation." *Design of Machines and Structures*, 10.1 (2020): 5-12.
4. Alhafadhi, mahmood hasan, and Gyorgy krallics. "The effect of heat input parameters on residual stress distribution by numerical simulation." IOP conference series: materials science and engineering. vol. 613. no. 1, Art. 012035, 2019, doi: 10.1088/1757-899X/613/1/012035
5. Alhafadhi, mahmood hasan, and Gyorgy krallics. "Numerical simulation prediction and validation of two-dimensional model weld pipe." *Machines. Technologies. Materials.* Vol. 13, No. 10 (2019): 447-450.
6. Alhafadhi, mahmood hasan, and Gyorgy krallics. "Prediction and numerical simulation of residual stress in multi-pass pipe welds", *Pollack Periodica*, Vol. 16, No. 2, pp. 7–12, 2021, doi: 710.1556/606.2020.00127
7. Mahmoodalhafadhi, Gyorgy Krallics, and Máté Szűcs. "Finite element analysis on the formation of residual stresses during welding of oil and gas pipe."

List of Conferences

1. Alhafadhi, mahmood hasan, and gyorgy krallics. "Simulation of the residual stress in a multi-pass oil and gas pipe weld joint." journal of physics: conference series. vol. 1527. No. 1. iop publishing, 2020.
2. Alhafadhi, mahmood hasan, and Gyorgy krallics. The effect of heat input parameters on residual stress distribution by femhungarian academy of sciences, Miskolc academic commitee erzsébet square, miskolc, 3530.
3. Alhafadhi, mahmood hasan, and Gyorgy krallics the effect of heat input parameters on residual stress distribution by numerical simulation5th international conference on competitive materials and technological processes (ic-cmtp5)

DOI: 10.14750/ME.2022.004

9. APPENDIX

A-1: Comparison of residual stresses measurement methods

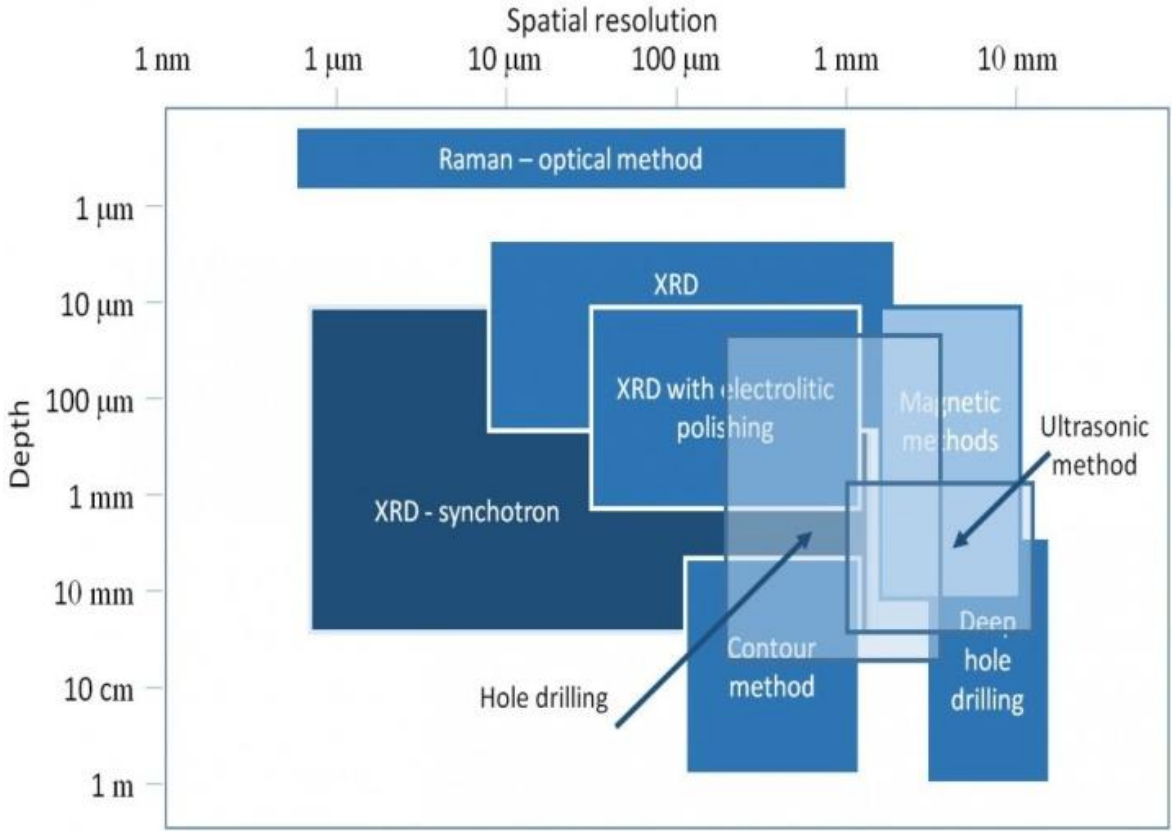

Figure A-1: Comparison of residual stresses measurement methods

Appendix B

B-1: CCC diagram for filler Continuous cooling transformation diagram for filler

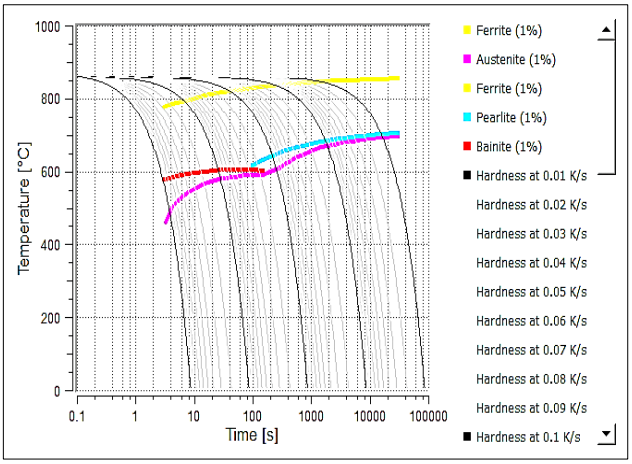

Figure B-1: Continuous cooling transformation diagram for filler Continuous cooling transformation diagram for filler

DOI: 10.14750/ME.2022.004

B-2: CCC diagram for filler Continuous cooling transformation diagram for E355K2

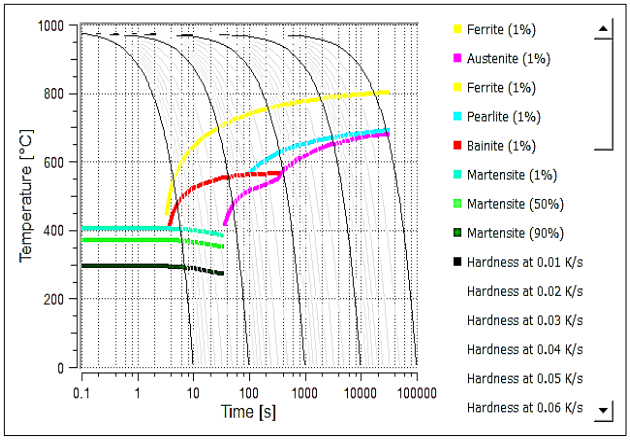

FigureB-2: Continuous cooling transformation diagram for E355K2

B-3: CCC diagram for filler Continuous cooling transformation diagram for P460NH_1

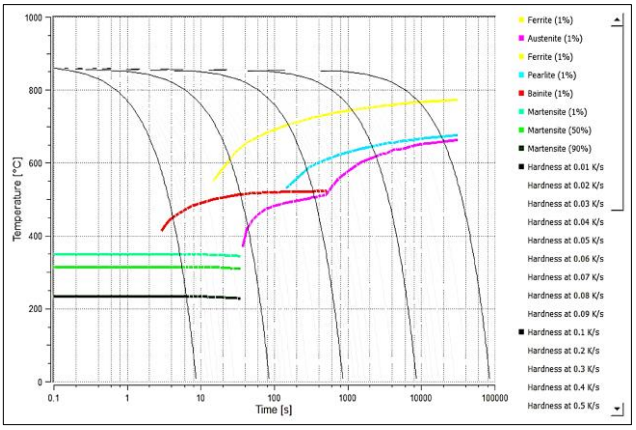

Figure B-3: Continuous cooling transformation diagram for P460NH_1

Appendix C

C-1: Prediction of Residual Stress in Welding Two Similar Material Pipes

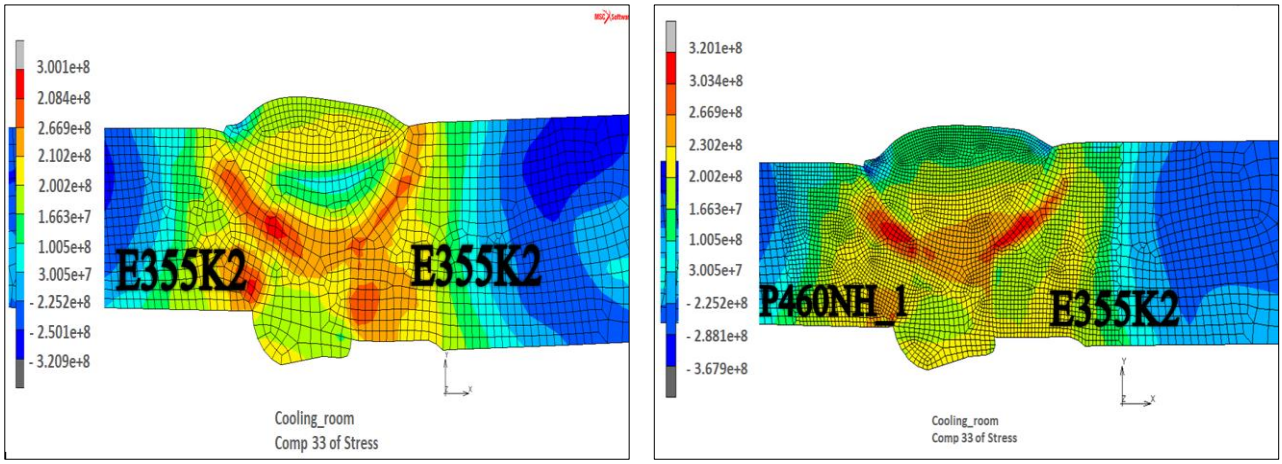

Figure C-1: Hoop stress (a) with similar material of pipe (E355K2) (b) with dissimilar material of pipe